

Development and Evaluation of CyclicRGD-tagged Nano-carrier System Containing Temozolomide and Rapamycin for the Treatment of Glioblastoma Multiforme

THESIS

Submitted in partial fulfillment of the requirements for the degree of

DOCTOR OF PHILOSOPHY

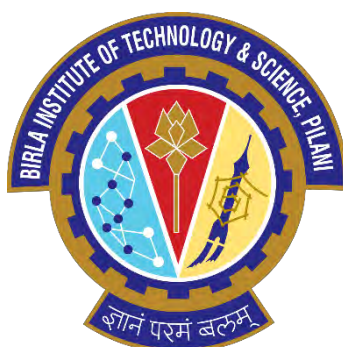
by

PRABHJEET SINGH

2018PHXF0044P

Under the Supervision of

Prof. Deepak Chitkara
(Supervisor)



**Prof. Gaikwad Anil
Bhanudas**
(Co-supervisor)

BIRLA INSTITUTE OF TECHNOLOGY & SCIENCE, PILANI

2024

Dedication



My father

I dedicate my thesis to my father
Mr. Gurmeet Singh for his
believe in me and his sacrifices
made all along my journey

My Mother

I dedicate my thesis to my mother
Mrs. Kanwaljeet Kaur for her
continuous support, prayers, and
being my best buddy during my
ups and down

Prabhjeet Singh

DECLARATION

I declare that the thesis entitled “**Development and Evaluation of CyclicRGD-tagged Nano-carrier System Containing Temozolomide and Rapamycin for the Treatment of Glioblastoma Multiforme**” has been prepared by me under the guidance of **Prof. Deepak Chitkara**, Associate Professor and **Prof. Gaikwad Anil Bhanudas**, Professor, Department of Pharmacy, BITS-Pilani, Pilani Campus, Rajasthan. No part of this thesis has formed the basis for the award of any degree or fellowship previously.


Prabhjeet Singh

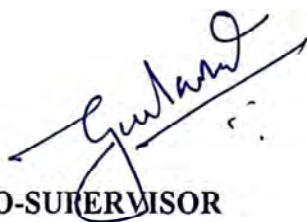
Department of Pharmacy,
BITS-Pilani, Pilani Campus,
333031-Rajasthan, India

Date: 14-09-2024

Place: Pilani, Rajasthan

CERTIFICATE

This is to certify that the thesis entitled “**Development and Evaluation of CyclicRGD-tagged Nano-carrier System Containing Temozolomide and Rapamycin for the Treatment of Glioblastoma Multiforme**” submitted by **Mr. Prabhjeet Singh**, ID No **2018PHXF0044P** for the award of Ph. D. Degree of the Institute embodies the original work done by him under my supervision.



CO-SUPERVISOR

Prof. Gaikwad Anil Bhanudas

Professor,

Department of Pharmacy,

BITS-Pilani, Pilani Campus,

333031-Rajasthan, India



SUPERVISOR

Dr. Deepak Chitkara

Associate Professor,

Department of Pharmacy,

BITS-Pilani, Pilani Campus,

333031-Rajasthan, India

Date: 14-09-2024

Place: Pilani, Rajasthan

Table of Contents

Contents	Page No.
<i>Acknowledgement</i>	i
<i>List of Abbreviations and Symbols</i>	v
<i>List of Tables</i>	x
<i>List of Figures</i>	xii
<i>Abstract</i>	xviii
Chapter 1	1
Introduction to Research work	
Chapter 2	43
Analytical and bioanalytical method development and validation of rapamycin, temozolomide, temozolomide acid, temozolomide hydrazide, and 5-aminoimidazole-4-carboxamide in biological matrix of rat	
Chapter 3	74
Design, synthesis, and characterization of polycarbonate-based polymeric conjugates of temozolomide	
Chapter 4	100
Formulation development, <i>in vitro</i> and <i>in vivo</i> evaluation of hybrid nanoconjugates of temozolomide in C6 cells-induced syngeneic orthotopic glioma model in rats	
Chapter 5	124
Development and evaluation of cRGD peptide-functionalized hybrid nanoconjugates of temozolomide coloaded with rapamycin in C6 cells-induced syngeneic orthotopic glioma model in rats	
Chapter 6	160
Conclusions and future prospective	
<i>Annexure I</i>	A
<i>List of Patents</i>	
<i>Annexure II</i>	B
<i>List of Publications</i>	
<i>Annexure III</i>	D
<i>List of Awards and Conferences</i>	
<i>Annexure IV</i>	E
<i>Biography of Supervisor and Co-supervisor</i>	
<i>Annexure V</i>	H
<i>Biography of Scholar</i>	

Acknowledgement

First and foremost, I am truly grateful and bow down to the **Waheguru** for his grace. By the grace of God, I have been able to past all my endeavors, blessing with strength, power, courage, wisdom, and bringing me this far in my academic career and enabling me to accomplish my Ph.D. work successfully.

Each of us poses individual note in the music of life, but when all notes unite, our unique melodies harmonize to form a sweet and mesmerizing symphony. The togetherness of the sweet tunes not only strengthens the melody, it also transforms the dreams into a meaningful and fulfilling reality. Toward the submission of the thesis, I would like to thank all those who extended their kind help and support in fulfilling this achievement.

My work would not have been possible without the leadership and support of my esteemed supervisor, **Prof. Deepak Chitkara**, Associate Professor at BITS-Pilani, for his unconditional support and encouragement throughout my whole journey. I owe my deepest thanks for his guidance, detailed discussion, caring nature, enthusiastic but calm approach, and, more importantly, allowing me to think independently, which kept me going further in the pursuit of excellence in research. Being well acquainted with my capabilities, he kept pushing me forward and guided me in all aspects, be it academic, research, or personal. His eagle-eyed dedication towards the advancements in the field of science and excellent ability to manage multiple tasks simultaneously have instilled great motivation in me and undoubtedly changed my view towards the research. His infinite patience guided me through challenges countless times, shaping the person I have become today. I will always be indebted for your valuable teachings, out-of-the-league support, and sustained encouragement.

I sincerely thank my co-supervisor, **Prof. Gaikwad Anil Bhanudas**, Professor, Department of Pharmacy, BITS-Pilani, for his kind and continuous support and encouragement

throughout my journey. I am very thankful to him for his care towards me and for giving me full freedom to reach new heights.

I want to express my sincere thanks to Doctoral Advisory Committee (DAC) members **Prof. Anil Jindal** and **Prof. Sandeep Sundriyal** for their continuous support, thorough analysis of my research work, and providing valuable and critical suggestions that have profoundly shaped my research proposal and thesis. Their commitment has been a guiding light, enriching my academic journey with their expertise.

I sincerely thank the faculty members of the Department of Pharmacy, BITS-Pilani, **Prof. R.N. Saha** (Retired Senior Professor), **Prof. R. Mahesh** (Senior Professor), **Prof. S. Murugesan**, **Prof. Rajeev Taliyan**, **Prof. Hemant R. Jadhav**, **Prof. Atish T. Paul**, **Prof. Anupama Mittal**, **Prof. Aniruddha Roy**, **Prof. M.M. Pandey**, **Prof. Gautam Singhvi**, **Prof. Richa Srivastava**, **Prof. Pragyanshu Khare**, and **Dr. Sunil Kumar Dubey** (former faculty), for providing essential learning and support.

My special thanks to **Dr. Sushil K. Yadav** (Sr. Vet. In-charge, Central Animal Facility) for his unquestioning belief and unwavering support in performing animal studies during my Ph.D. tenure.

I want to thank all non-teaching staff, including **Mr. Puran**, **Mr. Vishal**, **Mr. Laxman**, **Mr. Tarachand**, **Mr. Ram P. Suthar**, **Mr. Surender**, **Mr. Vikas**, **Mr. Naveen**, **Mr. Abhishek**, **Mr. Sandeep**, **Mr. Mukesh**, **Mr. Mahender**, and **Mr. Sultan** for their support in document management and timely provision of laboratory necessities.

I am thankful to **DBT-nanobiotechnology**, **DST-INSPIRE**, and **BITS-Pilani** for their financial support and providing research facilities during my Ph.D. journey.

I am very thankful to **Prof. Rajeev Sakhuja** and **Dr. Kiran Bajaj** for their continuous support during my Ph.D.

My heartiest thanks to my old buddy, **Mr. Shakti Nagpal**, for being perpetually supportive, encouraging, and believing in me throughout my journey. It would be incomplete without the thanks to my close buddies for being there in my ups and downs and being faithful throughout my journey. I thank **Dr. Vishal Singh**, **Dr. Kavya Sree Maravajjala**, **Mr. Shivanshu**, **Dr. Paramita Saha**, and **Mr. Anmol Arora** for supporting and believing in me throughout the journey.

I want to thank **Dr. Deepak Kumar Sahel** and **Reena Jatyan** for their extra-mile support during my Ph.D. journey. I would like to thank all my fantastic juniors and colleagues **Mr. Abhay Tharmatt**, **Ms. Sonia Guha**, **Mr. Gangadhari Giriprasad**, **Mr. Imran Ansari**, **Dr. J. Yogeswaran**, **Dr. Preety Rawal**, **Dr. Arihant Kumar Singh**, **Dr. Moumita Basak**, **Mr. Shubham Salunkhe**, **Mr. K. Sai Pradyuth**, **Mr. N. Sai Bhargav**, **Mr. Pratik Shinde**, for creating a pleasant workplace. I thank my seniors, **Dr. Saurabh Sharma**, **Dr. Sudeep Sudesh Pukhale**, **Dr. Kishan Italiya**, and **Dr. Samrat Mazumdar**, for their support and motivation during the early stages of my Ph.D. journey.

I am thankful to **Mrs. Proporna**, Department of Biology, **Dr. Bintu Kumar**, **Dr. Manish Mehra**, **Dr. Santosh Khandagale**, **Dr. Karishma**, **Dr. Mahesh Krishna**, **Mr. Ram P. Bhatt**, **Mr. Sumit**, **Mr. Ajit**, Department of Chemistry for their talks with a cup of tea and making the journey memorable.

I want to thank my seniors and colleagues from the department, **Dr. K.V. Krishna**, **Dr. Dhanashree Surve**, **Dr. Vajir Malek**, **Dr. Nisha Sharma**, **Dr. Ginson George**, **Dr. Pracheta Sengupta**, **Dr. Vamshi R. Krishna**, **Dr. Sarathlal K.C.**, **Dr. Geetika Wadhwa**, **Dr. Violina**, **Dr. Karan Kumar**, **Dr. Himanshu**, **Dr. Tejashree Waghule**, **Dr. Kedar Prayag**, **Dr.**

Srividya Gorantla, Mr. Rupesh Jain, Dr. Rajesh Pradhan, Dr. Amritansh Bhanot, Dr. Nikita Hinge, Dr. Mahipal Donthi, Dr. Ajinath Kale, Dr. Atharva R. Bhide, Dr. Prashant Auti, Dr. Sharyu Kesharwani, Ms. Manisha Choudhari, Ms. Karnam Sri Ravalli, Ms. Nisha, Mr. Mukesh, Ms. Shreya Das, Mr. Amit Sharma, Mr. Vishwadeep Shelke, Ms. Sakshi, Ms. Yashika, Ms. Shobha, Ms. Shikha, Ms. Neha, Mr. Chandu Ala, Mr. Jayant, Mr. Md. Muzaffar Rehaman, Ms. Lavanya, Mr. Utkarsh, Mr. Yash Patidar, Ms. Shivangi, Ms. Vaibhavi, Ms. Shivani, Ms. Priyanka, Ms. Jyotika, Ms. Aarti, Mr. Jagdish, Mr. Bhupendra, Mr. Animesh, Ms. Pranali, Mr. Sanat, for being a sport during my Ph.D. journey. I sincerely thank all who helped me directly or indirectly during my Ph.D.

The journey would not have been possible for me to come this far without their prayers, blessings, unconditional love, care, and support. I thank my sisters, **Mrs. Gurleen Kaur** and **Mrs. Jasleen Kaur**, for believing in me throughout my life. I am grateful to my elders and entire family for their blessings.

I would acknowledge the silent sacrifice of all animals during the course of study.

“Embarking on a journey, the road is long, but dreams have just begun.”

(Prabhjeet Singh)

List of Abbreviations and Symbols

%	Percent
~	Approximately equal to
<	Less than
>	Greater than
±	Plus or minus
μg	Microgram
μl	Microliter
μM	Micromolar
¹³ C NMR	Carbon-13- nuclear magnetic resonance
¹ H NMR	Proton nuclear magnetic resonance
AIC	5-aminoimidazole-4-carboxamide
BBB	Blood brain barrier
BBTB	Blood brain tumor barrier
BHMP	2, 2- bis (hydroxymethyl) propionic acid (bhmp)
BME	Brain microenvironment
CBTRUS	Central Brain Tumor Registry of the United States
CCSEA	Committee for Control and Supervision of Experiments on Animals
CDCl ₃	Chloroform-D
CNS	Central nervous system
CO ₂	Carbon dioxide
Conc.	Concentration
Const.	Constant

CPCSEA	Committee for the Purpose of Control and Supervision of Experiments on Animals
CPPs	Cell penetrating peptides
CV	Coefficient of variation
DAPI	4',6-diamidino-2-phenylindole
DCM	Dichloromethane
DEE	Diethyl ether
DIC	Differential interference contrast
DIPEA	N, n-diisopropylethylamine
DiR	1,1-Dioctadecyl-3,3,3,3-tetramethylindotricarbocyanine
DLS	Dynamic light scattering
DMEM	Dulbecco's modified eagle medium
DMSO	Dimethyl sulfoxide
DMSO- <i>d</i> ₆	Dimethyl sulfoxide- <i>d</i> ₆
DSB	Double strand break
EDC.HCl	1-ethyl-3-(3-dimethylaminopropyl) carbodiimide hydrochloride
ESI-TOF	Electrospray Ionization Time-of-Flight
FBS	Fetal bovine serum
FDA	Food and Drug Administration
FE-SEM	Field Emission Scanning Electron microscopy
GBM	Glioblastoma Multiforme
HoBt	Hydroxybenzotriazole
HPLC	High-performance liquid chromatography
HQC	High quality control
HRMS	High-resolution mass spectrometry

IAEC	Institutional Animal Ethics Committee
ICH	International Council for Harmonisation
IDH	Isocitrate dehydrogenase
IVIS	<i>In vivo</i> imaging system
KG	Kilogram
LC	Liquid chromatogram
LC/MS	Liquid chromatography-mass spectrometry.
LOD	Limit of Detection
LOQ	Limit of Quantitation
LQC	Low quality control
MBC	5-methyl-5-benzyloxycarbonyl-1, 3-dioxane-2-one
MDM2	Mouse double minute 2 homolog
MEM	Minimum essential medium
mg	Milligram
MGMT	O6-Methylguanine-methyltransferase
MHz	Megahertz
min	Minutes
ml	Milliliter
mM	Millimolar
mm	Millimeter
mPEG	Poly(ethylene glycol) monomethyl ether
MQC	Middle-quality control
MTIC	3-methyl-(triazene-1-yl)imidazole-4-carboximide
mTOR	Mammalian Target of Rapamycin
MTT	(3-(4,5-Dimethylthiazol-2-yl)-2,5-Diphenyltetrazolium Bromide)

mV	Milli volt
MWCO	Molecular weight cut-off
nab-sirolimus	Nanoparticle albumin-bound sirolimus
ng	Nanogram
nm	Nanometer
NMR	Nuclear magnetic resonance
°C	Degree centigrade
PBS	Phosphate buffer saline
Pd/C	Palladium on carbon
PDC	Polymer drug conjugate
PDI	Polydispersity index
PI	Propidium iodide
PI3K/Akt	Phosphoinositide 3-kinase/protein kinase B
PS	Particle size
PTEN	Phosphatase and tensin homolog
PyBOP	Benzotriazol-1-yloxytripyrrolidinophosphonium hexafluorophosphate
QC	Quality control
R ²	Regeression coefficient of determination
RAP	Rapamycin
RES	Reticuloendothelial system
RH/LH	Right hemisphere to left hemisphere
ROP	Ring-opening polymerization
RSD	Relative standard deviation
S/N	Signal to noise
SD	Standard deviation

SEM	Standard error of mean
TEA	Triethylamine
TLC	Thin layer chromatography
TMZ	Temozolomide
TMZ-A	Temozolomide acid
TMZ-BOC	BOC-protected Temozolomide
TMZ-H	Temozolomide hydrazide
UV-Vis	Ultraviolet-visible
v/v	Volume per volume
Var.	Variable
w/w	Weight by Weight
WHO	World Health Organization
ZP	Zeta potential

List of Tables

Table No.	Title	Page No.
1.1	Polymeric conjugates of TMZ	25
2.1	Intra-day and Inter-day accuracy and precision of TMZ-H	47
2.2	Stability studies of TMZ-H	47
2.3	Calibration curve details of RAP, TMZ, TMZ-A, TMZ-BOC, TMZ-H, and AIC	52
2.4	Intra-day and Inter-day accuracy and precision of RAP, TMZ, TMZ-A, TMZ-BOC, TMZ-H, and AIC	54-55
2.5	Stability studies of RAP, TMZ, TMZ-A, TMZ-BOC, TMZ-H, and AIC	55-57
2.6	UPLC-MS/MS parameters for RAP, TMZ, TMZ-A, TMZ-H, AIC, and TAC	63
2.7	Mass parameters for RAP, TMZ, TMZ-A, TMZ-H, AIC, and TAC	63
2.8	Calibration curve equation and sensitivity for RAP, TMZ, TMZ-A, TMZ-H, and AIC	67
2.9	Intra-day and Inter-day accuracy and precision of RAP, TMZ, TMZ-A, TMZ-H, and AIC in whole blood as a biological matrix	68-69
2.10	Stability studies of RAP, TMZ, TMZ-A, TMZ-H, and AIC in whole blood as a biological matrix	69-71
3.1	Loading capacity of nanoconjugates	91

4.1	Preparation of Hybrid TMZ NCs using different ratios of mPEG-b-P(CB- $\{g$ -COOH; g-TMZ ₄₀ : mPEG-PLA)	110
5.1	Pharmacokinetic parameters of TMZ, TMZ-A, TMZ-H, AIC and RAP after intravenous (i.v.) administration of free TMZ, free RAP, Hybrid TMZ/R NCs, and cRGD-Hybrid TMZ/R NCs in C6-glioma bearing rats. Data represented as mean \pm SEM	146

List of Figures

Fig. No.	Caption	Page No.
1.1	Overview of the biological barriers for brain delivery	7
1.2	Blood–brain barrier and blood–brain tumor barrier	11
1.3	Overview of temozolomide (TMZ) and mTOR inhibitor-rapamycin (RAP) in glioma	17
2.1	TMZ-H characterisation. A) UV-Visible spectrum and B) Calibration curve	46
2.2	Chromatographic elution of AIC, TMZ, TMZ-A, TMZ-BOC, and TMZ-H (<i>top to bottom</i>) on C18 column using methanol and sodium acetate buffer (pH 4.0) as a mobile phase	51
2.3	Calibration curve of A) RAP, B) TMZ, C) TMZ-A, D) TMZ-BOC, E) TMZ-H, and F) AIC in mobile phase	52
2.4	Specificity of the analytes A) TMZ→TMZ-A, B) TMZ-A→TMZ-BOC, C) TMZ-BOC→TMZ-H	53
2.5	Cone and collision potential optimisation for parent ion and daughter ion for RAP, TMZ, TMZ-A, TMZ-H, AIC, and TAC	64
2.6	Representative chromatogram for A) RAP, B) TAC, C) TMZ-H, D) TMZ-A, E) TMZ, and F) AIC (<i>top to bottom</i>)	66
3.1	Reaction scheme for the synthesis of TMZ-polymer conjugates. A) Synthesis of TMZ hydrazide: i) NaNO ₂ , H ₂ SO ₄ , 4-8 °C, overnight, ii) t-butyl carbazate, PyBOP, triethylamine, overnight, iii) 1,4-dioxane.HCl, 4-6 h, B) Synthesis of polycarbonate polymer with free COOH group: iv) Benzyl bromide, KOH, 100 °C, overnight,	76

	then triphosgene, pyridine, acetone-dry ice bath, 4 h, v) mPEG (Mn. 5000), tin(II)-ethylhexanoate, microwave-assisted ring-opening polymerization, 130 °C, 1 h, vi) Palladium on carbon, H ₂ , 5 h, C) Synthesis of TMZ-polymer conjugates (<i>mPEG-b-P(CB-{g-COOH; g-TMZ_n})</i>): vii) EDC/HOBt coupling, DIPEA, N ₂ , 4-8 °C	
3.2	Characterization of TMZ and its derivatives. A) ¹ H NMR and B) ESI-TOF HR-Mass spectrometry of TMZ (1), TMZ-A (2), TMZ-BOC (3), and TMZ-H (4)	81
3.3	Characterization of TMZ and its derivatives using UV-Visible spectroscopy	82
3.4	Characterization of TMZ and its derivatives. ¹³ C NMR spectrometry of A) TMZ (1), B) TMZ-A (2), C) TMZ-BOC (3), and D) TMZ-H (4)	83
3.5	Characterization of MBC cyclic carbonate monomer using A) ¹ H NMR, B) ¹³ C NMR, and C) ESI-TOF HR-mass spectrometry	85
3.6	Characterization of <i>mPEG-b-P(CB)</i> carbonate polymer using A) ¹ H NMR and B) ¹³ C NMR spectroscopy	86
3.7	¹ H-NMR spectrum of A) polycarbonate polymer with free COOH group (<i>mPEG-b-P(CB-{g-COOH})</i>), and B) TMZ-polymer conjugate (<i>mPEG-b-P(CB-{g-COOH; g-TMZ₄₀})</i>)	87
3.8	¹³ C NMR of A) <i>mPEG-b-P(CB-{g-COOH})</i> and B) <i>mPEG-b-P(CB-{g-COOH; g-TMZ₄₀})</i>	89
3.9	¹ H NMR of A) <i>mPEG-b-P(CB-{g-COOH; g-TMZ₂₀})</i> and B) <i>mPEG-b-P(CB-{g-COOH; g-TMZ₆₀})</i>	90

3.10	Characterization of TMZ-polymer conjugates (<i>mPEG-b-P(CB-{g-COOH; g-TMZ₂₀})</i> , <i>mPEG-b-P(CB-{g-COOH; g-TMZ₄₀})</i> , <i>mPEG-b-P(CB-{g-COOH; g-TMZ₆₀})</i>) in various dispersive mediums (PBS; 10 mM pH 5.0, PBS; 10 mM pH 6.0, and PBS; 10 mM pH 7.4) using Dynamic light scattering (DLS), Scanning electron microscopy (SEM) images, and their pictograms	92
3.11	Characterisation of <i>mPEG-b-P(CB-{g-COOH; g-TMZ_n})</i> NCs. A) UV-based TMZ stability and B) DLS-based colloidal stability of <i>mPEG-b-P(CB-{g-COOH; g-TMZ₂₀})</i> and B) <i>mPEG-b-P(CB-{g-COOH; g-TMZ₄₀})</i> NCs	93
4.1	Scheme for the synthesis of TMZ-polymer conjugate (<i>mPEG-b-P(CB-{g-COOH; g-TMZ₄₀})</i>)	102
4.2	Scheme for the synthesis of mPEG-poly(lactic acid) (mPEG-PLA) copolymer	103
4.3	Characterisation of <i>mPEG-b-P(CB-{g-COOH; g-TMZ₄₀})</i> using A) ¹ H-NMR and B) ¹³ C NMR	108
4.4	Characterization of hybrid nanoconjugates. A) Schematic representation of hybrid nanoconjugates in combination with <i>mPEG-b-P(CB-{g-COOH; g-TMZ₄₀})</i> and mPEG-PLA, B) particle size with SEM image and pictograph, C) surface zeta potential, D) DLS-based colloidal stability, and E) UV-based TMZ stability evaluation of Hybrid TMZ NCs in phosphate buffered saline (PBS; pH 7.4) at 4 °C and 37 °C	110
4.5	<i>In vitro</i> cell-based evaluation of Hybrid TMZ NCs in glioma cells. Cell cytotoxicity using MTT assay in A) C6 and B) U87MG glioma	112

-
- cells. Annexin-V/PI-based apoptosis assay in C) C6 and D) U87MG glioma cells
- 4.6 *In vitro* cell-based evaluation of Hybrid TMZ NCs in glioma cells. Coumarin (C6)-based cellular uptake assay. A) & B) Qualitative evaluation using microscopy in C6 and U87MG glioma cells, C) & D) Quantitative uptake using flow cytometry in C6 and U87MG glioma cells, respectively 113
- 4.7 *In vivo* efficacy of hybrid nanoconjugates in C6-cells induced orthotopic syngeneic glioma model in SD rats. A) Treatment schedule. B) Representative brain images of treatment groups (negative control, positive control, TMZ-treated, and Hybrid TMZ NCs treated) and its C1-C4) brain histopathological (H&E) evaluation of the right hemisphere (at the site of injection). D), E), F), and G) represents mean brain weight, hemispherical width ratio (RH/LH), body weight, and Kaplan-Meier survival plot of treated animals, respectively (scale bar: 100 μ m) (*, *** indicates p value <0.05, <0.001, respectively) 115
- 4.8 *In vivo* H&E evaluation of hybrid nanoconjugate in majorly excised organs (heart, lungs, liver, kidney, and spleen) in C6-induced orthotopic glioma model in SD rats. (lungs: arrow indicates the presence of mitotic nucleus) (scale bar: 100 μ m) 117
- 5.1 Scheme for the A) preparation and fate of nanoconjugates after *in vivo* administration and B) synthesis of cRGD-targeted poly lactide polymer (cRGD-PEG-PLA) 128
-

5.2	Characterisation of polymer. ¹ H NMR A) Mal-PEG-PLA and B) cRGD-PEG-PLA polymer	134
5.3	A) Particle size and B) surface zeta potential analysis of cRGD-Hybrid TMZ/R NCs	136
5.4	Particle size distribution of coumarin-6 dye loaded cRGD-Hybrid TMZ/R NCs	136
5.5	<i>In vitro</i> evaluation of cRGD-Hybrid TMZ NCs in C6 glioma cells. A) Cell cytotoxicity assay B) & C) Combination index analysis for TMZ, RAP, and its combination using Chou-Talalay method. D) Annexin-V-FITC/PI-based apoptosis assay E) & F) Cellular uptake determination using coumarin-6 dye as a fluorescent probe	138
5.6	<i>In vitro</i> evaluation of cRGD-Hybrid TMZ NCs in U87MG glioma cells. A) Cell cytotoxicity assay B) & C) Combination index analysis for TMZ, RAP, and its combination using Chou-Talalay method. D) Annexin-V-FITC/PI-based apoptosis assay E) Cellular uptake determination using coumarin-6 dye as a fluorescent probe	139
5.7	<i>In vivo</i> efficacy of cRGD-Hybrid TMZ NCs in C6 cells induced orthotropic syngeneic glioma model in rats. A) Scheme for the <i>in vivo</i> study design. B) Representative brain images of treatment groups and B1-B7) brain histopathology (H&E) evaluation of the right hemisphere of brain (injection site). C) and E) mean body and brain weight of treated animals, D), and F) hemispherical width ratio (RH/LH) and Kaplan-Meier survival plot of treated animals, respectively (scale bar: 100 μm) (*, **, ***, @@, ### represents p value <0.05, <0.01, <0.001, <0.01, and <0.001 respectively)	141

5.8	Histopathological toxicity (H&E) evaluation of cRGD-Hybrid TMZ/R NCs in major organs (heart, lungs, liver, kidney, and spleen) in C6-glioma tumour bearing animals (scale bar: 100 μ m) (Black arrow: mononuclear cell infiltration in lungs, blue arrow: degeneration of hepatocytes in liver, green arrow: atrophic renal tubules with abnormal peritubular space, light blue arrow: moderate white and red pulp depletion)	143
5.9	Pharmacokinetic concentration-time profile of TMZ, TMZ-A, TMZ-H, AIC and RAP in whole blood after intravenous (i.v.) administration of free TMZ, free RAP, Hybrid TMZ/R NCs, and cRGD-Hybrid TMZ/R NCs in C6-glioma bearing rats. Data represented as mean \pm SD	145
5.10	Biodistribution of cRGD-Hybrid nanoconjugates in glioma bearing rats (Br: Brain, H: Heart, Lu: Lungs, Li: Liver, Ki: Kidney, and Sp: spleen)	147

Abstract

Abstract

Glioblastoma multiforme is a malignant and aggressive form of glioma arising from an astrocytic lineage, commonly found in CNS with grade IV malignancy, accounting for 80% of all malignant primary brain tumors. GBM is a type IV glioma characterized by its dedifferentiated, angiogenic, multiforme structure, making it more lethal. Moreover, multistep tumorigenesis of the malignancy of the glial cells accounts for nearly 90% of GBM IDH-wild type cases, and the remaining 10% is developed from the progression of low-grade astrocytoma or oligodendrogliomas, forming secondary glioblastoma. GBM is considered to be highly lethal, with a median survival rate of up to ~15 months; even after completion of the treatment, only ~25% of patients survive for more than 24 months after diagnosis. Currently, the standard-of-care treatment of GBM involves the administration of Temozolomide (TMZ) as a chemotherapeutic adjuvant alongside debulking surgery and radiotherapy. Despite intensive treatment, the average survival of GBM-affected patients remains around 50-65 weeks. This could be attributed due to the short half-life (1.8 h), rapid pH-dependent hydrolysis, and speedy clearance, resulting in a minimal amount of TMZ reaching the brain in the effective form, resulting in lesser accumulation in the brain, eventually causing the development of resistance and sub-therapeutic outcomes. In order to achieve the therapeutic effect, high doses of TMZ are given, resulting in dose-dependent toxicities. However, several molecules have been tested alongside TMZ to determine their efficacy in treating gliomas. These molecules include mTOR inhibitors, such as rapamycin (RAP), temsirolimus, and ridaforolimus. These rapalogues (especially RAP) mainly inhibit mTORC1 activity, which remains upregulated in tumor growth and progression. RAP is primarily known for effectively blocking the PI3K/Akt/mTOR pathway (causes activation of tumor suppressor genes), low therapeutic window, and good organ distribution. Nevertheless, the molecule still lacks the clinical translation for glioma therapy. This could be mainly ascribed due to the low solubility, bioavailability (~15%), poor pharmacokinetic behavior, and off-target effects, making it more challenging for its deployment in the treatment of GBM. Although both the molecules, including TMZ and RAP, demonstrate the antitumor action against the GBM differently. When administered together, both compounds can work synergistically to strengthen the effectiveness of the treatment, specifically by overcoming the development of resistance and inhibiting the downstream pathway of tumor survival and progression. This thesis primarily focuses on developing and evaluating a nanocarrier system that can efficiently deliver the dual payloads TMZ and RAP across the blood-brain barrier/blood-brain tumor barrier (BBB/BBTB) to the site of action in

the intact form. The synthesized copolymers were prepared and characterized thoroughly using UV and NMR spectroscopy.

In Chapter 1, we discussed the debilitating GBM disease with current treatment strategies and possible barriers that hinder the treatment phase. Thereafter, we thoroughly discussed the advanced therapeutic strategies to overcome the barriers. We have also covered the non-viral-based nanomaterials for dual drug delivery in treating GBM.

In Chapter 2, the analytical method was developed and validated using the ultraviolet-visible (UV-Vis) spectroscopy and HPLC-UV-based method, followed by UPLC-MS/MS-based bioanalytical method development and validation of RAP, TMZ and its metabolites. Initially, a simple UV-based analytical method was developed for temozolomide hydrazide (TMZ-H) to quantitate the drug molecule in the polymeric conjugate of temozolomide. The calibration curve was prepared, ranging from 0.62 to 40 $\mu\text{g/ml}$, with a regression coefficient of 1. The method was validated on UV-Vis spectroscopy as per the ICH guidelines. Thereafter, an HPLC-UV-based analytical method for rapamycin, temozolomide (TMZ), and its derivatives (TMZ-A, TMZ-BOC, TMZ-H, AIC) were developed and validated per the ICH guidelines. The calibration curve was prepared for all the analytes in the mobile phase ranging from 0.390 to 200 $\mu\text{g/ml}$ with a regression coefficient of >0.999 . The developed method was then utilized to determine the interferences and purity of the analytes. After that, a UPLC-MS/MS-based bioanalytical method was developed ranging from 0.976 ng/ml to 1000 ng/ml for RAP, TMZ, TMZ-A, TMZ-H, and AIC in whole blood as a biological matrix. Tacrolimus was used as an internal standard for all the analytes. The developed method exhibited a linearity for all the analytes with a regression coefficient of >0.99 and was later validated as per the ICH bioanalytical guidelines. The developed and validated method will be used to determine the *in vivo* pharmacokinetics in C6-glioma-bearing animals.

In Chapter 3, the work was started with the synthesis of an amphiphilic polycarbonate copolymer, $m\text{PEG-}b\text{-}P(\text{CB-}\{g\text{-COOH}\})$, with carboxyl pendant groups in a multistep reaction, wherein MBC carbonate monomer was co-polymerized with mPEG as macroinitiator using ring-opening polymerization with mPEG as macroinitiator to yield $m\text{PEG-}b\text{-}P(\text{CB})$ copolymer. The protective benzylic pendant was removed using catalytic hydrogenation to obtain the $m\text{PEG-}b\text{-}P(\text{CB-}\{g\text{-COOH}\})$. Simultaneously, the TMZ-hydrazide derivative was synthesized using a multistep reaction. Briefly, TMZ was converted to TMZ acid, then reacted with t-butyl carbazate to form TMZ-Boc-protected hydrazine, followed by cleavage of Boc using saturated

dioxane-HCl to afford unprotected TMZ hydrazide. After that, TMZ hydrazide derivative was reacted to *mPEG-b-P(CB- $\{g-COOH\}$)* copolymer using EDC/HOBt coupling to obtain a series of polymer conjugate of TMZ (*mPEG-b-P(CB- $\{g-COOH; g-TMZ_n\}$)*), with 20, 40, and 60 units of TMZ grafted to the polycarbonate backbone group exhibiting drug loading capacity of 16.8%, 28.8%, and 37.99% w/w, respectively. Out of which, *mPEG-b-P(CB- $\{g-COOH; g-TMZ_{40}\}$)* with 40 units of TMZ attached demonstrated pH-dependent change in particle size, i.e., the size of nanoparticles was found to reduce as the pH increased from pH 5.0 to pH 7.4 ranging from 207.2 to 90.9 nm, with stability half-life of 5.88 h compared to 1.8 h of free TMZ under physiological conditions (37 °C; pH 7.4). Though conjugating TMZ with polycarbonate has overcome the limitations associated with TMZ, there is still a lot of scope for further improvement in the stability and delivery of the molecule.

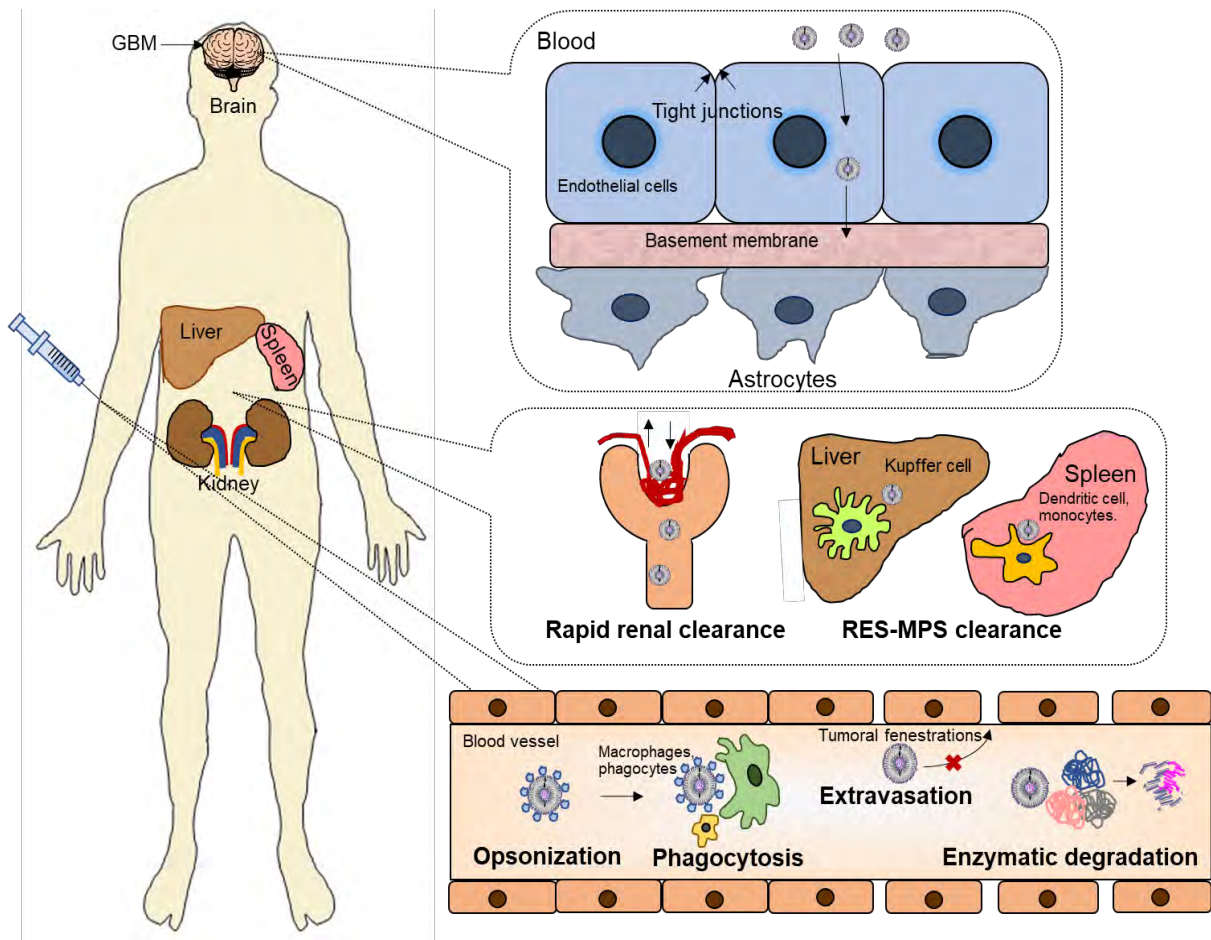
In Chapter 4, In order to improve the TMZ stability, we synthesised polyester-based mPEG-PLA polymer using ring-opening polymerization of DL-lactide and mPEG as macroinitiator in the presence of tin(II) ethylhexanoate as a catalyst. The polymer was then purified and characterized using ¹H NMR spectroscopy, indicating an average molecular weight of ~10 KDa with ~70 units of lactic acid. The polymer was then used to prepare polymer hybrid TMZ nanoconjugates composed of a mixture of *mPEG-b-P(CB- $\{g-COOH; g-TMZ_{40}\}$)* and mPEG-PLA using the thin film hydration method. The resulting hybrid TMZ polymer nanoconjugates (Hybrid TMZ NCs) exhibited better particles of 105.7 nm with a loading capacity of up to 21.6% w/w. Interestingly, the resulting Hybrid TMZ NCs showed a marked improvement in the half-life up to ~194 h compared to 1.8 h free TMZ and improved colloidal stability for over 7 days under physiological conditions (37 °C; pH 7.4). The Hybrid TMZ NCs showed enhanced cellular uptake efficiency up to 74% and 79% in C6 and U87MG glioma cells that resulted in an IC₅₀ of Hybrid TMZ NCs at ~645 and 866 μM compared to 1125 and 738 μM for free TMZ in C6 and U87MG glioma cells, respectively. Moreover, the Hybrid TMZ NCs demonstrated improved apoptosis rate up to 27.6% and 42.75% compared to 15.5% and 21.33% free TMZ in C6 and U87MG glioma cells, respectively. After confirming the *in vitro* potential, the Hybrid TMZ NCs were evaluated *in vivo* potential in a C6 cells-induced orthotropic syngeneic glioma model in *Sprague Dawley* rats. *In vivo* administration of Hybrid TMZ NCs has demonstrated an improvement in the antitumor outcome compared to the free TMZ, with a significant improvement in the brain weight, hemispherical width ratio, improved overall survival of rats, better biocompatibility, and reduced drug-dependent organ toxicities.

Chapter 5 extensively studies TMZ and RAP as combinational therapeutics, especially focusing on their delivery across the BBB/BBTB for treating gliomas. Therefore, the Hybrid TMZ NCs were coloaded with mTOR inhibitor RAP and targeted with cRGD peptide using thin film hydration method and maleimide-thiol coupling, respectively, to improve its *in vivo* efficiency. The dual payload carrying cRGD-targeted hybrid TMZ NCs (cRGD-Hybrid TMZ/R NCs) showed a particle size and surface zeta potential of 141.83 ± 10.05 nm and -0.168 ± 0.03 mV, respectively. The cRGD-Hybrid TMZ/R NCs have demonstrated better cellular uptake efficiency, resulting in improved cellular toxicity and apoptotic potential against C6 and U87MG glioma cells. Upon confirming the *in vitro* potential, we established and validated the C6-cells-induced syngeneic orthotropic glioma model in *Sprague Dawley* rats. Subsequently, the effect of the cRGD-Hybrid TMZ/R NCs was evaluated in tumor-bearing animals, wherein the tumor burden was found to be reduced with improved survival of rats. The histopathological toxicity analysis of major organs also indicated no significant signs of toxicity in the heart, liver, lungs, kidney, and spleen, demonstrating the biocompatibility of the developed cRGD-Hybrid TMZ/R nanoconjugates. Simultaneously, the pharmacokinetic study was performed in C6-glioma-bearing animals, indicating reduced circulation half-life and volume of distribution and improved the C_{max} , AUC, and clearance of RAP, post-treatment with cRGD-Hybrid TMZ/R NCs. Further, *in vivo* tissue bio-distribution was performed in C6-glioma-bearing rats, where the cRGD-Hybrid TMZ/R NCs exhibited an intense signal in tumor-bearing brain and liver at 6 h of administration, indicating the beneficial outcome of cRGD peptide functionalization with improved BBB permeability.

Overall, we have developed and evaluated cRGD-Hybrid TMZ/R NCs for their *in vitro* and *in vivo* delivery of TMZ and RAP as dual payload across the BBB/BBTB for anti-glioma activity. Such therapeutic strategies offer a promising avenue in addressing a wide range of diseases, potentially transforming the landscape of brain tumor therapeutics.

Chapter 1

Introduction



1.1. Introduction

Cancer is considered a deadly and debilitating disease, primarily characterized by abnormal cell growth with an ability to invade adjoining tissues, organs, and other parts of the body. According to the WHO Globocan report, around 18.1 million new cases of cancer were reported in 2018 out of which 9.6 million cancer patients died. Also, as per 5-year global cancer prevalence data, a total of 43.8 million have cancer, out of which 17.38 million people are Asian [1,2], highlighting the unmet medical attention required for cancer management and treatment. Among neurological cancers, glioblastoma multiforme (GBM) is a common brain malignancy with a significant increase in incidences per year. According to the central brain tumor registry of the United States (CBTRUS) statistical report, the average incidence rate of GBM is 3.22 per 100,000 cases and is profoundly seen higher in a patient with hereditary tumor syndromes like turcot and li-fraumeni syndrome [3,4]. GBM is a heterogeneous type of malignancy, usually known as astrocytoma, that arises from neoplastic glial cells and is considered one of the most lethal forms of brain cancer [5]. Unlike other tumors, GBM only invades the exposed organ but does not undergo metastasis. It is usually located in the frontal, temporal-parietal, and occipital lobes of the brain, with higher incidence rates in frontal and multiple lobes with overlapping tumors, and very rarely located in the spinal cord [3].

The current treatment for GBM includes tumor resection, with concomitant radiation therapy and chemotherapy. Despite intensive treatment, the average survival of GBM-affected patients remains around 50-65 weeks [6]. The reason behind the cases of tumor relapse is not clearly known; however, it could be attributed to the physiological barrier, the effect of drug action on tumor cells, and the development of resistance. During the treatment phase, access of most of the drugs to the target site is altered because of physiological barriers, including a blood-brain barrier (BBB) and blood-brain tumor barrier (BBTB), which they must cross after the systemic administration [7]. BBB is characterized by the monolayered, tightly packed epithelial cells preventing the entry of foreign or non-permissive substances. Whereas, BBTB constitutes the existing and newly formed components that are mainly responsible for the nutrient and oxygen delivery to the glioma cells [8]. Temozolomide, an alkylating agent, is currently used as the primary chemotherapeutic agent for GBM treatment [9]. TMZ was initially described in the year 2005 for GBM treatment with the aid of radiotherapy, wherein, the median survival rate of patients treated with TMZ was increased to 26.5% from 10.4% with radiotherapy alone [10]. TMZ is mainly marketed as Temodal capsules with 5-250 mg of TMZ given orally five days per week for four weeks and in vials (with 100 mg TMZ) for intravenous

injection. It is known to prevent G2/M transition that ultimately leads to the initiation of cellular apoptosis and shows cytotoxicity *via* methylation of guanine at the O-6 site, resulting in the addition of thymine in place of cytosine and further resulting in cell death. Concomitant therapy using both Temodal and radiation has improved the overall median survival by 2.5 months in newly diagnosed adult GBM patients as compared to those treated with radiation alone, but the major problem with the TMZ and radiotherapy is the tumoral relapse resulting from drug resistance. TMZ resistance is primarily ascribed to different DNA repair mechanisms, especially *via* the O-6-methylguanine-DNA methyltransferase (MGMT) enzyme. MGMT acts by reversing the TMZ effect by removing the methyl attached to the O-6 of guanine residue, thereby leading to the failure of therapy [11]. Hence, the lower cellular concentration of MGMT is directly correlated with higher sensitivity towards TMZ treatment [12]. To resolve this issue, developing efficient strategies is required that can directly circumvent the resistance mechanisms and effectively target GBM at the molecular level. In order to develop an efficient system, it is necessary to understand the pathophysiology of GBM vis-à-vis properties of therapeutic molecule/s.

1.2. Glioblastoma multiforme: Epidemiology, Etiology, and Pathophysiology

Glioblastoma multiforme is a malignant and aggressive form of glioma of an astrocytic lineage that is commonly found in CNS with grade IV malignancy and accounts for 80% of all malignant primary brain tumors. According to WHO standards of classification, gliomas are classified into four grades (I to IV) based on the extent of malignancy of the tumor. Grade I and II depict low-grade tumors with low proliferative potential, while grade III and grade IV tumors are comparatively malignant, dedifferentiated, aggressive, and lethal [13]. Moreover, multistep tumorigenesis of the malignancy of the glial cells accounts for nearly 90% of GBM IDH-wild type cases, and the remaining 10% is developed from the progression of low-grade astrocytoma or oligodendrogliomas, forming secondary glioblastoma. The development of secondary glioblastoma is comparatively slower and can take around 4-5 years to develop, while primary glioblastoma usually takes around three months with nearly negligible diagnosis [14,15]. The standard treatment for GBM includes surgical removal of the tumor, wherein >95% of the cancer can be removed, followed by chemotherapy and radiotherapy. In a randomized clinical trial, patients treated with TMZ adjuvant with radiotherapy exhibited improvement in median survival rate to 14.6 months compared to 12.1 months with radiotherapy alone. In addition, 2-year progression-free survival was found to be improved up to 10.7% with TMZ plus radiotherapy compared to 1.5% in the radiotherapy alone [10]. Despite

the fact that advanced multimodal therapy, including surgical resection, radiotherapy, and chemotherapy, the overall prognosis and survival are still limited in GBM patients. Further, the associated decline in neurological function leads to a hampered quality of life for the patients and their families [16,17].

1.2.1. Epidemiology

Central nervous system (CNS) tumor cases have been estimated globally in multiple age groups, including children, adults, and aged individuals, with an estimation of 7-11 cases per 1 million. In a Global Burden of Disease study, CNS cancer incidence was found to be around 330,000 cases, with a significantly higher death rate of 227,000 cases worldwide. Besides, 7.7 million CNS cancer patients have been estimated to suffer from disability-adjusted life-years due to the severity of brain damage. Global age-standardized incidence rates have also increased by 17.3% between the year 1990 to 2016, with a rate of 4.63 cases per 100,000 individuals [18,19]. According to Globocan (WHO), brain and CNS-related cancers were newly diagnosed in 308,102 cases, accounting for 1.6% cases of all cancers, and 251,329 deaths were reported worldwide in 2020 (© International agency for research on cancer 2024) both in males and females, including all age brackets. The 5-year prevalence data also indicates the majority of cases are prevalent in Asians, with 435,532 cases with a total count of 837,152 individuals worldwide. Furthermore, demographic data indicates that the majority (54.2%) of incidences and deaths were observed in Asians, followed by the European population [20]. By 2040, the incidence rate is expected to rise to 435,000 individuals. The worldwide Age-standardized incidences rates were observed to be higher in males compared to females, with 3.9 to 3.4 cases per 100,000 individuals, respectively. In the U.S. alone, all brain and CNS-related tumors with 17th position account for 24,538 new cases. Moreover, it has accounted for 3% and 18,133 deaths, acquiring the 9th rank in the list [21]. Wherein primary GBM is uncommon in children and grows rapidly with the average patient age of 62 years, the incidence increases till the 75-84 years and decreases after 85 years, with an annual age-adjusted incidence of 5.6 compared with 3.5 per 100,000 individuals. The mean patient's age for secondary GBM is 45 years and is commonly found in children and adults [3,22]. In a hospital-based clinico-epidemiology cancer profiling, a total of 1450 glioma cases were analyzed with a mean age of 39 years, wherein glioma was more prevalent in the male population, up to 66.6%. Out of 1450 cases, 41.4% of cases were of high-grade glioma (glioblastoma) followed by astrocytoma (22.8%), pilocytic astrocytoma (6.2%), and oligodendroglioma (4.5%) [23].

1.2.2. Etiology

The complete etiology of GBM has not been fully discovered by the scientific community, as no specific underlying reason for the occurrence of GBM can be identified. To date, few risk factors have been identified responsible for the development of glioblastoma. Exposing ionizing radiation is the only strongest and validated risk factor; more than 100 cases of glioblastoma have been diagnosed from radiation exposure with an overall risk of 2.5%. Also, the high-dose of radiotherapy and chemotherapy for treatment of the cancers are found to have a positive correlation in the development of intracranial tumors. The patients treated for acute lymphoid leukemia with radiotherapy and antimetabolite chemotherapeutic agents were more inclined to the incidence of GBM [24,25]. In retrospective cohort data, patients treated with radiation have demonstrated intensified risk of cancer in various groups. For instance, exposure to ionizing radiation due to the atomic bomb explosion in Hiroshima and Nagasaki resulted in increased incidences of all cancers, including gliomas. Furthermore, several other factors, including exposure to chemical carcinogens like pesticides, organochlorides, alkylureas, vinyl chlorides, N-nitroso compounds, aspartame, etc., are suspected to increase the risk of cancer [13,26–28]. While in a meta-analysis study, patients suffering from asthma and other allergenic conditions have shown an inverse association with the development of GBM due to activation of immune surveillance mechanisms [29]. Furthermore, the genetic predisposition syndromes are found to be associated with 5-10% of the cases associated with the development of glioblastoma, including Li–Fraumeni syndrome, Cowden's disease, and neurofibromatosis Turcot's syndrome and multiple hamartomas, providing strong, suitable candidates for understanding the possible underlying cause and molecular pathway in GBM [3,27]. Han et al. reported a supporting relationship between the head trauma and the development of glioma, describing the trauma as a cocarcinogen in the presence of initiating carcinogen [30]. Besides, the role of retroviruses and herpesviruses have been studied extensively in inducing gliomas in experimental models, suggesting a potential association between the gliomas and the viral onco-modulation in tumor malignancy [31].

1.2.3. Pathophysiology

Based on the histopathological evaluation, GBM cells are poorly differentiated cells with neoplastic properties, characterized by pseudo-palisading foci, nuclear hyperchromasia, increased angiogenesis, mitotic activity, thrombosis, cellular and nuclear atypia, and reduced apoptosis, resulting in abnormal proliferation, growth, and survival of GBM cells. The most

frequent location of occurrence of GBM is in the Supratentorial region (95% of cases), with tumor incidences in frontal, temporal, and parietal lobes [32], followed by the cerebellum, brain stem, and spinal cord [33]. According to WHO based classification, GBM is subdivided as per the histopathological criteria wherein, Grade I tumor or juvenile pilocytic astrocytoma is characterized by benign and slow-growing tumor, Grade II or anaplastic astrocytoma is characterized by increased cellularity with minimal necrosis, Grade III tumor or anaplastic astrocytoma shows tumor hypercellularity, poorly differentiated, mitosis with a high rate of reoccurrence, and Grade IV tumor or glioblastoma is a highly deadly form of tumor possess a high rate of hypercellularity, minimal cellular differentiation, angiogenesis, and necrosis, disrupting BBB and forms a cystic and gelatinous region in the brain. GBM can be identified macroscopically with a characteristic feature of the development of gross appearance in the white matter of brain tissue. In a few cases, a portion of affected tissue appears to be necrotic or yellowish, while some of the tumor tissue appears to show angiogenesis and hemorrhage [13]. The tumor can be observed as an individual large, irregular-shaped lesion arising in the white matter that can be perceived as anaplastic astrocytoma, demonstrating the tumor heterogeneity, ranging from poorly differentiating cells to highly differentiated cells with their angiogenic, invading, proliferation, and survival feature.

The development of tumor may occasionally develop symptoms, mainly because of the site of the tumor, tissue necrosis, and increased intracranial pressure, resulting in the development of seizures (could be focal, partial, complex, or generalized seizures), cognitive, hearing, and visual impairment, gait disfigurement, headaches, etc.; which is usually be mistaken for the stroke [34]. Due to tumor heterogeneity, disruption in the brain microenvironment (BME) causes reduced tight junction proteins, loss of pericytes, and astrocytic protection, exhibiting an increased permeability and distribution of foreign substances to the BME. Furthermore, the presence of leaky, fenestrated, and damaged lymphatic vessels in GBM attributes to the accumulation of metabolic and waste proteins, resulting in the formation of edema [35]. Likewise, using contrast-enhanced MRI, glioma-bearing mice depicted enhanced vasculature leakage in the BME that demonstrated the formation of brain edema. Furthermore, the outflow of CSF was also found to be significantly reduced in glioma-bearing mice, depicting the damage in the lymphatic drainage in glioma cases [36].

Based on the severity and clinical evaluation, GBM is classified into primary and secondary glioblastoma. Primary glioblastoma or *de novo* grade IV glioblastoma develops into

undifferentiated tumor cells without prominent evidence directly from a malignant precursor or stem cell. Molecular and gene alterations in primary glioblastoma usually includes alteration in epidermal growth factor receptor (EGFR), Phosphatase and Tensin homolog (PTEN), Telomerase Reverse Transcriptase (TERT), Mouse Double Minute 2 (MDM2), deletion of p16, and Loss of heterozygosity (LOH) at chromosome 10q, etc. Secondary GBM develops from lower-grade astrocytoma, which eventually mutates to higher-grade tumors *via* distinct molecular pathways, including isocitrate dehydrogenase 1 and 2 (IDH1/2), TP53 gene, platelet-derived growth factor receptor A (PDGFRA/ α), Retinoblastoma (R.B.), and Loss of heterozygosity (LOH) at 17p, 19q, and 10q, Alpha Thalassemia/Mental Retardation Syndrome X-linked (ATRX) [13,17,37–39]. The development of glioblastoma eventually results in alteration in the endothelial tight junctions of the blood-brain barrier (BBB), leading to an increased moment of molecules, blood-borne factors, and pathogens to the brain, causing cerebral malfunctions [40]. Currently going advancements in pathological techniques have attributed the correlation between the molecular downstream pathways with their clinical outcome. For instance, in a clinical high-grade glioma cohort population-based study, patients with grade III and IV glioma were evaluated for their genetic pathology. Wherein, involvement of MGMT promoter methylation, 1p19q co-deletion, IDH1 mutation, and ATRX loss was observed in HGG. Further, the prominent association of MGMT promoter methylation was found to be associated with improved overall survival and could be served as a prognostic marker in HGGs [41]. Other multiple factors, including PDGFR, Crk, p130CAS, HEF1 c-Met, HIF- α , etc., are also found to be pathologically active in the promotion of glioma survival, migration, and invasion [42].

1.3. Barrier in therapeutic delivery: The Blood-Brain Barrier

Understanding the brain microcellular environment is pivotal to design the new therapeutic approaches for GBM treatment. CNS barrier micro-environment is majorly composed of three components that include epithelia of choroid plexus, sub-arachnoid epithelium and blood-brain barrier (BBB). The BBB is a highly specialized structural and functional barrier, characterized by very low permeability, low pinocytosis, lacking fenestration and higher compartmental resistance across the blood and brain. It comprises of a group of different types of cells, including astrocytes, microglial cells, pericytes, and brain endothelium, performing different series of functions as a well-organized single neurovascular unit. Though the BBB provides strength to the CNS, it also serves several other roles including the exchange of essential nutrients with metabolic waste, maintaining ionic regulation through

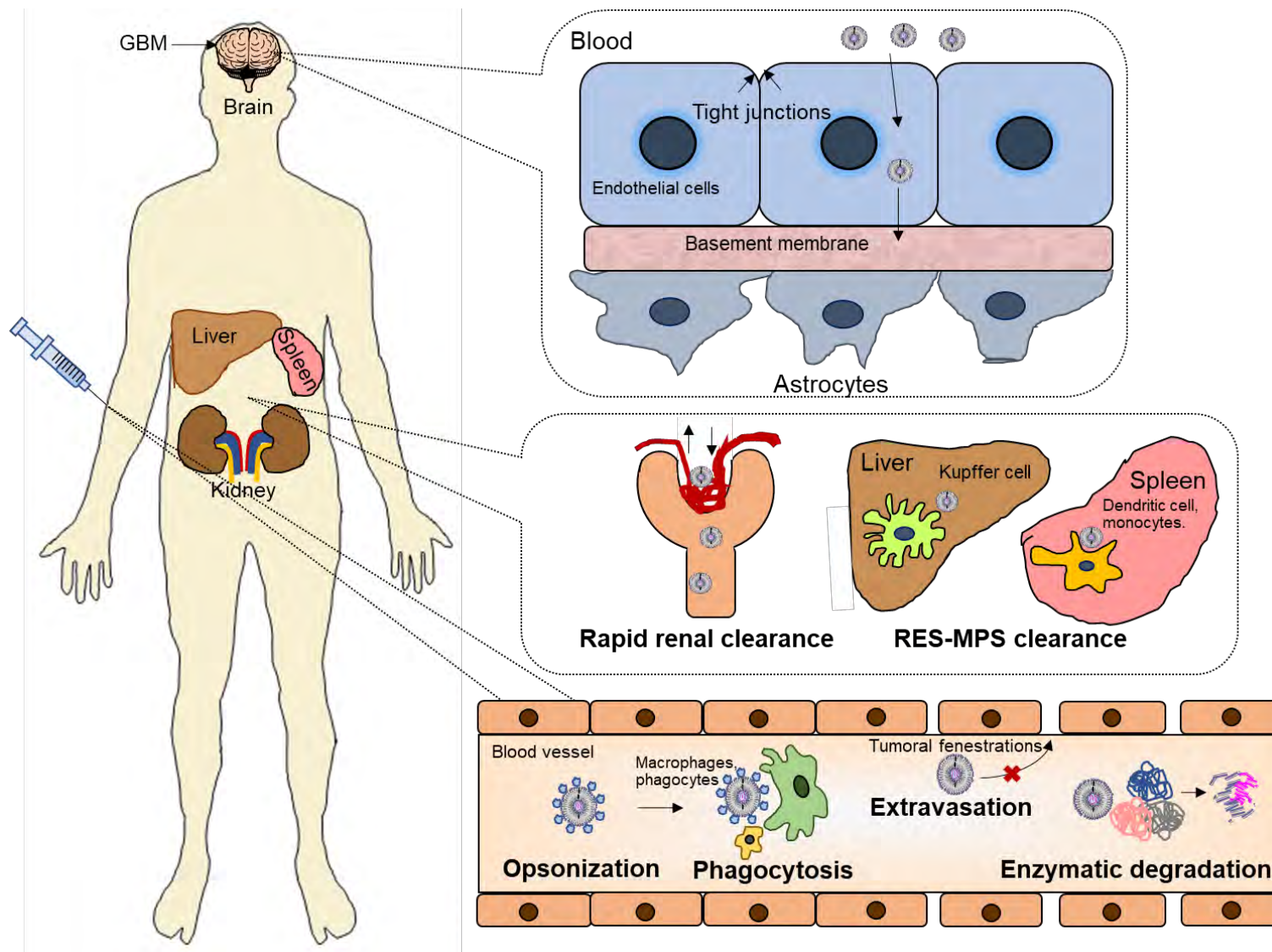


Figure 1.1. Overview of the biological barriers for brain delivery

selective ion transporters, circumventing crosstalk between the brain and peripheral neuroactive agents [43–45]. The presence of tight and adherent junctions of BBB restricts the movement of active drug molecules through the paracellular route across the endothelial layer and facilitates the movement *viz.* transcellular route [46]. Thus, BBB is responsible for aiding homeostasis and protection of the brain microcellular environment, maintaining the healthy status of the brain (Figure 1.1).

The blood-brain barrier (BBB) plays a vital role in filtering the blood components and other blood-mediated infections, critical for the normal functioning of the central nervous system and the homeostasis of the brain microenvironment. It is found in all organisms having well-developed CNS comprises multiple cellular and extracellular components such as endothelial cells, pericytes, astrocytes, and extracellular matrix [47]. The presence of claudins, occludin, junction adhesion, and cytoplasmic accessory proteins are the building blocks of the blood-brain barrier [48], forming tight junctions that primarily impede the paracellular diffusion and exhibit a low degree of transcytosis from blood to brain. In addition, cellular components, including astrocytes, pericytes, and endothelial cells, work together as a single neovascular unit and release several vasoactive adhering proteins that help in the regulation of vascular tension, expression of tight junction proteins, transport enzymes, and proteins [49,50]. Such a dense network of barriers facilitates the endothelial cells to regulate the brain homeostasis, neuronal functions and protects the brain by imparting the combination of physical, transport, and the metabolic barrier between the blood and brain compartment, thus creating a high paracellular resistance for pathogens, injury, molecules, proteins, inflammatory markers, neuro-active molecules, extracellular ligands, and other blood-borne components. The BBB properties are not stringently fixed; rather, it remains dynamic, which can be physiologically and pathologically regulated by the manifestation in the endothelial cell. However, in GBM, dysfunction of the BBB results in the impairment in the tight endothelial junctions, resulting in the loss of BBB characteristics, including damage in tight junctions, depletion of adhesion proteins (tenascin, agrin claudin, occludin), increased vessel permeability, endothelial fenestrations, pericytic detachment, and alteration in the extracellular matrix and thus termed as blood-brain tumor barrier (BBTB) [51,52]. The loss in the BBB integrity causes the development of several other complications such as stroke, neuroinflammatory shock, edema, altered neuronal signaling, immune cell infiltration, eventually leading to neuronal dysregulation or degeneration. The hypercellularity and neoangiogenesis behavior of glioblastoma deals in the alteration in the integrity of tight junctions, endothelial fenestrations,

perivascular space, and other components of the neovascular unit of BBB. Also, the glioma cell growth degenerates the vascular system and reduces vascular perfusion resulting in the secretion of hypoxia-related angiogenesis factors like VEGF, BFGF, IL-8, etc. Such growth factors stimulate neovascularisation and form different types of blood vessels, characterized by modulation in tight junctions and ECM [52,53]. Wherein, type I vessels depict the nominal agrin and claudin expression, type II and III exhibit either lowered or loss of expression of tenascin and claudin ECM. The type IV vessels showed complete loss of agrin and tight junctions of BBB, resulting in leaky blood vessels. Furthermore, dysfunction in BBB related ECM can be correlated with other extracellular enzymes like matrix metalloproteinase-3, matrix metalloproteinase-9, matrix metalloproteinase-12, cathepsin B, plasminogen activator, and scatter factor/ hepatocyte growth factor (SF/HGF) [54,55], which are found to be upregulated in proliferating glioma cells. Interestingly, upregulation in MMPs, TIMPs, and other proteases imparted parallel degradation in BBB integrity *via* degradation of BBB ECM growth factors, cleavage of basal laminal proteins, and remodeling of ECM, causing initiation, growth, survival, and angiogenesis of glioma cells [55]. For the effective treatment of cancer, an active moiety must be able to penetrate the barriers present alongside the tumor, including blood-borne barrier (pH, enzymes, ions, immune system), blood-brain barrier (pericytes, basal membrane, tight junctions), blood-brain tumor barrier (pH, tumor defense system), and tumor cell penetration (cellular uptake, efflux system, endosomal degradation). The aforementioned factors play a vital role directly or indirectly behind the poor delivery and treatment within the tumor. Nearly 100% of macromolecules and 98% of neurotherapeutics are not able to permeate through the presence of stringent BBB/BBTB [45,52,56]. The physiochemical properties of a molecule are as highly important as it allows the molecule to penetrate the barriers involved in the delivery to tumor cells. For instance, according to the Lipinski rule of 5, the drug can be said to be poorly absorbed when it has a molecular weight of greater than 500 Da, log p of >5, carrying more than 5 hydrogen bond donors, >10 hydrogen bond acceptor, and except biological transporters dependent substrates. In conclusion, size, lipophilicity, polar surface area, charge, plasma protein interaction, rotatable bond count, an affinity for uptake, and efflux of the molecule, provide a better idea in the delivery of molecules across the BBB [56,57]. Multiple approaches have been developed to deliver the molecule to the tumor tissue, *viz.*, bypassing the physiochemical, cellular, and molecular barriers of BBB/BBTB. The chemotherapeutics otherwise are unable to cross the intact BBB, but they partially can cross the BBTB due to the EPR effect. Thus, the permeation through the disrupted BBTB does not

ensure the complete accumulation near the tumor site, resulting in the mortified efficiency of chemotherapeutics in GBM therapy [52,56] (Figure 1.1).

BBB also plays a vital role in maintaining a stable microenvironment in the neural parenchyma located in the endothelial cells, limiting the paracellular movement of hydrophilic molecules *viz.* tight junctions (T.J.) and low degree of transcytosis, which is a part of transcellular transport. Small lipophilic compounds, can transcellularly diffuse through the BBB, involving the transportation of molecules through a non-saturable and non-competitive mechanism. In contrast, hydrophilic molecules do not cross through passively mediated transcellular transport; rather, they follow passively mediated paracellular transport. However, the passage of such molecules is quite limited due to the presence of tight junctions. BBB is known for its dynamic interaction with the brain microenvironment and further responds according to the needs of the brain. Depending upon the requirement and affinity of molecules, polar molecules like amino acids, nucleoside, peptide, vitamin and glucose, are transported to the brain *viz.* carrier-mediated active transport while large-bulky peptides and proteins like insulin, cytokines, transferrin and other large peptides are facilitated through receptor-mediated endocytosis by binding to a specific surface receptor on membrane accompanied with endocytosis [21,22] (Figure 1.2).

Presence of physiological and electrostatic barriers for the transport, another form of barrier is also formed by the cell, which is generally known as a metabolic barrier. Several intracellular and extracellular enzymes like nuclease, peptidase, monoamine oxidase and other hepatic enzymes are responsible for the formation of such barriers. These barriers manage the conversion of the active substance into less permeable products, leading to a reduction in the passage through the BBB [21]. In GBM, morphological changes tend to occur in the BBB that leads to an increase in neurovascular permeability and drug uptake. In a study conducted by cheng and co-workers, it was found that gancyclovir eliminates the pericytes that result in disruption and inhibition of tumor vessels and its growth [3]. Due to the changes in BBB, pericytes (GBM derived cells) start to detach, leading to an alteration in the extracellular matrix (ECM) that could be correlated to the changes occurring in the ECM components of GBM vessels. Several ECM molecules, like agrin and tenascin, can be analyzed in certain tissues with certain characteristic properties such as barrier like activity, cell adhesion, proliferation, migration of astrocytes, etc. Other studies also suggest that maintenance of BBB is actively done by agrin and its down-regulation may lead to an increase in BBB permeability [23].

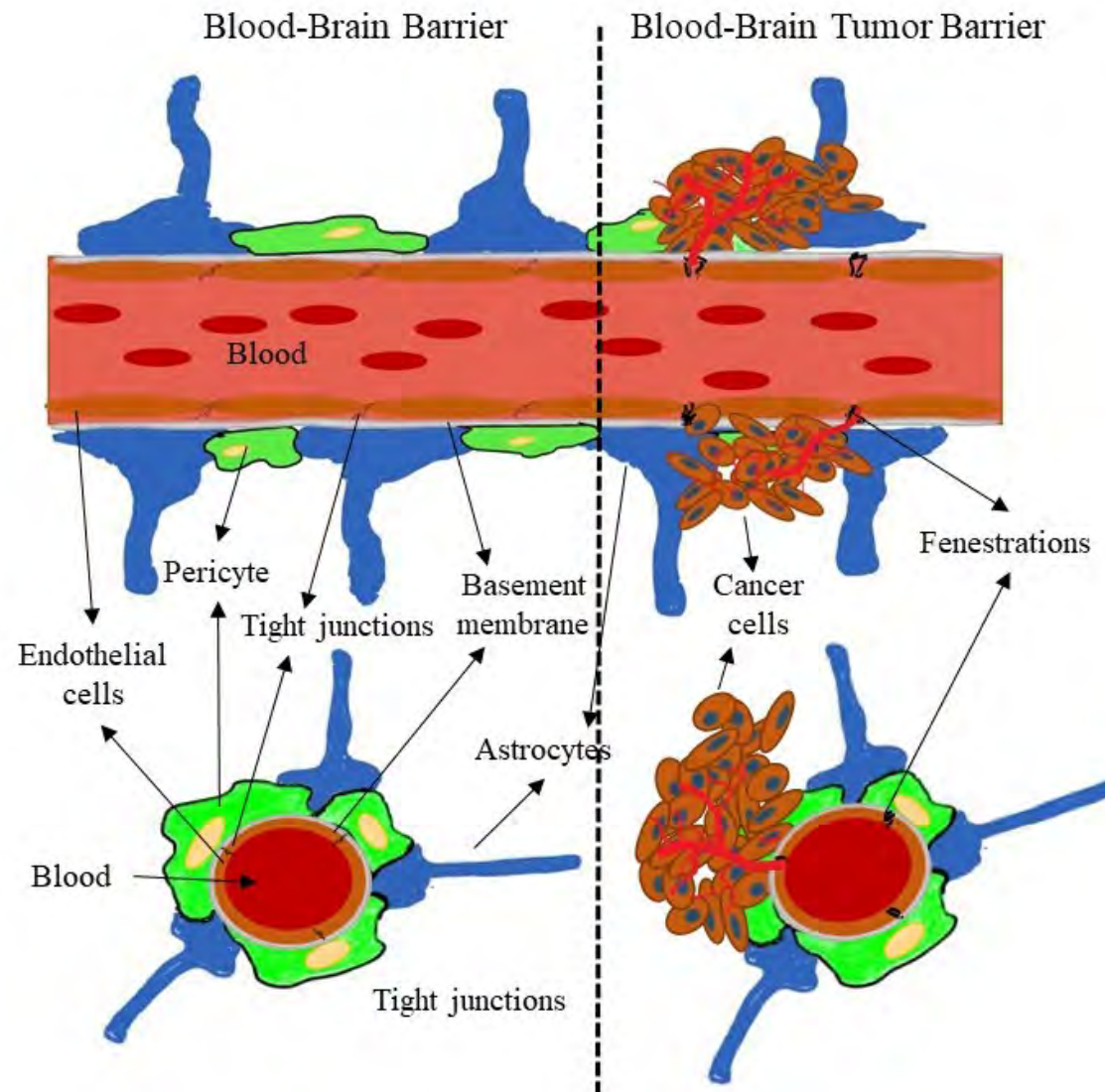


Figure 1.2. Blood-brain barrier and blood-brain tumor barrier

1.4. Current Treatment strategy

The conventional treatment of GBM primarily involves chemotherapy with DNA alkylating agent (TMZ) prior to debulking surgery and radiotherapy, mainly to improve the survival of the patient. The outcome of the surgical resection of the tumor is limited due to the heterogeneity and tumor infiltration to the neighboring tissue, rendering the treatment to limited scope. Therefore, coupling surgical resection with TMZ chemotherapy and radiotherapy is required for the destruction of tumors, even a minimal number of residual tumors can result in tumor relapse [58,59].

The treatment of newly diagnosed GBM patients initiates with the debulking surgery, wherein the neurosurgeon obtains the tissue for diagnosis, followed by the surgical reduction of tumor cells and hypoxic core of the tumor, which is comparatively resistant to external radio-chemotherapy. The surgical removal of each tumor is individual specific depending upon tumor shape, size, location, nature (diffused or distinct, benign or malignant), etc. [60,61]. Certain advancements in image-guided surgical techniques such as cortical mapping, intraoperative fluorescence imaging, MRI, and stereotactic surgery have reduced the tumor burden significantly by removal of a portion of the brain, but the meaningful removal of deep-located tumor tissue is still debatable, requiring additional treatment approaches [62,63]. Hence, the debulking process is coupled with both individual radiotherapy and chemotherapy. Radiation therapy (X-ray, gamma, protons energy), in addition to the surgical resection, has provided local control to the tumoral tissue, which is evident by the randomized clinical trial exhibiting the patients given 50-60 Gy of radiation has significantly improved the median survival to 36 weeks compared to 14 weeks without radiation therapy. Additionally, the extent of the intensity of the radiation impacts the tumoral cell death. As proven by the study, treatment with radiation less than 60Gy has shown poor outcomes in the patients [60,64]. On the other hand, the higher doses of radiation also affect the neighboring healthy cells adjoining the tumor cells. However, the determination of radiation intensity mainly depends on the extent of the tumor growth and nature. Although radiotherapy has shown improvement in patient survival, still continuous treatment with radiotherapy also imparts the development of resistance in the tumor cells, thus making it more difficult to treat [60]. To overcome certain limitations associated, chemotherapy is given as an adjuvant treatment to tumor-bearing patients. For instance, TMZ is considered the gold-standard chemotherapeutic agent with debulking surgery and radiotherapy [59,65]. TMZ is the most widely used chemotherapeutic agent for the GBM, *viz.*, alkylating the DNA base pair, causing cell cycle arrest and apoptosis. Several other FDA-

approved DNA alkylating drugs have been used to treat the gliomas, namely, carmustine (BCNU), lomustine (CCNU), Bevacizumab, Gliadel® wafers, etc. [58]. Nevertheless, the treatment fails, mainly due to the enzyme alkyl guanine transferase (AGT) *via* reversing the alkylation of DNA, rendering the treatment nullified. However, the breakthrough was reported by Stupp et. al. in 2005, wherein TMZ was used as a chemotherapeutic agent as an adjuvant therapy with surgical resection followed by radiotherapy. The results indicated significant improvement in the 2-year survival rate up to 26.5% compared to the radiotherapy alone [10]. Gilbert et al. 2002 studied the effect of TMZ in patients in adjuvant to radiotherapy in newly diagnosed GBM and observed a good response rate of 39% and a short median overall survival of 13.2 months [66]. Furthermore, surgical resection with radiotherapy and chemotherapy also improved the two-year survival of 26.5 percent compared to the 10.4% radiotherapy alone [10]. Mineo et al. reported that treatment with temozolomide with surgery and radiotherapy significantly improved the median survival of 19 months compared to the 16 months with other chemotherapeutic agents [67]. Later on, studies have also shown no improvement in the overall survival of the patients after treatment with the TMZ. This observation could be attributed due to the overexpression of MGMT-dependent development of resistance in patients due to negative promoter methylation status or wild-type glioma IDH expression, causing tumor relapse [60,62,63,68]. However, to overcome the limitations with TMZ alone, the patients were treated in combination with second-line chemotherapeutics against glioma. Likewise, In a pilot phase II trial, patients with grade IV malignant glioma were treated with TMZ + bevacizumab, TMZ+ sorafenib showed an overall survival of 16.3 and 12 months, respectively [69,70]. In another phase 2 open-label, multicenter clinical trial was evaluated in patients with surgical resection, followed by radiation therapy with TMZ and Bevacizumab showed complete response up to 22.5% of patients with progression-free survival and overall survival of 0.96 and 1.68 years [71]. In a single-arm phase 2 non-randomized clinical trial, the combination of Erlotinib plus Sirolimus showed median progression and overall survival of 6.9 and 33.8 weeks [72]. In phase 2 open-label interventional trials, the combination of albumin-bound rapamycin (nab-rapamycin) was evaluated with various drugs in combination, including nab-sirolimus+ temozolomide, nab-sirolimus+ bevacizumab, nab-sirolimus+ lomustine, nab-sirolimus+ marizomib, nab-sirolimus+ TMZ+ radiotherapy for the treatment of high-grade, recurrent glioma and newly diagnosed glioblastoma. Whereas, treatment with nab-rapamycin + TMZ showed better median progression-free survival and overall survival of 11.7 and 13.8 months compared to the other treatment combination [73]. Furthermore, prior treatment with mTOR inhibitor everolimus with surgery exhibited marked improvement in the progression-free

survival of 25.9 weeks compared to surgery alone [74]. Despite the conventional treatment approaches and multimodal diagnostic techniques, the conventional treatment only leads to nominal improvement in the patient's overall survival, making room for advancements in the clinical strategies to treat GBM by overcoming the existing limitations.

1.4.1. Temozolomide (TMZ): background, mechanism of action and limitations

It is a small molecule (molecular weight: 194 Da) belonging to the imidazotetrazine class, known for its potent monofunctional DNA alkylating properties for treating gliomas. TMZ was initially developed by the Aston University of Great Britain in the early 1980s, later being utilized for its antitumor activity. TMZ is marketed as Temodar® (US) and Temodal® (Europe) in the form of capsules and powder for intravenous infusion. After being launched for its anticancer properties, the drug became the biggest-selling blockbuster drug, with sales of more than \$1 billion in 2008 [58,75]. It is a prodrug that remains stable under acidic conditions allowing for oral absorption, but when it comes in contact with alkaline or physiological pH (i.e. above 7), it spontaneously undergoes breakdown into 5-(3-methyltriazene-1-yl)-imidazole-4-carboxamide (MTIC) followed by liberation of 5-aminoimidazole-4-carboxamide (AIC) and highly reactive methyldiazonium carbocation. The active moiety of carbocation acts as an electrophile and causes methylation to susceptible sites of DNA, especially at O⁶-methylguanine (O⁶-MG), N⁷-methylguanine (N⁷-MG), and N³-methyladenine (N³-MA), resulting in mismatching of base pairs and DNA double-strand break, causing cell cycle arrest and eventually cell death (Figure 1.3). TMZ is administered orally and poses an oral bioavailability of >95%, with a half-life of 1.8 h. The pharmacokinetic parameters, such as clearance and volume of distribution, also correspond to 17 L/m² and 0.4 L/kg, respectively, with C_{max} reaching within 60 min after oral administration. TMZ is also known to cross the blood-brain barrier in limited quantity as only <1% of the administered dose reaches the brain, making the dose insufficient to reach the brain. Thus, TMZ is administered at a higher dose equivalent to >150 mg/m²/day to maintain the therapeutic dose in the brain. The higher administered doses of TMZ into the systemic circulation also impart the off-target effects due to its non-specific DNA binding, especially onto the hematopoietic lineage, causing dose-dependent toxicities including grade 3 or grade 4 hematological toxic effects such as leukopenia, neutropenia, thrombocytopenia, and anemia [58].

Although TMZ has shown improvement in the treatment of glioma, still the curable therapeutic outcome is far from being achieved. It could be attributed to the limiting

physiochemical properties (short half-life, rapid degradation, and fast clearance) and the development of resistance, resulting in poor prognosis. Additionally, the development of TMZ-based resistance is mainly due to the repair mechanism pathways, namely, MGMT-dependent direct repair, mismatch repair, base excision repair, etc. MGMT (O⁶-Alkylguanine-DNA alkyltransferase) present in the cell is responsible for the repair mechanism, *viz.* removal of methyl, ethyl, hydroxyethyl, etc. groups on the DNA susceptible sites (O⁶-methylguanine (O⁶-MG), N⁷-methylguanine (N⁷-MG), and N³-methyladenine (N³-MA) [58] (Figure 1.3). MGMT is a small protein of 22KDa that is present in normal cells and protects the cells from carcinogens, but it is overexpressed in cancer cells up to 300 folds compared to the normal cells, and a positive correlation has been observed in MGMR expression, and resistance development. Similarly, the mismatch repair recognizes and corrects the mismatched bases and plays a vital role in maintaining the corrective measures during replication. Base excision repair aids in the removal and repair of damaged nucleotides, DNA strand breaks, and sites generated by TMZ and other treatment processes [76].

1.4.2. Rapamycin: background, mechanism of action, and limitations

Rapamycin (a.k.a. sirolimus) is a macrocyclic lactone molecule isolated from the bacteria *Streptomyces hygroscopicus*, with a potent multifunctional activity including antimicrobial, immunosuppressant, and antitumor activity. Rapamycin is mainly used as an immunosuppressant to block allograft rejection during transplantation [77]. It is given in combination with other agents, such as prednisone and cyclosporine, to reduce organ rejection in cardiac and renal transplants [78]. Later on, due to its common downstream pathway with cancer, the drug has been explored for its antitumor activity in various cancers, namely, cancers of glioma, breast, prostate, ovarian, skin, etc. It primarily acts by inhibiting the mammalian target of rapamycin (mTOR), which regulates protein and glucose homeostasis. mTOR is directly correlated with the activation of the PI3K/Akt downstream pathway which is particularly important for the cancer cells for their survival, replication, and angiogenesis. Once the receptor tyrosine kinase is activated by certain cytokines namely, VEGF, EGFR, PDGFR, etc, it leads to the activation of PI3 kinases, causes the production of PIP3 and other downstream effectors, resulting in phosphorylation of Akt and eventually activates the mTOR components (mTORC1, Raptor complex) [79,80]. The activation of mTOR plays a critical role in the progression and synthesis of proteins, nucleic acids, and cell cycle progression from late G1 to S phase. Rapamycin directly binds to the active site of mTOR and blocks its functions, resulting in the inhibition of protein and nucleotide synthesis, cell cycle arrest at the late G1

phase, and autophagy stimulation [81] (Figure 1.3). Similarly, several clinical trials have reported the role of autophagy and mTOR modulators in the treatment of cancers [73,82,83]. Deployment of sirolimus has provided proof-of-principle in clinical settings, however, it imparts off-target toxicities, including leucopenia, thrombocytopenia, renal, cardiac impairment, hyperlipidemia, etc, rendering the treatment with limited scope. The pharmacokinetics of rapamycin is still the limiting factor for the delivery across the tumor site with systemic bioavailability of ~14% and a half-life of 60-80 h. The distribution of rapamycin has shown significant partitioning towards the red blood cells, plasma, and lymphocytes equivalent to ~95%, 3%, and 1%, respectively, resulting in a blood-to-plasma ratio of ~35-37. The volume of distribution and clearance of the rapamycin was observed to be 12-20 L/Kg and 173 ml/h/Kg with >90% of the drug bound to the albumin protein, making it less bioavailable to the target tissue (FDA Approved Drug Products: RAPAMUNE (sirolimus) for oral use [84]. Additionally, the undergoes an extensive liver and intestinal metabolism, giving out various hydroxylated and demethylated byproducts (34-hydroxy sirolimus, 39-O-demethyl sirolimus, 12-hydroxy sirolimus, and 34-hydroxy sirolimus) with pharmacological efficacy several folds lesser than the intact molecule rapamycin [85–88]. Therefore, due to its challenging structure and physiochemical behavior of the molecule, the protection of the drug molecule and ensuring the delivery to the target site of action is need of an hour to fully harness the potential of the molecule in combating glioma.

1.4.3. TMZ and mTOR inhibitor combination to treat glioma

TMZ is considered a drug of choice for the treatment of GBM, which can cross the BBB and target the tumor tissue, causing DNA methylation and cell cycle arrest at the G2/M phase and eventually resulting in cell apoptosis and autophagy [58]. While Rapamycin demonstrates its anti-glioma action, *viz.* alteration in the common downstream pathway including PI3K/Akt/mTOR, eventually leading to inhibition of protein, nucleic acid, and other proliferative components. Thus causing cell cycle arrest at G1 phase and cell tumor cell death [81].

Both molecules, including TMZ and RAP, demonstrate the antitumor action against the GBM differently, *i.e.*, TMZ exhibits its action *viz.* DNA alkylation while RAP shows its action, *viz.* inhibition of multiple downstream proliferative pathways (PI3K/Akt/mTOR) involved in

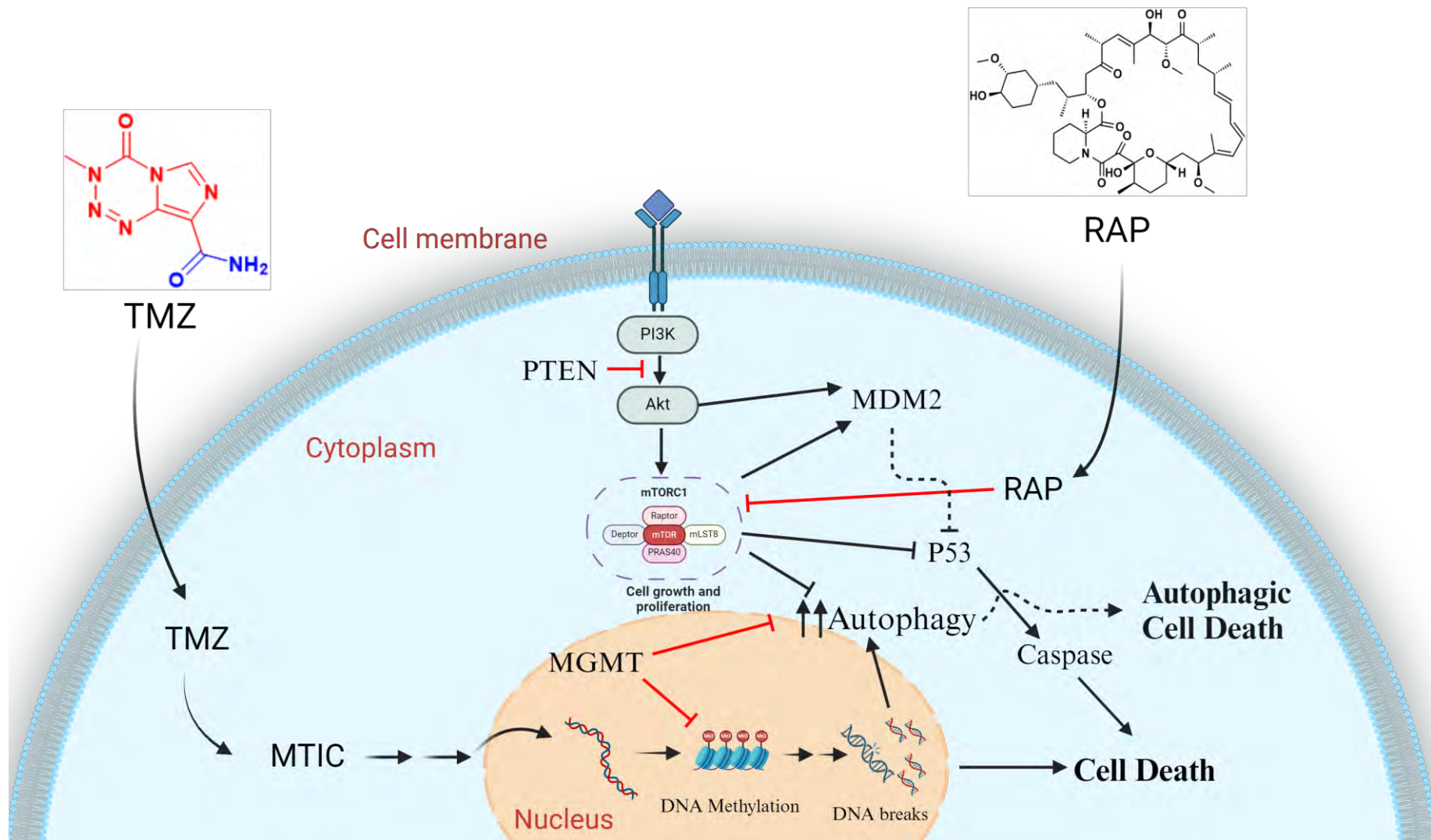


Figure 1.3. Overview of temozolomide (TMZ) and mTOR inhibitor-rapamycin (RAP) in glioma

tumor survival and growth. When administered together, both compounds work synergistically to strengthen the effectiveness of the treatment outcome, specifically by overcoming the development of resistance. Nevertheless, the TMZ and RAP combination carry ample advantages over the conventional treatment; still, the outcome of therapy is nominal. It is mainly observed due to the different physiochemical properties of the drug, including the TMZ being a hydrophilic molecule with a solubility of 5 mg/ml and high permeability. At the same time, rapamycin is considered to be highly hydrophobic with log p of >5, solubility of 0.00173 mg/ml, and less permeable across the biological membrane, making it highly challenging to cross the BBB and deliver simultaneously to the target site of action [58,89] (Figure 1.3).

Overall, the strategic deployment of the drug combination (TMZ and RAP) could be a potential approach in cancer therapeutics, particularly for GBM. However, the physiochemical constraints of these molecules hinder the utilization of their full potential. Therefore, devising an innovative delivery approach that can co-deliver TMZ and RAP could mitigate their drawbacks and play a pivotal role in unlocking the full therapeutic potential against the GBM.

1.5. Nanotechnology based delivery strategies

Nanotechnology especially nanomaterials, has shown significant advancements in the field of medicine. The concept of nanomaterial was initiated in the mid-20th century by Jatzkewitz till then major improvement has been observed in nanotechnology in terms of safety, efficacy, biocompatibility, and patient compliance for the delivery of molecules to the targeted site [90]. In the past 2 decades, the healthcare industry has shown highlighted interest in the design and development of the nanocarrier for the delivery of payloads (aka nano drugs). Owing to its nanomaterials, multiple critical attributes (such as structure, size, composition, surface charge, etc.) are involved in delivering the payload to the target site of action with minimal off-target effects. Both organic (polymeric, lipidic) and inorganic (gold, silica, metallic) materials have been used to develop the nano drugs that showed advantages, including targeted delivery, improved stability, biocompatibility, low off-target effects, biodegradability, with minimal adverse effects in a preclinical and clinical setting [58]. Numerous studies have demonstrated the usage of inorganic materials to deliver the molecules to the target site, such as mesoporous silica nanoparticles, metal-organic framework, gold nanoparticles, quantum nanodots, etc., that could benefit medical and diagnostic applications. For instance, Rathnayake et al. prepared dual-targeted mesoporous silica core encapsulating the paclitaxel and coated with liposome, showed particle size ranging from 83-138 nm and

improved *in vitro* effectiveness in cancer therapy compared to free PTX [91]. Zhang et al., co-loaded TMZ and chloroquine into the polydopamine-coated mesoporous silica nanoparticles and showed a particle size ranging from 190-200 nm, depicted improved reduction in tumor growth *viz.* autophagy and apoptosis compared to the free drug [92]. Recently, metal-organic frameworks have gained attention for their potential in the field of medicine, mainly due to their high surface area, porosity, and ease of fabrication for numerous theranostic applications. Likewise, preparation of Fucoidan-coated metal-organic frameworks coloaded with temozolomide and talazoparib, exhibiting improvement in the *in vitro* and *in vivo* tumor accumulation and reduced tumor growth in a syngeneic colorectal cancer mice model [93]. Pulvirenti et al. prepared nanometric hybrid Fe₃O₄ magnetic nanoparticles with improved TMZ loading capacity equivalent to 12 mg/g of TMZ for the antitumor activity against the A172 glioma cells [94].

Apart from inorganic material, studies have shown the use of biocompatible polyester-based polymer to deliver the TMZ for GBM. Utilizing polycarbonate/polyester polymers confers multiple benefits over conventional and inorganic material therapeutic modalities. These mainly include better biocompatibility, biodegradability, improved drug loading and encapsulation efficiencies, precise control over the drug release kinetics, and notably the tailorable properties inherent to these materials, giving a competitive edge over the other therapeutic approaches against glioma. Likewise, Lee et al. prepared PLGA-polymer-based nanoparticles loaded with TMZ using solvent evaporation and nanoprecipitation method, depicting the loading capacity ranging from 0.2 to 2% w/w [95]. Meteoglu et al. prepared PLGA-based polymeric nanoparticles co-loaded with genistein and TMZ for delivery against glioblastoma. The resulting coloaded nanoparticles showed a particle size of ~135 nm with PDI 0.139 and encapsulation efficiency of ~50% [96]. In another study, polysorbate 80-coated PLGA-based nanoparticles loaded with rapamycin were prepared for anti-glioma activity. The resulting nanoparticles were prepared using the emulsification-diffusion method, exhibiting particle size and PDI of 247 nm and 0.103 with an encapsulation efficiency of 28.5% and showed better *in vitro* cytotoxicity profile compared to the uncoated and free rapamycin alone in C6 glioma cells [97]. Similarly, Zhao et al. prepared mPEG-PLGA-based nanoparticles loaded with rapamycin for hepatic disease, exhibiting a particle size and PDI of 154 nm and 0.166 with better uptake of nanoparticles in hepatic cells [98]. Pape et al. prepared rapamycin-loaded PLGA polymer-based nanoparticles for intra-articular injection. The drug-loaded nanoparticles showed a particle size and PDI of 393 nm and 0.173, respectively, with a drug

encapsulation efficiency of ~100% at a drug loading capacity of 9.09% w/w and a process recovery yield of 61% [99].

Liposomal nanoparticles are lipid-based systems known for their structural composition, similar to the cell membrane. It comprises a lipid-bilayered structure encapsulating an aqueous core, providing a suitable environment for encapsulating a diverse range of drugs, peptides, and nucleic acids. Liposomes elicit advantages, including protection from degradation, extended circulation time, other pharmacokinetic parameters, and biocompatibility, and they also facilitate the enhanced permeability and retention effect against tumors. Likewise, Song et al. prepared liposomal preparation composed of DPPC and cholesterol loaded with TMZ for anti-glioblastoma activity. The TMZ-loaded liposomes exhibited particle size and PDI of 150 nm and 0.23, respectively, with an encapsulation efficiency of 52% at drug loading of 7.2% w/w. The TMZ-lipo showed a better pharmacokinetic profile and inhibited tumor growth than free TMZ in C6 orthotopic tumor-bearing rats. [100]. Huang et al. prepared TMZ-loaded solid lipid nanoparticles of stearic acid and lecithin using emulsification and low-temperature solidification. The TMZ-SLN nanoparticles showed particle size and zeta potential of 65.9 nm and -37.2 mV, respectively, with an encapsulation efficiency of 58.9% at drug loading of 0.94% w/w. The *in vivo* administration of TMZ-SLN showed an improved pharmacokinetic profile and TMZ accumulation in the brain compared to free TMZ [101]. Chen et al. prepared a loaded Nanostructured lipid carrier composed of 888 ATO, Cremophor ELP, and SPC, which showed a particle size of ~179 nm with an encapsulation efficiency of 83%. *In vivo* administration of TMZ-NLCs reduced the tumor growth significantly compared to the free TMZ and positive control group in U87MG solid tumors in mice [102]. Mazuryk et al. prepared rapamycin-loaded SLNs using cold high-pressure homogenization and ultrasound-assisted emulsion. The resulting nanoparticles exhibited a flat ellipsoidal structure with a hydrodynamic radius of ~46 nm and 8-9 nm thickness, which could be utilized for its *in vivo* therapeutic potential [103]. Chen et al. prepared rapamycin-loaded liposomal preparation composed of soy phosphatidylcholine:cholesterol: PEG-DSPE, showed a particle size of 100 nm and a narrow polydispersity index. The nanoparticles showed better tumor cell uptake and accumulation in tumor-bearing mice. *In vivo* administration of rapa-lipo improved tumor growth inhibition and reduction in tumor parameters compared to free rapamycin in HCT-116 xenograft tumor-bearing mice [104]. While the advancements in the delivery approaches utilizing both organic and inorganic nanomaterials have shown enhanced outcomes in disease treatment, but certain limitations still persist, constraining the treatment to a limited extent. Consequently, warranting

the design and development of alternative approaches to effectively deliver the payload to an intended site, thereby yielding a curable therapeutic outcome.

1.6. Polymer conjugates approach

Conjugation-based approach have witnessed a drastic increasing trend in the medical field for their theranostic applications. Till now, research has been carried out in the field of polymer chemistry to functionalize them as polymer-based nanomedicines that could be used clinically for the treatment of various cancers [105,106]. Synthetic polymer chemistry helps to design and develop polymers with different molecular weights and chemical compositions containing specific types of functional groups playing a vital role in the preparation of polymer conjugates such as carboxylic, amine, alcohols, to which the other bioactive molecules could be tethered to deliver it to target site of action. The conjugation of bioactive molecules (small molecules/drugs, nucleic acids, lipids, peptides, DNA, etc.) to the polymeric unit imparts numerous benefits, including, improved stability, molecule solubilization, pharmacokinetics, permeability, biocompatibility, and reduced metabolism, clearance and excretion from the body [105,107,108]. The polymer conjugates could be synthesized in various ways including, the copolymerization of bioactive functional units with the formation of polymer units or the direct attachment of the bioactive molecule to the polymer backbone in a specific stoichiometric ratio. Although the conjugation approach has shown various advantages over the conventional delivery of the molecules to the targeted site, the major challenge involved in the preparation of the polymer conjugates includes the presence of free functional groups for the site of attachment, molecular weight of the polymer, nature of the polymer, polymer stability, nature of bioactive payload, etc. furthermore, the conjugation of the bioactive molecule to the polymeric backbone renders the molecule as the new chemical entity that requires the additional studies across the preclinical and clinical setting to reach the market for their respective medical application [105].

1.6.1. History of conjugates

The realm of drug conjugates has undergone a transformative journey, expanding beyond traditional drug conjugates (D.C.s), fueled by clinical successes, technological advances, and an evolving understanding of molecular biology. Nearly sixty years ago, the conjugation of drugs to synthetic and natural macromolecules marked a pivotal moment in targeted drug delivery. Jatzkewitz pioneered this field, using a dipeptide spacer to attach mescaline to polyvinylpyrrolidone in the early fifties [109], and Ushakov's work in the sixties and seventies

synthesized water-soluble polymer conjugates, laying the foundation for subsequent evolution [110–112]. Early pioneers like Mathé et al. contributed to targeted delivery by conjugating drugs to immunoglobulins [113]. Simultaneously, DeDuve's discovery of enzyme localization in the lysosomal compartment underscored the importance of lysosomotropic design polymer–drug conjugates [114]. Ringsdorf's concept of using polymers as targetable drug carriers added another dimension to drug conjugation, detailing the polymer backbone on which the bioactive molecule, spacer, and other molecules could be attached covalently to yield the polymer–drug conjugate [115]. This journey continued with detailed studies on the biocompatibility of soluble and crosslinked hydrophilic polymers, leading to the application of hydrogels in clinical settings and the selection of HPMA polymers and copolymers as biocompatible drug carriers [116–122]. Comprehensive studies on enzyme-catalyzed cleavage of oligopeptide sequences in hybrid HPMA copolymers resulted in choosing the GFLG oligopeptide spacer as a drug attachment/release site, widely adopted in numerous studies worldwide. HPMA copolymer-based macromolecular therapeutics entered clinical trials for therapeutic validation in the early 1990s, including HPMA copolymer–doxorubicin (DOX), HPMA copolymer–DOX–galactosamine, HPMA copolymer–camptothecin, HPMA copolymer–paclitaxel, and HPMA copolymer–platinates [122–126]. These trials demonstrated the advantages of binding low molecular weight drugs to polymer-carriers, the biocompatibility of conjugates, and decreased side effects, resulting in a higher maximum tolerated dose (MTD) of polymer conjugates compared to free drugs. Thereon, several modifications have been made in the field of polymer and conjugation chemistry to yield polymer therapeutics such as polymer–drug conjugate, polymer–peptide conjugate, polymer–oligonucleotide conjugate, polymer lipid conjugate, polymer DNA conjugate, etc. However, during the design of polymer conjugates their biocompatibility, stability, and efficacy must be considered to deliver the payload to the targeted site of action with minimal adverse effects

1.6.2. Polymer conjugates of Temozolomide

Polymer drug conjugates have acquired special attention in the delivery of both small molecules as well as macromolecules, as they have demonstrated improved safety profile and desired clinical outcome [127–129]. In the 1950s, the synthesis of the first polymer–drug conjugate was reported by von Horst Jatzkewitz using a dipeptide linker of leucine and glycine [128]. Thereafter, the concept of polymer–drug conjugates was detailed by Helmut Ringsdorf in the mid-1970s, characterized by the presence of polymeric backbone to which low molecular bioactive molecule (for bioactivity), solubilizer (for imparting hydrophilicity), and a targeting

moiety (for biological targeting) are covalently attached through a bioresponsive linker. The concept of the ideal Ringsdorf model of polymeric therapeutics provides various chemical modalities that can be modified, including the polymeric backbone, bioresponsive spacer, and functionality of a drug molecule for the desired application [127,130,131]. The polymeric backbone provides the platform to the nanomedicine, which can be modified with free and selective end group functionalities, while the presence of end group functionalities provides a basic ground for the attachment of spacers and bioactive molecules. Another area of interest is the attachment of the bioactive molecule *via* spacer to the polymeric backbone itself. The nature of free end group functionalities of polymeric backbone, bioactive molecule and spacer are of primary interest in the designing of such system. Certain functionalities including amines, carboxylic acids, hydrazone, acyl, alcohols, and thiols, provide better support in the conjugation process, resulting in a stimuli-based system responsive to pH, enzyme, light, external field, etc. [132,133]. On the other hand, some molecules do not possess such free end group functionalities, in such cases, the attachment to the backbone is a difficult task. For such molecules, initially, free functionalities are generated which were subsequently conjugated to the polymeric backbone using a specialized linker, yielding the polymeric prodrug. The third area of interest is the presence of ligand or a transport system that directs the movement of the conjugate to the specific targeted site of action with minimal non-specific binding. Specific targeting can be achieved by the presence of the homing (receptor-active) components including enzymes, hormones, peptides, immunoglobulins, etc., resulting in a tissue-specific targeting with minimal toxicity [134]. Since then, multiple works based on Ringsdorf model have been carried out by various researchers in the development process, eliciting advancements in the translational process. For instance, in 1990, Adagen, the first clinical approval of a polymer protein conjugate was acquired for the enzyme replacement therapy for adenosine deaminase deficiency (ADA) [128]. Several other polymeric prodrugs including NKTR-118, CT-2106, AP5346, AP5280, Xyotax, IT-101, PK1, PK2, etc, are in the clinical development stage and require detailed clinical evaluation [134,135]. The hydrophilic drugs are hard to load in the hydrophobic core of the nanocarriers; therefore, the concept of polymer drug-conjugate came in the scenario for such molecules, wherein the drug is conjugated in the end or grafted on the backbone of the polymer with a bioresponsive spacer. Various reported polymer drug conjugates are shown in Table 1.1.

The delivery of TMZ payload by encapsulation techniques has demonstrated significantly lower carrying capacity, thus requiring a significantly large amount of carrier with

the drug to achieve the desired effect. For instance, PLGA based nanoparticles encapsulating TMZ using solvent evaporation technique exhibited drug load ranging 0.4 to 4.4% w/w with maximum encapsulation efficiency up to 27%, along with the burst release in the first 6 h [136]. Lee et al. prepared folate-targeted PEG-PLGA nanoparticles using solvent evaporation, and nanoprecipitation method showed drug loading up to 2% w/w with encapsulation efficiency ranging 2.6 to 12.6% [95]. Dilnawaz et al. prepared TMZ and curcumin-loaded magnetic nanoparticles delivery system. Drugs were allowed to partition into the glyceryl monooleate shells surrounding the magnetic nanoparticles, exhibiting encapsulation efficiency of 75% and 30% at drug loading less than 5% for curcumin and TMZ, respectively [137]. On the other hand, the polymer-drug conjugates (PDC) have shown significant improvement in drug payload with controlled physico-biochemical properties, not only ensuring the stability, biocompatibility, non-toxic behavior but also ensuring the targeted delivery and release to a specific site [128,133,138]. The polymer-TMZ conjugate has exhibited numerous benefits, including improvement in TMZ stability, efficacy, improved pharmacokinetics, systemic circulation half-life, and reduced toxicity. Likewise, Patil et al. synthesized multifunctional targetable conjugates of TMZ with poly(β -L-malic acid) polymeric backbone, containing targeting monoclonal transferrin receptor antibody (TfR), trileucine (LLL) for pH-dependent endosomal escape, Alexa fluor 680 for identification, and PEG for protection. The water-soluble multifunctional TMZ nanoconjugates exhibited hydrodynamic diameter ranging from 6.5 to 14.8 nm with zeta potential ranging -6.3 to -17.7 mV. Further, the nanoconjugates had significant improvement in TMZ payload up to 30% w/w in the form of TMZ hydrazide, demonstrating improved stability by 3-4 times and uptake in glioma cells, especially in the presence of TfR targeted conjugate [139]. In another study, Fang et al. prepared chlorotoxin-targeted TMZ conjugated chitosan-based delivery system (NP-TMZ-CTX), exhibiting stable and significantly higher TMZ loading with an average particle size of less than 100 nm. The actively functionalized TMZ-conjugated nanosystem was able to target and penetrate 2-6 folds efficiently and reduce the IC₅₀ by 50-90%, compared to non-targeted nanoparticles against GBM cells [140]. Emrick group developed a series of TMZ conjugated poly(2-methacryloyloxyethyl phosphorylcholine) (polyMPC-TMZ) using controlled free-radical copolymerization of MPC and TMZ-substituted methacrylate. The resulting conjugate showed TMZ loading more than 50 mol%, which may require tissue specific biorecognition using targeting molecules like peptides, targeting ligands, and antibodies to facilitate BBB trans permeability [141]. Afterward, the polyMPC-TMZ was prepared *via* RAFT polymerization and used to prepare the nanoformulation with a size ranging from 7 to 40 nm that enhanced the

Table 1.1. Polymeric conjugates of TMZ

Polymer Conjugate	Linker	IC ₅₀	Formulation	Outcomes	Ref.
Poly MPC polymer	Methacrylate linker	396-1282 μ M 1477-9260 μ M	Micelles	1) Enhanced drug stability 2) Half-life improved 2-19 times from free TMZ	[142]
Poly(β -L-malic acid)	Hydrazine linker	-	Nanoconjugate	1) Half-life improved from 1.8h to 5-7 hr 2) Cell viability reduced	[139]
Poly(2-ethyl-2-oxazoline)	Ester	PEtOz ₄₇ -TMZ - 22.43 μ g/ml PEG ₁₁₃ -TMZ- 26.08 μ g/ml	Nano conjugation micelles	1) Enhanced the stability of TMZ 2) Prolonged the circulation time <i>in vivo</i> 3) Increased the TMZ accumulation in glioblastoma	
Conjugated Gold Nanoparticles	Ester	5.74 \pm 0.02 μ mol/L 64.06 \pm 0.16 μ mol/L	Gold nano formulation	1) IC ₅₀ of anti-EphA3-TMZ@GNPs (64.06 \pm 0.16 μ M) was 18.5-fold 2) Down-modulated expression of O6 -methylguanine-DNA methyltransferase 3) Increased chemosensitivity of T98G to TMZ 4) Prolonged the median survival time to 42 days and increased tumor-cell apoptosis	[143]
PEtOz-TMZ polymer micelles	Ester	22.43 μ g/ml for PEtOz ₄₇ -TMZ 26.08 μ g/ml for PEG ₁₁₃ -TMZ	Micelles	1) Reduces TMZ degradation rate with half-life upto 13.7h compared to free TMZ with t _{1/2} of 1.1h in plasma 2) Median survival of polymer-drug conjugates significantly improved upto 45 days 3) no significant morphological change or tissue damage in toxicity analysis	[144]

half-life of TMZ by 19 folds compared to free TMZ [142]. The attachment on drug conjugates with targeting ligand has a significant role in the delivery of TMZ to the specific site of action with minimum adverse effects *in vivo*. Likewise, Wang et. al. fabricated anti-ephrin type-A receptor functionalized TMZ-PEG-Gold nanoparticle conjugates, wherein, TMZ was conjugated to PEG thiol, which was further reacted with gold nanoparticles to yield TMZ-PEG-GNPs. The prepared anti-EphA3-TMZ-PEG-GNPs exhibited loading efficiency up to 7% w/w with an average particle size of 46.12 nm. The results showed enhanced cellular uptake, apoptosis, and reduced IC₅₀ by 18.5 folds compared to free TMZ in glioma cell lines. Furthermore, *in vivo* administration of targeted nanoparticles improved the median survival time to 42 days, found to be safe and biocompatible as compared to TMZ treatment [143]. Recently Xu et. al. synthesized poly(2-ethyl-2-oxazoline) (PEtOz)-TMZ conjugate using ester linker, with the TMZ loading up to 4% w/w of the conjugate. The nanoconjugates yielded micelles, exhibiting a significant improvement in the stability by 5.5 folds up to 13.8 h compared to free TMZ. *In vivo* systemic administration resulted in reduction in the degradation rate of TMZ and extended the systemic half-life from 1.1 h to 13.7 h in plasma with improvement in survival time to 45 days compared to 26 days in the free TMZ treatment group in the C6 orthotopic xenograft mouse model [144].

1.7. Hybrid carrier system for the combined delivery

The era of the development of nanoparticles has shown improvement in the delivery perspective of the molecule to the specific site of action, eliciting the desired therapeutic outcome. The organic and inorganic delivery nanomaterials must be designed to elicit biocompatibility, stability, permeability, reduced toxicity, clearance, metabolism, RES absorption, and improved target-specific delivery with better pharmacokinetics and pharmacodynamic behavior [145–147]. The polymer-hybrid (polymer-polymer, polymer-lipid, polymer-inorganic material) system shows the combined advantages of including components with beneficial desired outcomes with tailor-made properties over the individual components. One of the key advantages of hybrid carrier systems is their ability to accommodate a wide range of therapeutic agents, encompassing small molecule, proteins, nucleic acid, and other compounds, tailored for many diseases and theranostic applications. Hybrid nanocarriers can be engineered to respond to stimuli such as pH, redox, temperature, or enzymatic activity to acquire spatiotemporal control over the therapeutic delivery with minimal off-target effects. Likewise, lipid-polymer hybrid nanoparticles have aided in improving the delivery. For instance, Jain et al. prepared lipid-polymeric hybrid nanoparticles coloaded with MTX and

beta-carotene, exhibited drug loading capacity of 8.5% and 2.85% w/w, resulting in better cellular internalization, better *in vivo* antitumor efficacy, reduced toxicity, and better biocompatibility [148]. Khan et al. prepared curcumin and cisplatin-loaded lipid-polymer hybrid nanoparticles composed of lipoid S75 and chitosan exhibiting particle size of 225 nm with an encapsulation efficiency of >80%, resulting in improved uptake efficiency and chemosensitization of 3D ovarian cancer spheroid model [148]. Zeng et al. prepared lipid-polymer hybrid nanoparticles composed of DSPE-PEG and cholic acid functionalized PLA copolymer coloaded with PTX and celecoxib for overcoming drug resistance in breast cancer. The LPHNPs showed particle size and PDI of 121 nm and 0.12, respectively, with an encapsulation efficiency of ~80% for both PTX and CXB at a drug loading capacity of 7.1 and 2.4% w/w, respectively. The hybrid nanoparticles showed sustained drug release kinetics, effectively reducing cell growth in both resistance and non-resistant cell lines [148]. Tran et al. co-loaded DTX and vorinostat into the lipid polymer hybrid nanoparticles composed of Capryol 90, TPGS, DDAB lipid, and PEG-b-PAsp polymer with particle size and PDI of 232 nm and 0.297 with encapsulation efficiency of 73.7 and 75.8 for vorinostat and DTX, respectively. The LPHNPs showed sustained and pH-dependent release kinetics and were effectively taken up by the cells, resulting in improved apoptosis and tumor (SCC-7, MCF-7, and MDA-MB-231) growth inhibition [149].

1.8. Actively targeted hybrid nanocarrier delivery system

The hybrid nanocarrier-based drug delivery system is utilized to deliver and improve the physiochemical properties, pharmacokinetics, and pharmacodynamics of the drug. The utilization of the polymer hybrid complexes, combining polycarbonate and polyester block polymer, signifies a significant improvement in addressing the challenges related to delivering a wide array of molecules with diverse physiochemical properties. The innovative polymer hybrid approach enabled the delivery of hydrophilic/hydrophobic moieties with varying ionization coefficients while ensuring the stability of the molecule. Especially, it enhances the drug loading and encapsulation capacity, protection against degradation, controlled drug release kinetics, and facilitating surface functionalization with the targeting ligands. However, the unspecificity of the nanomaterial system makes it much more difficult to deliver the therapeutic concentration of payload to the site of action with minimal toxicity to the non-cancerous cells. Utilizing the ligand-based targeted delivery approach to the cancer cells has drastically reduced the side effects of the treatment compared to conventional chemotherapy [150,151]. Over the past three decades, the ligand-based targeted strategy has shown marked

improvement in the field of medicine for their biomedical applications (for diagnosis and treatment). Nanoparticles could be made active targeted by functionalization with specific ligands such as peptides, antibodies, DNA/RNA fragments, aptamers, carbohydrates, and other small molecules, making the nanoparticles that can specifically recognize and bind to the target site specifically to the cancer cells [151,152]. Several peptides, such as CooP, Angiopep-2, RGD motif, tLyP-1, C6, UNO, and TAT, have been explored to specifically target the glioma, facilitating better cellular internalization *viz.* receptor-mediated endocytosis. Thus, enabling tumor-specific targeting and better therapeutic outcomes in managing gliomas and other malignancies. [153]. Amongst, RGD peptide motif have exhibited higher binding affinity towards integrin $\alpha\beta3$ and $\alpha\beta5$ receptors that are over-expressive in components of BBB/BBTB in many tumors and other components of tumor microenvironment, including glioblastoma, melanoma, breast, prostate, and ovarian cancer. Likewise, Zhang et al. prepared RGD-peptide targeted polymer lipidic nanoparticles coloaded with DOX and MMC to treat lung metastases of TNBC in mice. The utilization of tumor-homing peptide RGD demonstrated the highest distribution and accumulation in tumors and low toxicity to the liver and heart in the murine lung metastatic model of MDA-MB231 breast cancer. *In vivo* administration of RGD-targeted LPHNPs reduced the tumor burden and progression of metastasis, indicating the role of RGD peptide in the lung metastasis mouse model of TNBC [154]. Yang et al. fabricated cRGD-modified LPHNPs as promising candidates to deliver the therapeutic payload to human breast cancer. The cRGD-targeted hybrid nanoparticles have shown higher drug loading capacity and improved the cell endocytic capability in MDA-MB-435s and MCF-7 breast cancer cells [155]. Gao et al. prepared tumor homing iRGD peptide surface modified on LPHNPs, exhibiting better cellular accumulation and *in vivo* tumor growth inhibition compared to non-targeted counterpart in 4T1- breast-tumor bearing mouse model [156]. Belhadj at al, prepared cRGD and p-hydroxybenzoic acid (pHA) dual functionalized liposomal preparation encapsulating DOX for the treatment of glioblastoma. The utilization of cRGD peptide could targeted integrin receptors on BBTB and glioma cells, while pHA could target dopamine receptor on the BBB, facilitating an effective uptake and delivery of the payload to the site of action. *In vivo* administration of dual targeted liposomal preparation demonstrated improvement in the accumulation in the tumor and median survival time upto 2.3 folds compared to the non-targeted counterpart in U87 cells bearing tumor in nude mice [157]. similarly, cRGD-targeted polymeric micelles demonstrated rapid accumulation and improved permeation into the tumor parenchyma compared to the non-targeted polymeric micelles in U87MG bearing orthotropic BALB/c nude mice model [158]. Multiple reports suggest the

active targeting strategy using the cell penetrating peptides have shown substantial improvement in the delivery of the payload to the intended site of action *viz.* bypassing the BBB/BBTB. Such advanced approach holds a promise as a potential candidate in combating glioma.

1.9. Outline of current research work

Temozolomide and Rapamycin, being different in physiochemical properties, pose challenges in their simultaneous delivery to the brain for their effective synergistic therapeutic potential. To achieve its optimal therapeutic synergism, the current study aims to design, develop, and evaluate actively targeted nanocarrier systems that can effectively deliver rapamycin and temozolomide for treating GBM. The research work initiated with the synthesis and screening of polycarbonate-based polymer-drug conjugate of temozolomide and further coupled with mPEG-PLA copolymer in a fixed proportion to yield polymer Hybrid TMZ nanoconjugates. Subsequently, cRGD peptide-functionalized polymer (cRGD-PEG-PLA) was coupled with the Hybrid TMZ nanoconjugates and co-loaded with the drug mTOR inhibitor rapamycin to achieve active targeting. Such a novel delivery system supports the nanodrugs in transversing across the BBB/BBTB and reaches the intended site of action, thereby demonstrating the synergistic potential of TMZ and rapamycin in combating glioma.

The proposed cRGD peptide-functionalized hybrid nanoconjugate delivery system not only delivers multiple payloads at the same time but offers several other advantages, including improved stability, physiochemical properties of the TMZ, better intracellular fate of the nanocarrier and its payload system, and the presence of PEG chains to protect the nanocarrier from RES system. Additionally, the tumor homing capabilities of cRGD peptide enhance the permeability towards the tumor cells, improving the site and target-specific delivery of the payload towards the cancer cells.

1.10. Objectives of research work

The following objectives have been designed to achieve the aim of the research work. The objectives are further divided into various chapters, focussing on the designated purpose of the work.

Objective 1. Analytical and bioanalytical method development and validation of rapamycin, temozolomide, temozolomide acid, temozolomide hydrazide, and 5-aminoimidazole-4-carboxamide in biological matrix of rat

Objective 2. Design, synthesis, and characterization of polycarbonate-based polymeric conjugates of temozolomide

Objective 3. Formulation development, *in vitro* and *in vivo* evaluation of hybrid nanoconjugates of temozolomide in C6 cells-induced syngeneic orthotopic glioma model in rats

Objective 4. Development and evaluation of cRGD peptide-functionalized hybrid nanoconjugates of temozolomide coloaded with rapamycin in C6 cells-induced syngeneic orthotopic glioma model in rats

1.11. References

- [1] Bray F, Ferlay J, Soerjomataram I, Siegel RL, Torre LA, Jemal A. Global cancer statistics 2018: GLOBOCAN estimates of incidence and mortality worldwide for 36 cancers in 185 countries. *CA Cancer J Clin* 2018;68:394–424. <https://doi.org/https://doi.org/10.3322/caac.21492>.
- [2] WHO-IARC. All Cancers: Globocan 2018. 2018.
- [3] Tamimi AF, Juweid M. Epidemiology and Outcome of Glioblastoma. In: De Vleeschouwer S, editor., Brisbane (AU): 2017. <https://doi.org/10.15586/codon.glioblastoma.2017.ch8>.
- [4] Ostrom QT, Cioffi G, Gittleman H, Patil N, Waite K, Kruchko C, et al. CBTRUS Statistical Report: Primary Brain and Other Central Nervous System Tumors Diagnosed in the United States in 2012–2016. *Neuro Oncol* 2019;21:v1–100. <https://doi.org/10.1093/neuonc/noz150>.
- [5] Sasmita AO, Wong YP, Ling APK. Biomarkers and therapeutic advances in glioblastoma multiforme. *Asia Pac J Clin Oncol* 2018;14:40–51. <https://doi.org/https://doi.org/10.1111/ajco.12756>.
- [6] Nachbichler SB, Schupp G, Ballhausen H, Niyazi M, Belka C. Temozolomide during radiotherapy of glioblastoma multiforme. *Strahlentherapie Und Onkol* 2017;193:890–6. <https://doi.org/10.1007/s00066-017-1110-4>.
- [7] Carlsson SK, Brothers SP, Wahlestedt C. Emerging treatment strategies for glioblastoma multiforme. *EMBO Mol Med* 2014;6:1359–70. <https://doi.org/https://doi.org/10.15252/emmm.201302627>.
- [8] Meng J, Agrahari V, Youm I. Advances in Targeted Drug Delivery Approaches for the Central Nervous System Tumors: The Inspiration of Nanobiotechnology. *J Neuroimmune Pharmacol* 2017;12:84–98. <https://doi.org/10.1007/s11481-016-9698-1>.
- [9] Sharma S, Italiya K, Mittal A, Chitkara D. New strategies for cancer management: how can temozolomide carrier modifications improve its delivery? *Ther Deliv* 2017;8:475–7.
- [10] Stupp R, Mason WP, van den Bent MJ, Weller M, Fisher B, Taphoorn MJB, et al. Radiotherapy plus Concomitant and Adjuvant Temozolomide for Glioblastoma. *N Engl J Med* 2005;352:987–96. <https://doi.org/10.1056/NEJMoa043330>.
- [11] Lee SY. Temozolomide resistance in glioblastoma multiforme. *Genes Dis* 2016;3:198–210.
- [12] Chen X, Zhang M, Gan H, Wang H, Lee J-H, Fang D, et al. A novel enhancer regulates MGMT expression and promotes temozolomide resistance in glioblastoma. *Nat Commun* 2018;9:2949.
- [13] Hanif F, Muzaffar K, Perveen K, Malhi SM, Simjee SU. Glioblastoma Multiforme: A Review of its Epidemiology and Pathogenesis through Clinical Presentation and Treatment. *Asian Pac J Cancer Prev* 2017;18:3–9. <https://doi.org/10.22034/APJCP.2017.18.1.3>.

- [14] Thakkar JP, Dolecek TA, Horbinski C, Ostrom QT, Lightner DD, Barnholtz-Sloan JS, et al. Epidemiologic and Molecular Prognostic Review of Glioblastoma. *Cancer Epidemiol Biomarkers & Prev* 2014;23:1985 LP – 1996. <https://doi.org/10.1158/1055-9965.EPI-14-0275>.
- [15] Urbańska K, Sokołowska J, Szmidt M, Sysa P. Glioblastoma multiforme - an overview. *Contemp Oncol (Poznan, Poland)* 2014;18:307–12. <https://doi.org/10.5114/wo.2014.40559>.
- [16] Tan AC, Ashley DM, López GY, Malinzak M, Friedman HS, Khasraw M. Management of glioblastoma: State of the art and future directions. *CA Cancer J Clin* 2020;70:299–312. <https://doi.org/https://doi.org/10.3322/caac.21613>.
- [17] Batash R, Asna N, Schaffer P, Francis N, Schaffer M. Glioblastoma Multiforme, Diagnosis and Treatment; Recent Literature Review. *Curr Med Chem* 2017;24:3002–9. <https://doi.org/http://dx.doi.org/10.2174/0929867324666170516123206>.
- [18] Mohammadi E, Ghasemi E, Azadnajafabad S, Rezaei N, Saeedi Moghaddam S, Ebrahimi Meimand S, et al. A global, regional, and national survey on burden and Quality of Care Index (QCI) of brain and other central nervous system cancers; global burden of disease systematic analysis 1990-2017. *PLoS One* 2021;16:e0247120.
- [19] Beghi E, Giussani G, Nichols E, Abd-Allah F, Abdela J, Abdelalim A, et al. Global, regional, and national burden of epilepsy, 1990–2016: a systematic analysis for the Global Burden of Disease Study 2016. *Lancet Neurol* 2019;18:357–75. [https://doi.org/https://doi.org/10.1016/S1474-4422\(18\)30454-X](https://doi.org/https://doi.org/10.1016/S1474-4422(18)30454-X).
- [20] Globocan, International Agency for Research on cancer W. Brain, central nervous system. 2020.
- [21] Ostrom QT, Cioffi G, Waite K, Kruchko C, Barnholtz-Sloan JS. CBTRUS Statistical Report: Primary Brain and Other Central Nervous System Tumors Diagnosed in the United States in 2014–2018. *Neuro Oncol* 2021;23:iii1–105. <https://doi.org/10.1093/neuonc/noab200>.
- [22] Miller KD, Ostrom QT, Kruchko C, Patil N, Tihan T, Cioffi G, et al. Brain and other central nervous system tumor statistics, 2021. *CA Cancer J Clin* 2021;71:381–406. <https://doi.org/https://doi.org/10.3322/caac.21693>.
- [23] Singh S, Deora H, Neyaz A, Das KK, Mehrotra A, Srivastava AK, et al. Trends in clinico-epidemiology profile of surgically operated glioma patients in a tertiary care center over 12 years—through the looking glass! *Egypt J Neurosurg* 2021;36:32. <https://doi.org/10.1186/s41984-021-00118-w>.
- [24] Salvati M, Frati A, Russo N, Caroli E, Polli FM, Minniti G, et al. Radiation-induced gliomas: report of 10 cases and review of the literature. *Surg Neurol* 2003;60:60–7. [https://doi.org/https://doi.org/10.1016/S0090-3019\(03\)00137-X](https://doi.org/https://doi.org/10.1016/S0090-3019(03)00137-X).
- [25] Relling M V, Rubnitz JE, Rivera GK, Boyett JM, Hancock ML, Felix CA, et al. High incidence of secondary brain tumours after radiotherapy and antimetabolites. *Lancet* 1999;354:34–9. [https://doi.org/https://doi.org/10.1016/S0140-6736\(98\)11079-6](https://doi.org/https://doi.org/10.1016/S0140-6736(98)11079-6).
- [26] Wingren C, James P, Borrebaeck CAK. Strategy for surveying the proteome using

- affinity proteomics and mass spectrometry. *Proteomics* 2009;9:1511–7. <https://doi.org/https://doi.org/10.1002/pmic.200800802>.
- [27] Adamson C, Kanu OO, Mehta AI, Di C, Lin N, Mattox AK, et al. Glioblastoma multiforme: a review of where we have been and where we are going. *Expert Opin Investig Drugs* 2009;18:1061–83. <https://doi.org/10.1517/13543780903052764>.
- [28] Omuro A, DeAngelis LM. Glioblastoma and Other Malignant Gliomas: A Clinical Review. *JAMA* 2013;310:1842–50. <https://doi.org/10.1001/jama.2013.280319>.
- [29] Schwartzbaum JA, Fisher JL, Aldape KD, Wrensch M. Epidemiology and molecular pathology of glioma. *Nat Clin Pract Neurol* 2006;2:494–503. <https://doi.org/10.1038/ncpneuro0289>.
- [30] HAN Z, DU Y, QI H, YIN W. Post-Traumatic Malignant Glioma in a Pregnant Woman: Case Report and Review of the Literature. *Neurol Med Chir (Tokyo)* 2013;53:630–4. <https://doi.org/10.2176/nmc.cr2013-0029>.
- [31] Kofman A, Marcinkiewicz L, Dupart E, Lyshchev A, Martynov B, Ryndin A, et al. The roles of viruses in brain tumor initiation and oncomodulation. *J Neurooncol* 2011;105:451–66. <https://doi.org/10.1007/s11060-011-0658-6>.
- [32] Chakrabarti I, Cockburn M, Cozen W, Wang Y-P, Preston-Martin S. A population-based description of glioblastoma multiforme in Los Angeles County, 1974–1999. *Cancer* 2005;104:2798–806. <https://doi.org/https://doi.org/10.1002/cncr.21539>.
- [33] Nakada M, Kita D, Watanabe T, Hayashi Y, Teng L, Pyko I V, et al. Aberrant Signaling Pathways in Glioma. *Cancers* 2011;3. <https://doi.org/10.3390/cancers3033242>.
- [34] Hanif F, Muzaffar K. kakhkashan Perveen, S. Malhi, and S. Simjee, “Glioblastoma Multiforme: A Review of its Epidemiology and Pathogenesis through Clinical Presentation and Treatment,.” *Asian Pac J Cancer Prev* 2017;18.
- [35] Sharma HS, Muresanu DF, Castellani RJ, Nozari A, Lafuente JV, Tian ZR, et al. Chapter One - Pathophysiology of blood-brain barrier in brain tumor. Novel therapeutic advances using nanomedicine. In: Bryukhovetskiy I, Sharma A, Zhang Z, Sharma HSBT-IR of N, editors. *Nov. Ther. Adv. Glioblastoma*, vol. 151, Academic Press; 2020, p. 1–66. <https://doi.org/https://doi.org/10.1016/bs.irm.2020.03.001>.
- [36] Ma Q, Schlegel F, Bachmann SB, Schneider H, Decker Y, Rudin M, et al. Lymphatic outflow of cerebrospinal fluid is reduced in glioma. *Sci Rep* 2019;9:14815. <https://doi.org/10.1038/s41598-019-51373-9>.
- [37] Yeini E, Ofek P, Albeck N, Rodriguez Ajamil D, Neufeld L, Eldar-Boock A, et al. Targeting Glioblastoma: Advances in Drug Delivery and Novel Therapeutic Approaches. *Adv Ther* 2021;4:2000124. <https://doi.org/https://doi.org/10.1002/adtp.202000124>.
- [38] Tso C-L, Freije WA, Day A, Chen Z, Merriman B, Perlina A, et al. Distinct Transcription Profiles of Primary and Secondary Glioblastoma Subgroups. *Cancer Res* 2006;66:159 LP – 167. <https://doi.org/10.1158/0008-5472.CAN-05-0077>.
- [39] Ohgaki H, Dessen P, Jourde B, Horstmann S, Nishikawa T, Di Patre P-L, et al. Genetic Pathways to Glioblastoma. *Cancer Res* 2004;64:6892 LP – 6899.

- <https://doi.org/10.1158/0008-5472.CAN-04-1337>.
- [40] C. Papadopoulos D. C. Davies, B. A. Bell, M. SS. Emerging molecular mechanisms of brain tumour oedema. *Br J Neurosurg* 2001;15:101–8. <https://doi.org/10.1080/02688690120036775>.
- [41] Ang SYL, Lee L, See AAQ, Ang TY, Ang BT, King NKK. Incidence of biomarkers in high-grade gliomas and their impact on survival in a diverse SouthEast Asian cohort - a population-based study. *BMC Cancer* 2020;20:79. <https://doi.org/10.1186/s12885-020-6536-x>.
- [42] Gladson CL, Prayson RA, Liu WM. The Pathobiology of Glioma Tumors. *Annu Rev Pathol Mech Dis* 2010;5:33–50. <https://doi.org/10.1146/annurev-pathol-121808-102109>.
- [43] Sweeney MD, Zhao Z, Montagne A, Nelson AR, Zlokovic B V. Blood-brain barrier: from physiology to disease and back. *Physiol Rev* 2018.
- [44] Rhea EM, Banks WA. Role of the blood-brain barrier in central nervous system insulin resistance. *Front Neurosci* 2019;13:457034.
- [45] Abbott NJ, Patabendige AAK, Dolman DEM, Yusof SR, Begley DJ. Structure and function of the blood–brain barrier. *Neurobiol Dis* 2010;37:13–25. <https://doi.org/https://doi.org/10.1016/j.nbd.2009.07.030>.
- [46] Warren KE. Beyond the blood: brain barrier: the importance of central nervous system (CNS) pharmacokinetics for the treatment of CNS tumors, including diffuse intrinsic pontine glioma. *Front Oncol* 2018;8:239.
- [47] Abbott NJ. Dynamics of CNS Barriers: Evolution, Differentiation, and Modulation. *Cell Mol Neurobiol* 2005;25:5–23. <https://doi.org/10.1007/s10571-004-1374-y>.
- [48] Ballabh P, Braun A, Nedergaard M. The blood–brain barrier: an overview: Structure, regulation, and clinical implications. *Neurobiol Dis* 2004;16:1–13. <https://doi.org/https://doi.org/10.1016/j.nbd.2003.12.016>.
- [49] Van Itallie CM, Anderson JM. Claudins and epithelial paracellular transport. *Annu Rev Physiol* 2006;68:403–29. <https://doi.org/10.1146/annurev.physiol.68.040104.131404>.
- [50] Van Itallie CM, Holmes J, Bridges A, Gookin JL, Coccaro MR, Proctor W, et al. The density of small tight junction pores varies among cell types and is increased by expression of claudin-2. *J Cell Sci* 2008;121:298–305. <https://doi.org/10.1242/jcs.021485>.
- [51] Rascher G, Fischmann A, Kröger S, Duffner F, Grote E-H, Wolburg H. Extracellular matrix and the blood-brain barrier in glioblastoma multiforme: spatial segregation of tenascin and agrin. *Acta Neuropathol* 2002;104:85–91. <https://doi.org/10.1007/s00401-002-0524-x>.
- [52] Arvanitis CD, Ferraro GB, Jain RK. The blood–brain barrier and blood–tumour barrier in brain tumours and metastases. *Nat Rev Cancer* 2020;20:26–41. <https://doi.org/10.1038/s41568-019-0205-x>.
- [53] Wang Y, Zhang F, Xiong N, Xu H, Chai S, Wang H, et al. Remodelling and Treatment

- of the Blood-Brain Barrier in Glioma. *Cancer Manag Res* 2021;13:4217–32. <https://doi.org/10.2147/CMAR.S288720>.
- [54] Schneider SW, Ludwig T, Tatenhorst L, Braune S, Oberleithner H, Senner V, et al. Glioblastoma cells release factors that disrupt blood-brain barrier features. *Acta Neuropathol* 2004;107:272–6. <https://doi.org/10.1007/s00401-003-0810-2>.
- [55] Wolburg H, Noell S, Fallier-Becker P, Mack AF, Wolburg-Buchholz K. The disturbed blood–brain barrier in human glioblastoma. *Mol Aspects Med* 2012;33:579–89. <https://doi.org/https://doi.org/10.1016/j.mam.2012.02.003>.
- [56] Wang D, Wang C, Wang L, Chen Y. A comprehensive review in improving delivery of small-molecule chemotherapeutic agents overcoming the blood-brain/brain tumor barriers for glioblastoma treatment. *Drug Deliv* 2019;26:551–65. <https://doi.org/10.1080/10717544.2019.1616235>.
- [57] Dréan A, Goldwirt L, Verreault M, Canney M, Schmitt C, Guehenec J, et al. Blood-brain barrier, cytotoxic chemotherapies and glioblastoma. *Expert Rev Neurother* 2016;16:1285–300. <https://doi.org/10.1080/14737175.2016.1202761>.
- [58] Jatyan R, Singh P, Sahel DK, Karthik YG, Mittal A, Chitkara D. Polymeric and small molecule-conjugates of temozolomide as improved therapeutic agents for glioblastoma multiforme. *J Control Release* 2022;350:494–513. <https://doi.org/https://doi.org/10.1016/j.jconrel.2022.08.024>.
- [59] Rong L, Li N, Zhang Z. Emerging therapies for glioblastoma: current state and future directions. *J Exp Clin Cancer Res* 2022;41:142.
- [60] Grossman SA, Batara JF. Current management of glioblastoma multiforme. *Semin Oncol.*, vol. 31, Elsevier; 2004, p. 635–44.
- [61] Zhang X, Zhang WEI, Cao W-D, Cheng G, Zhang Y-Q. Glioblastoma multiforme: Molecular characterization and current treatment strategy. *Exp Ther Med* 2012;3:9–14.
- [62] Wu W, Klockow JL, Zhang M, Lafortune F, Chang E, Jin L, et al. Glioblastoma multiforme (GBM): An overview of current therapies and mechanisms of resistance. *Pharmacol Res* 2021;171:105780.
- [63] Bhaskaran M, Devegowda VG, Gupta VK, Shivachar A, Bhosale RR, Arunachalam M, et al. Current perspectives on therapies, including drug delivery systems, for managing glioblastoma multiforme. *ACS Chem Neurosci* 2020;11:2962–77.
- [64] Anton K, Baehring JM, Mayer T. Glioblastoma multiforme: overview of current treatment and future perspectives. *Hematol Oncol Clin North Am* 2012;26:825–53.
- [65] Ozdemir-Kaynak E, Qutub AA, Yesil-Celiktas O. Advances in glioblastoma multiforme treatment: new models for nanoparticle therapy. *Front Physiol* 2018;9:291105.
- [66] Gilbert MR, Friedman HS, Kuttlesch JF, Prados MD, Olson JJ, Reaman GH, et al. A phase II study of temozolomide in patients with newly diagnosed supratentorial malignant glioma before radiation therapy. *Neuro Oncol* 2002;4:261–7.
- [67] Mineo J-F, Bordron A, Baroncini M, Ramirez C, Maurage C-A, Blond S, et al. Prognosis factors of survival time in patients with glioblastoma multiforme: a multivariate analysis

- of 340 patients. *Acta Neurochir (Wien)* 2007;149:245–53.
- [68] Stylli SS. Novel treatment strategies for glioblastoma. *Cancers (Basel)* 2020;12:2883.
- [69] NCT01209442. Hypofractionated Intensity-Modulated Radiation Therapy With Temozolomide and Bevacizumab for Glioblastoma Multiforme 2010. <https://clinicaltrials.gov/study/NCT01209442?tab=history> (accessed March 29, 2024).
- [70] NCT00544817. Radiation Therapy and Temozolomide Followed by Temozolomide Plus Sorafenib for Glioblastoma Multiforme 2007. <https://clinicaltrials.gov/study/NCT00544817?tab=history> (accessed March 29, 2024).
- [71] NCT00590681. Bevacizumab and Temozolomide Following Radiation and Chemotherapy for Newly Diagnosed Glioblastoma Multiforme 2008. <https://classic.clinicaltrials.gov/ct2/show/results/NCT00590681> (accessed March 29, 2024).
- [72] NCT00672243. Ph II Erlotinib + Sirolimus for Pts w Recurrent Malignant Glioma Multiforme 2008. <https://clinicaltrials.gov/study/NCT00672243?cond=NCT00672243&rank=1&tab=history> (accessed March 29, 2024).
- [73] NCT03463265. Nab-sirolimus in Recurrent High Grade Glioma and Newly Diagnosed Glioblastoma 2018. <https://clinicaltrials.gov/study/NCT03463265?cond=NCT03463265&rank=1> (accessed March 29, 2024).
- [74] NCT00515086. Study of Everolimus (RAD001) in Patients With Recurrent Glioblastoma Multiforme (GBM) 2007. <https://clinicaltrials.gov/study/NCT00515086?cond=NCT00515086&rank=1&tab=history> (accessed March 29, 2024).
- [75] Wesolowski JR, Rajdev P, Mukherji SK. Temozolomide (temodar). *Am J Neuroradiol* 2010;31:1383–4.
- [76] Zhang J, F.G. Stevens M, D. Bradshaw T. Temozolomide: Mechanisms of Action, Repair and Resistance. *Curr Mol Pharmacol* 2012;5:102–14. <https://doi.org/http://dx.doi.org/10.2174/1874467211205010102>.
- [77] Law BK. Rapamycin: an anti-cancer immunosuppressant? *Crit Rev Oncol Hematol* 2005;56:47–60.
- [78] Kahan BD. Sirolimus: a comprehensive review. *Expert Opin Pharmacother* 2001;2:1903–17.
- [79] Koehl GE, Schlitt HJ, Geissler EK. Rapamycin and tumor growth: mechanisms behind its anticancer activity. *Transplant Rev* 2005;19:20–31.
- [80] Saxton RA, Sabatini DM. mTOR signaling in growth, metabolism, and disease. *Cell* 2017;168:960–76.
- [81] Tanemura M, Ohmura Y, Deguchi T, Machida T, Tsukamoto R, Wada H, et al. Rapamycin causes upregulation of autophagy and impairs islets function both in vitro and in vivo. *Am J Transplant* 2012;12:102–14.

- [82] NCT00877773. Phosphatidylinositol 3 Kinase and Mammalian Target of Rapamycin (PI3K-mTOR) in Advanced Cancer Patients 2009. <https://clinicaltrials.gov/study/NCT00877773?cond=NCT00877773&rank=1&tab=history> (accessed March 29, 2024).
- [83] NCT02023905. Everolimus With and Without Temozolomide in Adult Low Grade Glioma 2013. <https://clinicaltrials.gov/study/NCT02023905?cond=NCT02023905&rank=1&tab=history> (accessed March 29, 2024).
- [84] Trepanier DJ, Gallant H, Legatt DF, Yatscoff RW. Rapamycin: distribution, pharmacokinetics and therapeutic range investigations: an update. *Clin Biochem* 1998;31:345–51.
- [85] Streit F, Christians U, Schiebel HM, Meyer A, Sewing KF. Structural identification of three metabolites and a degradation product of the macrolide immunosuppressant sirolimus (rapamycin) by electrospray-MS/MS after incubation with human liver microsomes. *Drug Metab Dispos* 1996;24:1272 LP – 1278.
- [86] Paine MF, Leung LY, Lim HK, Liao K, Oganessian A, Zhang M-Y, et al. Identification of a Novel Route of Extraction of Sirolimus in Human Small Intestine: Roles of Metabolism and Secretion. *J Pharmacol Exp Ther* 2002;301:174 LP – 186. <https://doi.org/10.1124/jpet.301.1.174>.
- [87] Filler G, Bendrick-Peart J, Strom T, Zhang YL, Johnson G, Christians U. Characterization of sirolimus metabolites in pediatric solid organ transplant recipients. *Pediatr Transplant* 2009;13:44–53. <https://doi.org/https://doi.org/10.1111/j.1399-3046.2008.00956.x>.
- [88] Christians U, Sattler M, Schiebel HM, Kruse C, Radeke HH, Linck A, et al. Isolation of two immunosuppressive metabolites after in vitro metabolism of rapamycin. *Drug Metab Dispos* 1992;20:186 LP – 191.
- [89] DrugBank. Sirolimus n.d. <https://go.drugbank.com/drugs/DB00877> (accessed March 29, 2024).
- [90] Aslan B, Ozpolat B, Sood AK, Lopez-Berestein G. Nanotechnology in cancer therapy. *J Drug Target* 2013;21:904–13. <https://doi.org/10.3109/1061186X.2013.837469>.
- [91] Rathnayake K, Patel U, Hunt EC, Singh N. Fabrication of a Dual-Targeted Liposome-Coated Mesoporous Silica Core–Shell Nanoassembly for Targeted Cancer Therapy. *ACS Omega* 2023;8:34481–98.
- [92] Zhang P, Cao F, Zhang J, Tan Y, Yao S. Temozolomide and chloroquine co-loaded mesoporous silica nanoparticles are effective against glioma. *Heliyon* 2023;9.
- [93] DuRoss AN, Landry MR, Thomas Jr CR, Neufeld MJ, Sun C. Fucoidan-coated nanoparticles target radiation-induced P-selectin to enhance chemoradiotherapy in murine colorectal cancer. *Cancer Lett* 2021;500:208–19.
- [94] Pulvirenti L, Monforte F, Lo Presti F, Li Volti G, Carota G, Sinatra F, et al. Synthesis of MIL-Modified Fe₃O₄ Magnetic Nanoparticles for Enhancing Uptake and Efficiency of Temozolomide in Glioblastoma Treatment. *Int J Mol Sci* 2022;23.

- <https://doi.org/10.3390/ijms23052874>.
- [95] Lee CY, Ooi IH. Preparation of Temozolomide-Loaded Nanoparticles for Glioblastoma Multiforme Targeting—Ideal Versus Reality. *Pharm* 2016;9. <https://doi.org/10.3390/ph9030054>.
- [96] Meteoglu I, Erdemir A. Genistein and Temozolomide-Loaded Polymeric Nanoparticles: A Synergistic Approach For Improved Anti-Tumor Efficacy Against Glioblastoma. *Process Biochem* 2021;110:9–18. <https://doi.org/10.1016/j.procbio.2021.07.015>.
- [97] Escalona-Rayó O, Fuentes-Vázquez P, Jardon-Xicotencatl S, García-Tovar CG, Mendoza-Elvira S, Quintanar-Guerrero D. Rapamycin-loaded polysorbate 80-coated PLGA nanoparticles: optimization of formulation variables and in vitro anti-glioma assessment. *J Drug Deliv Sci Technol* 2019;52:488–99.
- [98] Zhao R, Zhu M, Zhou S, Feng W, Chen H. Rapamycin-loaded mPEG-PLGA nanoparticles ameliorate hepatic steatosis and liver injury in non-alcoholic fatty liver disease. *Front Chem* 2020;8:407.
- [99] Pape E, Parent M, Pinzano A, Sapin-Minet A, Henrionnet C, Gillet P, et al. Rapamycin-loaded Poly (lactic-co-glycolic) acid nanoparticles: Preparation, characterization, and in vitro toxicity study for potential intra-articular injection. *Int J Pharm* 2021;609:121198.
- [100] Song Z, Huang X, Wang J, Cai F, Zhao P, Yan F. Targeted Delivery of Liposomal Temozolomide Enhanced Anti-Glioblastoma Efficacy through Ultrasound-Mediated Blood–Brain Barrier Opening. *Pharm* 2021;13. <https://doi.org/10.3390/pharmaceutics13081270>.
- [101] Huang G, Zhang N, Bi X, Dou M. Solid lipid nanoparticles of temozolomide: Potential reduction of cardiac and nephric toxicity. *Int J Pharm* 2008;355:314–20. <https://doi.org/10.1016/j.ijpharm.2007.12.013>.
- [102] Chen Z, Lai X, Song S, Zhu X, Zhu J. Nanostructured lipid carriers based temozolomide and gene co-encapsulated nanomedicine for gliomatosis cerebri combination therapy. *Drug Deliv* 2016;23:1369–73. <https://doi.org/10.3109/10717544.2015.1038857>.
- [103] Mazuryk J, Deptuła T, Polchi A, Gapiński J, Giovagnoli S, Magini A, et al. Rapamycin-loaded solid lipid nanoparticles: morphology and impact of the drug loading on the phase transition between lipid polymorphs. *Colloids Surfaces A Physicochem Eng Asp* 2016;502:54–65.
- [104] Chen Y-Q, Zhu W-T, Lin C-Y, Yuan Z-W, Li Z-H, Yan P-K. Delivery of rapamycin by liposomes synergistically enhances the chemotherapy effect of 5-fluorouracil on colorectal cancer. *Int J Nanomedicine* 2021:269–81.
- [105] van Dongen MA, Dougherty CA, Banaszak Holl MM. Multivalent polymers for drug delivery and imaging: the challenges of conjugation. *Biomacromolecules* 2014;15:3215–34.
- [106] Duncan R. Polymer conjugates as anticancer nanomedicines. *Nat Rev Cancer* 2006;6:688–701.
- [107] Gauthier MA, Klok H-A. Peptide/protein–polymer conjugates: synthetic strategies and

- design concepts. *Chem Commun* 2008:2591–611.
- [108] Stevens CA, Kaur K, Klok H-A. Self-assembly of protein-polymer conjugates for drug delivery. *Adv Drug Deliv Rev* 2021;174:447–60.
- [109] Jatzkewitz H. Peptamin (glycyl-L-leucyl-mescaline) bound to blood plasma expander (polyvinylpyrrolidone) as a new depot form of a biologically active primary amine (mescaline). *Z Naturforsch* 1955;10:27–31.
- [110] Givental NI, Ushakov SN, Panarin EF, Popova GO. Experimental studies on penicillin polymer derivatives. *Antibiotiki* 1965;10:701–6.
- [111] Shumikhina KI, Panarin EF, Ushakov SN. Experimental study of polymer salts of penicillins. *Antibiotiki* 1966;11:767–70.
- [112] Panarin EF, Ushakov SN. Synthesis of polymer salts and amides of penicillins. *Pharm Chem J* 1968;2:260–2.
- [113] Mathé G, Lou TB, Bernard J. Effet sur la leucemie 1210 de la souris d'une combinaison par diazotation de methoptérine et de gamma-globulines de hamsters porteurs de cette leucemie par hétérogreffe. *Press. MEDICALE*, vol. 66, MASSON EDITEUR 120 BLVD SAINT-GERMAIN, 75280 PARIS 06, FRANCE; 1958, p. 571.
- [114] De Duve C, De Barse T, Poole B, Tulkens P. Lysosomotropic agents. *Biochem Pharmacol* 1974;23:2495–531.
- [115] Ringsdorf H. Structure and properties of pharmacologically active polymers. *J. Polym. Sci. Polym. Symp.*, vol. 51, Wiley Online Library; 1975, p. 135–53.
- [116] Kopeček J, Šprincl L, Lim D. New types of synthetic infusion solutions. I. Investigation of the effect of solutions of some hydrophilic polymers on blood. *J Biomed Mater Res* 1973;7:179–91.
- [117] Paluska E, Cinátl J, Korčáková L, Štěrba O, Kopeček J, Hrubá A, et al. Immunosuppressive effects of a synthetic polymer poly N-(2-hydroxypropyl) methacrylamide (Duxon). *Folia Biol (Praha)* 1980;26:304–11.
- [118] Korčáková L, Paluska E, Hašková V, Kopeček J. A simple test for immunogenicity of colloidal infusion solutions—the draining lymph node activation. *Zeitschrift Für Immunitätsforschung, Exp Und Klin Immunol* 1976;151:219–23.
- [119] Šprincl L, Exner J, Štěrba O, Kopeček J. New types of synthetic infusion solutions. III. Elimination and retention of poly-[N-(2-hydroxypropyl) methacrylamide] in a test organism. *J Biomed Mater Res* 1976;10:953–63.
- [120] Paluska E, Hrubá A, Štěrba O, Kopeček J. Effect of a synthetic poly N-(2-hydroxypropyl) methacrylamide (Duxon) on haemopoiesis and graft-versus-host reaction. *Folia Biol (Praha)* 1986;32:91–102.
- [121] Šprincl L, Vacík J, Kopeček J, Lím D. Biological tolerance of poly (N-substituted methacrylamides). *J Biomed Mater Res* 1971;5:197–205.
- [122] Kopeček J, Rejmanová P, Chytrý V. Polymers containing enzymatically degradable bonds, 1. Chymotrypsin catalyzed hydrolysis of p-nitroanilides of phenylalanine and

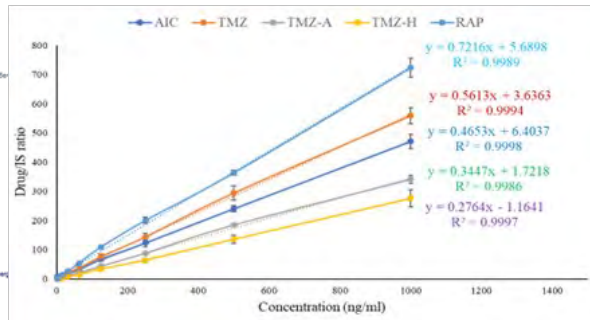
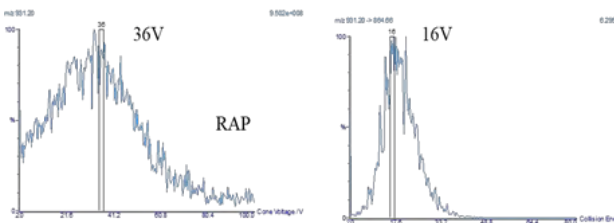
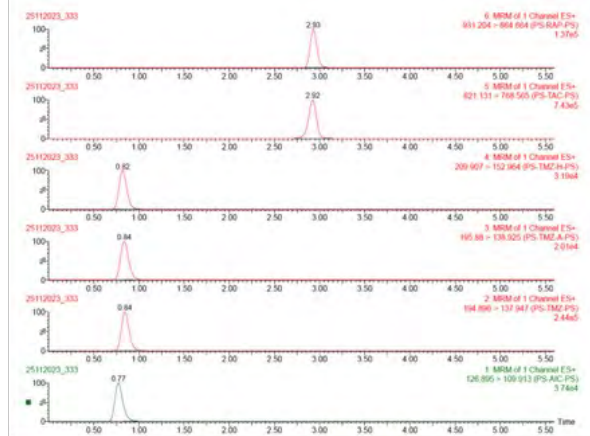
- tyrosine attached to side-chains of copolymers of N-(2-hydroxypropyl) methacrylamide. *Die Makromol Chemie Macromol Chem Phys* 1981;182:799–809.
- [123] Kopeček J. Reactive copolymers of N-(2-hydroxypropyl) methacrylamide with N-methacryloylated derivatives of l-leucine and l-phenylalanine, 1. Preparation, characterization, and reactions with diamines. *Die Makromol Chemie Macromol Chem Phys* 1977;178:2169–83.
- [124] Ulbrich K, Strohaln J, Kopeček J. Polymers containing enzymatically degradable bonds, 3. Poly [N-(2-hydroxypropyl) methacrylamide] chains connected by oligopeptide sequences cleavable by trypsin. *Die Makromol Chemie Macromol Chem Phys* 1981;182:1917–28.
- [125] Ulbrich K, Zacharieva EI, Obereigner B, Kopeček J. Polymers containing enzymatically degradable bonds V. Hydrophilic polymers degradable by papain. *Biomaterials* 1980;1:199–204.
- [126] Duncan R, Cable HC, Lloyd JB, Rejmanová P, Kopeček J. Polymers containing enzymatically degradable bonds, 7. Design of oligopeptide side-chains in poly [N-(2-hydroxypropyl) methacrylamide] copolymers to promote efficient degradation by lysosomal enzymes. *Die Makromol Chemie* 1983;184:1997–2008.
- [127] Khandare J, Minko T. Polymer–drug conjugates: Progress in polymeric prodrugs. *Prog Polym Sci* 2006;31:359–97. <https://doi.org/https://doi.org/10.1016/j.progpolymsci.2005.09.004>.
- [128] Ekladios I, Colson YL, Grinstaff MW. Polymer–drug conjugate therapeutics: advances, insights and prospects. *Nat Rev Drug Discov* 2019;18:273–94. <https://doi.org/10.1038/s41573-018-0005-0>.
- [129] Ansari I, Singh P, Mittal A, Mahato RI, Chitkara D. 2,2-Bis(hydroxymethyl) propionic acid based cyclic carbonate monomers and their (co)polymers as advanced materials for biomedical applications. *Biomaterials* 2021;275:120953. <https://doi.org/https://doi.org/10.1016/j.biomaterials.2021.120953>.
- [130] Wadhwa S, Mumper RJ. Polymer-Drug Conjugates for Anticancer Drug Delivery. *Crit Rev Ther Drug Carrier Syst* 2015;32:215–45. <https://doi.org/10.1615/critrevtherdrugcarriersyst.2015010174>.
- [131] Duro-Castano A, Movellan J, Vicent MJ. Smart branched polymer drug conjugates as nano-sized drug delivery systems. *Biomater Sci* 2015;3:1321–34. <https://doi.org/10.1039/C5BM00166H>.
- [132] Girase ML, Patil PG, Ige PP. Polymer-drug conjugates as nanomedicine: a review. *Int J Polym Mater Polym Biomater* 2020;69:990–1014. <https://doi.org/10.1080/00914037.2019.1655745>.
- [133] Alven S, Nqoro X, Buyana B, Aderibigbe BA. Polymer-Drug Conjugate, a Potential Therapeutic to Combat Breast and Lung Cancer. *Pharm* 2020;12. <https://doi.org/10.3390/pharmaceutics12050406>.
- [134] Fante C, Greco F. Polymer-Drug Conjugates BT - Fundamentals of Pharmaceutical Nanoscience. In: Uchehgbu IF, Schätzlein AG, Cheng WP, Lalatsa A, editors., New

- York, NY: Springer New York; 2013, p. 159–82. https://doi.org/10.1007/978-1-4614-9164-4_7.
- [135] Duncan R, Vicent MJ, Greco F, Nicholson RI. Polymer-drug conjugates: towards a novel approach for the treatment of endocrine-related cancer. *Endocr Relat Cancer* 2005;12 Suppl 1:S189-99. <https://doi.org/10.1677/erc.1.01045>.
- [136] Ananta JS, Paulmurugan R, Massoud TF. Temozolomide-loaded PLGA nanoparticles to treat glioblastoma cells: a biophysical and cell culture evaluation. *Neurol Res* 2016;38:51–9. <https://doi.org/10.1080/01616412.2015.1133025>.
- [137] Dilnawaz F, Sahoo SK. Enhanced accumulation of curcumin and temozolomide loaded magnetic nanoparticles executes profound cytotoxic effect in glioblastoma spheroid model. *Eur J Pharm Biopharm* 2013;85:452–62. <https://doi.org/10.1016/j.ejpb.2013.07.013>.
- [138] Chang M, Zhang F, Wei T, Zuo T, Guan Y, Lin G, et al. Smart linkers in polymer–drug conjugates for tumor-targeted delivery. *J Drug Target* 2016;24:475–91. <https://doi.org/10.3109/1061186X.2015.1108324>.
- [139] Patil R, Portilla-Arias J, Ding H, Inoue S, Konda B, Hu J, et al. Temozolomide Delivery to Tumor Cells by a Multifunctional Nano Vehicle Based on Poly(β -L-malic acid). *Pharm Res* 2010;27:2317–29. <https://doi.org/10.1007/s11095-010-0091-0>.
- [140] Fang C, Wang K, Stephen ZR, Mu Q, Kievit FM, Chiu DT, et al. Temozolomide Nanoparticles for Targeted Glioblastoma Therapy. *ACS Appl Mater Interfaces* 2015;7:6674–82. <https://doi.org/10.1021/am5092165>.
- [141] Skinner M, Ward SM, Emrick T. Versatile Synthesis of Polymer-Temozolomide Conjugates. *ACS Macro Lett* 2017;6:215–8. <https://doi.org/10.1021/acsmacrolett.7b00007>.
- [142] Ward SM, Skinner M, Saha B, Emrick T. Polymer–Temozolomide Conjugates as Therapeutics for Treating Glioblastoma. *Mol Pharm* 2018;15:5263–76. <https://doi.org/10.1021/acs.molpharmaceut.8b00766>.
- [143] Wang L, Tang S, Yu Y, Lv Y, Wang A, Yan X, et al. Intranasal Delivery of Temozolomide-Conjugated Gold Nanoparticles Functionalized with Anti-EphA3 for Glioblastoma Targeting. *Mol Pharm* 2021;18:915–27. <https://doi.org/10.1021/acs.molpharmaceut.0c00911>.
- [144] Xu K, Zhang L, Gu Y, Yang H, Du B, Liu H, et al. Increased the TMZ concentration in brain by poly(2-ethyl-2-oxazoline) conjugated temozolomide prodrug micelles for glioblastoma treatment. *Eur Polym J* 2021;145:110232. <https://doi.org/10.1016/j.eurpolymj.2020.110232>.
- [145] Jose C, Amra K, Bhavsar C, Momin MM, Omri A. Polymeric lipid hybrid nanoparticles: properties and therapeutic applications. *Crit Rev Ther Drug Carr Syst* 2018;35.
- [146] Hood MA, Mari M, Muñoz-Espí R. Synthetic strategies in the preparation of polymer/inorganic hybrid nanoparticles. *Materials (Basel)* 2014;7:4057–87.
- [147] Gajbhiye KR, Salve R, Narwade M, Sheikh A, Kesharwani P, Gajbhiye V. Lipid polymer hybrid nanoparticles: a custom-tailored next-generation approach for cancer

- therapeutics. *Mol Cancer* 2023;22:160.
- [148] Jain A, Sharma G, Kushwah V, Garg NK, Kesharwani P, Ghoshal G, et al. Methotrexate and beta-carotene loaded-lipid polymer hybrid nanoparticles: A preclinical study for breast cancer. *Nanomedicine* 2017;12:1851–72.
- [149] Tran TH, Nguyen HT, Yong CS, Truong DH, Kim JO. Synergistic therapeutic strategy of dual drug-loaded lipid polymer hybrid nanoparticles for breast cancer treatment. *Indian J Pharm Sci* 2019;81:474–82.
- [150] Gu FX, Karnik R, Wang AZ, Alexis F, Levy-Nissenbaum E, Hong S, et al. Targeted nanoparticles for cancer therapy. *Nano Today* 2007;2:14–21.
- [151] Accardo A, Aloj L, Aurilio M, Morelli G, Tesaro D. Receptor binding peptides for target-selective delivery of nanoparticles encapsulated drugs. *Int J Nanomedicine* 2014:1537–57.
- [152] Koo H, Huh MS, Sun I-C, Yuk SH, Choi K, Kim K, et al. In vivo targeted delivery of nanoparticles for theranosis. *Acc Chem Res* 2011;44:1018–28.
- [153] Ayo A, Laakkonen P. Peptide-Based Strategies for Targeted Tumor Treatment and Imaging. *Pharmaceutics* 2021;13. <https://doi.org/10.3390/pharmaceutics13040481>.
- [154] Zhang T, Prasad P, Cai P, He C, Shan D, Rauth AM, et al. Dual-targeted hybrid nanoparticles of synergistic drugs for treating lung metastases of triple negative breast cancer in mice. *Acta Pharmacol Sin* 2017;38:835–47. <https://doi.org/10.1038/aps.2016.166>.
- [155] Yang Z, Luo X, Zhang X, Liu J, Jiang Q. Targeted delivery of 10-hydroxycamptothecin to human breast cancers by cyclic RGD-modified lipid–polymer hybrid nanoparticles. *Biomed Mater* 2013;8:25012.
- [156] Gao F, Zhang J, Fu C, Xie X, Peng F, You J, et al. iRGD-modified lipid–polymer hybrid nanoparticles loaded with isoliquiritigenin to enhance anti-breast cancer effect and tumor-targeting ability. *Int J Nanomedicine* 2017:4147–62.
- [157] Belhadj Z, Zhan C, Ying M, Wei X, Xie C, Yan Z, et al. Multifunctional targeted liposomal drug delivery for efficient glioblastoma treatment. *Oncotarget* 2017;8:66889.
- [158] Miura Y, Takenaka T, Toh K, Wu S, Nishihara H, Kano MR, et al. Cyclic RGD-Linked Polymeric Micelles for Targeted Delivery of Platinum Anticancer Drugs to Glioblastoma through the Blood–Brain Tumor Barrier. *ACS Nano* 2013;7:8583–92. <https://doi.org/10.1021/nn402662d>.

Chapter 2

Analytical and bioanalytical method development and validation of rapamycin, temozolomide, temozolomide acid, temozolomide hydrazide, and 5-aminoimidazole-4-carboxamide in biological matrix of rat



The current chapter comprises three sub-sections, i.e., section 2.2, 2.3, and 2.4, encompassing the development of the analytical method and its validation using the ultraviolet-visible (UV-Vis) spectroscopy, HPLC-UV-based method, and UPLC-MS/MS based bioanalytical method development and validation. Section 2.2 details the analytical method for the temozolomide hydrazide (TMZ-H), while section 2.3 details the HPLC-UV-based analytical method for rapamycin, temozolomide (TMZ) and its derivatives (TMZ-A, TMZ-BOC, TMZ-H, AIC) have been developed, followed by its thorough validation as per the ICH Q2-guidelines. Section 2.4 entails the detailed bioanalytical method development using UPLC-MS/MS for RAP, TMZ, TMZ-A, TMZ-H, and AIC, followed by validation using ICH M10 guidelines.

2.1. Chemical and reagents

Temozolomide (TMZ, >98%), 5(4)-Amino-4(5)-(aminocarbonyl)imidazole Hydrochloride (AIC, >98%) was purchased from TCI chemicals (Tokyo, Japan). Sirolimus (rapamycin, >99%) from Alfa Aesar (ThermoFisher Scientific (Massachusetts, United States)). Temozolomide acid (TMZ-A, >99%) and temozolomide hydrazide (TMZ-H, >99%) were synthesized in house as per the reported protocol [1]. HPLC grade Methanol and Formic acid (98 - 100%) were obtained from Merck (Massachusetts, United States). All other reagents and chemicals were procured from local vendors.

2.2. Analytical method for the analysis of TMZ-H using ultraviolet-visible (UV-Vis) spectroscopy method

2.2.1. Instrumentation conditions

UV-visible spectra for TMZ-H were recorded using a Jasco-V750 spectrophotometer (Hachioji, Tokyo, Japan) at room temperature with a path length of 1 cm over the 200-800 nm wavelength range.

2.2.2. Preparation of stock and working solution

The stock solution of TMZ-H (2 mg/ml) was prepared by dissolving 10 mg of TMZ-H in 5 ml of HPLC-grade methanol. The solution was vortexed for 10 min to ensure the solubility of the sample. The working solution was prepared by diluting the stock solution with 50% methanol in milli-Q water.

2.2.3. Preparation of calibrators and quality control samples

The working solution of TMZ-H was prepared by diluting the stock solution with 50% methanol to prepare the calibration curve using a serial dilution method ranging from 0.62 µg/ml to 40 µg/ml, and a calibration curve was prepared using an absorbance-concentration profile. Thereafter, quality control (QC) samples were prepared in a similar manner in triplicates, including Low-level QC (LQC), Mid-level quality control (MQC), High-level quality control (HQC) were prepared with a concentration equivalent to 0.9, 9.5, and 30 µg/ml, respectively. All the stock and working standard solutions were stored at -20 °C until further use. Further, the regression equation was used to calculate the concentration of the unknown and QC samples for further evaluation.

2.2.4. Assay Validation

The method was developed and validated as per the International Council for Harmonisation (ICH) for linearity, sensitivity (LOD and LOQ), specificity, accuracy, and precision [2].

2.2.4.1. Linearity of the calibration curve

Calibration standards were prepared ranging from 0.62 µg/ml to 40 µg/ml and analyzed using JASCO UV V-750. The obtained data was plotted for absorbance to the concentration of the analyte (TMZ-H). The linearity of the calibration curve was determined using the regression line expressed as equation $y=mx+c$, where m is the slope and c is the intercept of the regression line.

2.2.4.2. Sensitivity

The sensitivity was determined through the limit of detection (LOD) and limit of quantitation (LOQ) method. The LOD and LOQ could be calculated as per the below formula:

$$LOD = 3.3 \times \sigma/m \quad eq. 2.1$$

$$LOQ = 10 \times \sigma/m \quad eq. 2.2$$

Where σ is the standard deviation of the response, and m is the slope of the calibration curve

2.2.4.3. Accuracy and precision

Accuracy and precision can be determined using the quality control samples (LQC, MQC, and HQC). The samples were prepared with at least three replicates of each QC sample

(n=03/each QC level). The acceptance criteria for accuracy and precision must fall within the % relative standard deviation (% RSD) and % Bias of 98-102%.

2.2.4.4. Stability

Stability studies of the analyte were performed by keeping the QC samples (LQC, MQC, and HQC) based on bench-top stability (25 ± 2 °C, 24 h) and short-term storage stability (8 ± 2 °C, 7 days). A minimum of three replicates of QC (n=03/each QC level) sets must be evaluated and fall within the acceptance criteria of % RSD and % Bias of not more than 2% for all the samples.

2.2.5. Result and discussion

The analytical method using a simple UV-Vis spectrophotometer for the TMZ-H was developed and validated as per the ICH Q2 guidelines. The spectrum for the TMZ-H is shown in the figure 2.1A. At wavelength λ_{\max} 328 nm (Figure 2.1A), the calibration curve, QC, and unknown samples were evaluated. The developed analytical method was found to be linear over the range of 0.62 $\mu\text{g/ml}$ to 40 $\mu\text{g/ml}$. The developed calibration curve demonstrated the line equation and regression coefficient (R^2) of $y=0.04040x-0.00246$ and 0.99998, respectively, for TMZ-H, as shown in figure 2.1B. The method was sensitive with an LOD and LOQ of 84.2 and 255.1 ng/ml, respectively. The developed method was validated as per the ICH guidelines, and all the values for accuracy, precision, and stability were found within the recommended limit range, as mentioned in Table 2.1 and 2.2.

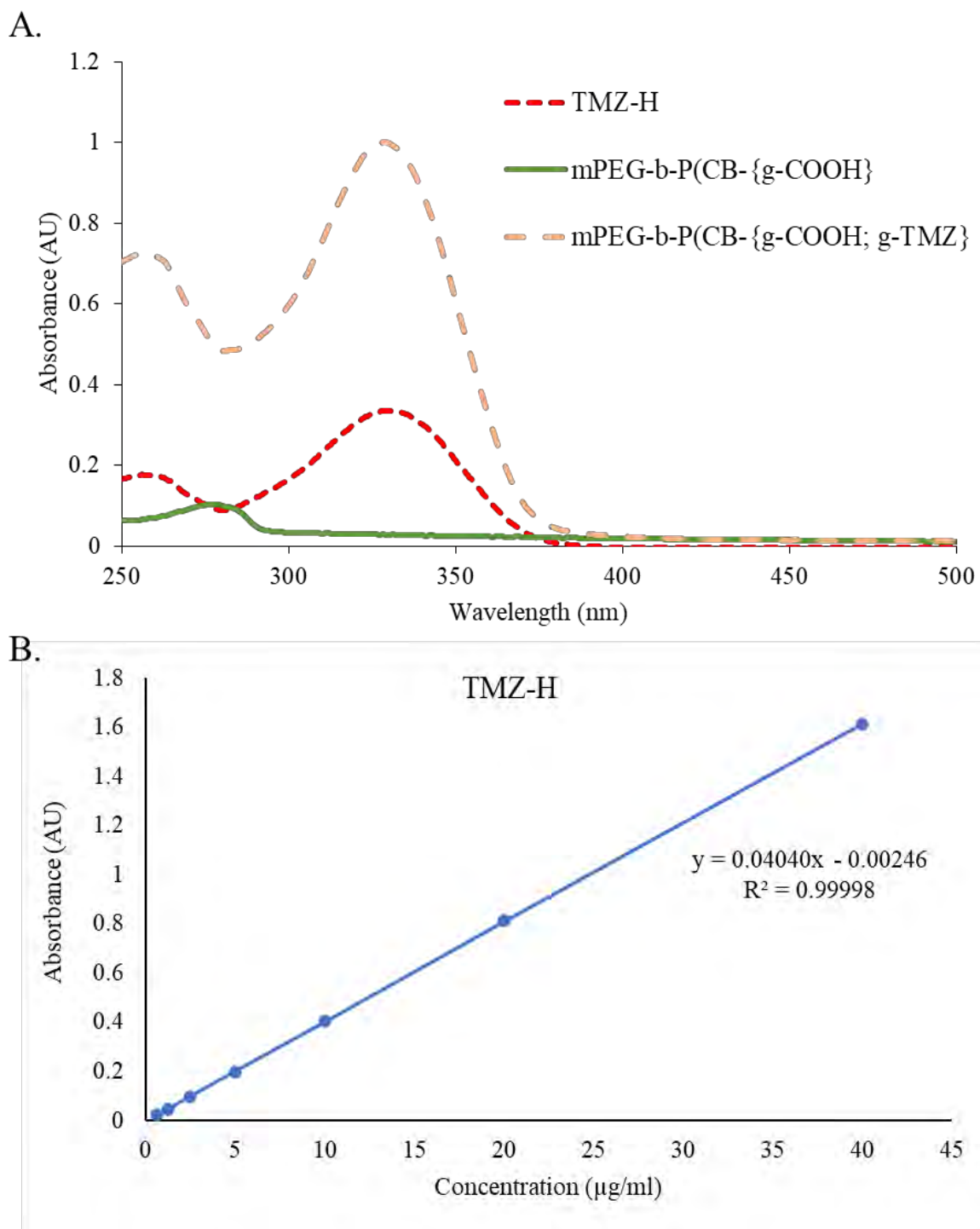


Figure 2.1. TMZ-H characterisation. A) UV-Visible spectrum and B) Calibration curve

Table 2.1. Intra-day and Inter-day accuracy and precision of TMZ-H

Level	Intra day				Inter day		
	Nominal conc. ($\mu\text{g/ml}$)	Observed conc. ($\mu\text{g/ml}$)	% RSD	% Bias	Observed conc. ($\mu\text{g/ml}$)	% RSD	% Bias
		Mean \pm SD			Mean \pm SD		
LQC	0.9	0.902 \pm 0.016	1.78	0.21	0.904 \pm 0.017	1.83	0.39
MQC	9.5	9.594 \pm 0.171	1.78	0.99	9.623 \pm 0.157	1.63	1.3
HQC	30	29.603 \pm 0.522	1.76	-1.32	29.739 \pm 0.348	1.17	-0.87

Table 2.2. Stability studies of TMZ-H

Conditions	Level	Nominal conc. ($\mu\text{g/ml}$)	Observed conc. ($\mu\text{g/ml}$)	% RSD	% Bias
			Mean \pm SD		
t= 0 h (for initial samples)	LQC	0.9	0.899 \pm 0.015	1.65	-0.12
	MQC	9.5	9.587 \pm 0.181	1.89	0.91
	HQC	30	29.635 \pm 0.548	1.85	-1.22
Benchtop stability	LQC	0.9	0.901 \pm 0.017	1.91	0.16
	MQC	9.5	9.549 \pm 0.112	1.17	0.52
24 h	HQC	30	29.560 \pm 0.541	1.83	-1.47
Short-term stability (4 $^{\circ}\text{C}$, 7 days)	LQC	0.9	0.902 \pm 0.017	1.92	0.24
	MQC	9.5	9.599 \pm 0.182	1.9	1.04
	HQC	30	29.578 \pm 0.553	1.87	-1.41

2.3. HPLC-UV-based analytical method development and validation

The analytical method for rapamycin, temozolomide (TMZ), and its derivatives (TMZ-A, TMZ-BOC, TMZ-H, AIC) using HPLC-UV was developed and validated per the ICH Q2 guidelines [2].

2.3.1. Liquid chromatographic conditions

Chromatographic elution of RAP, TMZ, TMZ-A, TMZ-BOC, TMZ-H, and AIC was performed on Waters® HPLC system equipped with dual binary pump (#515), autosampler (#2707), and TUV detector (#2489). The analyte analysis was achieved on the Inertsil-ODS 3V column (250 × 4.6 mm, 5 µm) using methanol and sodium acetate buffer (pH 4.0) as a mobile phase. For RAP, the mobile phase ratio was kept at 92:08% v/v for methanol and sodium acetate buffer (pH 4.0) and monitored at 278 nm at a flow rate of 1 ml/min. While, TMZ, TMZ-A, TMZ-BOC, TMZ-H, and AIC were eluted using methanol and sodium acetate buffer (pH 4.0) at a ratio of 27:73% v/v as mobile phase. The eluted analytes were monitored at 328 and 267 nm at a flow rate of 1 ml/min. The injection volume for all the analytes was fixed at 20 µl. The obtained data were recorded and interpreted using Breeze 2 software.

2.3.2. Preparation of stock and working solutions

A stock solution of RAP, TMZ, TMZ-A, TMZ-BOC, TMZ-H, and AIC (2 mg/ml) was weighed and dissolved in 10 ml of HPLC-grade mobile phase. All stock solutions were stored immediately at -20 °C until further use.

2.3.3. Preparation of Quality control samples

The QC samples were prepared by diluting the stock solution to give three QC samples in triplicates, including Low-level QC (LQC), Mid-level quality control (MQC), and High-level quality control (HQC) with a concentration equivalent to 5, 40, and 150 µg/ml, respectively. Further, the regression equation was utilized to determine the concentration of the unknown and QC samples for further evaluation.

2.3.4. Analytical method validation

The developed analytical method was validated as per the International Council for Harmonisation ICH-Q2 guidelines. The following parameters were evaluated for the developed method [2].

2.3.4.1. Selectivity and specificity

The selectivity and specificity of the developed analytical method was performed to determine the interference from the previously synthesized analyte by keeping the other parameters constant.

2.3.4.2. Linearity of the calibration curve

Nine calibration points were eluted on the LC system from 0.390 µg/ml to 200 µg/ml. The obtained data was analyzed, and the area under the curve was plotted over the concentration and expressed by an equation $y=mx+c$, where m is the slope and c is the intercept of the regression line. The linearity of the calibration curve was determined using the regression coefficient (R^2) using the obtained regression equation.

2.3.4.3. Sensitivity, LOD, and LOQ

The sensitivity of the method was determined through the visual analysis of the signal-to-noise ratio (S/N), which was compared by measuring the signals from the samples of known low concentrations to the blank samples. A S/N ratio of 3:1 and 10:1 is considered as the limit of detection (LOD), and a limit of quantitation (LOQ), respectively, is considered within the limits.

Additionally, the LOD and LOQ could be calculated as per the below formula:

$$LOD = 3.3 \times \sigma/m \quad eq. 2.3$$

$$LOQ = 10 \times \sigma/m \quad eq. 2.4$$

Where σ is the standard deviation of the response and m is the slope of the calibration curve

2.3.4.4. Accuracy and precision

The intra and inter-day accuracy and precision were determined using the quality control samples (LQC, MQC, and HQC). The samples were prepared with at least three replicates of each QC sample ($n=03$ /each QC level). The acceptance criteria for accuracy and precision must fall within the % relative standard deviation (% RSD) and % Bias of 98-102%.

2.3.4.5. Carryover effect

The carryover was analyzed by injecting the HQC sample, followed by injecting two blank samples (zero samples) to determine the presence of impurities and remnants of the

previously injected sample. For zero samples, an acceptable criterion should be less than 2% of the injected sample.

2.3.4.6. Stability studies

Stability studies of the analyte were performed by keeping the QC samples (LQC, MQC, and HQC) based on bench-top stability (25 ± 2 °C, 24 h), autosampler stability (8 ± 2 °C, 24 h). A minimum of three replicates of QC (n=03/each QC) sets must be evaluated and fall within the acceptance criteria of % RSD and % Bias of not more than 20% for all the samples.

2.3.5. Results and discussion

2.3.5.1. Analytical method development

The analytical method was developed for various analytes on the Waters LC system equipped with a C18 column. For RAP, the elution time of the analytes was 4.99 min using a 92:08% v/v ratio of methanol and sodium acetate buffer (pH 4.0) as a mobile phase. The other analytes, TMZ, TMZ-A, TMZ-BOC, TMZ-H, and AIC, were eluted at 4.43, 3.30, 25.91, 3.75, and 3.10 min, respectively, detected at 328 and 267 nm using 27:73% v/v ratio of methanol and sodium acetate buffer (pH 4.0) as a mobile phase (Figure 2.2).

2.3.5.2. Method validation

The analytical method was developed and validated as per the ICH-Q2 guidelines. The method was found to show the selectivity and specificity towards the respective analyte of interest, demonstrating no interference from the previously synthesized analytes (Figure 2.4). The analytes obtained were more than 99% pure. The developed method exhibited linearity over the range of 0.390 µg/ml to 200 µg/ml, with regression equations of $y=43678x-23862$, $y=43195x+9301$, $y=34100x-16229$, $y=40150x+29451$, $y=33238x-17430$, and $y=70023x-8526.2$ with regression coefficient (R^2) of 0.99986, 0.99999, 0.99938, 0.99902, 0.99965, and 0.99997 for RAP, TMZ, TMZ-A, TMZ-BOC, TMZ-H, and AIC, respectively as mentioned in table 2.3. The calibration curve was plotted across the area under the curve to the concentration axis (Figure 2.3). The method was found to be sensitive with LOD and LOQ for various analytes, as mentioned in table 2.3. Furthermore, the method showed intraday and interday accuracy and precision parameters within the acceptable range for the analytes, as mentioned in table 2.4. Also, the developed method did not show any sign of a carryover effect, and stability data were found to be within acceptable limits as per the guidelines (Table 2.5).

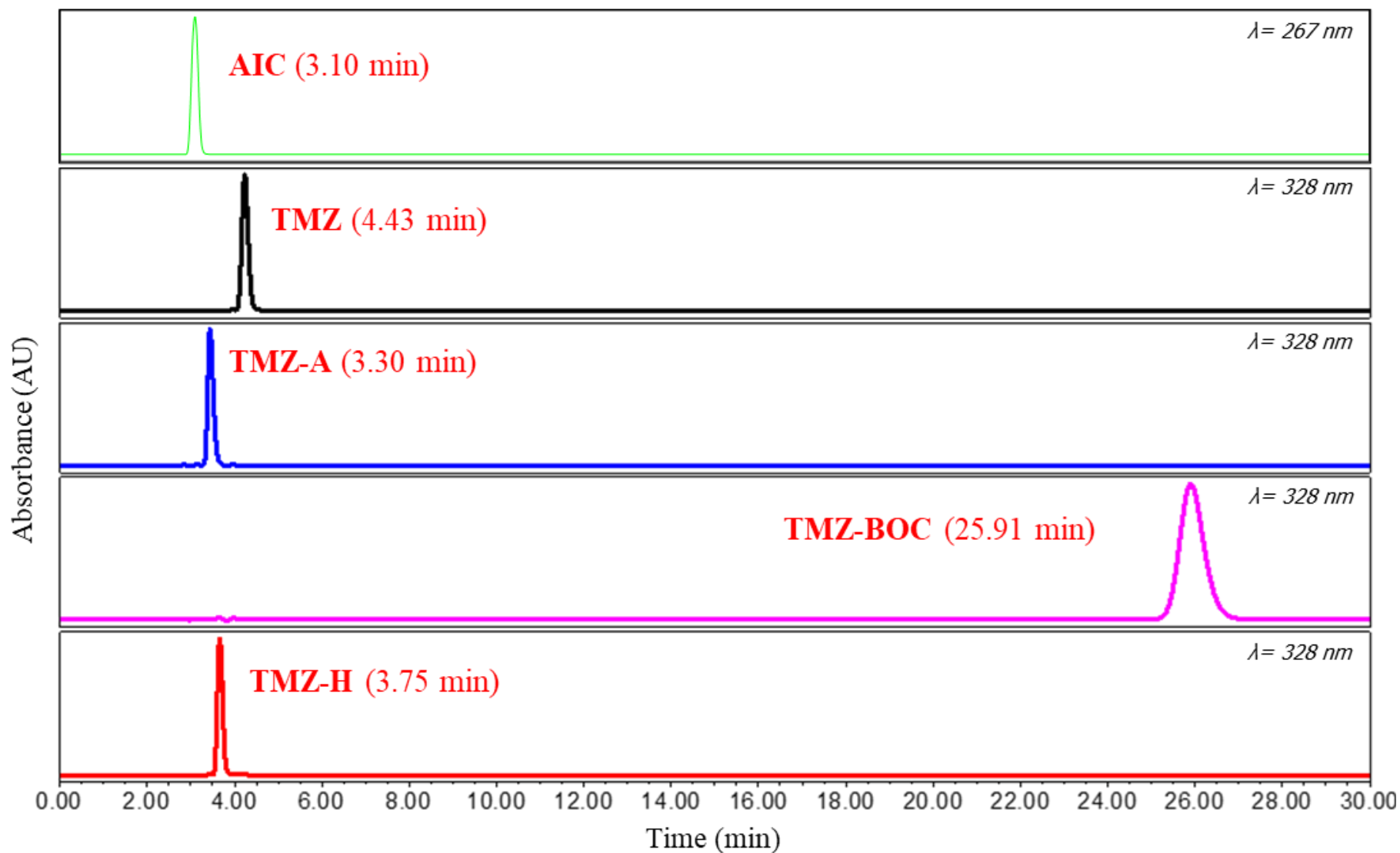


Figure 2.2. Chromatographic elution of AIC, TMZ, TMZ-A, TMZ-BOC, and TMZ-H (*top to bottom*) on C18 column using methanol and sodium acetate buffer (pH 4.0) as a mobile phase

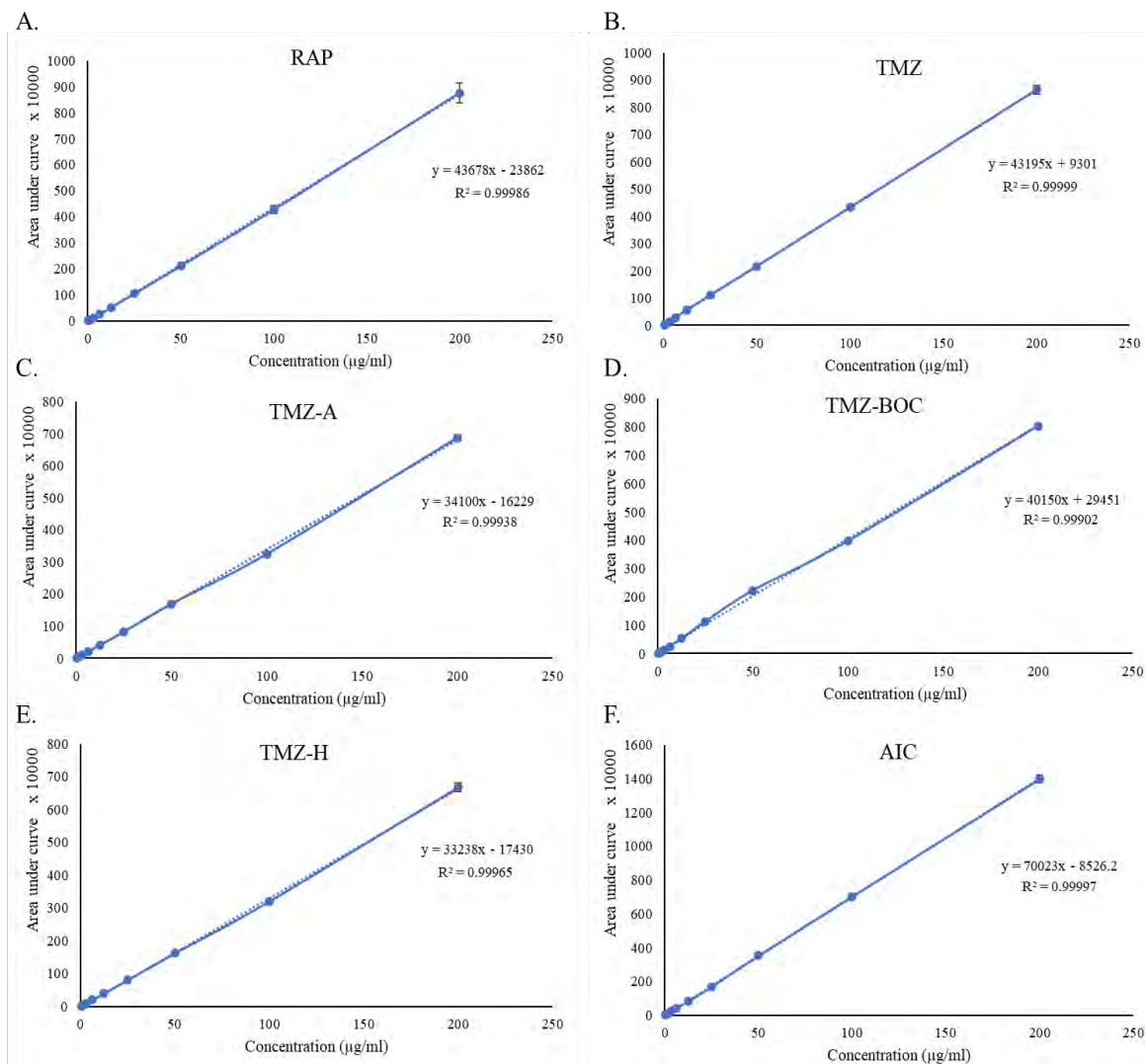


Figure 2.3. Calibration curve of A) RAP, B) TMZ, C) TMZ-A, D) TMZ-BOC, E) TMZ-H, and F) AIC in mobile phase

Table 2.3. Calibration curve details of RAP, TMZ, TMZ-A, TMZ-BOC, TMZ-H, and AIC

Molecule	Regression equation	Regression coefficient (R^2)	LOD (ng/ml)	LOQ (ng/ml)
RAP	$y=43678x-23862$	0.99986	21.7	65.7
TMZ	$y=43195x+9301$	0.99999	20.5	62.3
TMZ-A	$y=34100x-16229$	0.99938	27.9	84.5
TMZ-BOC	$y=40150x+29451$	0.99902	32.6	98.6
TMZ-H	$y=33238x-17430$	0.99965	30.0	91
AIC	$y=70023x-8526.2$	0.99997	13.4	40.8

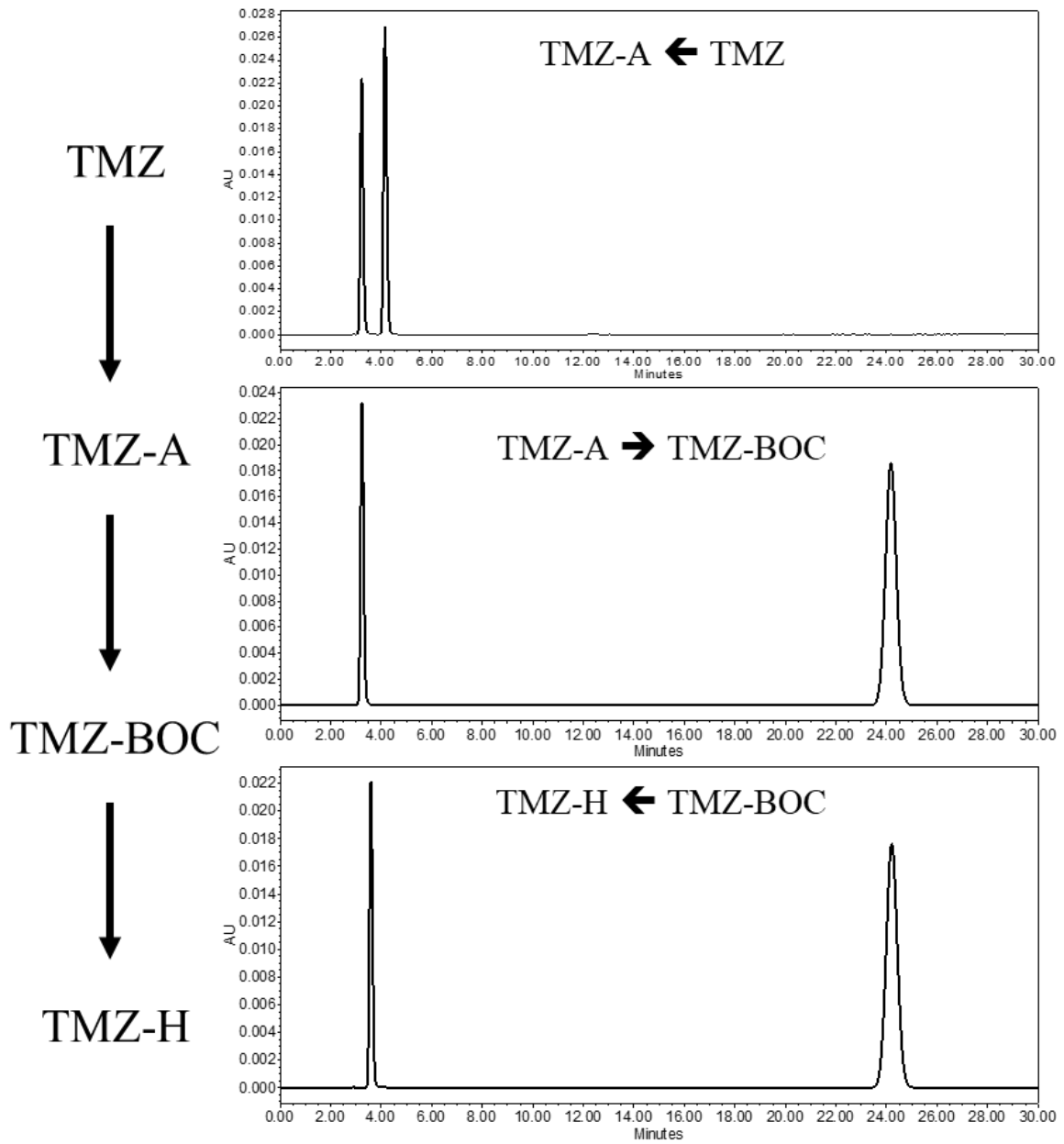


Figure 2.4. Specificity of the analytes A) $TMZ \rightarrow TMZ-A$, B) $TMZ-A \rightarrow TMZ-BOC$, C) $TMZ-BOC \rightarrow TMZ-H$

Table 2.4. Intra-day and Inter-day accuracy and precision of RAP, TMZ, TMZ-A, TMZ-BOC, TMZ-H, and AIC

RAP							
Level	Nominal conc. (µg/ml)	Intra day			Inter day		
		Observed conc. (µg/ml)	% RSD	% Bias	Observed conc. (µg/ml)	% RSD	% Bias
		Mean ± SD			Mean ± SD		
LQC	5	5.077 ± 0.084	1.65	1.54	5.075 ± 0.093	1.82	1.5
MQC	40	39.245 ± 0.602	1.53	-1.89	39.227 ± 0.658	1.68	-1.93
HQC	150	148.324 ± 2.824	1.9	-1.12	147.930 ± 2.928	1.98	-1.38

TMZ							
Level	Nominal conc. (µg/ml)	Intra day			Inter day		
		Observed conc. (µg/ml)	% RSD	% Bias	Observed conc. (µg/ml)	% RSD	% Bias
		Mean ± SD			Mean ± SD		
LQC	5	5.020 ± 0.074	1.47	0.4	5.006 ± 0.073	1.47	0.13
MQC	40	40.651 ± 0.533	1.31	1.63	40.637 ± 0.595	1.46	1.59
HQC	150	152.406 ± 1.511	0.99	1.6	152.722 ± 1.449	0.95	1.81

TMZ-A							
Level	Nominal conc. (µg/ml)	Intra day			Inter day		
		Observed conc. (µg/ml)	% RSD	% Bias	Observed conc. (µg/ml)	% RSD	% Bias
		Mean ± SD			Mean ± SD		
LQC	5	5.095 ± 0.054	1.06	1.91	5.092 ± 0.060	1.17	1.85
MQC	40	40.015 ± 0.660	1.65	0.04	39.941 ± 0.710	1.78	-0.15
HQC	150	152.320 ± 2.625	1.72	1.55	152.146 ± 2.896	1.9	1.43

TMZ-BOC							
Level	Nominal conc. (µg/ml)	Intra day			Inter day		
		Observed conc. (µg/ml)	% RSD	% Bias	Observed conc. (µg/ml)	% RSD	% Bias
		Mean ± SD			Mean ± SD		
LQC	5	5.030 ± 0.077	1.52	0.59	4.992 ± 0.017	0.35	-0.16
MQC	40	39.980 ± 0.389	0.97	-0.05	39.887 ± 0.419	1.05	-0.28
HQC	150	150.146 ± 1.207	0.8	0.1	149.931 ± 1.381	0.92	-0.05

TMZ-H							
Level	Nominal conc. (µg/ml)	Intra day			Inter day		
		Observed conc. (µg/ml)	% RSD	% Bias	Observed conc. (µg/ml)	% RSD	% Bias
		Mean ± SD			Mean ± SD		
LQC	5	5.084 ± 0.085	1.67	1.67	5.083 ± 0.059	1.16	1.66
MQC	40	40.596 ± 0.729	1.79	1.49	40.703 ± 0.760	1.87	1.76
HQC	150	152.806 ± 2.464	1.61	1.87	152.774 ± 2.344	1.53	1.85

AIC							
Level	Nominal conc. (µg/ml)	Intra day			Inter day		
		Observed conc. (µg/ml)	% RSD	% Bias	Observed conc. (µg/ml)	% RSD	% Bias
		Mean ± SD			Mean ± SD		
LQC	5	5.060 ± 0.079	1.55	1.2	5.039 ± 0.067	1.33	0.79
MQC	40	40.138 ± 0.529	1.32	0.35	40.220 ± 0.547	1.36	0.55
HQC	150	152.003 ± 1.414	0.93	1.34	151.786 ± 1.465	0.96	1.19

Table 2.5. Stability studies of RAP, TMZ, TMZ-A, TMZ-BOC, TMZ-H, and AIC

RAP						
Conditions	Level	Nominal conc. (µg/ml)	Observed conc. (µg/ml)	% RSD	% Bias	
			Mean ± SD			
t= 0 h (for initial samples)	LQC	5	5.064 ± 0.074	1.46	1.28	
	MQC	40	39.221 ± 0.626	1.59	-1.95	
	HQC	150	148.286 ± 2.958	1.99	-1.14	
Benchtop stability (24 h)	LQC	5	5.053 ± 0.069	1.36	1.07	
	MQC	40	39.280 ± 0.587	1.49	-1.8	
	HQC	150	149.095 ± 2.380	1.6	-0.6	
Autosampler stability (24 h)	LQC	5	5.069 ± 0.049	0.96	1.39	
	MQC	40	39.280 ± 0.587	1.49	-1.8	
	HQC	150	148.821 ± 2.387	1.6	-0.79	

TMZ					
Conditions	Level	Nominal conc. ($\mu\text{g/ml}$)	Observed conc. ($\mu\text{g/ml}$) Mean \pm SD	% RSD	% Bias
t= 0 h (for initial samples)	LQC	5	5.015 \pm 0.081	1.62	0.29
	MQC	40	40.648 \pm 0.596	1.47	1.62
	HQC	150	152.346 \pm 1.681	1.1	1.56
Benchtop stability (24 h)	LQC	5	5.031 \pm 0.077	1.53	0.62
	MQC	40	40.773 \pm 0.494	1.21	1.93
	HQC	150	152.795 \pm 1.309	0.86	1.86
Autosampler stability (24 h)	LQC	5	5.019 \pm 0.083	1.64	0.38
	MQC	40	40.458 \pm 0.273	0.68	1.14
	HQC	150	152.001 \pm 1.276	0.84	1.33
TMZ-A					
Conditions	Level	Nominal conc. ($\mu\text{g/ml}$)	Observed conc. ($\mu\text{g/ml}$) Mean \pm SD	% RSD	% Bias
t= 0 h (for initial samples)	LQC	5	5.086 \pm 0.055	1.08	1.73
	MQC	40	39.929 \pm 0.700	1.75	-0.18
	HQC	150	152.180 \pm 2.910	1.91	1.45
Benchtop stability (24 h)	LQC	5	5.089 \pm 0.058	1.13	1.78
	MQC	40	40.081 \pm 0.716	1.79	0.2
	HQC	150	152.030 \pm 2.727	1.79	1.35
Autosampler stability (24 h)	LQC	5	5.098 \pm 0.060	1.17	1.96
	MQC	40	39.960 \pm 0.722	1.81	-0.1
	HQC	150	151.951 \pm 2.756	1.81	1.3
TMZ-BOC					
Conditions	Level	Nominal conc. ($\mu\text{g/ml}$)	Observed conc. ($\mu\text{g/ml}$) Mean \pm SD	% RSD	% Bias
t= 0 h (for initial samples)	LQC	5	5.037 \pm 0.092	1.82	0.75
	MQC	40	39.854 \pm 0.362	0.91	-0.37
	HQC	150	150.682 \pm 0.675	0.45	0.45
Benchtop stability (24 h)	LQC	5	5.049 \pm 0.082	1.62	0.97
	MQC	40	40.062 \pm 0.433	1.08	0.16
	HQC	150	149.762 \pm 1.141	0.76	-0.16
Autosampler stability (24 h)	LQC	5	5.041 \pm 0.090	1.78	0.81
	MQC	40	40.119 \pm 0.336	0.84	0.3
	HQC	150	150.208 \pm 1.470	0.98	0.14

TMZ-H					
Conditions	Level	Nominal conc. ($\mu\text{g/ml}$)	Observed conc. ($\mu\text{g/ml}$) Mean \pm SD	% RSD	% Bias
t= 0 h (for initial samples)	LQC	5	5.071 \pm 0.088	1.74	1.42
	MQC	40	40.428 \pm 0.672	1.66	1.07
	HQC	150	152.626 \pm 2.711	1.78	1.75
Benchtop stability (24 h)	LQC	5	5.059 \pm 0.066	1.31	1.18
	MQC	40	40.416 \pm 0.649	1.61	1.04
	HQC	150	152.355 \pm 2.463	1.62	1.57
Autosampler stability (24 h)	LQC	5	5.086 \pm 0.094	1.86	1.73
	MQC	40	40.772 \pm 0.656	1.61	1.93
	HQC	150	152.219 \pm 2.238	1.47	1.48
AIC					
Conditions	Level	Nominal conc. ($\mu\text{g/ml}$)	Observed conc. ($\mu\text{g/ml}$) Mean \pm SD	% RSD	% Bias
t= 0 h (for initial samples)	LQC	5	5.043 \pm 0.074	1.46	0.85
	MQC	40	40.192 \pm 0.573	1.42	0.48
	HQC	150	152.053 \pm 1.574	1.04	1.37
Benchtop stability (24 h)	LQC	5	5.075 \pm 0.077	1.52	1.51
	MQC	40	40.111 \pm 0.586	1.46	0.28
	HQC	150	152.378 \pm 1.201	0.79	1.59
Autosampler stability (24 h)	LQC	5	5.065 \pm 0.087	1.71	1.3
	MQC	40	40.186 \pm 0.576	1.43	0.47
	HQC	150	151.793 \pm 1.472	0.97	1.2

2.4. UPLC-MS/MS-based bioanalytical method development and validation

2.4.1. Instrumentation conditions: Chromatographic and MS/MS parameters

Mass parameters for the determination and quantitation of all drugs and internal standard (tacrolimus (TAC)) was achieved on Waters® Xevo TQD mass spectrometer equipped with electrospray ionization (ESI) probe for better sensitivity operated in positive mode (Waters, Milford, Massachusetts, USA). The source capillary potential was set to 3.78 KV, ion source temperature to 150 °C, desolvation source temperature to 400 °C, desolvation source gas flow to 800 L/h and cone source gas flow to 5 L/h. The multiple reaction monitoring (MRM) mode with ion transition were optimized and used to quantify the drugs and IS in the samples

Chromatographic analysis was performed on Waters® Acquity H-Class UPLC-MS/MS equipped with Xevo TQD mass analyser (Waters, Milford, Massachusetts, USA). UPLC-MS/MS is combined with series of assemblies namely, UPLC-Quaternary solvent manager, UPLC-sample manage-FTN, with active column heater, automated high vacuum rotary turbo pump and automated nitrogen generator for its peak performance. Mass Lynx software (V4.1) was used for system control, data collection, peak analysis.

Liquid chromatographic separation of analytes (RAP, TMZ, TMZ-A, TMZ-H, AIC, and TAC (IS)) was performed on Waters ACQUITY UPLC BEH C18 Column (2.1 × 100 mm, 1.7 µm). The mobile phase consisted of A) Ammonium acetate buffer with 0.1% formic acid, B) Methanol. The column temperature was maintained at 35 °C with linear gradient elution at flow of 0.3 ml/min: 0-0.6 min A-60%, 0.6-0.7 min A-60% to 0%, 0.7-2.9 min A- hold at 0%, 2.9-2.95 min A- 0% to 60%, 2.95-5.6 min A-60%. Thereafter, a linearity curve plot was prepared for drugs ranging from 0.976 ng/ml to 1000 ng/ml and tacrolimus as IS was kept constant. The sample temperature was set at 15 °C and injection volume was set at 10 µl.

2.4.2. Stock solutions, dilutions, calibrators and quality control samples

The stock solution of RAP, TMZ, TMZ-A, TMZ-H, AIC, and TAC were prepared by dissolving 10 mg of accurately weighed standard in methanol to give stock of 2 mg/ml. The stock solutions were diluted using methanol to give final working analytical standard solution of calibration standards equivalent ranging from 19.52 to 20,000 ng/ml. The internal standard (TAC; IS) was prepared by dissolving 2 mg of TAC in methanol to give stock solution of 2 mg/ml and further diluted using methanol to give working standard of 500 ng/ml. All the stock and working standard solutions were stored at -20 °C until further use.

Final calibrators and quality control samples were prepared by spiking 5 µl of working standard solution and 5 µl of IS to 90 µl of solvent or biological matrix. The concentrations of drug calibrators were prepared ranging from 0.976 to 1000 ng/ml with IS equivalent to 25 ng/ml. The four concentration level of quality control (QCs) samples were prepared in a similar manner including Lower limit of quantification (LLOQ), Low-level QC (LQC), Mid-level quality control (MQC), and High-level quality control (HQC) with minimum of 5 replicates of each QC level. The spiked standards were prepared and validated as per the ICH guidelines.

2.4.3. Sample preparation and drug extraction

The whole blood containing Na-EDTA was initially acidified with 10 µl of 0.1M L-ascorbic acid followed by spiking with 5 µl of drug solution and 5 µl of IS to 90 µl of acidified blood sample. The spiked blood sample was then allowed to incubate for 15 min for proper mixing. Furthermore, the obtained sample was processed using series of hybrid extraction method including lysis solution followed by protein precipitation or liquid-liquid extraction. The sample was screened with the addition of 50 µl of lysis solution (such as ammonium sulphate, zinc sulphate, ammonium acetate, 5% glacial acetic acid, 10% glacial acetic acid, 1% HCl, 1% formic acid, etc) and vortexed vigorously for 2 min.

For protein precipitation method, the precipitating agent (such as methanol, acetonitrile, and methanol: acetonitrile mixture (1:1)) was added and vortexed for 15 min followed by centrifugation at 15000 rpm for 10 min at 4 °C. The obtained supernatant was then taken and 10 µl of sample was injected and analyzed using developed simultaneous UPLC-MS/MS method.

For liquid-liquid extraction, the drug and IS spiked blood sample was taken and lysis solution was added and 1.5 ml of water immiscible solvent or extracting solvent (such as ethyl acetate, dichloromethane, tBME, diethyl ether, ethyl acetate:tBME mixture (1:1), ethylacetate: diethyl ether (1:1), etc) was added and vortexed for 15 min followed by centrifugation at 5000 rpm for 5 min at 4 °C. The supernatant was taken and dried under low vacuum at 37 °C. The dried sample was reconstituted in 100 µl of mobile phase and 10 µl of sample was injected and analysed using developed simultaneous UPLC-MS/MS method.

2.4.4. Assay validation

The developed UPLC-MS/MS method for the various analytes including RAP, TMZ, TMZ-A, TMZ-H, and AIC was developed and validated according to the ICH-bioanalytical

method validation guidelines [3]. The method was validated in terms of selectivity, linearity, sensitivity, accuracy, precision, recovery, matrix effect, carry over effects, and stability.

2.4.4.1. Selectivity

Selectivity of the developed method was investigated in the presence and absence of the biological matrix components. The test was performed by comparing 3 replicates of analytical spiked sample (drug/IS in MeOH) with 3 replicates of matrix blank (processed whole blood) and 3 replicates of spiked matrix sample (drug/IS in extracted sample) at low and high QC level each. The obtained chromatogram must be free of interference at the elution time of the analyte and IS of interest with % RSD in limits (analyte $\leq 20\%$ for LLOQ and $\leq 15\%$ for LQC, MQC and HQC).

2.4.4.2. Linearity

The developed method was assessed for the linearity range of the analyte of interest and IS spiked into the whole blood with the final concentration ranging from 0.976 ng/ml to 1000 ng/ml. The analyte/IS spiked into matrix was extracted as mentioned in section 2.4.3. The peak area ratio of analyte of interest and IS with a minimum of 3 calibration curve is run over the period of several days were used to evaluated for the linearity of the assay and the calibration with R^2 value greater than 0.99 and minimum of 75% of the calibrators must fall within the limit of acceptance were considered for further experimentation.

2.4.4.3. LLOQ, LOD, LOQ, Sensitivity

The sensitivity of the developed method will be determined in terms of Lower Limit of Quantification (LLOQ), which is considered as the lowest concentration that could be measured with % RSD within $\leq 20\%$ with signal to noise (S/N) ≥ 10 compared to drug free extracted matrix. The calibrators were utilized to determine the Limit of Detection (LOD) and Limit of Quantification (LOQ) using the below mentioned formula:

$$LOD = 3.3 \times \sigma/m \quad eq. 2.5$$

$$LOQ = 10 \times \sigma/m \quad eq. 2.6$$

Where, σ is standard deviation of intercept of regression and m is slope of calibration.

The S/N ratio was determined using minimum of 6 chromatograms of analyte/IS extracted from pooled biological matrix.

2.4.4.4. Accuracy and precision

The developed method was assessed for accuracy and precision using the quality control samples (LLOQ, LQC, MQC, HQC). The freshly prepared QC samples were performed in the format with minimum of 3 replicates per each QC level analyzed on 3 different working days. The acceptance criteria for intraday and interday accuracy and precision must fall within the limits with % RSD and % Bias of ≤ 15 and $\leq 15\%$, respectively, except for LLOQ the acceptance criteria was $\leq 20\%$ in all the runs.

2.4.4.5. Recovery and matrix effect

The recovery of the extraction process was determined using the QC levels (LQC, MQC, and HQC) compared with the peak area ratio response from the drug/IS spiked in both pre- and post-extraction samples. The extraction recovery process need not to be 100%, the process must be efficient and reproducible in all the sets.

The matrix effect was evaluated using the post extraction addition method, wherein, the biological samples from the multiple sources (atleast 6) was pooled to determine the interference of the biological matrix/metabolites with the analyte and IS. Minimum of 3 replicates of QC sets were utilized to determine the effect by comparing the peak area ratio responses of the spiked neat solution in mobile phase (set 1) with the blank post-extraction samples spiked at equivalent concentration (set 2). The matrix effect is calculated using the below mentioned formula, and expressed as % ME, that should be $\leq 15\%$:

$$\%ME = \frac{\text{Response of set 1} - \text{Response of set 2}}{\text{response of set 1}} \times 100$$

If % ME is equals to zero, means no matrix effect, while % ME < 0 or > 0 is considered as ion enhancement or suppression, respectively.

2.4.4.6. Carry over effect

Carry over effect of analyte and IS was evaluated by injecting highest analyte concentration followed by two blank injections. The process was performed thrice for every biological matrix and must follow the criteria with carry over NMT $\leq 20\%$ of LLOQ and $\leq 5\%$ for the IS. Additionally, an extensive method was used to wash the needle using the mixture of methanol: acetonitrile: water (45:45:10) for 10 sec, followed by next injection.

2.4.4.7. Stability

Stability studies of analytes and IS were performed on the basis of short-term stability by keeping the QC samples (LLOQ, LQC, MQC, and HQC) in laboratory conditions (bench-top stability) at 25 °C for 4 h, autosampler stability of the extracted samples was evaluated at 8 °C after 24 h. Minimum of three replicates of QC sets must be evaluated and fall within the acceptance criteria of % Bias \leq 15% for all the samples.

2.4.5. Result and discussion

2.4.5.1. Chromatographic and MS/MS conditions

The analyte and IS detection and quantification method were developed using electrospray ionization (ESI) probe set in positive mode (ESI+). The positive ionization mode produced $[M+H]^+$, $[M+Na]^+$, and $[M+K]^+$ adducts for the analyte and IS. MS/MS based parameters were optimized for better sensitivity with capillary potential of 3.78 KV and desolvation temperature was set at 400 °C. The MRM transitions of molecules were obtained. The transitions for RAP (931.2 \rightarrow 864.66), TMZ (194.9 \rightarrow 137.95), TMZ-A (195.88 \rightarrow 138.93), TMZ-H (209.91 \rightarrow 152.96), AIC (126.89 \rightarrow 109.91), and IS TAC (821.13 \rightarrow 768.56), with cone potential of 36, 22, 22, 22, 22, and 34V, at collision energy equivalent to 16, 10, 8, 10, 8, and 22 V, respectively, were used to determine the concentration of the drugs and IS in the samples. All other working parameters of UPLC-MS/MS are listed in below mentioned table 2.6. The detailed MS and MRM transitions are mentioned in table 2.7. Figure 2.5 shows the parent ion and daughter ion optimization (at their respective cone and collision energy potential) for the analytes and IS.

For extraction of drug, a hybrid method (salting out with liquid-liquid extraction) was adopted, wherein, initially, 50 μ l of 0.5 M ammonium sulfate as lysis salt was added and vortexed for 2 min, followed by extraction of analytes using 1200 μ l of ethyl acetate (EA) and vortexed for 30 min as mentioned in section 2.4.3. The samples were centrifuged at 5000 rpm for 5 min at 4 °C. The supernatant was carefully collected and transferred to vials, and the same process was repeated for the second time. The collected organic layer was evaporated to dryness and reconstituted with 100 μ l of mobile phase, followed by 10 μ l of sample volume injected and analysed using developed simultaneous UPLC-MS/MS method. Liquid chromatographic separation for detection and quantification of RAP, TMZ and its derivatives were obtained in a gradient elution mode due to different physiochemical properties of the analytes. The developed LC method eluted the RAP (2.93 min), TAC (2.92 min), TMZ

Table 2.6. UPLC-MS/MS parameters for RAP, TMZ, TMZ-A, TMZ-H, AIC, and TAC

Waters® UPLC-MS/MS parameters	
Capillary potential	3.78 KV
Desolvation temp	400 °C
Desolvation gas	800 L/h
Cone gas	5 L/h
Source temp	150 °C
Mobile phase	Methanol: Ammonium acetate (pH 3.6)
Flow rate	0.3 ml/min
Mode of elution	Gradient
Linearity	0.976-1000 ng/ml
Elution time	RAP (2.93 min)
	TAC (2.92 min)
	TMZ (0.84 min)
	TMZ-A (0.84 min)
	TMZ-H (0.82 min)
AIC (0.77 min)	

Table 2.7. Mass parameters for RAP, TMZ, TMZ-A, TMZ-H, AIC, and TAC

MS/MS parameters			
Analyte of interest	MRM transition	Cone Potential	Collision energy
RAP	931.2 → 864.66	36	16
TMZ	194.9 → 137.95	22	10
TMZ-A	195.88 → 138.93	22	8
TMZ-H	209.91 → 152.96	22	10
AIC	126.89 → 109.91	22	8
TAC (IS)	821.13 → 768.56	34	22

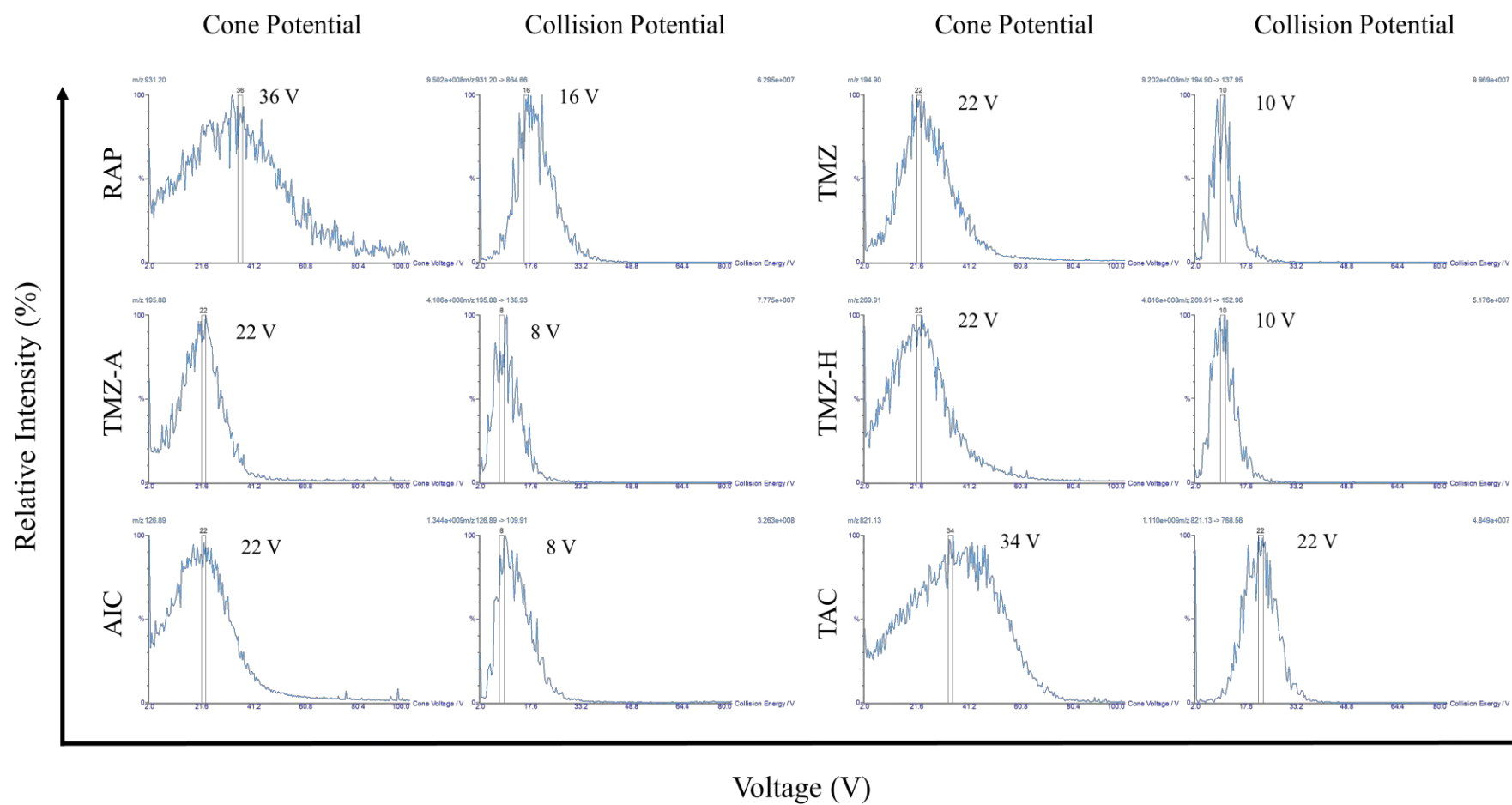


Figure 2.5. Cone and collision potential optimisation for parent ion and daughter ion for RAP, TMZ, TMZ-A, TMZ-H, AIC, and TAC

(0.84 min), TMZ-A (0.84 min), TMZ-H (0.82 min), and AIC (0.77 min) using methanol: ammonium acetate as a mobile phase. The simultaneous method yielded uniform peak shape for qualitative and quantitative analysis with improved sensitivity. Representative chromatogram for the respective analyte and IS are shown in figure 2.6, depicting the analyte standard of RAP, TAC, TMZ, TMZ-A, TMZ-H, and AIC.

2.4.5.2. Method validation

The developed UPLC-MS/MS method fulfilled and validated the criteria according to the ICH-bioanalytical method validation guidelines, in terms of selectivity, linearity, sensitivity, accuracy, precision, recovery, matrix effect, carry over effects, and stability. The developed method did not show any interference at the retention time of analyte and IS. Moreover, the analyte and IS extracted sample showed the similar retention time as of the analytical sample (neat sample in mobile phase) without any interference, suggesting the selectivity of the analysis. The developed method demonstrated the linearity for all the samples over the concentration range of 0.976-1000 ng/ml with IS equivalent to 25 ng/ml with a correlation regression coefficient (R^2) of >0.99 with calibration equation of the analytes mentioned in table 2.8.

The sensitivity of the method was estimated in terms of the LOD, and LOQ. The LOD of the developed UPLC-MS/MS assay in the whole blood was found to be 40, 68, 161, 891, and 80 pg/ml and LOQ of 122, 208, 488, 2700, and 244 pg/ml for RAP, TMZ, TMZ-A, TMZ-H, and AIC, respectively (Table 2.8). However, the % RSD of the LLOQ in all the extracted biological samples were within $\leq 20\%$ with S/N ratio ≥ 10 . The developed method was found to show intra-day and inter-day accuracy and precision with % RSD and % Bias within the acceptable limits of $\leq 15\%$, except for LLOQ the criteria is $\leq 20\%$ in all the runs, as per recommended in the bioanalytical method validation guidelines (Table 2.9). The developed extraction protocol matrix effect was found to be within the acceptable limits as per the guidelines. Also, no carryover effect was detected in the blank for the analyte and IS after injected with LQC, MQC, and HQC.

The stability of the analyte in the biological matrix (whole blood) was determined based on bench-top stability for 4 h at 25 °C. The samples were found to be stable with % RSD of less than 10% for all the samples. The autosampler stability studies were also performed to check the stability of the samples during the analysis for over the period of 24 h kept at 8 °C.

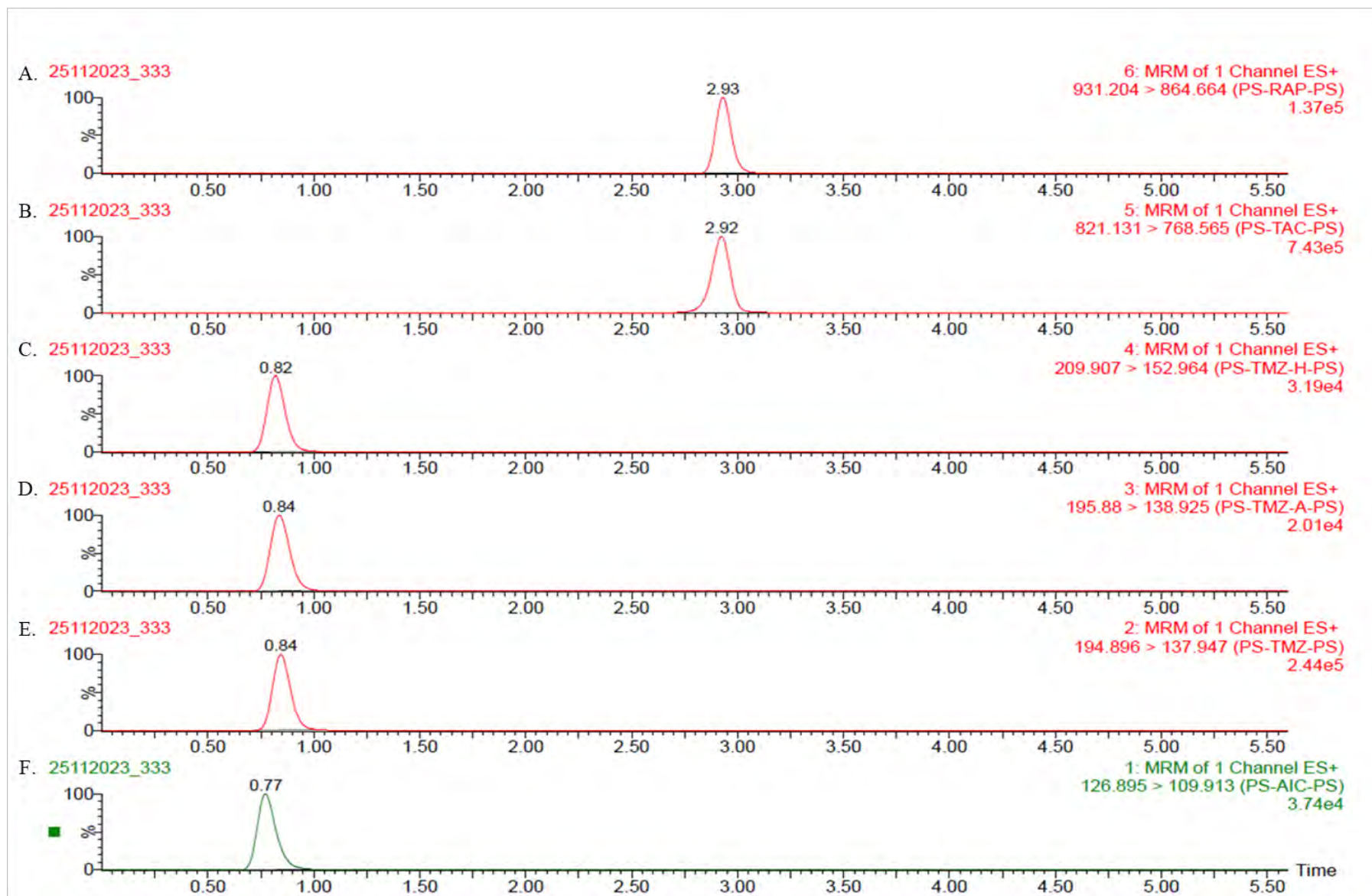


Figure 2.6. Representative chromatogram for A) RAP, B) TAC, C) TMZ-H, D) TMZ-A, E) TMZ, and F) AIC (top to bottom)

Table 2.8. Calibration curve equation and sensitivity for RAP, TMZ, TMZ-A, TMZ-H, and AIC

Molecule	Regression equation	Regression coefficient (R²)	LOD (pg/ml)	LOQ (pg/ml)
RAP	Y=0.7216x + 5.6898	0.9989	40	122
TMZ	Y=0.5613x + 3.6363	0.9994	68	208
TMZ-A	Y=0.3447x + 1.7218	0.9986	161	488
TMZ-H	Y=0.2764x – 1.1641	0.9997	891	2700
AIC	Y=0.4653x + 6.4037	0.9998	80	244

Table 2.9. Intra-day and Inter-day accuracy and precision of RAP, TMZ, TMZ-A, TMZ-H, and AIC in whole blood as a biological matrix

RAP							
Level	Nominal conc. (ng/ml)	Intra day			Inter day		
		Observed conc. (ng/ml) Mean \pm SD	% RSD	% Bias	Observed conc. (ng/ml) Mean \pm SD	% RSD	% Bias
LLOQ	3	2.81 \pm 0.19	6.86	-6.22	2.83 \pm 0.19	6.76	-5.78
LQC	100	106.7 \pm 7.29	6.83	6.7	107.03 \pm 6.62	6.19	7.03
MQC	450	431.74 \pm 25.16	5.83	-4.06	434.25 \pm 22.86	5.27	-3.5
HQC	800	814.68 \pm 41.05	5.04	1.83	822.45 \pm 37.48	4.56	2.81

TMZ							
Level	Nominal conc. (ng/ml)	Intra day			Inter day		
		Observed conc. (ng/ml) Mean \pm SD	% RSD	% Bias	Observed conc. (ng/ml) Mean \pm SD	% RSD	% Bias
LLOQ	1.5	1.49 \pm 0.19	12.61	-0.38	1.49 \pm 0.19	12.9 4	-0.88
LQC	100	103.65 \pm 13.70	13.21	3.65	106.25 \pm 7.15	6.73	6.25
MQC	450	469.05 \pm 33.31	7.1	4.23	462.51 \pm 31.88	6.89	2.78
HQC	900	918.97 \pm 82.98	9.03	2.11	899.46 \pm 76.60	8.52	-0.06

TMZ-A							
Level	Nominal conc. (ng/ml)	Intra day			Inter day		
		Observed conc. (ng/ml) Mean \pm SD	% RSD	% Bias	Observed conc. (ng/ml) Mean \pm SD	% RSD	% Bias
LLOQ	1.5	1.49 \pm 0.13	8.52	-0.9	1.47 \pm 0.13	9.07	-2
LQC	100	105.76 \pm 7.47	7.07	5.76	105.10 \pm 7.83	7.45	5.1
MQC	450	455.95 \pm 34.32	7.53	1.32	451.21 \pm 35.33	7.83	0.27
HQC	900	900.44 \pm 90.72	10.08	0.05	876.69 \pm 79.22	9.04	-2.59

TMZ-H							
Level	Nominal conc. (ng/ml)	Intra day			Inter day		
		Observed conc. (ng/ml) Mean \pm SD	% RSD	% Bias	Observed conc. (ng/ml) Mean \pm SD	% RSD	% Bias
LLOQ	5	5.37 \pm 0.56	10.45	7.36	5.48 \pm 0.47	8.56	9.69
LQC	100	96.77 \pm 1.04	10.05	3.47	94.21 \pm 8.64	9.17	-5.79
MQC	450	414.36 \pm 21.13	5.1	-7.92	409.99 \pm 18.73	4.57	-8.89
HQC	900	902.19 \pm 71.91	7.97	0.24	892.59 \pm 67.21	7.53	-0.82

Table 2.9. continued

AIC							
Level	Nominal conc. (ng/ml)	Intra day			Inter day		
		Observed conc. (ng/ml) Mean \pm SD	% RSD	% Bias	Observed conc. (ng/ml) Mean \pm SD	% RSD	% Bias
LLOQ	6	6.27 \pm 0.67	10.62	4.43	6.19 \pm 0.66	10.68	3.24
LQC	100	105.28 \pm 9.10	8.65	5.28	105.92 \pm 5.92	7.54	5.92
MQC	450	438.17 \pm 48.34	11.03	-2.63	438.43 \pm 47.30	10.79	-2.57
HQC	900	908.42 \pm 67.96	7.48	0.94	899.1 \pm 66.95	7.45	-0.10

Table 2.10. Stability studies of RAP, TMZ, TMZ-A, TMZ-H, and AIC in whole blood as a biological matrix

RAP						
Conditions	Level	Nominal conc. (ng/ml)	Observed conc. (ng/ml) Mean \pm SD	% RSD	% Bias	
t= 0 h (for initial samples)	LLOQ	3	2.82 \pm 0.2	7.12	-5.93	
	LQC	100	107.72 \pm 7.16	6.65	7.72	
	MQC	450	433.25 \pm 27.55	6.36	-3.72	
	HQC	800	811.89 \pm 44.2	5.44	1.49	
Benchtop stability 24 h	LLOQ	3	2.83 \pm 0.2	7.04	-5.56	
	LQC	100	105.47 \pm 7.41	7.02	5.47	
	MQC	450	432.4 \pm 25.29	5.85	-3.91	
	HQC	800	808.44 \pm 42.27	5.23	1.05	
Autosampler stability 24 h	LLOQ	3	2.77 \pm 0.15	5.55	-7.82	
	LQC	100	106.99 \pm 7.77	7.27	6.99	
	MQC	450	433.76 \pm 26.68	6.15	-3.61	
	HQC	800	814.79 \pm 44.70	5.49	1.85	

TMZ					
Conditions	Level	Nominal conc. (ng/ml)	Observed conc. (ng/ml)	% RSD	% Bias
			Mean \pm SD		
t= 0 h (for initial samples)	LLOQ	1.5	1.53 \pm 0.19	12.21	1.99
	LQC	100	102.58 \pm 14.67	14.3	2.58
	MQC	450	466.73 \pm 36.31	7.78	3.72
	HQC	900	914.38 \pm 89.79	9.82	1.6
Benchtop stability 24 h	LLOQ	1.5	1.45 \pm 0.18	12.16	-3.03
	LQC	100	104.82 \pm 14.83	14.14	4.82
	MQC	450	476.33 \pm 31.61	6.64	5.85
	HQC	900	940.33 \pm 72.42	7.7	4.48
Autosampler stability 24 h	LLOQ	1.5	1.48 \pm 0.18	12.22	-1.18
	LQC	100	102.33 \pm 14.59	14.26	2.33
	MQC	450	465.18 \pm 34.12	7.33	3.37
	HQC	900	927.87 \pm 78.47	8.46	3.1
TMZ-A					
Conditions	Level	Nominal conc. (ng/ml)	Observed conc. (ng/ml)	% RSD	% Bias
			Mean \pm SD		
t= 0 h (for initial samples)	LLOQ	1.5	1.49 \pm 0.13	8.71	-0.77
	LQC	100	104.54 \pm 7.54	7.21	4.54
	MQC	450	455.22 \pm 37.90	8.32	1.16
	HQC	900	898.55 \pm 99.64	11.09	-0.16
Benchtop stability 24 h	LLOQ	1.5	1.49 \pm 0.13	8.78	-0.46
	LQC	100	108.21 \pm 5.24	4.84	8.21
	MQC	450	464.21 \pm 28.23	6.08	3.16
	HQC	900	920.99 \pm 85.09	9.24	2.33
Autosampler stability 24 h	LLOQ	1.5	1.48 \pm 0.13	8.88	-1.45
	LQC	100	105.5 \pm 7.95	7.54	5.5
	MQC	450	451.91 \pm 36.02	7.97	0.42
	HQC	900	908.87 \pm 97.31	10.71	0.99

TMZ-H					
Conditions	Level	Nominal conc. (ng/ml)	Observed conc. (ng/ml) Mean \pm SD	% RSD	% Bias
t= 0 h (for initial samples)	LLOQ	5	5.47 \pm 0.47	8.62	9.44
	LQC	100	96.24 \pm 9.01	9.36	-3.76
	MQC	450	415.95 \pm 22.34	5.37	-7.57
	HQC	900	911.21 \pm 73.65	8.08	1.25
Benchtop stability 24 h	LLOQ	5	5.34 \pm 0.62	11.53	6.85
	LQC	100	97.85 \pm 10.66	10.9	-2.15
	MQC	450	414.75 \pm 19.94	4.81	-7.83
	HQC	900	902.19 \pm 71.91	7.97	0.24
Autosampler stability 24 h	LLOQ	5	5.27 \pm 0.57	10.74	5.4
	LQC	100	97.2 \pm 10.2	10.49	-2.8
	MQC	450	413.9 \pm 20.86	5.04	-8.02
	HQC	900	915.63 \pm 72.0	7.86	1.74
AIC					
Conditions	Level	Nominal conc. (ng/ml)	Observed conc. (ng/ml) Mean \pm SD	% RSD	% Bias
t= 0 h (for initial samples)	LLOQ	6	6.2 \pm 0.67	10.74	3.29
	LQC	100	103.87 \pm 9.38	9.03	3.87
	MQC	450	442.08 \pm 52.05	11.77	-1.76
	HQC	900	904.14 \pm 73.79	8.16	0.46
Benchtop stability 24 h	LLOQ	6	6.24 \pm 0.69	11.13	4.01
	LQC	100	106.83 \pm 8.42	7.88	6.83
	MQC	450	444.89 \pm 49.84	11.2	-1.13
	HQC	900	925.31 \pm 59.44	6.42	2.81
Autosampler stability 24 h	LLOQ	6	6.37 \pm 0.59	9.3	6.15
	LQC	100	105.45 \pm 9.2	8.72	5.45
	MQC	450	435.91 \pm 44.59	10.23	-3.13
	HQC	900	900.58 \pm 59.52	6.61	0.06

The results indicated the % RSD was within the accepted criteria with % RSD value within the limits. The detailed values of the stability analysis are shown in table 2.10.

2.5. Conclusion

In section 2.2, a simple UV-Vis spectrophotometer-based analytical method was developed and validated as per the ICH guidelines. Thereafter, in section 2.3, a simple isocratic reverse phase HPLC-UV-based analytical method was developed and validated to analyze multiple analytes, including RAP, TMZ, TMZ-A, TMZ-BOC, TMZ-H, and AIC. The calibration curve showed linearity over a wide concentration range from 0.390 µg/ml to 200 µg/ml for multiple analytes with a regression coefficient (R^2) of >0.99. The analytical method was validated as per the ICH guidelines for selectivity, linearity, accuracy, precision, sensitivity, carryover, and stability. Thus, the developed analytical method could be utilized to monitor the reaction, purity profiling, and determine the concentration of analytes in an unknown sample.

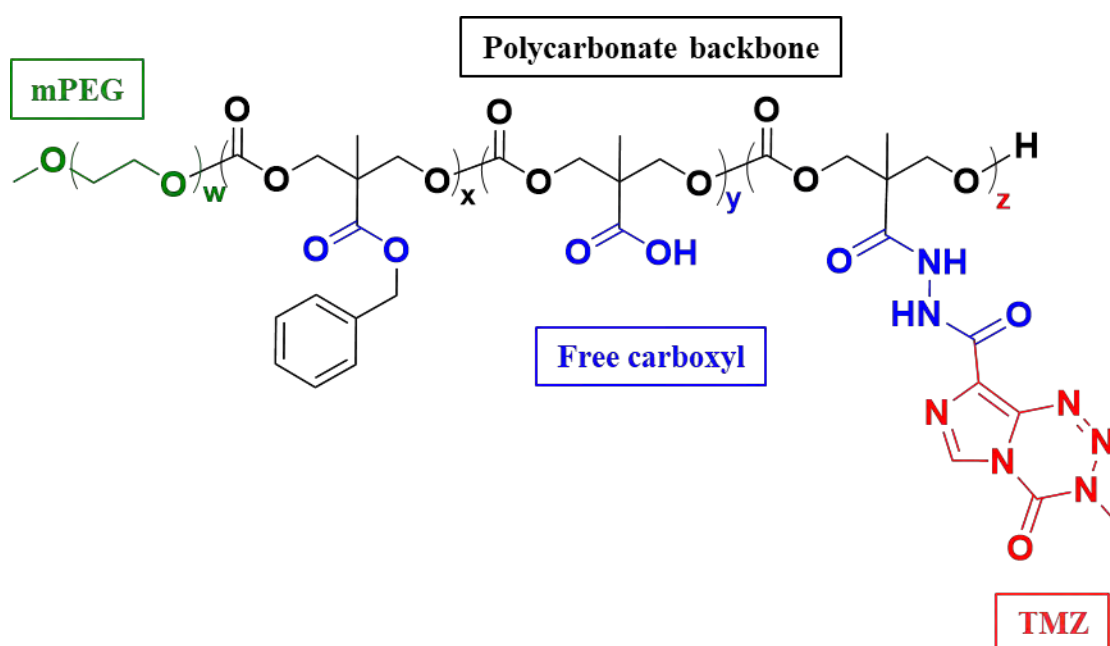
After that, in section 2.4, a highly sensitive, UPLC-MS/MS based simultaneous method for RAP, TMZ, and its derivatives was developed and validated as per the ICH guidelines. The developed method exhibited a linearity over the range of 0.976 to 1000 ng/ml in whole blood as a biological matrix with correlation regression coefficient (R^2) of >0.99. The method was found to show selectivity, accuracy, precision, with no matrix and carryover effect in whole blood was observed. The developed and validated method could be utilized for *in vivo* pharmacokinetics of analytes in animals.

2.6. References

- [1] Jatyan R, Sahel DK, Singh P, Sakhuja R, Mittal A, Chitkara D. Temozolomide-fatty acid conjugates for glioblastoma multiforme: In vitro and in vivo evaluation. *J Control Release* 2023;23:S0168-3659. <https://doi.org/10.1016/j.jconrel.2023.05.012>.
- [2] ICH-Q2R2. VALIDATION OF ANALYTICAL PROCEDURES 2023:36. https://database.ich.org/sites/default/files/ICH_Q2%28R2%29_Guideline_2023_1130.pdf.
- [3] ICH. Bioanalytical Method Validation and Study Sample Analysis M10 2022:1–59. https://database.ich.org/sites/default/files/M10_Guideline_Step4_2022_0524.pdf.

Chapter 3

Design, synthesis, and characterization of polycarbonate-based polymeric conjugates of temozolomide



3.1. Introduction

Temozolomide (TMZ) is a second-generation DNA alkylating agent and used as a standard-of-care chemotherapeutic agent for the treatment of glioblastoma multiforme (GBM). Though a potent molecule, TMZ exhibits several limitations, such as short half-life, rapid pH-dependent hydrolysis, and speedy clearance, resulting in lesser accumulation in the brain. Hydrolysis of the molecule under physiological conditions results in the conversion of TMZ into its metabolite, MTIC (3-methyl-(triazene-1-yl)imidazole-4-carboxamide) and AIC (5-aminoimidazole-4-carboxamide), which cannot permeate into the cells effectively. Only <1% of the dose reaches the brain intact, thereby rendering the drug with sub-therapeutic outcomes. In order to achieve the therapeutic effect, high doses of TMZ are given, resulting in dose-dependent hematological toxicities. Several approaches have been explored to overcome these limitations, including its encapsulation in nanocarriers of organic (lipids, polymers, dendrimers, etc.) and inorganic (silica, quantum dots, gold, silver, etc.) materials that showed improved TMZ delivery as well as preparation of conjugates with small molecules and polymers [1]. TMZ has a solubility of 5 mg/ml, posing challenges in encapsulating into the nanocarriers. In the conjugation approach TMZ has been conjugated with small molecules such as doxorubicin, γ -carbolines, 5-nitro-2-(3-phenylpropylamino)-benzoate (NPPB), perillyl alcohol, etc. and polymer including poly-(2-methacryloyloxyethyl phosphorylcholine) (MPC), poly(β -L-malic acid), poly(2-ethyl-2-oxazoline), etc [2–8]. TMZ conjugated to the polymeric backbone demonstrated improved drug loading capacity, systemic circulation, tissue targeting, ease in fabrication, and better biocompatibility. Likewise, a series of polymer-TMZ conjugates depicted an effecting drug loading capacity up to 35-50 mol% with improved stability half-life ranging from 2-19 folds compared to free TMZ. The *in vitro* cell-based assay also depicted marked enhancement in the cytotoxicity and uptake in glioma cell lines [6]. In another study, multifunctional targeted poly(β -L-malic acid) conjugated to TMZ was synthesized, resulting in particles of 6.5-14.8 nm, improved loading capacity up to 17% w/w with enhanced stability of TMZ from 1.8 h to 5-7 h [7]. We have previously reported the drug conjugates using PEG-polycarbonate, providing ample opportunity to attach the drug to the polycarbonate backbone with improved loading capacity, stability, and efficacy [9]. Similarly, Jiang et al. conjugated doxorubicin to amphiphilic block copolymer, mPEG-b-P(ATMC-co-DTC) *via*. hydrazone linkage. The resulting self-assembled nanoconjugate showed 90-140 nm particles with a loading capacity of 9.9-12.5% w/w. The polymer-DOX conjugate demonstrated stimuli-sensitive drug release kinetics, effective cellular uptake, and cytotoxicity profile against HeLa

cells [10]. Liang et al. fabricated pegylated aliphatic polycarbonate copolymer DOX conjugate using a benzoic imine linker. The conjugate self-assembles to form a particle of 49 nm with a drug loading efficiency of 18.3% w/w. The drug-polymer conjugate NP showed better colloidal stability under physiological conditions and exhibited stimuli-based drug release in tumor microenvironment condition, consequently becoming a potential candidate for an effective and safer drug delivery system [11].

In the current research, a series of PEG-based TMZ-polymer conjugates (*mPEG-b-P(CB-{g-COOH}; g-TMZ_n)*) (wherein, n= 20, 40, and 60 units) were prepared consisting of polymer backbone and temozolomide covalently attached *viz.* hydrazine linker. A thorough screening and characterization were performed using NMR, and its nanoformulation was prepared and evaluated using DLS and UV spectroscopy for particle size and stability.

3.2. Experimental section

3.2.1. Materials

Temozolomide (TMZ, >98%), tert-butyl carbazate, 1H-Benzotriazol-1-yloxytripyrrolidinophosphonium Hexafluorophosphate (PyBOP), N,N-Diisopropylethylamine (DIPEA) were purchased from TCI chemicals (Tokyo, Japan). SnakeSkin™ Dialysis Tubing (MWCO. 10 KDa) was procured from ThermoFisher Scientific (Massachusetts, United States). Methoxy poly(ethylene glycol) (mPEG, 5000 Da) and Tin(II) 2-ethylhexanoate were obtained from Sigma-Aldrich (St. Louis, Missouri, United States). 1,4-Dioxane and Palladium on carbon (Pd/C) were purchased from Spectrochem (Mumbai, India). 1-(3-Dimethylaminopropyl)-3-ethylcarbodiimide hydrochloride (EDC.HCl) and Hydroxybenzotriazole (HOBt) were obtained from Sisco Research Laboratories (Mumbai, India). All other reagents and chemicals used were of analytical grade and bought from local vendors.

3.2.2. Synthesis of polymeric drug conjugate of TMZ (*mPEG-b-P(CB-{g-COOH}; g-TMZ_n)*)

A series of polymeric conjugates of TMZ were synthesized by reacting TMZ hydrazide derivative with amphiphilic *mPEG-b-P(CB-{g-COOH})* copolymer. TMZ-hydrazide derivative was synthesized using a multistep reaction (Figure 3.1). Initially, TMZ (**1**) was converted to TMZ acid (**2**), then reacted with t-butyl carbazate to form TMZ-Boc-protected TMZ hydrazide (**3**), followed by cleavage of Boc using saturated dioxane-HCl to afford unprotected TMZ hydrazide (**4**). An amphiphilic copolymer, *mPEG-b-P(CB-{g-COOH})*, with carboxyl pendant

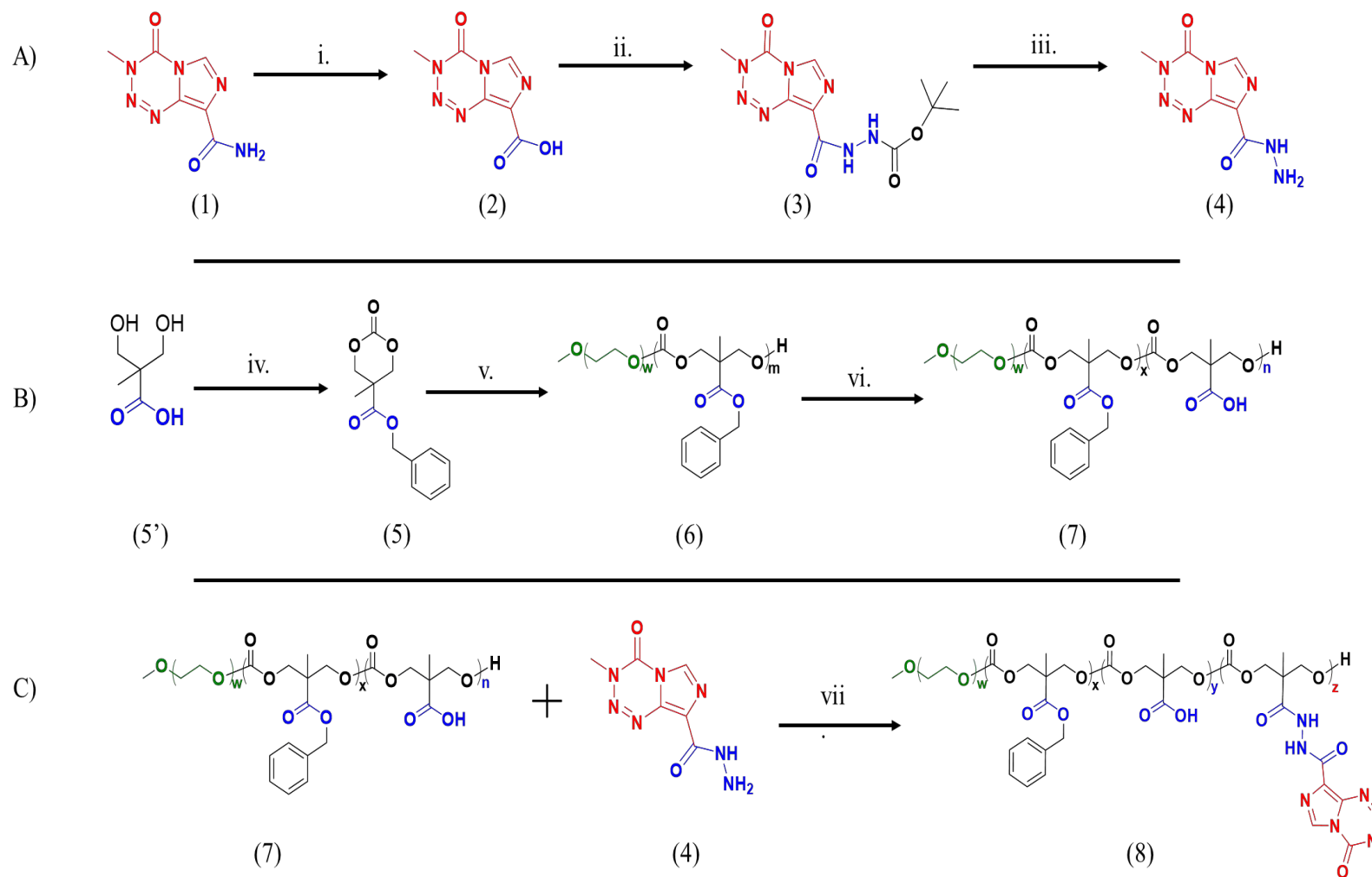


Figure 3.1. Reaction scheme for the synthesis of TMZ-polymer conjugates. A) Synthesis of TMZ hydrazide: i) NaNO_2 , H_2SO_4 , 4–8 °C, overnight, ii) *t*-butyl carbazate, PyBOP, triethylamine, overnight, iii) 1,4-dioxane.HCl, 4–6 h, B) Synthesis of polycarbonate polymer with free COOH group: iv) Benzyl bromide, KOH, 100 °C, overnight, then triphosgene, pyridine, acetone-dry ice bath, 4 h, v) *m*PEG (Mn. 5000), tin(II)-ethylhexanoate, microwave-assisted ring-opening polymerization, 130 °C, 1 h, vi) Palladium on carbon, H_2 , 5 h, C) Synthesis of TMZ-polymer conjugates (*m*PEG-*b*-*P*(CB-*g*-COOH; *g*-TMZ_{*n*}): vii) EDC/HOBt coupling, DIPEA, N_2 , 4–8 °C

groups was synthesized in a multistep reaction, wherein MBC (**5**) carbonate monomer was synthesized by reported procedure [12], followed by ring-opening polymerization with mPEG as macroinitiator to yield *mPEG-b-P(CB)* (**6**) copolymer. The protective benzylic pendant was removed using catalytic hydrogenation to obtain the *mPEG-b-P(CB-{g-COOH})* (**7**). TMZ hydrazide derivative (**4**) was reacted to *mPEG-b-P(CB-{g-COOH})* (**7**) copolymer using EDC/HOBt coupling to obtain polymer conjugate of TMZ (*mPEG-b-P(CB-{g-COOH}; g-TMZ_n)*) (**8**). All reactions were carried out under a dry nitrogen atmosphere using the standard protocol. The synthesized intermediates, monomers, and polymers were thoroughly characterized using ¹H NMR (400MHz) and ¹³C NMR (101MHz) spectra using Bruker AVANCE III 400 MHz NMR spectrometer (Billerica, Massachusetts, United States) at 20 °C either using DMSO-*d*₆ or CDCl₃ with tetramethylsilane (TMS) as an internal reference. High-resolution mass (HRMS) spectra were recorded using an Agilent Technologies 6545 Q-TOF LC/MS system (Agilent Technologies, Inc., California, United States) with electrospray ionization mode to detect the mass of monomers and their adducts. UV-visible spectra for synthesized compounds were recorded using a Jasco-V750 spectrophotometer (Tokyo, Japan) at room temperature with a path length of 1 cm over the 200-800 nm wavelength range.

3.2.2.1. Synthesis of Temozolomide acid (TMZ-A) (**2**)

TMZ (**1**) with an amide group was converted to a free -COOH group by the reported procedure [13]. TMZ-A (**2**) was prepared by dissolving TMZ (**1**) (0.5 g, 2.577 mmol) in 4 ml conc. H₂SO₄, a sodium nitrite solution (9.4 mmol, 0.65 g), was added dropwise with continuous nitrogen flow under ice-chilled conditions to remove the gaseous by-product, and the reaction mixture was allowed to stir overnight at room temperature. Further, the reaction mixture containing TMZ-A (**2**) was precipitated by adding ice-chilled water for 30 min. The precipitated product was thus filtered and dried under vacuum to yield final TMZ-A (**2**).

3.2.2.2. Synthesis of Boc-protected Temozolomide-hydrazide (TMZ-Boc) (**3**)

TMZ-A (**2**) containing free COOH group was attached with the *t*-butyl carbazate to prepare the TMZ-Boc (**3**) using PyBOP coupling chemistry. Briefly, a mixture of TMZ-A (**2**) (1 g, 5.128 mmol, 1 equiv.), Benzotriazol-1-yl-oxytripyrrolidinophosphonium hexafluorophosphate (PyBOP) (2.93 g, 5.64 mmol, 1.1 equiv.) and triethylamine (TEA) (1.07 ml, 0.778 g, 7.69 mmol, 1.5 equiv.) was added in 30 ml of dried acetonitrile. After that, *t*-butyl carbazate (0.745 g, 5.64 mmol, 1.1 equiv.) was added to the reaction mixture under ice-cold conditions and stirred at room temperature overnight under a nitrogen atmosphere. After

completion of reaction, solvent was evaporated under reduced pressure and crude precipitate was dissolved in dichloromethane (DCM) and was washed with a saturated sodium chloride solution twice. Organic layer was collected, dried over anhydrous sodium sulfate and evaporated to obtain a thick light yellow waxy liquid. The mixture was then purified using column chromatography, followed by washing with ice-cold diethyl ether to yield pure compound (**3**)

3.2.2.3. Synthesis of Temozolomide hydrazide (TMZ-H) (**4**)

After that, compound **3** containing protective Boc group was cleaved under the acidic environment to get TMZ-H (**4**) as reported previously [7]. TMZ-H (**4**) was synthesized by deprotecting compound **3** (1 g, 3.23 mmol) using 40 ml of 1,4-dioxane saturated with HCl in a 100 ml round bottom flask under cold conditions for 4-6 h. Reaction was monitored by using thin layer chromatography (TLC). Upon completion of the reaction, the solvent was removed using a vacuum, and the solid obtained was washed with diethyl ether to yield TMZ-H (**4**) having free amine (-NH₂) end group of hydrazine attached to imidazotetrazine derivative.

3.2.2.4. Synthesis of mPEG-polycarbonate polymer (mPEG-b-P(CB)) (**6**)

The *mPEG-b-P(CB)* (**6**) copolymer was synthesized using microwave-assisted ring-opening polymerization (ROP) of MBC (**5**) carbonate monomer with mPEG as macroinitiator using tin(II) ethyl hexanoate as a catalyst at 130 °C for 1 h. MBC (**5**) monomer was synthesized as reported earlier [12]. The crude polymer was purified using precipitation method by dissolving it in chloroform and precipitating with isopropyl alcohol and diethyl ether, twice. The purified copolymer was then dried under a vacuum and characterized using ¹H-NMR spectroscopy.

3.2.2.5. Synthesis of mPEG-carboxylic polycarbonate copolymer (mPEG-b-P(CB-{g-COOH})) (**7**)

mPEG-b-P(CB) (**6**) was subjected to catalytic hydrogenation to remove the protective benzylic group and obtain free carboxyl groups on the polycarbonate backbone. Briefly, *mPEG-b-P(CB)* (**6**) (2.0 g) was dissolved in dried tetrahydrofuran and methanol in a ratio 1:1 and taken in a glass vial to which 400 mg of Palladium on carbon (Pd/C) was added under nitrogen flow at ambient temperature. Hydrogenation of copolymer was done in hydrogenation parr apparatus at 40-45 psi pressure for 5 h. The copolymer was centrifuged and filtered using Celite 545[®] as a filter aid to remove the remaining Pd/C, followed by solvent removal and

drying under vacuum to give *mPEG-b-P(CB-{g-COOH})* containing free COOH as pendent groups (**7**). The free COOH groups were determined using the relative method by keeping mPEG (Mn. 5000 Da) as a constant.

3.2.2.6. Synthesis of temozolomide polymer-drug conjugate (*mPEG-b-P(CB-{g-COOH}; g-TMZ_n)*) (**8**)

A series of temozolomide-conjugated amphiphilic copolymers were synthesized using EDC-HOBT coupling chemistry. Briefly, a mixture of *mPEG-b-P(CB-{g-COOH})* (**7**) (0.3 g, 1.285 mmol of COOH, 1 equiv.), 1-Ethyl-3-(3-dimethylaminopropyl) carbodiimide hydrochloride (EDC.HCl) (0.37 g, 1.93 mmol, 1.5 equiv.), *N,N*-diisopropylethylamine (DIPEA) (560 μ l, 3.21 mmol, 2.5 equiv.) and hydroxybenzotriazole (HOBT) (0.26 g, 1.93 mmol, 1.5 equiv.) were added to 5 ml of dried dimethylformamide (DMF) under ice-cold conditions. After that, the mixture was activated under a nitrogen atmosphere for 0.5 h, followed by the addition of compound **4** (0.8 equiv. (215 mg, 1.03 mmol), 1.0 equiv. (269 mg, 1.29 mmol), and 1.2 equiv. (322 mg, 1.54 mmol)). The reaction mixture was allowed to stir overnight under a nitrogen atmosphere. After this, the reaction mixture was dialyzed using a snakeskin dialysis membrane (MWCO. 10 KDa) against purified water for 6-8 h, and water was replaced every 1 h. The resulting dialysate was taken from the dialysis bag and freeze-dried to yield the *mPEG-b-P(CB-{g-COOH}; g-TMZ_n)* (**8**). The obtained product was characterised using ¹H-NMR spectroscopy and the number of TMZ units attached was calculated using the relative method by keeping mPEG (Mn. 5000 Da) (macroinitiator) as a constant.

3.2.3. Development of TMZ nanoconjugate formulation (*mPEG-b-P(CB-{g-COOH}; g-TMZ_n) NPs*)

TMZ nanoconjugate formulation (*mPEG-b-P(CB-{g-COOH}; g-TMZ_n) NPs*) (n = 20, 40, and 60 units of TMZ) was prepared using the simple dispersion method. Briefly, *mPEG-b-P(CB-{g-COOH}; g-TMZ_n)* (9 mg) were weighed accurately, and 3 ml of dispersive medium (phosphate-buffered saline, 10 mM) was added to it, followed by simple pipetting to yield a dispersion mixture. The dispersion was probe sonicated for 20 s at 20% amplitude under ice-cold conditions and subjected to evaluation for particle size (PS), polydispersity index (PDI), zeta potential (ZP), and surface morphology. Further, the *mPEG-b-P(CB-{g-COOH}; g-TMZ_n) NPs* were evaluated for TMZ content and colloidal stability. The loading amount of TMZ was

calculated from the weight ratio method using the simple UV-Vis spectrophotometer (at λ_{\max} 328 nm) and calculated as per the below-mentioned formulae:

$$\%TMZ \text{ loading in compound } \mathbf{8} = \frac{\text{Amount of TMZ present}}{\text{Amount of compound } \mathbf{8} \text{ taken}} \times 100 \quad \text{eq. 3.1}$$

The particle size distribution, and surface zeta potential (ζ) were measured using dynamic light scattering (DLS) (Zetasizer Nano ZS, Malvern Panalytical Ltd, UK). The surface morphology was evaluated by prior surface coating with gold/chromium target Q150TES sputter coater, Quorum Technologies (Lewes, UK), followed by evaluation using Field Emission-Scanning Electron Microscopy (FE-SEM) (FEI, Apreo S LoVac, Thermo Fisher Scientific, MA, USA).

3.2.4. Stability studies

The stability studies of the developed *mPEG-b-P(CB-{g-COOH; g-TMZ_n})* NPs were performed under physiological conditions (pH at 4 °C and 37 °C). The samples were kept in a closed vial and incubated for specific period, followed by determination of change in particle size and %TMZ remaining in the *mPEG-b-P(CB-{g-COOH; g-TMZ_n})* NPs using DLS and UV method, respectively. For the DLS measurements, *mPEG-b-P(CB-{g-COOH; g-TMZ_n})* NPs were taken at a concentration of 3 mg/ml and analyzed for the change in particle size for 7 days. Furthermore, the same samples were used to determine the %TMZ remaining in the conjugates. For the UV stability analysis, the samples (free TMZ, *mPEG-b-P(CB-{g-COOH; g-TMZ_n})* (**8**)) were taken and analyzed at time points (0, 6, 12, 24, 48, 72, 96, 120 h) using UV-Vis spectrophotometry. The samples analyzed were withdrawn from the stock and diluted, and UV absorbance was evaluated at 328 nm for the %TMZ remaining, and the stability graph of %TMZ remaining was plotted over time.

3.3. Statistical analysis

The data and results are presented as mean \pm SD.

3.4. Results

3.4.1. Characterisation of TMZ conjugated amphiphilic copolymer (*mPEG-b-P(CB-{g-COOH; g-TMZ_n})*) (**8**)

A series of TMZ-conjugated amphiphilic copolymers (*mPEG-b-P(CB-{g-COOH; g-TMZ_n})*) were synthesized in a multistep reaction, as shown in figure 3.1. Initially, TMZ

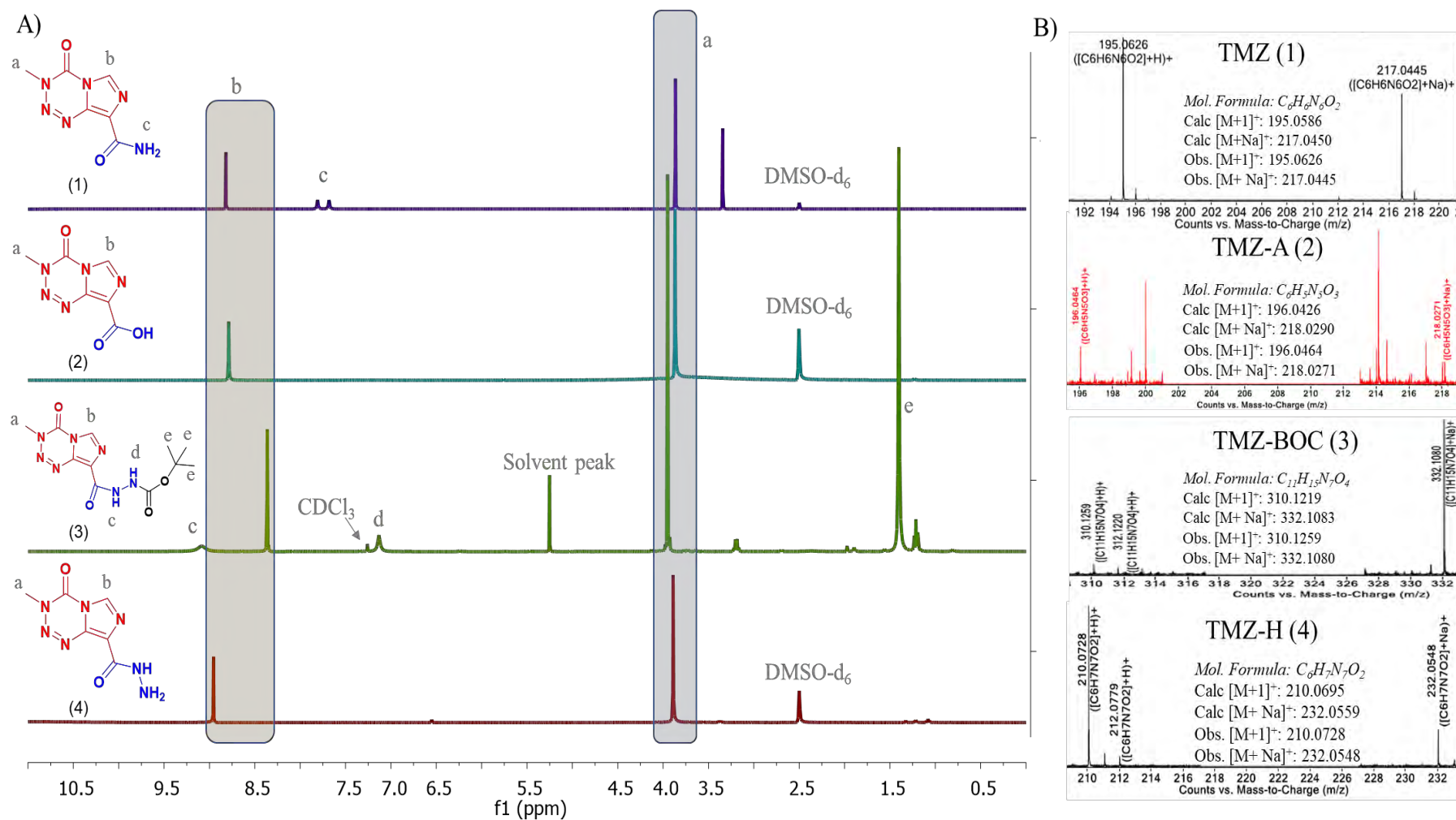


Figure 3.2. Characterization of TMZ and its derivatives. A) ¹H NMR and B) ESI-TOF HR-Mass spectrometry of TMZ (1), TMZ-A (2), TMZ-BOC (3), and TMZ-H (4)

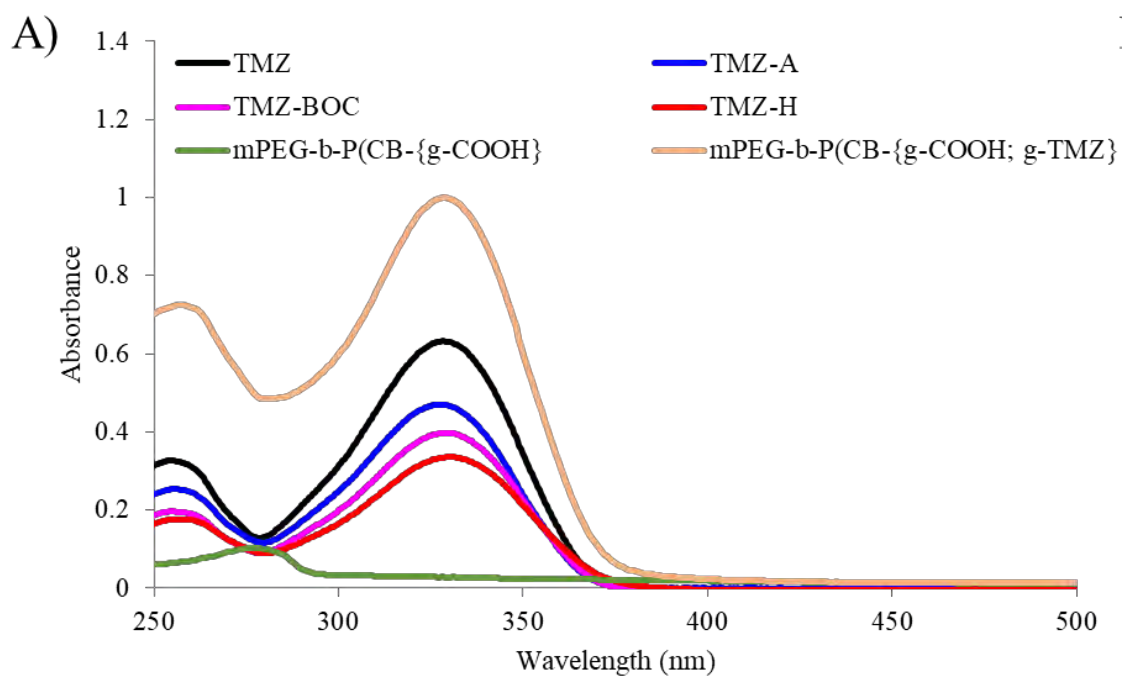


Figure 3.3. Characterization of TMZ and its derivatives using UV-Visible spectroscopy

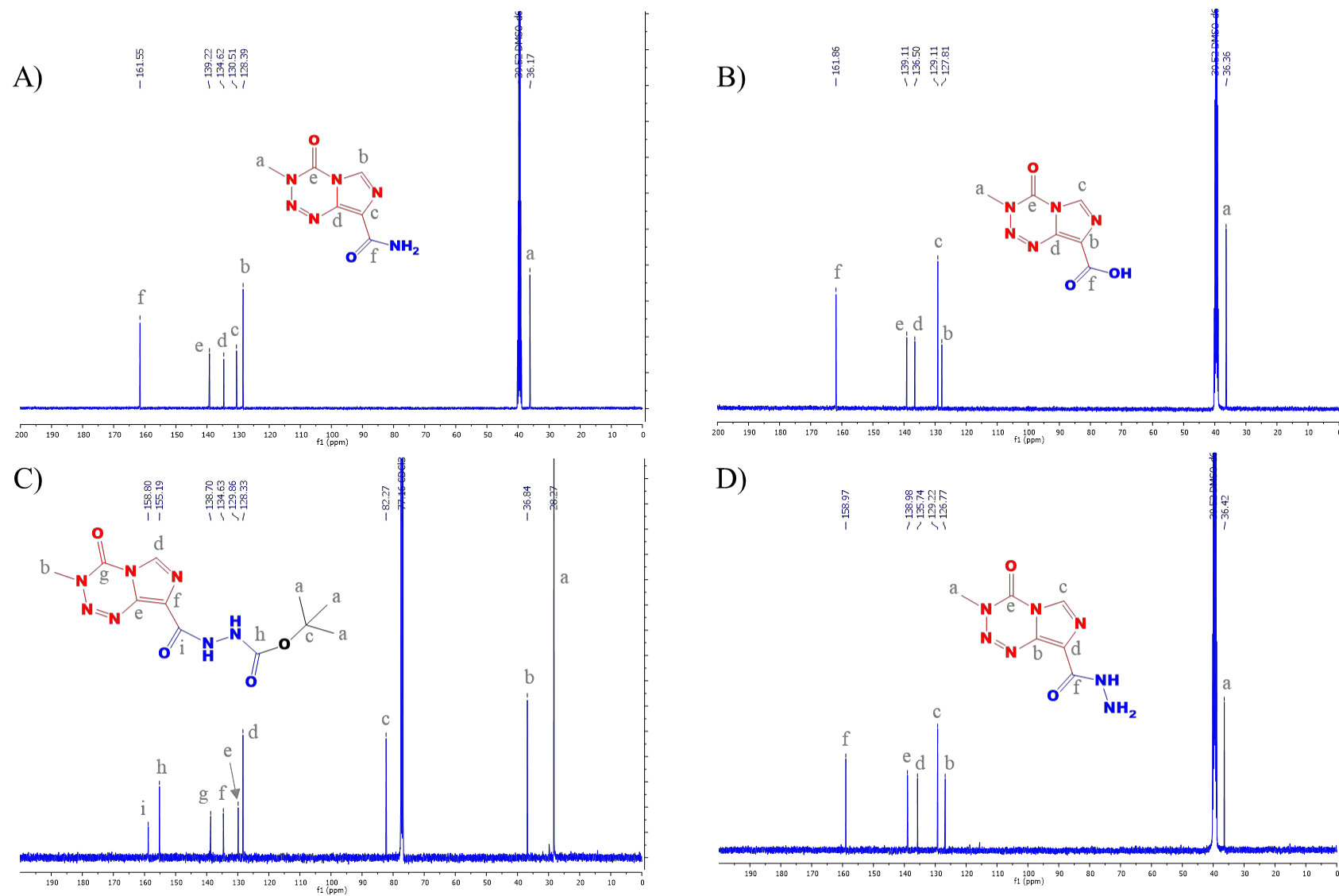


Figure 3.4. Characterization of TMZ and its derivatives. ^{13}C NMR spectrometry of A) TMZ (1), B) TMZ-A (2), C) TMZ-BOC (3), and D) TMZ-H (4)

hydrazide (**4**) was synthesized from TMZ (**1**). Wherein the free -NH₂ group of TMZ (**1**) was converted to temozolomide acid (TMZ-A) (**2**) with free -COOH group to yield white precipitate (~91% yield) and characterized. ¹H NMR (400 MHz, DMSO-*d*₆) of compound **2** showed peaks corresponding to δ 8.79 (s, 1H) and 3.87 (s, 3H). Further, the disappearance of two protons of -CONH₂ of TMZ at δ 7.68-7.81 confirms the conversion of free -CONH₂ to the COOH group (Figure 3.2A). ¹³C NMR showed peaks at δ 161.86, 139.11, 136.50, 129.11, 127.81 and 36.36 (Figure 3.4B). Mass spectroscopy ESI-TOF data showed [M+Na]⁺ at 218.0271 m/z and [M+1]⁺ ion peak at 196.0464 (mol. formula C₆H₅N₅O₃; cal. [M+1]⁺=196.0426) (Figure 3.2B) and the HPLC retention time of compound **2** shifted from 4.43 min to 3.30 min (Figure 2.2). The free -COOH of compound **2** was protected with *t*-butyl carbazate to yield Boc-protected TMZ hydrazide (TMZ-Boc) (**3**) using PyBOP coupling reagent. The crude product obtained was purified using column chromatography to yield a pure light-yellow solid (~62.1% yield). Figure 3.2A showed ¹H NMR (400 MHz, CDCl₃) of compound **3** with peaks at δ 9.08 (s, 1H), 8.36 (s, 1H), 7.13 (s, 1H), 3.95 (s, 3H), and 1.40 (s, 9H). ¹³C NMR (101 MHz, CDCl₃) showed δ 158.80, 155.19, 138.70, 134.63, 129.86, 128.33, 82.27, 36.84, and 28.27 (Figure 3.4C). Mass spectroscopy data showed [M+Na]⁺ at 332.1080 m/z and [M+H]⁺ peak at 310.1259 (mol formula C₁₁H₁₅N₇O₄; cal. [M+H]⁺=310.1219) (Figure 3.2B), and the HPLC elution of compound **3** shifted to 25.91 min from 3.30 min for compound **2** (Figure 2.2). Subsequently, the deprotection of the Boc group was done using dioxane saturated with HCl, followed by washing with diethyl ether to obtain white powder (~65% yield). Figure 3.2A showed ¹H NMR (400 MHz, DMSO-*d*₆) of compound **4** with peaks at δ 8.95 (s, 1H), 3.89 (s, 3H), with the disappearance of 9 protons from compound **3**. ¹³C NMR (101 MHz, DMSO-*d*₆) of compound **4** showed peak at δ 158.97, 138.98, 135.74, 129.22, 126.77, and 36.42 (Figure 3.4D). Mass spectroscopy ESI-TOF data reveals [M+Na]⁺ at 232.0548 m/z and [M+H]⁺ at 210.0728 (mol formula C₆H₇N₇O₂; cal. [M+H]⁺=210.0695) (Figure 3.2B), and the HPLC elution of compound **4** shifted to 3.75 min from 25.91 min for compound **3** (Figure 2.2), which is supported by UV spectroscopy data showing its absorption maxima at 328 nm (Figure 3.3), signifying the integrity of temozolomide after the synthesis of its hydrazine derivative (**4**).

In phase B, cyclic monomer 5-methyl-5-benzyloxycarbonyl-1, 3-dioxane-2-one (MBC) was synthesized in a two-step reaction as reported earlier [12]. The purified product was characterized using ¹H NMR and Mass spectroscopy. Figure 3.5A shows ¹H NMR (400 MHz, CDCl₃) of MBC with peaks at δ 7.36 (s, 5H), 5.22 (s, 2H), 4.70 (d, J = 10.9 Hz, 2H), 4.20 (d, J = 10.9 Hz, 2H), 1.33 (s, 3H) and ¹³C NMR (101 MHz, CDCl₃) with peaks at δ 171.03, 147.54,

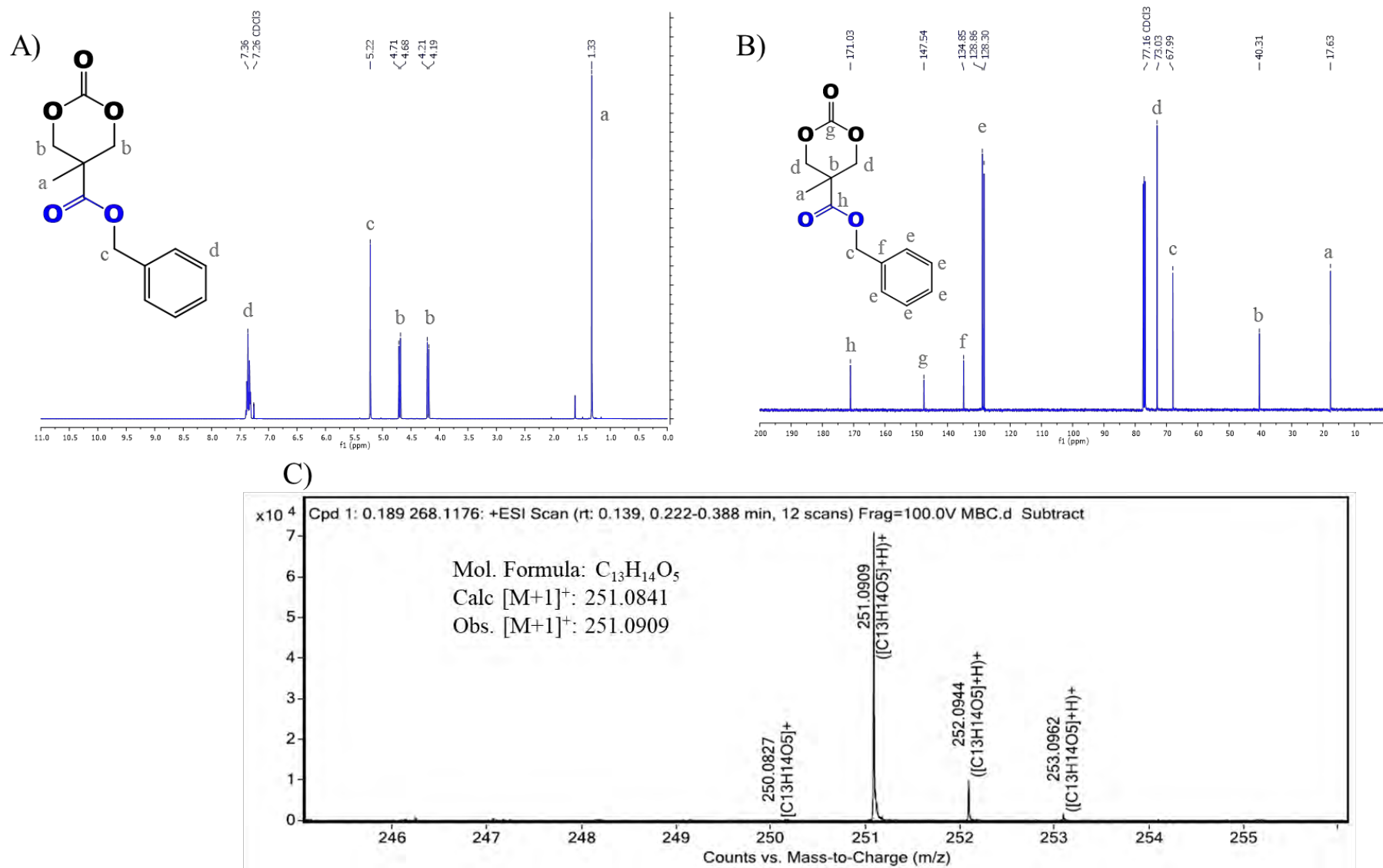


Figure 3.5. Characterization of MBC cyclic carbonate monomer using A) 1H NMR, B) ^{13}C NMR, and C) ESI-TOF HR-mass spectrometry

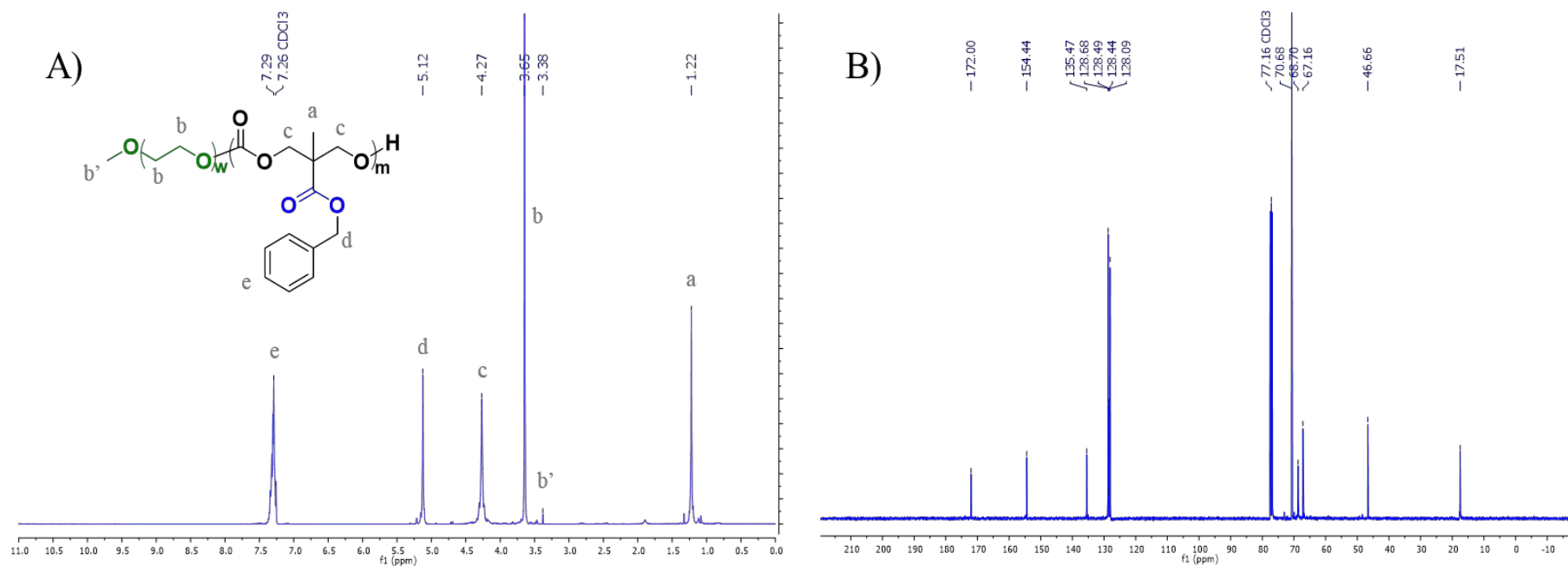


Figure 3.6. Characterization of *m*PEG-*b*-P(CB) carbonate polymer using A) ¹H NMR and B) ¹³C NMR spectroscopy

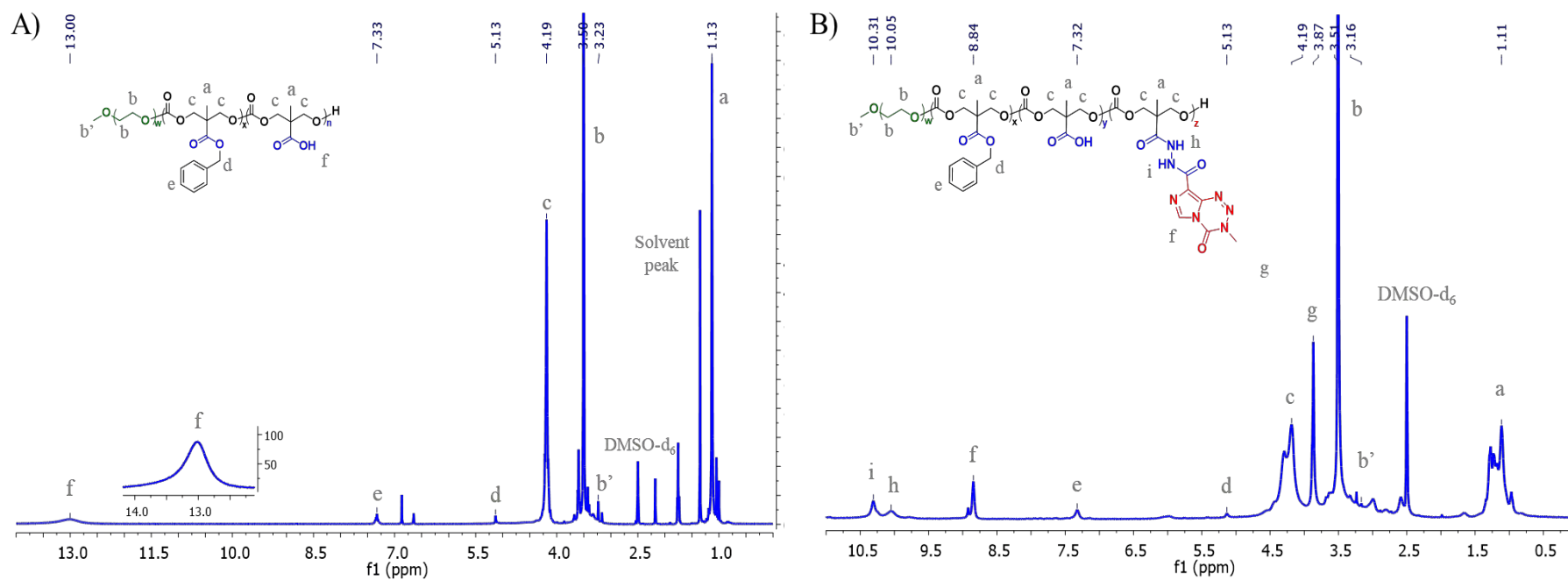


Figure 3.7. $^1\text{H-NMR}$ spectrum of A) polycarbonate polymer with free COOH group ($m\text{PEG-}b\text{-P}(\text{CB-}\{g\text{-COOH}\})$), and B) TMZ-polymer conjugate ($m\text{PEG-}b\text{-P}(\text{CB-}\{g\text{-COOH; } g\text{-TMZ}_{40}\})$)

134.85, 128.86, 128.30, 73.03, 67.99, 40.31, and 17.63 (Figure 3.5B). $[M+H]^+$ ion peak at m/z 251.0909 da (mol. formula= $C_{13}H_{14}O_5$; cal. $[M+H]^+$ = 251.0875 da) (Figure 3.5C) indicates successful synthesis of compound **5**. Microwave-assisted ring-opening polymerization of MBC (**5**) was initiated in the presence of mPEG as macroinitiator and tin(II) ethyl hexanoate as a catalyst to obtain *mPEG-b-P(CB)* (**6**) with a mass yield of 70%. Figure 3.6 shows 1H NMR (400 MHz, $CDCl_3$) characteristic peak at δ 7.37 – 7.26 (C_6H_5), δ 5.18 – 5.07 (CH_2 -Bn), δ 4.35 – 4.19 (CH_2 -O-*bisMPA*), δ 3.64 (CH_2 of PEG), δ 3.38 (CH_3 -O-PEG), δ 1.28 – 1.16 ($-CH_3$ of *bisMPA*) and ^{13}C NMR (101 MHz, $CDCl_3$) showed peaks at δ 172.00, 154.44, 135.47, 128.68, 128.49, 128.44, 128.09, 70.68, 68.70, 67.16, 46.66 and 17.51. The protective benzylic groups of compound **6** were removed using catalytic hydrogenation in the presence of Pd/C to obtain *mPEG-b-P(CB- $\{g-COOH\}$)* (**7**) with the free carboxylic pendant group on the polymer backbone (~60% mass yield). Figure 3.7A shows 1H NMR (400 MHz, DMSO- d_6) peak at δ 13.6-12.8 ($-COOH$), 4.22 – 4.11 (CH_2 -O-*bisMPA*), 3.50 ($-CH_2$ of PEG), 3.23 (CH_3 -O-PEG), 1.13 ($-CH_3$ of *bisMPA*) and reduction in the number of bulky benzylic protons at δ 7.33 ($-C_6H_5$) and 5.13 (CH_2 -Bn). ^{13}C NMR (101 MHz, DMSO- d_6) showed peaks at δ 176.62, 175.07, 173.51, 154.20, 153.97, 151.47, 139.18, 128.43, 128.04, 127.55, 124.92, 71.30, 69.81, 68.88, 67.03, 63.86, 63.58, 49.48, 47.48, 45.67, 34.39, 30.44, 25.14, 21.04 and 16.94 (Figure 3.8A). Carbodiimide/N-hydroxybenzotriazole (HOBt) coupling chemistry was utilized for grafting the hydrazine derivative of TMZ (**4**) to the free carboxylic pendent of the polycarbonate polymer backbone of compound **7** to yield the series of TMZ conjugated amphiphilic copolymer (*mPEG-b-P(CB- $\{g-COOH; g-TMZ_n\}$)*) (**8**). Figure 3.7B shows 1H NMR (400 MHz, DMSO- d_6) of *mPEG-b-P(CB- $\{g-COOH; g-TMZ_{40}\}$)* with peaks at δ 10.31($-NH-NH-$), 10.05 ($-NH-NH-$), 8.84 ($N-CH=N-$ of TMZ), 7.32 ($-C_6H_5$ of MBC), 5.13 (CH_2 -Bn), 4.19 (CH_2 -O-*bisMPA*), 3.87 ($N-CH_3$ of TMZ), 3.51 ($-CH_2$ of PEG), 3.16 (CH_3 -O-PEG), 1.11 ($-CH_3$ of *bisMPA*), indicating the synthesis of *mPEG-b-P(CB- $\{g-COOH; g-TMZ_{40}\}$)*. ^{13}C NMR (101 MHz, DMSO- d_6) showed peaks at δ 197.08, 173.81, 173.75, 173.70, 158.80, 154.12, 147.56, 139.13, 135.13, 128.76, 88.25, 74.13, 73.94, 69.80, 69.06, 45.70, 45.29, 36.23, 17.16 and 15.66 (Figure 3.8B). Figure 3.9 shows 1H NMR of *mPEG-b-P(CB- $\{g-COOH; g-TMZ_{20}\}$)* and *mPEG-b-P(CB- $\{g-COOH; g-TMZ_{60}\}$)*. The above-synthesized polymer-TMZ conjugates were characterized based on TMZ units attached equivalent to 20, 40, and 60 units grafted to the polymer backbone (**7**). The obtained *mPEG-b-P(CB- $\{g-COOH; g-TMZ_n\}$)* conjugates depicted the loading efficiency of 16.8%, 28.82%, and 37.99% w/w for 20, 40, and 60 units of TMZ units, respectively, and their loading efficiency is represented in Table 3.1.

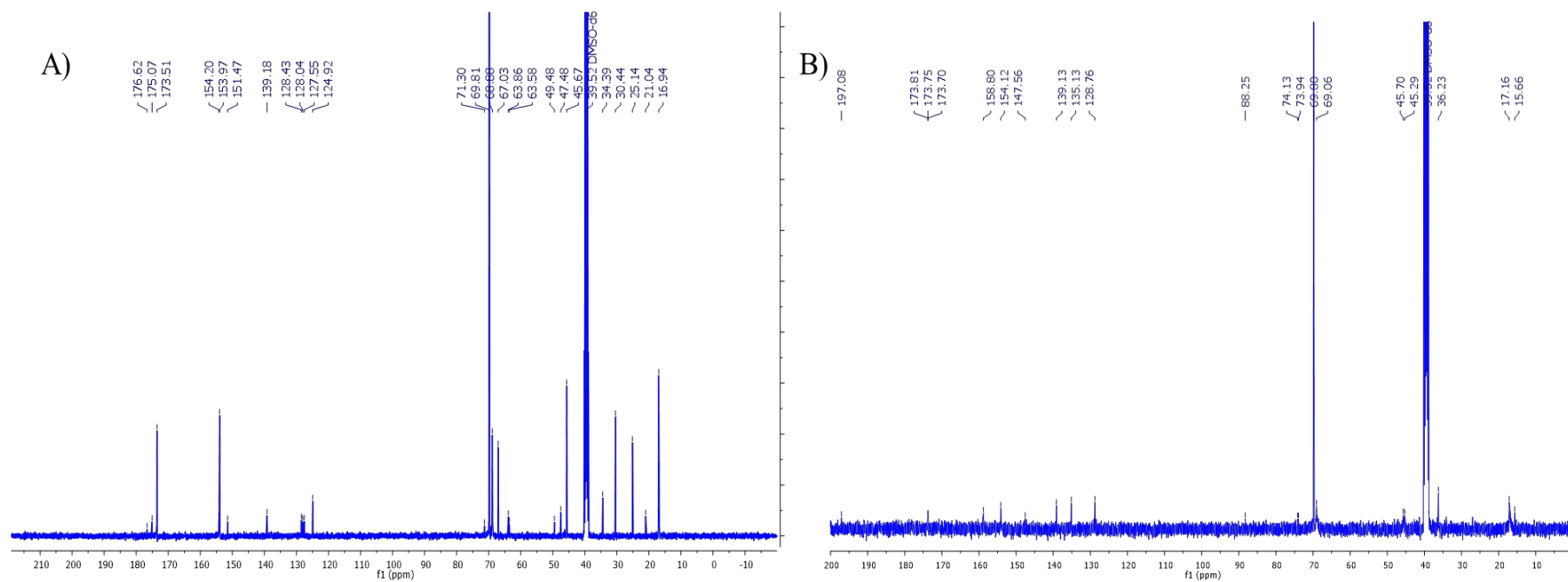


Figure 3.8. ^{13}C NMR of A) $m\text{PEG-}b\text{-P}(\text{CB-}\{g\text{-COOH}\})$ and B) $m\text{PEG-}b\text{-P}(\text{CB-}\{g\text{-COOH}; g\text{-TMZ}_{40}\})$

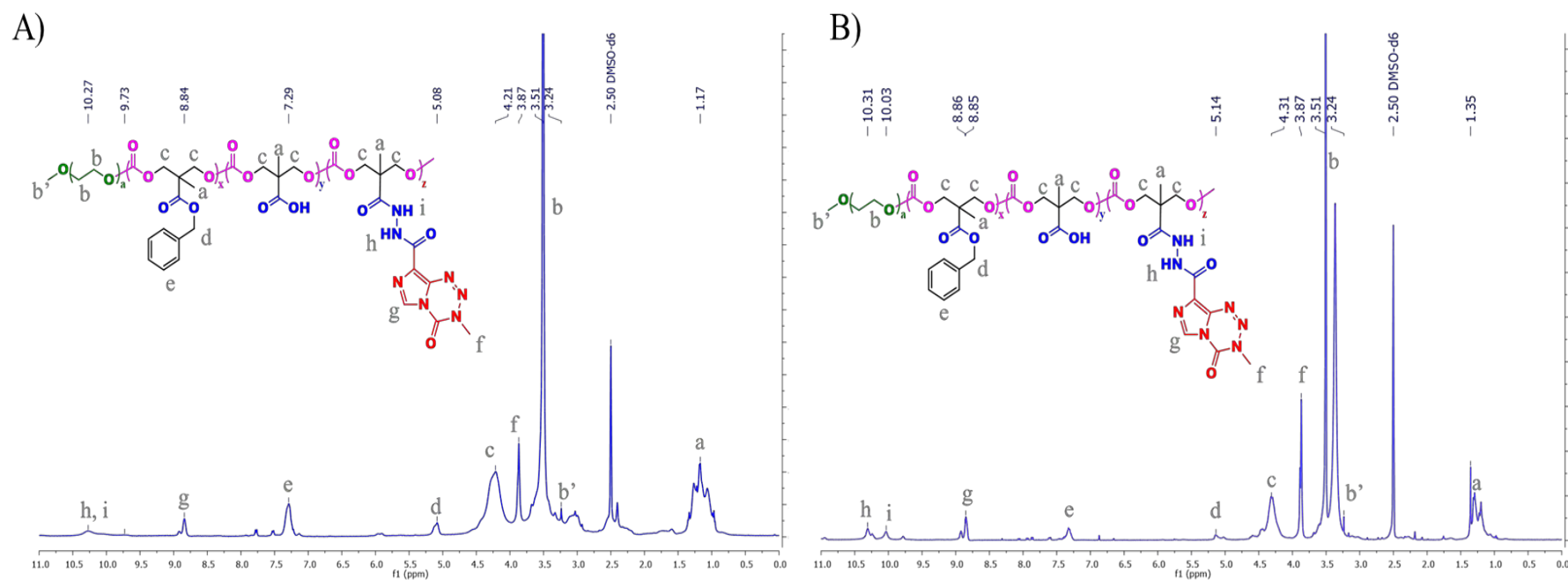


Figure 3.9. ^1H NMR of A) $m\text{PEG-}b\text{-P}(\text{CB-}\{g\text{-COOH; } g\text{-TMZ}_{20}\})$ and B) $m\text{PEG-}b\text{-P}(\text{CB-}\{g\text{-COOH; } g\text{-TMZ}_{60}\})$

3.4.2. mPEG-b-P(CB-{g-COOH; g-TMZ_n} (8) NPs characterization

The obtained *mPEG-b-P(CB-{g-COOH; g-TMZ₂₀}*, *mPEG-b-P(CB-{g-COOH; g-TMZ₄₀}*, and *mPEG-b-P(CB-{g-COOH; g-TMZ₆₀}* were initially screened based on the particle size and surface morphology using DLS and SEM, respectively, at pH 5.0, 6.0, and 7.4 (Figure 3.10). *mPEG-b-P(CB-{g-COOH; g-TMZ₂₀}* with 20 TMZ units, yielded nanosized particles with particle size of more than 200 nm and loading efficiency up to 16.8% w/w (Figure 3.10 and Table 3.1). The nanoconjugate yielded the pH-dependent change in particles with size of 323.7, 260.3, and 237.8 nm in pH 5.0, 6.0, and 7.4, respectively. While *mPEG-b-P(CB-{g-COOH; g-TMZ₆₀}* with 60 units of TMZ demonstrated higher loading capacity up to 37.99% w/w with significantly larger particle size of 552, 508.6, and 497.8 nm in pH 5.0, 6.0, and 7.4, respectively. Interestingly, *mPEG-b-P(CB-{g-COOH; g-TMZ₄₀}* with 40 TMZ units with a loading capacity of 28.7% w/w depicted pH-dependent change in particle size of 207.2, 205, and 90.9 ± 3.80 nm under pH 5.0, 6.0, and 7.4, respectively, which could be used as a potential nanoconjugate with optimal size and improved loading capacity (Figure 3.10 and Table 3.1).

Table 3.1. Loading capacity of nanoconjugates

Formulation	Loading efficiency (% w/w)
TMZ	n.a.
TMZH	n.a.
<i>mPEG-b-P(CB-{g-COOH; g-TMZ₂₀}</i>	$16.8 \pm 0.67\%$
<i>mPEG-b-P(CB-{g-COOH; g-TMZ₄₀}</i>	$28.7 \pm 0.81\%$
<i>mPEG-b-P(CB-{g-COOH; g-TMZ₆₀}</i>	$37.99 \pm 2.56\%$

3.4.3. Stability of TMZ nanoconjugate formulation (*mPEG-b-P(CB-{g-COOH; g-TMZ_n}* NPs)

The colloidal stability of the *mPEG-b-P(CB-{g-COOH; g-TMZ₂₀}* and *mPEG-b-P(CB-{g-COOH; g-TMZ₄₀}* was determined in physiological pH at 4 °C and 37 °C for up to 7 days. At 4 °C, *mPEG-b-P(CB-{g-COOH; g-TMZ₂₀}* and *mPEG-b-P(CB-{g-COOH; g-TMZ₄₀}* showed no significant change in particle size for 7 days. Surprisingly, on the next day, *mPEG-b-P(CB-{g-COOH; g-TMZ₂₀}* NPs showed significant change in particle size under physiological conditions (pH 7.4 and 37 °C). While *mPEG-b-P(CB-{g-COOH; g-TMZ₄₀}* NPs

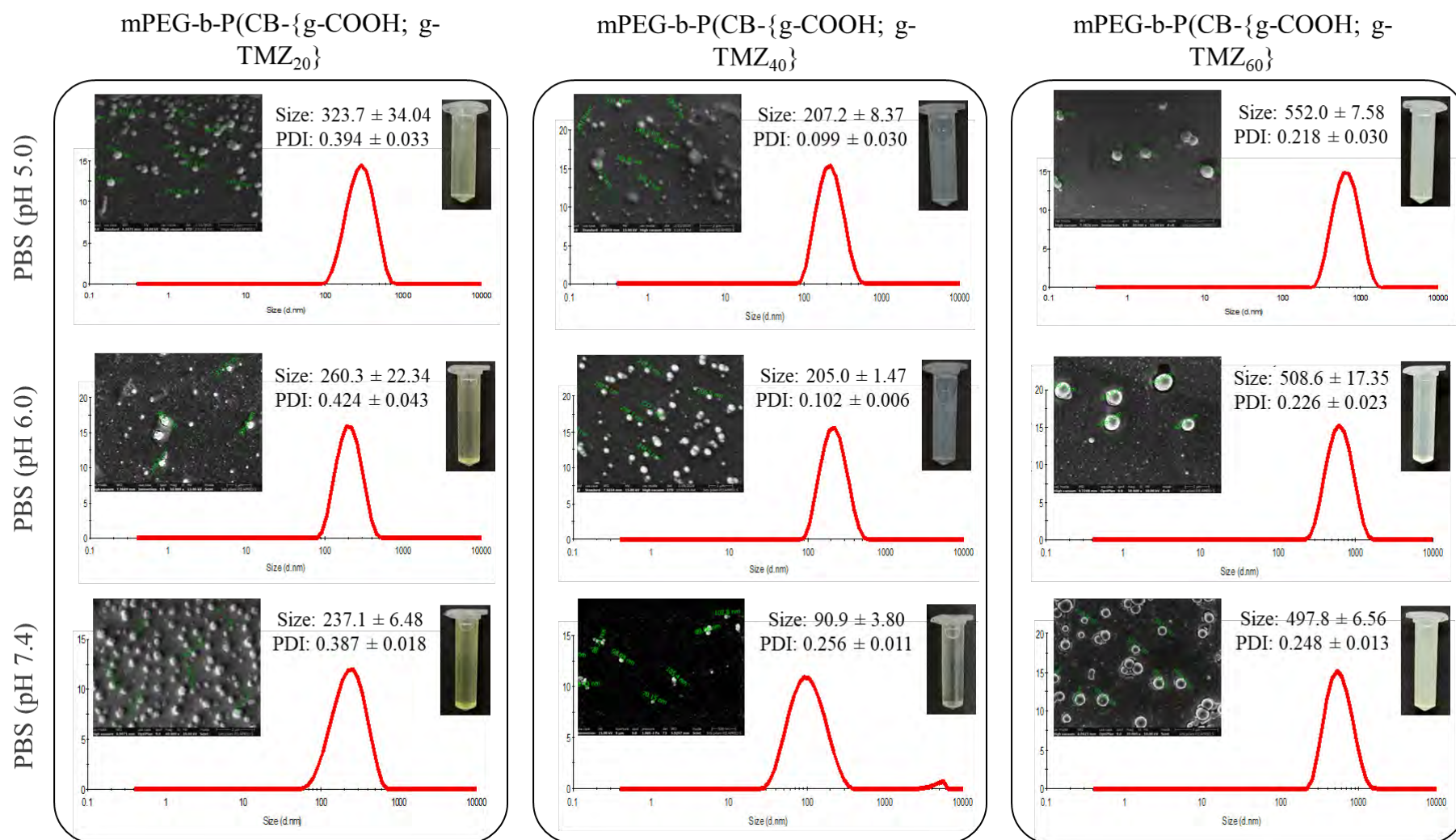


Figure 3.10. Characterization of TMZ-polymer conjugates (*mPEG-b-P(CB-{g-COOH; g-TMZ₂₀})*, *mPEG-b-P(CB-{g-COOH; g-TMZ₄₀})*, *mPEG-b-P(CB-{g-COOH; g-TMZ₆₀})*) in various dispersive mediums (PBS; 10 mM pH 5.0, PBS; 10 mM pH 6.0, and PBS; 10 mM pH 7.4) using Dynamic light scattering (DLS), Scanning electron microscopy (SEM) images, and their pictograms

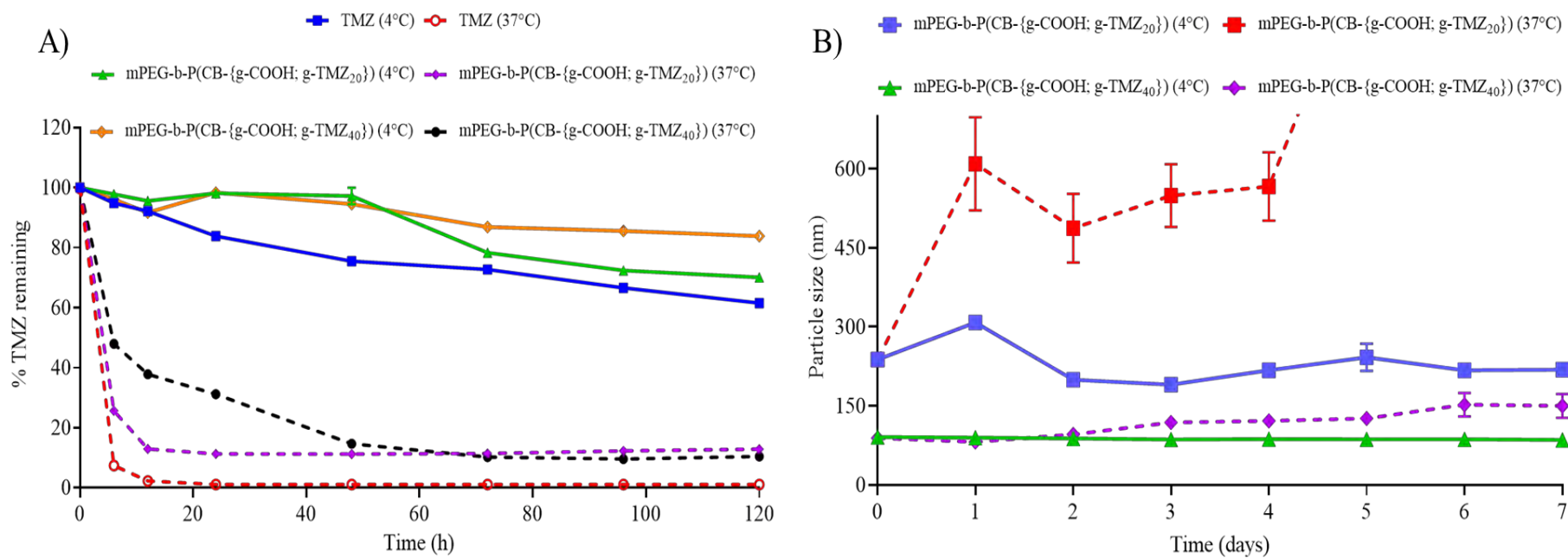


Figure 3.11. Characterisation of *mPEG-b-P(CB-{g-COOH; g-TMZ_n})* NCs. A) UV-based TMZ stability and B) DLS-based colloidal stability of *mPEG-b-P(CB-{g-COOH; g-TMZ₂₀})* and B) *mPEG-b-P(CB-{g-COOH; g-TMZ₄₀})* NCs

showed a change in particle size after 2 days with slightly better stability compared to *mPEG-b-P(CB-{g-COOH; g-TMZ₂₀}) NPs* (Figure 3.11B). TMZ exhibits hydrolytic degradation to form MTIC and AIC under physiological pH with a half-life of 1.8 h. The *mPEG-b-P(CB-{g-COOH; g-TMZ_n})* degradation behavior was determined using UV-Vis spectrophotometry at characteristic TMZ wavelength (328 nm) for 120 h and compared with free TMZ. The conjugation of TMZ to *mPEG-b-P(CB-{g-COOH; g-TMZ₂₀})* and *(mPEG-b-P(CB-{g-COOH; g-TMZ₄₀})* has moderately improved the half-life to 4.03 and 5.88 h, respectively (Figure 3.11A). Interestingly, the TMZ content was found to be intact in *mPEG-b-P(CB-{g-COOH; g-TMZ₂₀})* and *mPEG-b-P(CB-{g-COOH; g-TMZ₄₀})* at 4 °C.

3.5. Discussion

The standard of care therapy for GBM includes surgical resection, followed by radiotherapy and adjuvant chemotherapy with TMZ. TMZ is marketed as Temodal® in the form of capsules and injections, given *via.* oral and parenteral routes, respectively. It primarily shows its anticancer action by methylation of guanine and adenine residue of DNA, thereby causing cell death. TMZ, although demonstrated potent antitumor activity and is being used as a first-line chemotherapeutic agent, still faces several limitations, including a short half-life (~1.8-2 h), rapid metabolism, quick clearance, pH-dependent degradation, less brain bioavailability, and dose-dependent toxicity. Attempts have been made to overcome these limitations by encapsulating it in various systems, including polymeric carriers, lipidic carriers (liposomes, SLNs), and inorganic nanoparticles. For instance, Nordling-David *et al.* prepared TMZ-loaded PEGylated liposomes using a thin film hydration method, yielding a small vesicle of 121 nm with an encapsulation efficiency of 23%. *In vivo* assessment showed non-significant improvement in the survival rate compared to free TMZ [14]. Similarly, Duwa *et al.* prepared TMZ-loaded PLGA nanoparticles actively functionalized with cetuximab targeting EGFR receptors. Physicochemical characterization showed an average particle size of ~162 nm with a narrow PDI of 0.16 and encapsulation efficiency of 28.0% at drug loading of 1.4% w/w [15]. Pertaining to appreciable solubility of drug up to 5 mg/ml in water, TMZ exhibits a challenging process in achieving high drug loading in these nanocarriers. On the other hand, a conjugation-based approach could be utilized to overcome TMZ-related concerns such as loading capacity, encapsulation efficiency, drug stability, and its related toxicities. Likewise, polycarbonates have been used as biocompatible materials for improved mechanical support and delivery outcomes, giving desired therapeutic outcomes. Polycarbonates are composed of carbonate linkages that degrade slowly under physiological conditions and provide the controlled

hydrolysis carbonate group, producing carbon dioxide and alcohol, unlike the other polymers that release acids as a by-product. Furthermore, the ease in the tailoring of polycarbonates aids in developing targeted drug delivery, gene delivery, polymer-drug conjugates, polymer-protein conjugates, etc [16]. Chitkara *et al.* reported covalent conjugation of gemcitabine to polycarbonate poly(ethylene glycol)-block-poly(2-methyl-2-carboxyl-propylenecarbonate) polymer resulted in improved drug payload (12.8% w/w), protection from rapid metabolism, controlled release, and improved antitumor activity [9]. Liang *et al.* prepared a pH-responsive polycarbonate doxorubicin conjugate exhibiting a higher drug loading capacity of 18.3% w/w, good stability, and controlled release under *in vivo* conditions [11]. In the current research, a series of TMZ conjugated polymers were synthesized using a multistep reaction (Figure 3.1), wherein TMZ (**1**) was converted to its hydrazine derivative (**4**) in a three-step reaction. Simultaneously, amphiphilic block biocompatible polymer containing free COOH pendant (**7**) was synthesized using hydrogenation of mPEG-polycarbonate block polymer (**6**), followed by reaction with free NH₂ group of hydrazine derivative of TMZ to finally yield a series of polymer-drug conjugates, i.e., *mPEG-b-P(CB-{g-COOH; g-TMZ₂₀})*, *mPEG-b-P(CB-{g-COOH; g-TMZ₄₀})*, and *mPEG-b-P(CB-{g-COOH; g-TMZ₆₀})* containing 20, 40, and 60 units of TMZ conjugated to the polymer backbone as a pendant group with drug loading capacity of 16.8%, 28.8%, and 37.99% w/w, respectively. Interestingly, the synthesized conjugates yielded nanosized dispersions ranging from 90-552 nm (Figure 3.10). In previous reports, Xu *et al.* prepared a series of poly(2-ethyl-2-oxazoline) (PEtOz) conjugated TMZ (PEtOz-TMZ), exhibiting the drug loading capacity ranging from 2.2 to 4.1% w/w [8]. Ward *et al.* prepared TMZ conjugated 2-methacryloyloxyethylphosphorylcholine (MPC) based conjugate that showed TMZ loading capacity ranging from 15-35 mol% [6]. In another report, Patil *et al.* prepared TMZ conjugated multifunctional poly(β -L-malic acid) platform, resulting in the polymer TMZ conjugates with drug loading up to 17% w/w against the glioma cells [7].

The nanoconjugates of TMZ were prepared in various dispersive mediums (including pH 5.0, 6.0, and 7.4) and demonstrated varying particle sizes based on the units of TMZ units attached. *mPEG-b-P(CB-{g-COOH; g-TMZ₂₀})* demonstrated size ranging from 237.1 to 323.7, *mPEG-b-P(CB-{g-COOH; g-TMZ₄₀})* showed an average particle size ranging from 90.9 to 207.2, while, *mPEG-b-P(CB-{g-COOH; g-TMZ₆₀})* exhibited an average particle size from 497.8 to 552 nm with loading capacities of 16.8, 28.7, and 37.99% w/w, respectively (Figure 3.10, Table 3.1). The above-synthesized nanoconjugates exhibited pH-dependent change in particle size, i.e., the size of nanoparticles was found to reduce as the pH increased from pH

5.0 to pH 7.4. Similarly, Li *et al.* observed the increase in particle size as the pH of the dispersive medium was reduced from pH 7.4 to pH 5.5 using folate-functionalized soybean phosphatidylcholine complex-loaded PEG-lipid-PLA hybrid nanoparticles, showing the role of pH in the modulation of particle size of the nanocarrier system [17].

The stability of nanoconjugates in the biological environment is an important aspect that can impact the therapeutic outcome. The nanoconjugates with 20 and 40 units of TMZ attached were utilized for further evaluation as the particle size for the nanoconjugates was within range of interest for the experimentation. As reported previously, the junctions in tumor vasculature usually get compromised with intercellular gaps ranging from 60-300 nm with loose endothelial junctions [18]. Accordingly, colloidal and TMZ stability of *mPEG-b-P(CB-{g-COOH; g-TMZ₂₀})* and *mPEG-b-P(CB-{g-COOH; g-TMZ₄₀})* NPs under physiological conditions was investigated. The colloidal stability assay indicated no significant change in particle size at 4 °C up to 7 days, whereas, at 37 °C, a substantial change in particle size was observed from day 1 and day 2 in *mPEG-b-P(CB-{g-COOH; g-TMZ₂₀})* and *mPEG-b-P(CB-{g-COOH; g-TMZ₄₀})*, respectively (Figure 3.11B). The same samples were analysed for the %TMZ remaining, wherein *mPEG-b-P(CB-{g-COOH; g-TMZ₂₀})* and *(mPEG-b-P(CB-{g-COOH; g-TMZ₄₀})* showed a half-life of 4.03 and 5.88 h, respectively compared to 1.8 h for free TMZ (Figure 3.11A). A similar outcome was observed by Patil *et al.*, wherein conjugation of the molecule TMZ to the Poly(β -L-malic acid) yielded good loading efficiency of up to 17% w/w and slightly improved the stability half-life up to 5-7 h compared to 1.8 h of free TMZ [7]. Xu *et al.* conjugated TMZ to the poly(2-ethyl-2-oxazoline) (PEtOz) polymer, produced loading efficiency up to 4% w/w with stability ranging from 1.68-5.5 folds compared to free TMZ with a half-life of 2.5 h [8].

Overall, in the current work, the conjugation approach has significantly improved the physiochemical parameters of the TMZ with marked improvement in the loading capacity of the molecule. However, the betterment in the stability perspective of the TMZ is still warranted.

3.6. Conclusion

Although TMZ is a potent chemotherapeutic for the treatment of GBM, still the therapeutic outcome is limited due to drug-related limitations, including low stability, drug loading capacities, etc. For this, a synthetic route was developed describing the conjugation of TMZ to the PEG-based polycarbonate block copolymer. The covalent attachment of the TMZ has conveniently bypassed the barrier of low loading capacities, ranging from 16.8 to 37.99%

w/w. The varying units of TMZ attached played a significant role in preparing nanoformulation and envisaging the stability of the TMZ molecule. Although the improvement in the TMZ stability was observed, still there is a room for improvement, and more delivery strategies could be explored to deliver drugs for targeting glioma.

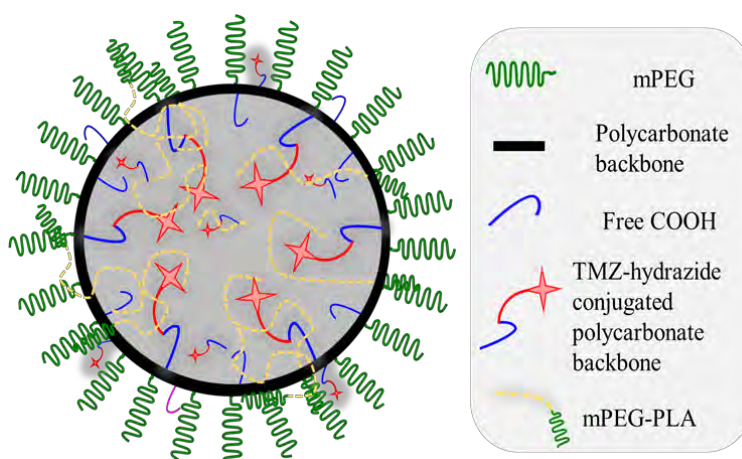
3.7. References

- [1] Jatyan R, Singh P, Sahel DK, Karthik YG, Mittal A, Chitkara D. Polymeric and small molecule-conjugates of temozolomide as improved therapeutic agents for glioblastoma multiforme. *J Control Release* 2022;350:494–513. <https://doi.org/https://doi.org/10.1016/j.jconrel.2022.08.024>.
- [2] Du K, Xia Q, Heng H, Feng F. Temozolomide–Doxorubicin Conjugate as a Double Intercalating Agent and Delivery by Apoferritin for Glioblastoma Chemotherapy. *ACS Appl Mater Interfaces* 2020;12:34599–609. <https://doi.org/10.1021/acsami.0c08531>.
- [3] Rai R, Banerjee M, Wong DH, McCullagh E, Gupta A, Tripathi S, et al. Temozolomide analogs with improved brain/plasma ratios – Exploring the possibility of enhancing the therapeutic index of temozolomide. *Bioorg Med Chem Lett* 2016;26:5103–9. <https://doi.org/https://doi.org/10.1016/j.bmcl.2016.08.064>.
- [4] Park M, Song C, Yoon H, Choi K-H. Double Blockade of Glioma Cell Proliferation and Migration by Temozolomide Conjugated with NPPB, a Chloride Channel Blocker. *ACS Chem Neurosci* 2016;7:275–85. <https://doi.org/10.1021/acschemneuro.5b00178>.
- [5] Cho H-Y, Swenson S, Thein TZ, Wang W, Wijeratne NR, Marín-Ramos NI, et al. Pharmacokinetic properties of the temozolomide perillyl alcohol conjugate (NEO212) in mice. *Neuro-Oncology Adv* 2020;2:vdaa160. <https://doi.org/10.1093/oaajnl/vdaa160>.
- [6] Ward SM, Skinner M, Saha B, Emrick T. Polymer–Temozolomide Conjugates as Therapeutics for Treating Glioblastoma. *Mol Pharm* 2018;15:5263–76. <https://doi.org/10.1021/acs.molpharmaceut.8b00766>.
- [7] Patil R, Portilla-Arias J, Ding H, Inoue S, Konda B, Hu J, et al. Temozolomide Delivery to Tumor Cells by a Multifunctional Nano Vehicle Based on Poly(β -L-malic acid). *Pharm Res* 2010;27:2317–29. <https://doi.org/10.1007/s11095-010-0091-0>.
- [8] Xu K, Zhang L, Gu Y, Yang H, Du B, Liu H, et al. Increased the TMZ concentration in brain by poly(2-ethyl-2-oxazoline) conjugated temozolomide prodrug micelles for glioblastoma treatment. *Eur Polym J* 2021;145:110232. <https://doi.org/https://doi.org/10.1016/j.eurpolymj.2020.110232>.
- [9] Chitkara D, Mittal A, Behrman SW, Kumar N, Mahato RI. Self-Assembling, Amphiphilic Polymer–Gemcitabine Conjugate Shows Enhanced Antitumor Efficacy Against Human Pancreatic Adenocarcinoma. *Bioconjug Chem* 2013;24:1161–73. <https://doi.org/10.1021/bc400032x>.
- [10] Jiang T, Li Y-M, Lv Y, Cheng Y-J, He F, Zhuo R-X. Amphiphilic polycarbonate conjugates of doxorubicin with pH-sensitive hydrazone linker for controlled release. *Colloids Surfaces B Biointerfaces* 2013;111:542–8.
- [11] Liang E, Guo Z, Hu Z, Chen Z, Reheman A, Wang J, et al. pH-Responsive expandable polycarbonate–doxorubicin conjugate nanoparticles for fast intracellular drug release. *New J Chem* 2021;45:7261–9. <https://doi.org/10.1039/D1NJ00598G>.
- [12] Sharma S, Mazumdar S, Italiya KS, Date T, Mahato RI, Mittal A, et al. Cholesterol and Morpholine Grafted Cationic Amphiphilic Copolymers for miRNA-34a Delivery. *Mol Pharm* 2018;15:2391–402. <https://doi.org/10.1021/acs.molpharmaceut.8b00228>.
- [13] Jatyan R, Sahel DK, Singh P, Sakhuja R, Mittal A, Chitkara D. Temozolomide–fatty acid

- conjugates for glioblastoma multiforme: In vitro and in vivo evaluation. *J Control Release* 2023;23:S0168-3659. <https://doi.org/10.1016/j.jconrel.2023.05.012>.
- [14] Nordling-David MM, Yaffe R, Guez D, Meirou H, Last D, Grad E, et al. Liposomal temozolomide drug delivery using convection enhanced delivery. *J Control Release* 2017;261:138–46. <https://doi.org/https://doi.org/10.1016/j.jconrel.2017.06.028>.
- [15] Duwa R, Banstola A, Emami F, Jeong J-H, Lee S, Yook S. Cetuximab conjugated temozolomide-loaded poly (lactic-co-glycolic acid) nanoparticles for targeted nanomedicine in EGFR overexpressing cancer cells. *J Drug Deliv Sci Technol* 2020;60:101928. <https://doi.org/https://doi.org/10.1016/j.jddst.2020.101928>.
- [16] Ansari I, Singh P, Mittal A, Mahato RI, Chitkara D. 2,2-Bis(hydroxymethyl) propionic acid based cyclic carbonate monomers and their (co)polymers as advanced materials for biomedical applications. *Biomaterials* 2021;275:120953. <https://doi.org/https://doi.org/10.1016/j.biomaterials.2021.120953>.
- [17] Li Y, Wu H, Yang X, Jia M, Li Y, Huang Y, et al. Mitomycin C-Soybean Phosphatidylcholine Complex-Loaded Self-Assembled PEG-Lipid-PLA Hybrid Nanoparticles for Targeted Drug Delivery and Dual-Controlled Drug Release. *Mol Pharm* 2014;11:2915–27. <https://doi.org/10.1021/mp500254j>.
- [18] Roberts WG, Delaat J, Nagane M, Huang S, Cavenee WK, Palade GE. Host microvasculature influence on tumor vascular morphology and endothelial gene expression. *Am J Pathol* 1998;153:1239–48.

Chapter 4

Formulation development, *in vitro* and *in vivo* evaluation of hybrid nanoconjugates of temozolomide in C6 cells-induced syngeneic orthotopic glioma model in rats



4.1. Introduction

Nanotechnology has emerged as a field of research from past 60 years that has demonstrated the promising and transformative outcomes utilized in multiple theranostic applications. Especially nanoparticles are a vital class of nanotechnology with a mesoscopic size, possessing a larger surface area to volume ratio and carrying capacity to manipulate the physiochemical properties of the drug molecules indirectly *via* encapsulation, complexation, or any other means. Due to the complex engineering and manufacturing of materials, it imparts an innovative paradigm to the system that makes it a suitable candidate for improved drug loading, endocytic uptake, specific targeting, systemic circulation time, and reduced minimal off-target responses [1,2]. Temozolomide (TMZ) is an imidazotetrazine derivative DNA-alkylating agent used as adjuvant chemotherapy with surgical resection with concomitant radiotherapy for the treatment of glioblastoma multiforme (GBM). TMZ is considered a gold standard in the treatment due to its excellent toxicity against the tumor cells compared to the neighbouring healthy cells. However, the outcome of the treatment is still nominal, resulting in tumor relapses in patients. This could be attributed due to the short half-life (1.8 h), rapid degradation, quick clearance, and off-target toxicity, which leads to a minimal amount of TMZ reaching the brain in the intact and effective form. Several reports have suggested reliable and effective ways to deliver the molecule intact, namely using the encapsulation, complexation, and conjugation approach. The encapsulation of TMZ to the nanomaterials have shown slightly better therapeutic outcomes than free drug treatment. However, the low encapsulation and loading efficiencies of the TMZ into the nanocarrier system has led to the outcome far from accomplished. Another conjugation-based approach has shown promising outcomes in improving several TMZ-related properties, including stability, loading efficiency, encapsulation, targeted delivery, and reduced off-target effects [3]. Likewise, Patil et al. prepared TMZ conjugated to the multifunctional poly(β -L-malic acid) platform and surface functionalized anti-TfR antibody, yielded 6.5-14.8 nm particles with a loading efficiency of 17% w/w. The TMZ-polymer conjugate particles showed improvement in TMZ stability up to 7 h compared to 1.8 h of free TMZ [4]. Previously, we have reported that polycarbonate conjugates significantly improve the physiochemical properties of the drug, including encapsulation, loading efficiency, stability, efficacy, and biocompatibility [5]. Similarly, in the previous chapter, we have synthesized and prepared a PEG-based polycarbonate copolymer conjugated with TMZ that has significantly improved the loading capacity of 16.8-37.99% w/w

with a stability half-life of 5.88 h under physiological conditions (37 °C; pH 7.4). Though conjugating TMZ with polycarbonate has overcome the limitations associated with TMZ, there is still a lot of scope for further improvement in the drug stability and delivery of the molecule. Similarly, other approaches, including hybrid nanoparticles, are the combination of two or more different components that are mixed in a definite ratio, yielding multiple advantages over the individual component alone, such as better stability, biocompatibility, controlled release, effective biodistribution, prolonged circulation, lowered toxicities, and improved *in vivo* efficacy [6]. Herein, we report a hybrid system comprising the TMZ nanoconjugates and mPEG-PLA. Combining biocompatible polymers with polymer-drug conjugates could provide benefits such as improved stability, biomimetic nature, reduced clearance, increased drug accumulation to the target site, and reduced toxicity. Several other hybrid nanosystems have been explored earlier. For instance, polymer-lipid hybrid nanoparticles were prepared using PLGA polymer, and HSPC, DSPC, and cholesterol as a lipid were prepared using the solvent emulsification method. The hybrid lipid-polymer nanosystem exhibited an average particle size of *ca.* 256 nm with an encapsulation efficiency of >60% at drug loading of ~3% w/w [7]. Previously, we have reported polymer-lipid hybrid systems to deliver small molecules, that has demonstrated improved outcome in the delivery perspective of the drug during the treatment process [8–10]. Therefore, combining the polymer-drug conjugates with other polymeric component provides an ample opportunity to modify and improve the delivery system.

In the current research, we prepared a hybrid system comprised of polymer-TMZ conjugate (mPEG-b-P(CB-{g-COOH; g-TMZ₄₀}) and mPEG-PLA and characterized for their *in vitro* and *in vivo* efficacy evaluation in the C6-induced syngeneic orthotropic glioma model, wherein brain physiology, survival rate, change in body weight, tumor burden, and organ toxicity using histopathology were assessed.

4.2. Experimental section

4.2.1. Materials

Temozolomide (TMZ, >98%), tert-butyl carbazate, 1H-Benzotriazol-1-yloxytripyrrolidinophosphonium Hexafluorophosphate (PyBOP), N,N-Diisopropylethylamine (DIPEA) were purchased from TCI chemicals (Tokyo, Japan). Dulbecco's Modified Eagle Medium (DMEM), Minimum Essential Media (MEM), Fetal Bovine Serum (FBS), SnakeSkin™ Dialysis Tubing (MWCO. 10 KDa), Annexin V Ready Flow Conjugates kit were

procured from ThermoFisher Scientific (Massachusetts, United States). Methoxy poly(ethylene glycol) (mPEG, 5000 Da), Tin(II) 2-ethylhexanoate, DL-lactide, and Propidium Iodide (PI) were obtained from Sigma-Aldrich (St. Louis, Missouri, United States). 1,4-Dioxane and Palladium on carbon (Pd/C) were purchased from Spectrochem (Mumbai, India). 3-(4,5-Dimethylthiazol-2-yl)-2,5-Diphenyltetrazolium Bromide (MTT), 1-(3-Dimethylaminopropyl)-3-ethylcarbodiimide hydrochloride (EDC.HCl), and Hydroxybenzotriazole (HOBt) were obtained from Sisco Research Laboratories (Mumbai, India). All other reagents and chemicals used were of analytical grade and bought from local vendors.

4.2.2. Synthesis of polymeric drug conjugate of TMZ ($mPEG-b-P(CB-\{g-COOH; g-TMZ_{40}\})$)

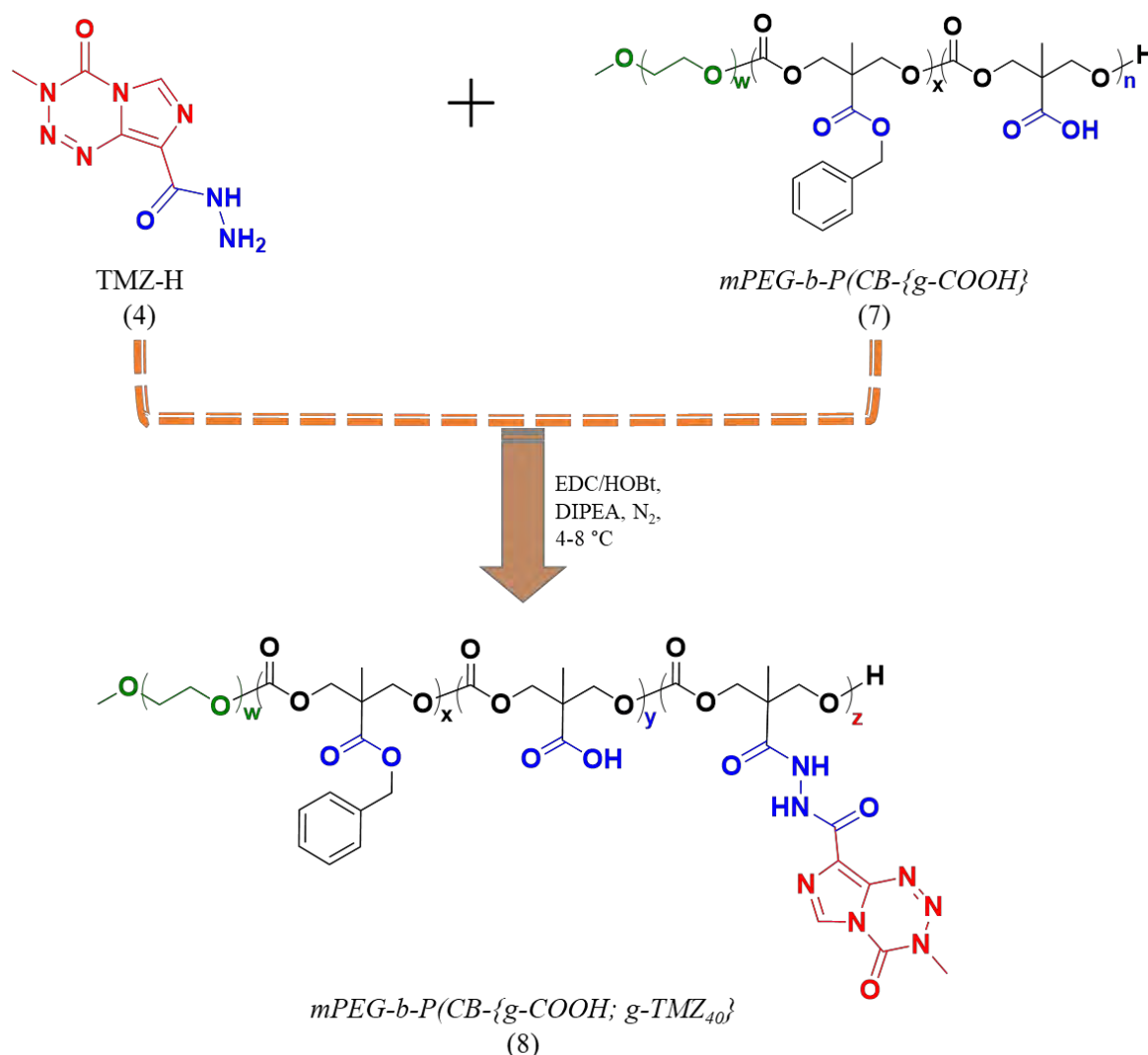


Figure 4.1. Scheme for the synthesis of TMZ-polymer conjugate ($mPEG-b-P(CB-\{g-COOH; g-TMZ_{40}\})$)

The polymer conjugate of TMZ was synthesized in a multistep reaction, as described in section 3.2.2. wherein TMZ-hydrazide (TMZ-H) (**4**) and PEG-based polycarbonate block copolymer was synthesized containing free COOH as a pendent group (**7**), followed by its EDC/HoBT coupling reaction to yield *m*PEG-*b*-P(CB- $\{g$ -COOH; g -TMZ₄₀) (Figure 4.1). Reactions were executed under dry nitrogen conditions using the standard protocols. All products were thoroughly characterized using ¹H NMR (400MHz) and ¹³C NMR (101MHz) spectra using Bruker AVANCE III 400 MHz NMR spectrometer (Billerica, United States). UV-visible spectra were recorded using a Jasco-V750 spectrophotometer (Tokyo, Japan) under ambient controlled conditions over the 200-800 nm wavelength range.

4.2.3. Synthesis of *m*PEG-poly(lactic acid) (*m*PEG-PLA) copolymer (**9**)

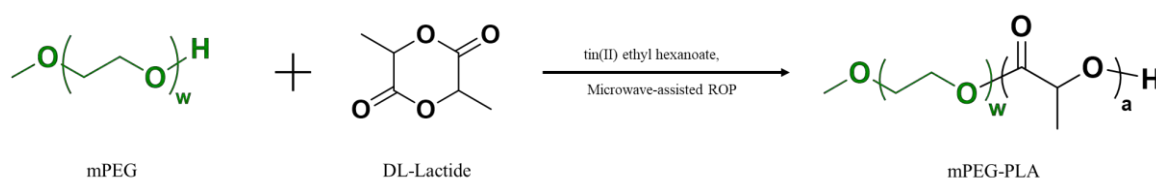


Figure 4.2. Scheme for the synthesis of *m*PEG-poly(lactic acid) (*m*PEG-PLA) copolymer

*m*PEG-PLA (**9**) was synthesized using the previously described microwave-assisted ring-opening polymerization (ROP) method with the scheme shown in Figure 4.2 [11]. Briefly, DL-Lactide (0.535 g, 3.71 mmol) was polymerized with *m*PEG (0.465 g, 93 mmol) as a macroinitiator in the presence of tin(II) ethyl hexanoate as a catalyst at 130 °C for 1 h. After that, the crude copolymer was allowed to cool at room temperature, followed by purification by dissolving it in chloroform and precipitating it in isopropyl alcohol and diethyl ether twice. The purified *m*PEG-PLA polymer was dried under a vacuum and analyzed using ¹H-NMR spectroscopy.

4.2.4. Development of hybrid TMZ nanoconjugate formulation (Hybrid TMZ NCs)

A hybrid TMZ nanoconjugate containing *m*PEG-*b*-P(CB- $\{g$ -COOH; g -TMZ₄₀) (**8**) and *m*PEG-PLA (**9**) was developed using a thin film hydration method, as reported earlier [12]. Briefly, *m*PEG-*b*-P(CB- $\{g$ -COOH; g -TMZ₄₀) (75 mg) and *m*PEG-PLA (25 mg) were dissolved in a DCM and ethanol mixture (3:1) and transferred to a 100 ml round bottom flask (RBF), followed by the formation of a thin film by removal of organic solvent using a rotary evaporator. The RBF with a thin film was purged with dried nitrogen gas for 60 min. After that, the thin film was redispersed slowly using a dispersive medium (phosphate-buffered saline, 10 mM) to yield a dispersion mixture. The dispersion was probe sonicated for 20 s at

20% amplitude under ice-cold conditions, followed by centrifugation at 12000 rpm for 10 min. The obtained supernatant was collected containing Hybrid TMZ NCs and subjected to evaluation for particle size (PS), polydispersity index (PDI), zeta potential (ZP), and surface morphology. Further, the Hybrid TMZ NCs were evaluated for TMZ and colloidal stability. The loading amount of TMZ was calculated from the weight ratio method using the simple UV-Vis spectrophotometer (at λ_{\max} 328 nm) and calculated as per the below-mentioned formulae:

$$\%TMZ \text{ loading in compound } \mathbf{8} = \frac{\text{Amount of TMZ present}}{\text{Amount of compound } \mathbf{8} \text{ taken}} \times 100 \quad \text{eq. 4.1}$$

$$\%TMZ \text{ loading in Hybrid nanoconjugate} = \frac{\text{Amount of TMZ in compound } \mathbf{8}}{\text{Total polymer (8 \& 9)}} \times 100 \quad \text{eq. 4.2}$$

The hydrodynamic diameter, particle size distribution, and surface zeta potential (ζ) were measured using dynamic light scattering (DLS) (Zetasizer Nano ZS, Malvern Panalytical Ltd, UK), measuring angle of 173 °. The surface morphology was evaluated by prior surface coating of Hybrid TMZ NCs with gold/chromium target for 120 s using Q150TES sputter coater, Quorum Technologies (Lewes, UK). After that, the coated particles were evaluated using Field Emission-Scanning Electron Microscopy (FE-SEM) (FEI, Apreo S LoVac, Thermo Fisher Scientific, MA, USA) with a spot size of 9 mm under vacuum.

4.2.5. Stability studies

The stability studies of the developed Hybrid TMZ NCs were performed under physiological pH at 4 °C and 37 °C. The samples were kept in a closed vial and incubated for a specific period, followed by the determination of change in particle size and %TMZ remaining in the *mPEG-b-P(CB-{g-COOH; g-TMZ₄₀})* and Hybrid TMZ NCs using dynamic light scattering (DLS) and UV method, respectively. For the DLS measurements, *mPEG-b-P(CB-{g-COOH; g-TMZ₄₀})* and Hybrid TMZ NCs were taken at a concentration of 3 mg/ml and analyzed for the change in particle size and PDI for 7 days. Furthermore, the same samples were used to determine the %TMZ remaining in the conjugates. For the UV stability analysis, the samples (free TMZ, *mPEG-b-P(CB-{g-COOH; g-TMZ₄₀})* (**8**), and Hybrid TMZ NCs) were taken and analyzed at predetermined time points (0, 6, 12, 24, 48, 72, 96, 120 h) using UV-Vis spectrophotometry. The samples analyzed were withdrawn from the stock and diluted, and UV absorbance was evaluated at 328 nm for the %TMZ remaining, and the stability graph of %TMZ remaining was plotted over time.

4.2.6. Cell culture studies

C6 and U87MG glioma cell lines were obtained from the National Centre for Cell Sciences (NCCS, Pune, India). C6 and U87MG cells were maintained in Dulbecco's Modified Eagle Medium (DMEM) and Minimum Essential Medium (MEM), respectively, supplemented with 10% fetal bovine serum (FBS) and 1% penicillin/streptomycin mixture, kept in an incubator at 37 °C with 5% CO₂. The cells were allowed to proliferate until 70-80% confluency was achieved for further experimentation.

4.2.6.1. Cell viability assay

C6 and U87MG glioma cells were trypsinized, and cells were seeded in a 96-well cell-culture plate at a cell density of 5000 cells/well and incubated at 37 °C/ 5% CO₂ for 24 h. The following day, cells were treated with free TMZ or Hybrid TMZ NCs in a concentration range of TMZ equivalent to 100-1500 µM and 25-1000 µM for C6 and U87MG cells, respectively. After 72 h of treatment, media was replaced with fresh media containing 5 mg/ml of 3-(4,5-dimethyl-thiazol-2-yl)-2, 5-diphenyl tetrazolium bromide (MTT) and kept for 4 h in an incubator. After the formation of formazan crystals, the media was discarded, and 200 µl of DMSO was added to each well to dissolve the crystals. The extent of metabolic activity was measured by determining the absorbance at 570 nm and 630 nm using an Epoch microplate spectrophotometer (Biotek Instruments, USA). The %cell viability was calculated using the below-mentioned equation [8].

$$\%Cell\ Viability = \left\{ \frac{[Absorbance\ of\ sample\ wells\ (560\ nm) - absorbance\ of\ sample\ wells\ (630\ nm)]}{[Absorbance\ of\ control\ wells\ (560\ nm) - absorbance\ of\ control\ wells\ (630\ nm)]} \right\} \times 100 \quad eq. 4.3$$

4.2.6.2. Apoptosis assay

Apoptosis analysis of Hybrid TMZ NCs was determined using the Annexin-V/PI-kit-based flow cytometry assay. Briefly, C6 and U87MG glioma cells were seeded in a 6-well plate (1×10^5 cells/well). The cells were incubated overnight, followed by the treatment with free TMZ and Hybrid TMZ NCs for 24 h. Thereafter, cells were washed with PBS, trypsinized, centrifuged, resuspended in 1X annexin binding buffer, and stained with annexin-V/ propidium iodide in a dark condition for 15 min. Flow cytometry (Beckman Coulter, USA) was used to analyze the apoptosis rate, and data were interpreted using CytExpert V3.0 software [8].

4.2.6.3. Cell uptake assay

The cellular uptake of Hybrid TMZ NCs was determined using qualitative and quantitative methods. Briefly, cells (C6 and U87MG) were seeded in a 6-well plate (1×10^5 cells/well) and allowed to adhere for 24 h. Thereafter, the cells were treated with blank coumarin-6 dye and coumarin-6-loaded Hybrid TMZ NCs and incubated for 4 h. Further, the cells were washed with PBS, fixed with 2% paraformaldehyde for 10 min, and counterstained with DAPI for 10 min to stain the nucleus. For qualitative analysis, fixed cells were observed under a fluorescence microscope (ZEISS, Germany), and respective microscopic images (DIC, DAPI, Coumarin-6, and Overlay) were acquired for the treatment groups. Obtained data were interpreted using Zen Blue software V3.4. For quantitative analysis, the samples were trypsinized, washed with PBS, and evaluated for the quantitative uptake of coumarin-6-dye in glioma cells using flow cytometry (Beckman Coulter, USA), and the obtained data were interpreted using CytExpert V3.0 software [8].

4.2.7. C6 cells induced orthotropic glioblastoma model development in rats

C6 glioma cells were incubated until 70% of confluency, and cells were trypsinized with (0.25% trypsin/EDTA solution), washed with DMEM medium, and suspended in 80 μ l of sterile phosphate-buffered saline. *Sprague Dawley* male rats, 6-8 weeks old, were used after the approval from the Institutional Animal Ethics Committee (IAEC) of BITS Pilani, with protocol no: IAEC/RES/23/08/Rev-3/32/26, and all the animal experiments were performed as per the Committee for the Purpose of Control and Supervision of Experiments on Animals (CPCSEA) guidelines. For C6 glioma cells implantation, rats were anesthetized with ketamine and xylazine at 90 mg/kg and 9 mg/kg, i.p., respectively. Animals were placed on the stereotaxic apparatus, and the head was shaved, followed by a small incision of 3 cm to expose the skull. A 1 mm burr hole was drilled, and C6 cells (2×10^6) were injected at 2 mm anterior, 3 mm lateral, and 4 mm depth to the bregma at a flow rate of 3 μ l/min using Hamilton's syringe. After injection, the needle was kept in the same position additionally for 2 min to avoid backflow. After that, the burr hole was sealed using biodegradable wax, and an incision was closed using a suture. Animals were placed back in their home cages and observed until they regained consciousness. Animals were observed daily for their change in neurological behaviour, body weight, and right eye bulging as an indicator of tumor development.

4.2.8. *In vivo* efficacy studies of Hybrid TMZ NCs in C6 cells induced orthotropic rat glioma model

Briefly, C6 glioma cells bearing rats were randomly taken and kept for 9 days, followed by the start of the treatment phase from day 10 with treatment groups (n=5) including positive control, free TMZ, and Hybrid TMZ NCs. All drug treatments were given intravenously (i.v.) at a dose equivalent to 10 mg/kg of TMZ thrice a week for the next 30 days. The animals were regularly monitored for their change in body weight, locomotion, and neurobehavioral activity. On day 40 (i.e., 30 days after treatment), animals were sacrificed, and the blood and major organs (heart, lungs, liver, spleen, kidney, etc.) were excised for histopathological evaluation. In addition, the excised brains of all the animals were isolated and evaluated for physical appearance, brain weight, hemispherical width ratio (RH/LH), and histopathological evaluation.

4.3. Statistical analysis

Results are expressed as mean \pm SD and mean \pm SEM. All the obtained data were analyzed using ANOVA (analysis of variance) followed by Tukey's test for comparison between treatment groups. $p < 0.05$ was considered statistically significant.

4.4. Results

4.4.1. Characterisation of TMZ conjugated amphiphilic copolymer (mPEG-b-P(CB-{g-COOH; g-TMZ₄₀}) (8)

The polymer TMZ conjugate was synthesized using a multistep reaction between compounds 4 and 7 to give *mPEG-b-P(CB-{g-COOH; g-TMZ₄₀})* using Carbodiimide/N-hydroxybenzotriazole (EDC/HOBt) coupling (Figure 4.1). Figure 4.3 shows ¹H NMR (400 MHz, DMSO-*d*₆) of *mPEG-b-P(CB-{g-COOH; g-TMZ₄₀})* with peaks at δ 10.31 (-NH-NH-), 10.05 (-NH-NH-), 8.84 (N-CH=N- of TMZ), 7.32 (-C₆H₅ of MBC), 5.13 (CH₂-Bn), 4.19 (CH₂-O-*bisMPA*), 3.87 (N-CH₃ of TMZ), 3.51 (-CH₂ of PEG), 3.16 (CH₃-O-PEG), 1.11 (-CH₃ of *bisMPA*), and ¹³C NMR (101 MHz, DMSO-*d*₆) showed peaks at δ 197.08, 173.81, 173.75, 173.70, 158.80, 154.12, 147.56, 139.13, 135.13, 128.76, 88.25, 74.13, 73.94, 69.80, 69.06, 45.70, 45.29, 36.23, 17.16 and 15.66. The synthesized *mPEG-b-P(CB-{g-COOH; g-TMZ₄₀})* consisting of 40 units of TMZ covalently attached to polymer backbone (7), with loading efficiency and average molecular weight equivalent to 28.82% w/w and ~29 KDa, respectively.

4.4.2. Characterization of mPEG-Poly lactic acid (mPEG-PLA) (9)

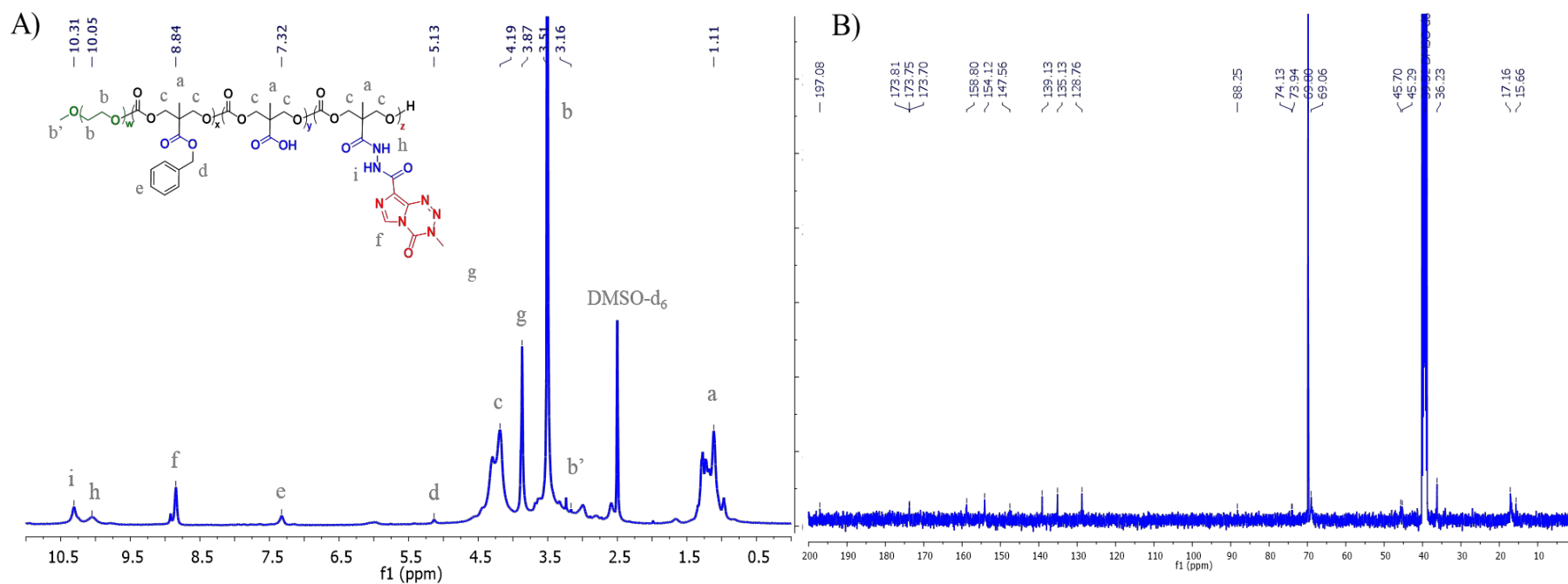


Figure 4.3. Characterisation of *mPEG-b-P(CB-{g-COOH; g-TMZ₄₀})* using A) $^1\text{H-NMR}$ and B) $^{13}\text{C-NMR}$

mPEG-PLA **9** was synthesized using ROP of the DL-lactide in the presence of mPEG as a macroinitiator using tin(II) ethyl hexanoate as a catalyst. ^1H NMR (400 MHz, CDCl_3) of mPEG-PLA **9** indicates an average molecular weight of 10 KDa with ~ 70 units of lactic acid.

4.4.3. Characterization of hybrid nanoconjugates composed of component **8** & **9** (Hybrid TMZ NCs)

Hybrid TMZ NCs consisting of *mPEG-b-P(CB-{g-COOH; g-TMZ₄₀})* (**8**) and mPEG-PLA (**9**) (3:1 ratio) were prepared using the thin film hydration method. The resulting Hybrid TMZ NCs depicted particle size of 105.7 ± 0.99 nm with a narrow polydispersity index of 0.106 ± 0.033 and a surface zeta potential of ζ : -6.79 ± 1.61 mV (Figure 4.4), compared to *mPEG-b-P(CB-{g-COOH; g-TMZ₄₀})* exhibited particle size of 90.9 ± 3.80 nm with PDI of 0.256 ± 0.011 , and surface zeta potential of ζ : -12.06 ± 0.86 mV. The SEM images of Hybrid TMZ NCs confirmed the particles obtained were uniform in size and spherical in morphology. Different ratios of *mPEG-b-P(CB-{g-COOH; g-TMZ₄₀})* (**8**) and mPEG-PLA (**9**) were screened ranging from 1:0, 3:1, 2:1, 1:1, 1:2, 1:3, and 0:1, exhibiting a particle size from 90 nm to 115 nm with variable loading capacities (Table 4.1). To achieve the maximum loading capacity, we selected *mPEG-b-P(CB-{g-COOH; g-TMZ₄₀})* (**8**) and mPEG-PLA (**9**) with 3:1 ratio wherein the loading capacity of the Hybrid TMZ NCs was found to be $\sim 21.6\%$ w/w. Thereafter, the experiments were performed using 3:1 ratio of compound **8** and **9**.

4.4.4. Stability of Hybrid TMZ nanoconjugate (Hybrid TMZ NCs)

The colloidal stability of the Hybrid TMZ NCs was determined in physiological pH at 4 °C and 37 °C for up to 7 days. At 4 °C, *mPEG-b-P(CB-{g-COOH; g-TMZ₄₀})* and Hybrid TMZ NCs showed no significant change in particle size for 7 days. At 37 °C, *mPEG-b-P(CB-{g-COOH; g-TMZ₄₀})* demonstrated a marked change in particle size after 2 days, while Hybrid TMZ NCs were stable for over 7 days. TMZ exhibits hydrolytic degradation to form MTIC and AIC under physiological pH with a half-life of 1.8-1.9 h. The Hybrid TMZ NCs degradation behavior was determined using UV-Vis spectrophotometry at characteristic TMZ wavelength (328 nm) for 120 h and compared with free TMZ and *mPEG-b-P(CB-{g-COOH; g-TMZ₄₀})*. The conjugation of TMZ (*mPEG-b-P(CB-{g-COOH; g-TMZ₄₀})*) has improved the half-life to 5.88 h, but it is still not significantly stable for the *in vivo* application. While at physiological conditions (pH 7.4, 37 °C), Hybrid TMZ NCs exhibited an improved stability half-life of ~ 194 h (Figure 4.4 D&E).

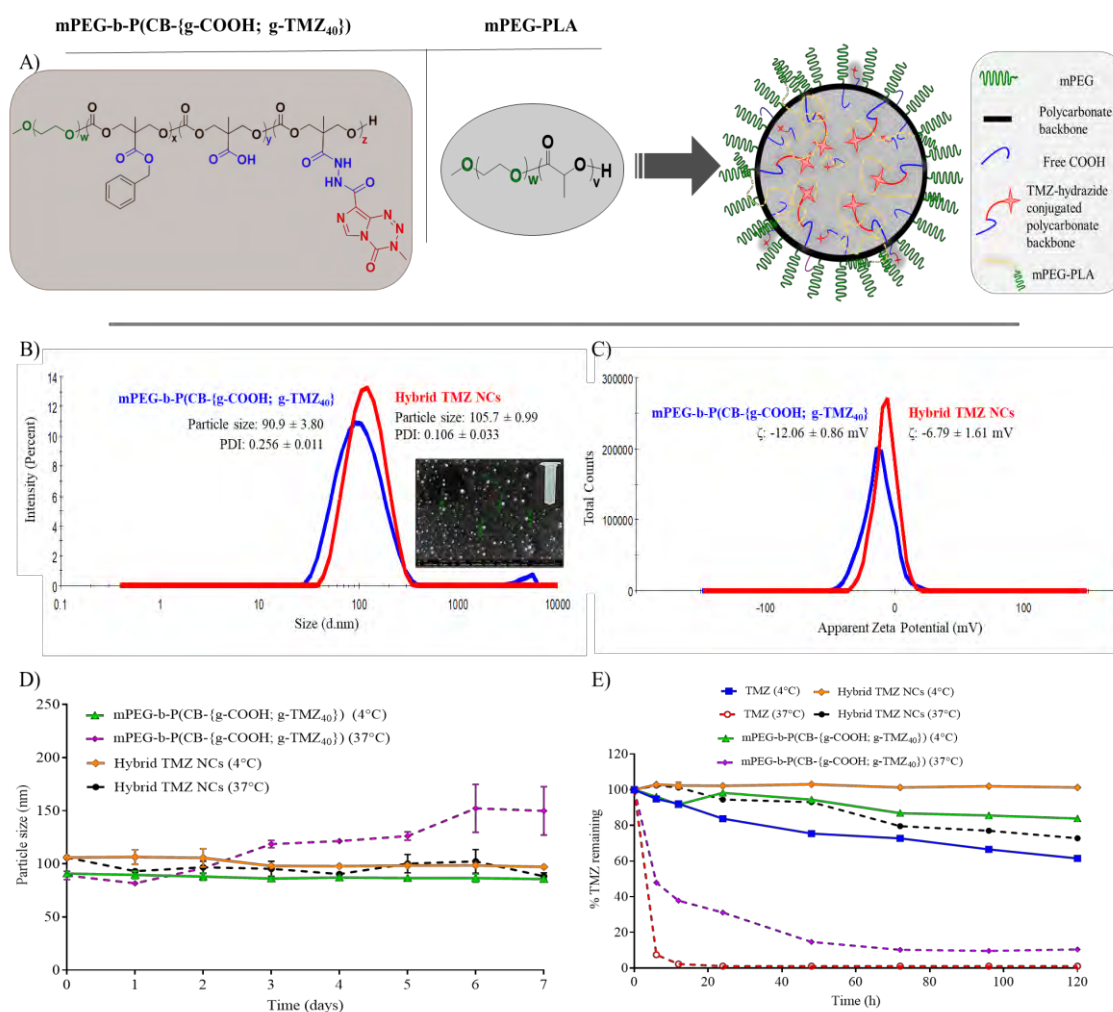


Figure 4.4. Characterization of hybrid nanoconjugates. A) Schematic representation of hybrid nanoconjugates in combination with $m\text{PEG-b-P}(\text{CB}\{-\text{g-COOH}; \text{g-TMZ}_{40}\})$ and $m\text{PEG-PLA}$, B) particle size with SEM image and pictograph, C) surface zeta potential, D) DLS-based colloidal stability, and E) UV-based TMZ stability evaluation of Hybrid TMZ NCs in phosphate buffered saline (PBS; pH 7.4) at 4 °C and 37 °C

Table 4.1. Preparation of Hybrid TMZ NCs using different ratios of $m\text{PEG-b-P}(\text{CB}\{-\text{g-COOH}; \text{g-TMZ}_{40}\})$: $m\text{PEG-PLA}$

Ratio ($m\text{PEG-b-P}(\text{CB}\{-\text{g-COOH}; \text{g-TMZ}_{40}\})$: $m\text{PEG-PLA}$)	Particle Size (nm)	PDI
1:0	90.9 ± 3.8	$0.256 \pm .011$
3:1	105.7 ± 0.99	0.106 ± 0.033
2:1	103 ± 2.09	0.218 ± 0.008
1:1	113.96 ± 1.49	0.168 ± 0.010
1:2	107.8 ± 2.71	0.141 ± 0.021
1:3	105.6 ± 4.91	0.254 ± 0.022
0:1	115.93 ± 7.266	0.264 ± 0.0374

4.4.5. *In vitro* uptake and cytotoxicity of Hybrid TMZ NCs

The cell viability profiles of treatment groups (including free TMZ and Hybrid TMZ NCs) were determined in C6 and U87MG glioma cell lines, as shown in Figure 4.5 A&B. The Hybrid TMZ NCs significantly improved IC_{50} to $\sim 645 \mu\text{M}$ compared to $\sim 1125 \mu\text{M}$ for free TMZ in C6 glioma cells. Similarly, in U87MG cells, the Hybrid TMZ NCs showed an IC_{50} of $\sim 866 \mu\text{M}$ compared to $\sim 738 \mu\text{M}$ for free TMZ.

The cellular uptake of Hybrid TMZ nanoconjugate was analyzed in C6 and U87MG glioma cells using coumarin-6 as a fluorescent dye, which showed an improved uptake in both glioma cells. Flow cytometry analysis also confirmed that the developed Hybrid TMZ NCs exhibited uptake efficiency of $\sim 74\%$ and $\sim 79\%$ in C6 and U87MG glioma cells, respectively (Figure 4.6).

4.4.6. Apoptosis assay

Apoptosis analysis was performed using the Annexin/PI staining method to determine the apoptosis in C6 and U87MG glioma cells after treatment with free TMZ and Hybrid TMZ NCs. Figure 4.5C represents the apoptosis in C6 glioma cells, wherein the Hybrid TMZ NCs demonstrated significant improvement in apoptosis of 27.6% (early apoptosis: 25.4% and late apoptosis: 2.1%) compared to free TMZ with apoptosis of 15.5% (early apoptosis: 15.45% and late apoptosis: 0.05%). Similarly, in U87MG cells, the Hybrid TMZ NCs showed a significantly improved apoptosis of 42.75% (early apoptosis: 40.99% and late apoptosis: 1.76%) compared to free TMZ with apoptosis of 21.33% (early apoptosis: 20.57% and late apoptosis: 0.76%) (Figure 4.5D), indicating the improved efficacy of Hybrid TMZ NCs.

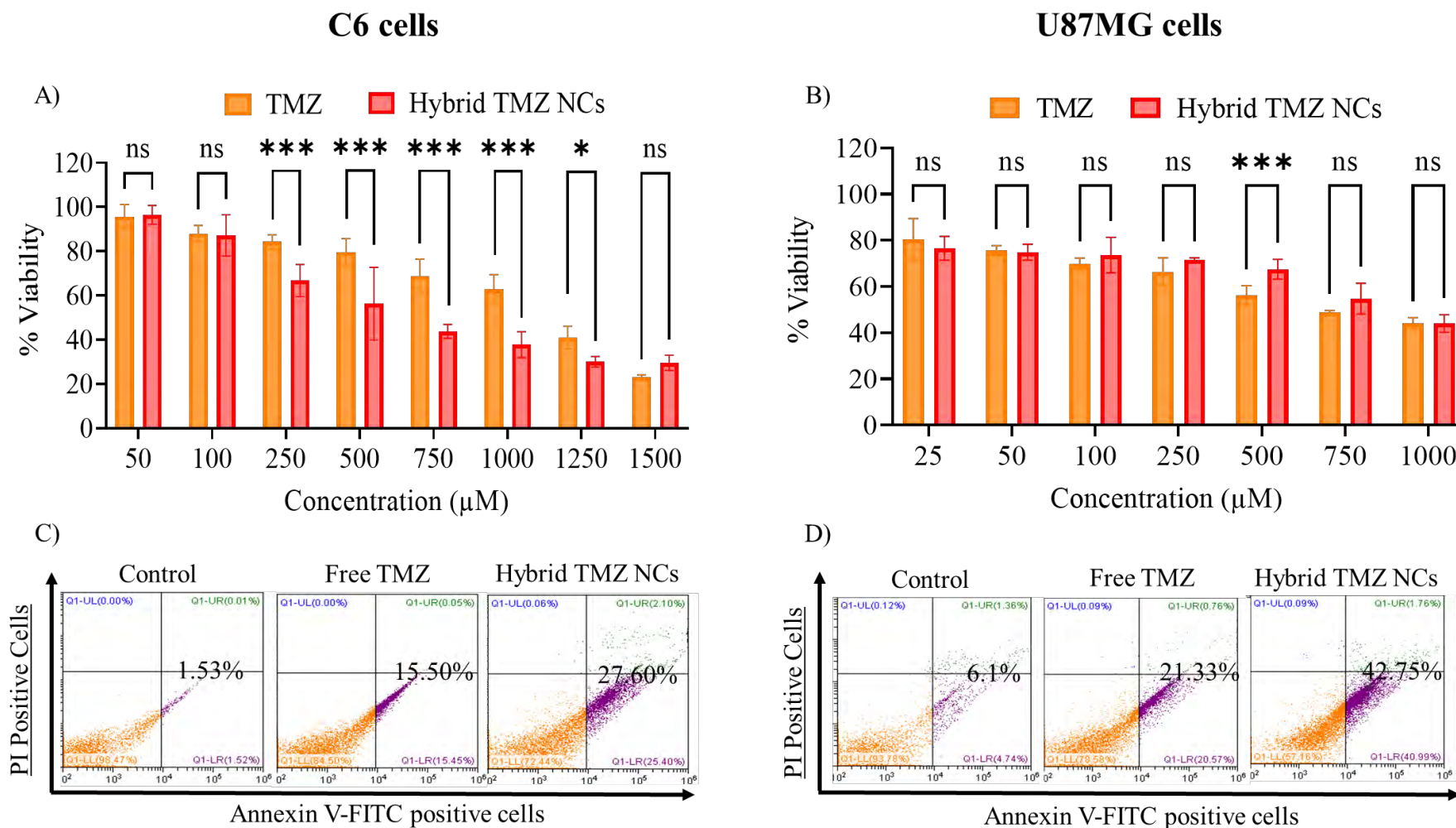


Figure 4.5. *In vitro* cell-based evaluation of Hybrid TMZ NCs in glioma cells. Cell cytotoxicity using MTT assay in A) C6 and B) U87MG glioma cells. Annexin-V/PI-based apoptosis assay in C) C6 and D) U87MG glioma cells

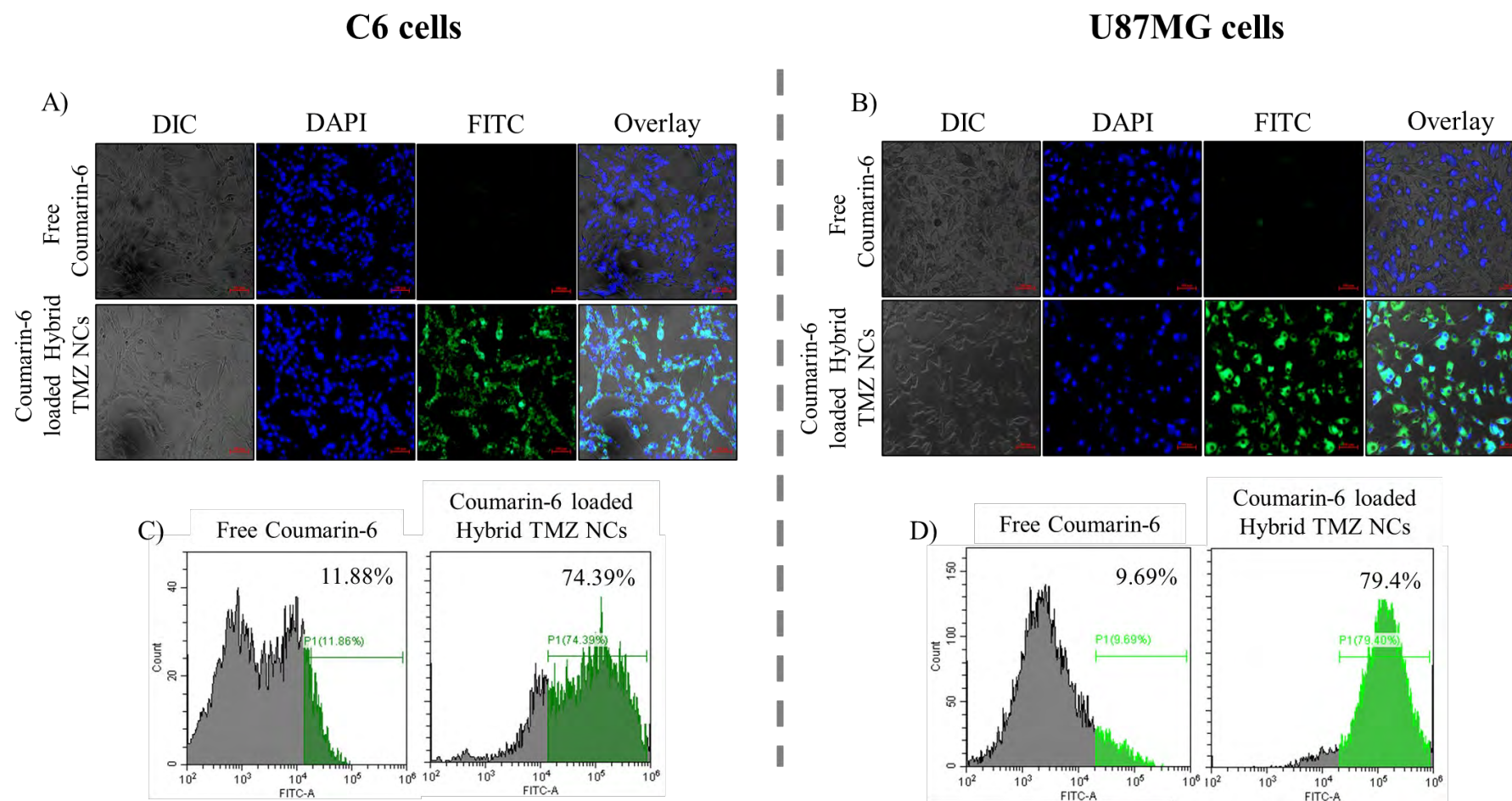


Figure 4.6. *In vitro* cell-based evaluation of Hybrid TMZ NCs in glioma cells. Coumarin (C6)-based cellular uptake assay. A) & B) Qualitative evaluation using microscopy in C6 and U87MG glioma cells, C) & D) Quantitative uptake using flow cytometry in C6 and U87MG glioma cells, respectively

4.4.7. *In vivo* efficacy

The *in vivo* antitumor efficacy of Hybrid TMZ NCs was evaluated in a C6-induced orthotropic syngeneic glioma model in *Sprague Dawley* rats (Figure 4.7). Animals were treated intravenously with free TMZ and Hybrid TMZ NCs at a dose equivalent to 10 mg/kg of TMZ thrice a week for 30 days. The group treated with normal saline (positive control) showed 100% mortality within 15 days after initiation of treatment, while the free TMZ-treated group showed mortality up to 40% till day 40 (30th day of treatment). Surprisingly, no mortality was observed in the Hybrid TMZ NCs treated group till 40 days. A noticeable weight loss was observed in all the animals after the injection of cells in the orthotropic site; later on, the animals showed recovery in body weight. The brain tissue of all animals was excised and evaluated for brain weight, and the right-to-left hemispherical width (RH/LH) ratio was examined to confirm tumor growth. It was observed that the positive control group showed significantly higher brain weight and RH/LH hemispherical width ratio as compared to the negative control group (normal animals). TMZ-treated animals showed a nominal reduction in brain weight and RH/LH hemispherical width ratio compared to the positive control group. Further, treatment with Hybrid TMZ NCs demonstrated a statistically significant decrease in the brain weight and the RH/LH hemispherical width ratio compared to the positive control group, indicating improved efficacy *in vivo* compared with the free TMZ-treated group. Further, the excised brain was subjected to histopathological toxicity evaluation. Figure 4.7 (C1-C4) shows the brain histopathological analysis of the positive control group with significantly higher infiltration of mononuclear cells/ tumor cells at the site of injection (dotted line) depicting the tumor growth. In contrast, no such infiltration was observed in the left hemisphere of the brain, showing normal cellular morphology with no infiltration of C6 cells (uninjected site) (*data not shown*). Treatment with Hybrid TMZ NCs showed a reduction in the mononuclear cells in the right hemisphere of the brain compared to the positive control group, indicating their effectiveness on the tumor burden in glioma-induced rats.

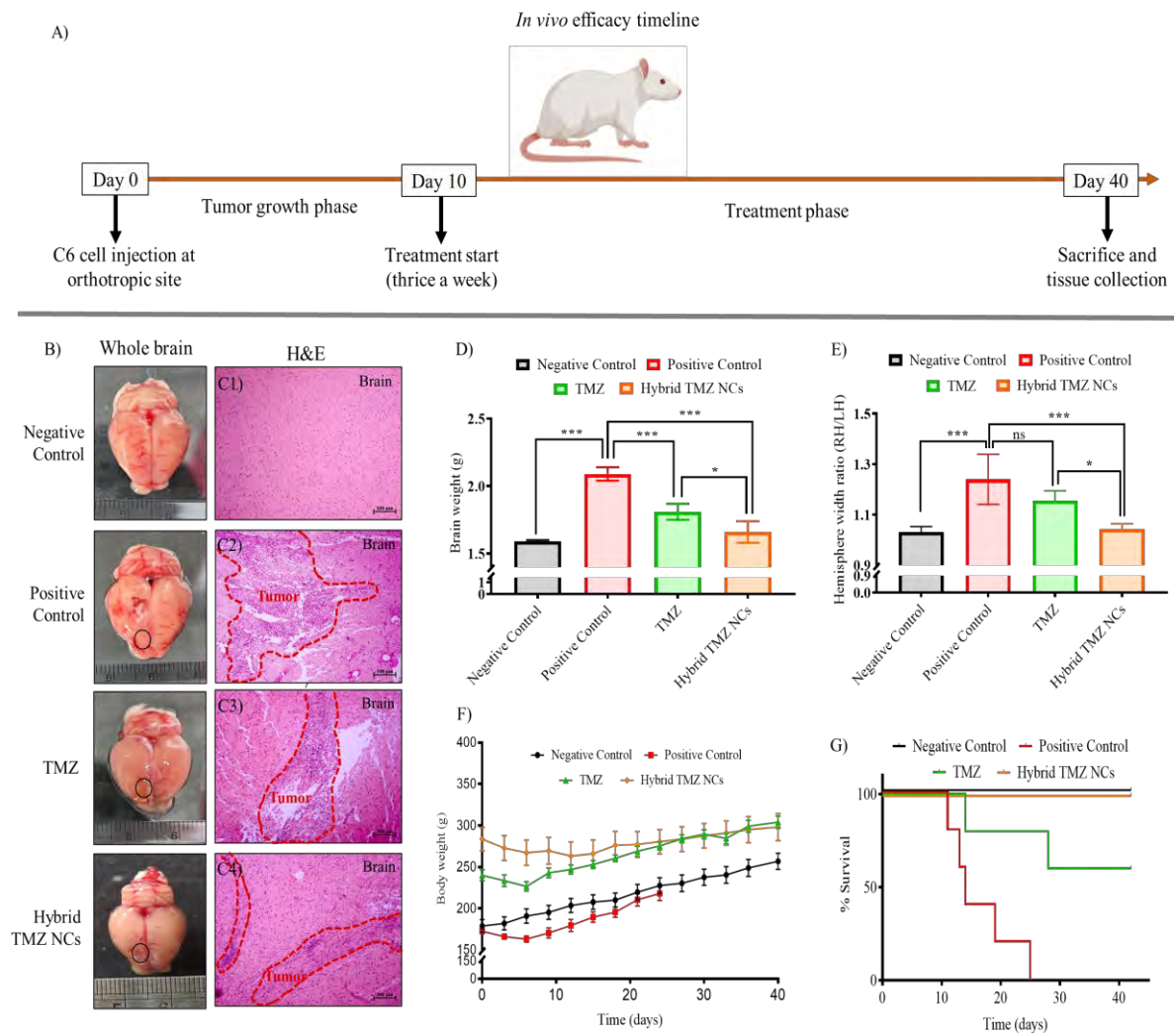


Figure 4.7. *In vivo* efficacy of hybrid nanoconjugates in C6-cells induced orthotopic syngeneic glioma model in SD rats. A) Treatment schedule. B) Representative brain images of treatment groups (negative control, positive control, TMZ-treated, and Hybrid TMZ NCs treated) and its C1-C4 brain histopathological (H&E) evaluation of the right hemisphere (at the site of injection). D), E), F), and G) represents mean brain weight, hemispherical width ratio (RH/LH), body weight, and Kaplan-Meier survival plot of treated animals, respectively (scale bar: 100 μ m) (*, *** indicates p value <0.05, <0.001, respectively)

4.4.8. Toxicity evaluation of hybrid nanoconjugates

The histopathological evaluation of various organs, including the heart, lungs, liver, kidney, and spleen, were evaluated using H&E staining to study the toxicity of the Hybrid TMZ NCs (Figure 4.8). The negative control (healthy animals) depicted normal morphology of the heart tissue with central nuclei and syncytial arrangement of fibers with intercalated disks. Similarly, treatment groups (positive control, free TMZ, and Hybrid TMZ NCs) showed similar histology regarding fiber arrangement and the presence of intercalated discs. Lungs are considered to be highly perfused organs and become the primary target of cancer cells. The positive control group treated with saline showed moderate tumor cell infiltration to the lungs with an increased mitotic cell infiltration compared to the negative control group. Upon treatment with free TMZ, a slight reduction in infiltration was observed. Interestingly, treatment with Hybrid TMZ NCs demonstrated a significant decrease in the mitotic nucleus and thickened alveolar septa, showing the positive anticancer outcome of the developed hybrid nanoconjugates on the lungs.

In histopathological analysis of the liver, the negative control group depicted the standard architecture of liver components consisting of hepatocytes, central vein, kupffer cells, bile duct cells, etc. In contrast, the positive control and TMZ-treated groups showed degenerative changes to the liver hepatocytes. In comparison, groups treated with Hybrid TMZ NCs demonstrated the normal architecture of the liver components (hepatocytes, kupffer cells, bile duct cells). Further, kidneys of the positive control tumor-bearing animals depicted alteration in the kidney components, such as atrophic renal tubules with increased peritubular space, and a similar trend was observed in free TMZ-treated animals. Treatment with Hybrid TMZ NCs yielded improved kidney histology with normal renal cortex, medulla, renal papilla, renal tubules, and glomerular tufts. The microscopic evaluation of splenic histology showed treatment with free TMZ, which showed moderate depletion in white pulp lymphoid components. At the same time, Hybrid TMZ NCs improved the splenic architecture with normal lymphoid follicles and sinuses with slight to minimal lymphoid depletion. Overall, the hybrid nanoconjugates exhibited better biocompatibility and recuperated organ components to normal levels with minimal to negligible toxicity comparable to the negative control group (Figure 4.8).

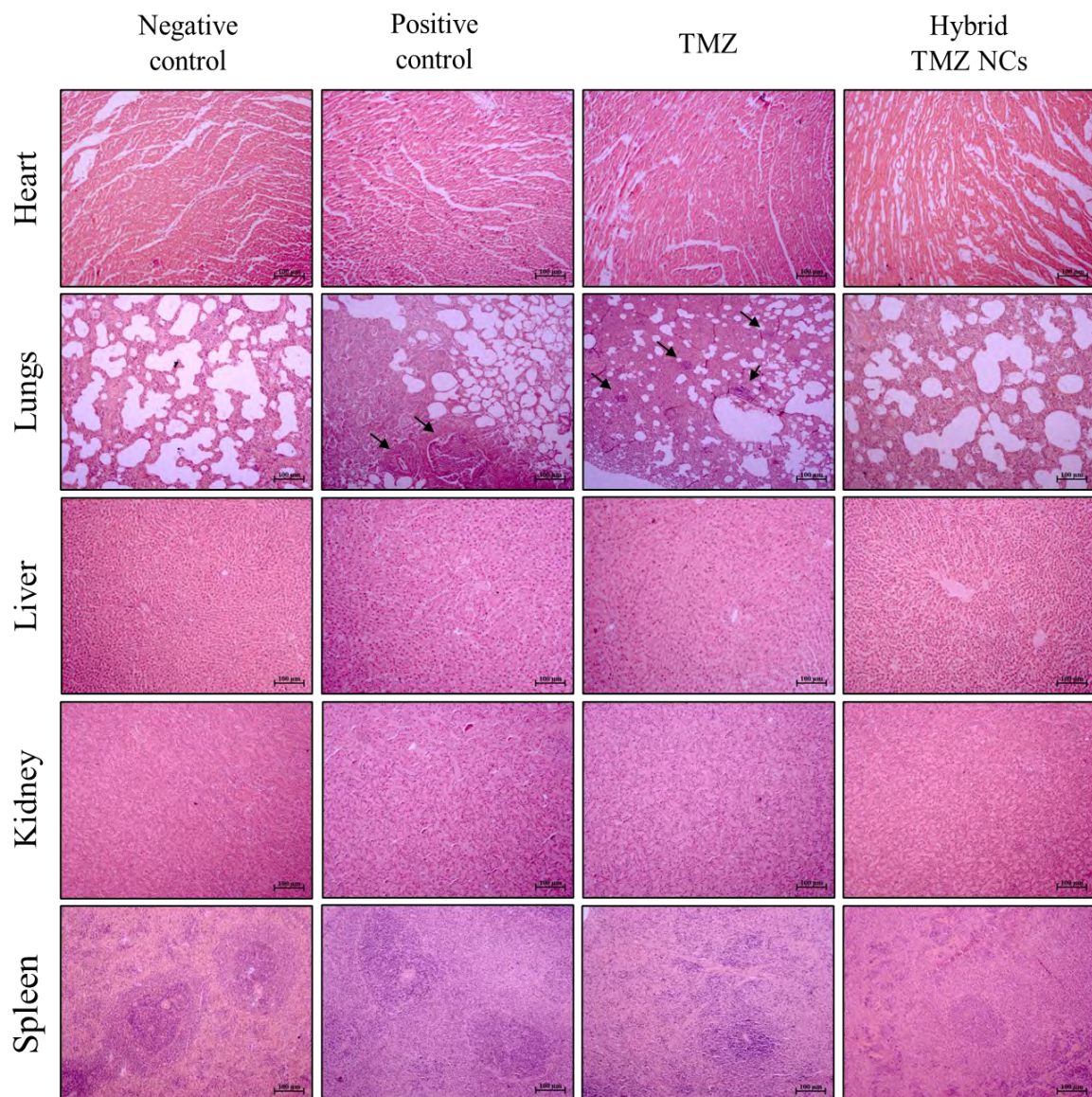


Figure 4.8. *In vivo* H&E evaluation of hybrid nanoconjugate in majorly excised organs (heart, lungs, liver, kidney, and spleen) in C6-induced orthotopic glioma model in SD rats. (lungs: arrow indicates the presence of mitotic nucleus) (scale bar: 100 μ m)

4.5. Discussion

Glioblastoma multiforme stands out as the most prevalent and deadly form of brain tumor among adults, representing 16% of all brain and central nervous systems. For treating GBM, temozolomide (TMZ) is considered the gold standard chemotherapeutic DNA alkylating agent with debulking surgery and concurrent radiotherapy. Currently, TMZ is given as capsules and parental injections, which go into circulation and finally to the target site of action. Although TMZ carries the potential for its antitumor efficacy, the molecule still possesses a series of limitations, including rapid clearance, short half-life, and pH-dependent degradation under physiological conditions, eventually resulting in <1% of the drug reaching the brain in intact form with additional off-target toxicities. However, newer strategies have been discovered to overcome the delivery and physiochemical-related limitations of the drug. Likewise, nanotechnology has significantly improved the physiochemical behavior of the hard-to-delivery molecules. Similarly, polymeric, lipidic, and inorganic materials have shown promising outcomes in overcoming TMZ-associated limitations [3]. Encapsulation of TMZ into solid-lipidic nanoparticles has shown particles of ~66 nm with an encapsulation efficiency of ~59% at a loading capacity of <1% w/w. *In vivo* administration of the TMZ-SLNs has shown improved brain accumulation and systemic circulation time compared to the free TMZ solution [13]. In another study, encapsulation of the drug into biocompatible polymer PLGA showed encapsulation of 12.6% at 2% of loading capacity, and other reports showed encapsulation of 28% at a loading capacity of 1.4% w/w [14]. Despite the significant advancements in TMZ delivery, the challenge remains while encapsulating TMZ mainly because of its unique physiochemical behaviour. Thereby, rendering the delivery process quite strenuous.

Another category, the polymer-drug therapeutics approach, has also been used to overcome the concerns associated with the physiochemical properties and delivery of molecules. Wherein the covalent conjugation of TMZ with the biocompatible polycarbonate copolymer could be utilized to overcome the low-loading, stability, tissue/organ targeting, and off-target toxicities. Additionally, polycarbonates offer several advantages in delivering drugs to the specific site, as discussed in section 3.5. Several reports have also stated covalent conjugation of the drug molecule with the polycarbonates as a side chain or pendent group has significantly overcome the drug-associated limitations, including low drug loading capacity, reduced systemic clearance, controlled release, improved circulation half-life, and tissue targeting, etc. [5,15]. Similarly, in the previous chapter, we designed and fabricated covalently

conjugated TMZ to PEG-based polycarbonate polymer-drug conjugates. The resulting conjugates have demonstrated significant enhancement in the physiochemical properties of the TMZ with improved drug loading capacity of 16.8 to 37.99% w/w and yielded nano-sized particles ranging from 90-552 nm. After that, the stability of nanoconjugates is the major concern in the biological milieu, playing an essential role in determining the outcome of the therapeutics. In the previous chapter, section 3.4.3, we have determined the colloidal and TMZ stability of *mPEG-b-P(CB-{g-COOH; g-TMZ₄₀})*, indicating a significant change in particle size from day 2 under physiological conditions. The same samples were evaluated for the %TMZ content that showed a slight improvement in the stability half-life up to 5.88 h compared to the 1.8 h of free TMZ. Despite the significant improvement in the loading capacity using the conjugation strategy, the stability perspective is still a concern. To enhance the stability, we prepared the Hybrid TMZ NCs, wherein different ratios of *mPEG-b-P(CB-{g-COOH; g-TMZ₄₀})* and mPEG-PLA polymer were screened ranging from 1:0, 3:1, 2:1, 1:1, 1:2, 1:3, and 0:1 (Table 4.1). These Hybrid TMZ NCs exhibited nearly similar particle size ranging from 105 to 115 nm in all the ratios, with a slight increase in particle size from individual *mPEG-b-P(CB-{g-COOH; g-TMZ₄₀})* component with size of 90.9 nm was observed. This is mainly observed due to utilisation of dual components in the Hybrid TMZ NCs. These system exhibited the loading capacity up to 21.6% w/w. Literature evidence also suggested that a hybrid system can provide advantages such as improved drug stability, colloidal stability, biocompatibility, combinational drug delivery, ease in fabrication, controlled release properties, and reduced toxicities [16]. For instance, Tahir *et al.* prepared lipid-polymer hybrid nanoparticles using PLGA polymer and DSPE-PEG lipid, yielding particle size ranging from 173-208 nm with excellent physical stability, biocompatibility, and a higher degree of internalization compared to free drug [17]. Similarly, Ebrahimian *et al.* prepared lipopolymeric nanoparticles using PLGA and PLGA-PC to enhance the stability of bromelain and facilitate oral delivery. The hybrid system showed stable nanoparticles with no significant change in particle size, PDI, and zeta potential for over 1 month of storage [18]. In the current study, we prepared the hybrid system containing the TMZ-conjugate with mPEG-PLA to yield Hybrid TMZ NCs. Hybrid TMZ NCs showed an average particle size of 105.7 nm and PDI of 0.106. Surprisingly, the colloidal and TMZ stability of the Hybrid TMZ NCs was significantly improved for over 7 days and 120 h, respectively, with half-life improved from 5.88 h to ~194 h (Figure 4.4). Overall, *in vitro* evaluation of the nanoconjugates has demonstrated the marked

enhancement of the physiochemical properties of the TMZ, wherein the stability and loading capacity of the TMZ were significantly improved using the above approach.

Lipid-polymeric hybrid nanosystems have demonstrated advancement in the development of the delivery platform for overcoming the physiological barriers involved in delivering the payload to the target region or site of action [10]. Likewise, Pukale *et al.* prepared lipid-polymer hybrid nanoparticles for the delivery of clobetasol propionate for psoriasis like skin condition, wherein, LPNs with particle size of 94.8 nm exhibited improved cellular uptake up to 99.81% with significantly improved *ex vivo* epidermis and dermis penetration into the psoriatic like skin [8]. Another study reported that the Lipid-polymeric hybrid nanoparticles loaded with erlotinib and bevacizumab exhibited improved uptake efficiency of up to 52.3% with reduced cellular viability compared to free drug treatment in A549 lung cancer cells [19]. Similarly, in our study, the Hybrid TMZ NCs exhibited improved cellular uptake efficiency up to 74% and 79% in C6 and U87MG glioma cells that resulted in an IC_{50} of Hybrid TMZ NCs at ~645 and 866 μM compared to 1125 and 738 μM for free TMZ in C6 and U87MG glioma cells, respectively. Likewise, previously, we have reported the cytotoxicity of TMZ in glioma cell lines with IC_{50} of >1000 μM and ~700 μM with total apoptosis of 18.8% and 25.32% in C6 and U87MG glioma cells, respectively [20]. Moreover, the Hybrid TMZ NCs demonstrated improved apoptosis rate up to 27.6% and 42.75% compared to 15.5% and 21.33% of free TMZ in C6 and U87MG glioma cells, respectively (Figure 4.5).

Thereafter, a C6 cells-induced orthotropic syngeneic glioma model was developed in *Sprague Dawley* rats. After the glioma model induction in rats, the change in physiological parameters, including right eye bulging, loss in body weight, reduced locomotion activity, etc., were observed to confirm the tumor growth. The animals were randomly divided, and the treatment was initiated. After the completion of the treatment phase, animals were sacrificed, and changes in brain parameters such as brain weight and hemispherical width ratio were noted. The Hybrid TMZ NCs resulted in a significant reduction in the brain weight brain hemispherical width ratio (RH/LH), and the mononuclear cell infiltration in the brain tissue was observed compared to the positive control and TMZ-treated group (Figure 4.7). Likewise, a similar observation has been made previously that induction of C6-cells orthotropic glioma model results in elevation of RH/LH ratio and the presence of tumor cell growth in the right hemisphere of the brain and metastatic cancer nodules in the lungs [20]. To understand the biocompatibility profile of the nanoconjugates, H&E staining of vital organs was performed,

showing no signs of toxicity with Hybrid TMZ NCs. Especially in the lungs, mononuclear cell infiltration was observed in positive control animals (saline-treated). Mononuclear cell infiltration was significantly reduced after treatment with Hybrid TMZ NCs, demonstrating the effective antitumor response against the glioma cells (Figure 4.8). As reported, polycarbonate and polyester polymers are biocompatible and have been deployed in the biomedical field with diagnostic and therapeutic applications [21]. A similar observation has been seen by Rana *et al.*, wherein no significant abnormalities were seen in major organs, including the brain, liver, heart, kidney, spleen, and lungs, and found to be safe post PEG-PLA administration [22]. Furthermore, He *et al.* prepared biodegradable polycarbonate micelles of mPEG-b-PMCC copolymer for the anticancer agent delivery, depicting good biocompatibility with blood and all the major tissues as no such toxicity was observed in histopathological evaluation [23]. Overall, the study demonstrated the conjugation and hybrid nanoformulation approach significantly improved the physiochemical and biological properties of the TMZ, especially the drug stability, loading capacity, and therapeutic effect.

4.6. Conclusion

Currently, TMZ is deployed as a standard of care chemotherapeutics against GBM. Despite the potential of TMZ as a suitable therapeutic candidate, the treatment outcome is constrained by the inherent TMZ-associated limitations. However, combining the conjugation approach and conversion to a hybrid nanocarrier has improved the loading capacity, stability half-life, and *in vitro* and *in vivo* efficacy. The hybrid nanoconjugates have enhanced cellular uptake, IC₅₀, and apoptosis in C6 and U87MG glioma cells. *In vivo* administration has demonstrated improvement in the antitumor outcome compared to the free TMZ, with a significant improvement in the brain weight, hemispherical width ratio, and improved overall survival of rats. Histopathological evaluation has shown a reduction in the mononuclear cell infiltration in the brain tissue, and no other significant signs of toxicity were observed in the heart, liver, lungs, kidney, and spleen, demonstrating the biocompatibility of the developed hybrid nanoconjugates. Thus, such a strategy could be explored for the delivery of drugs to target the glioma.

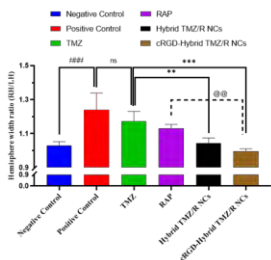
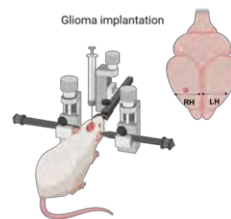
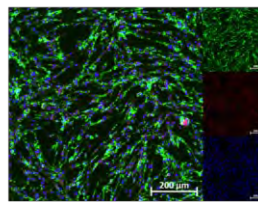
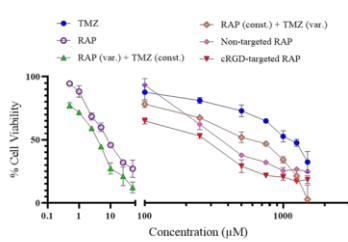
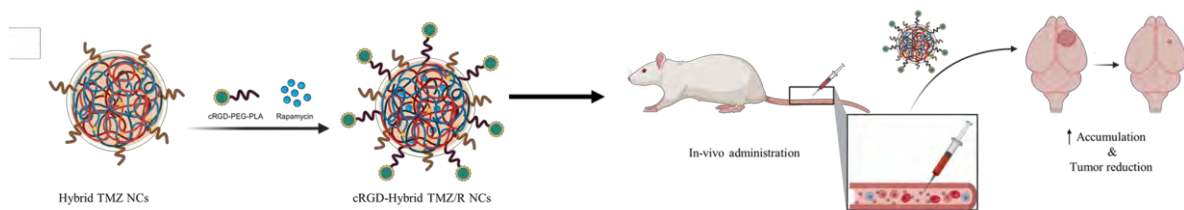
4.7. References

- [1] Aslan B, Ozpolat B, Sood AK, Lopez-Berestein G. Nanotechnology in cancer therapy. *J Drug Target* 2013;21:904–13. <https://doi.org/10.3109/1061186X.2013.837469>.
- [2] Bae KH, Chung HJ, Park TG. Nanomaterials for cancer therapy and imaging. *Mol Cells* 2011;31:295–302.
- [3] Jatyan R, Singh P, Sahel DK, Karthik YG, Mittal A, Chitkara D. Polymeric and small molecule-conjugates of temozolomide as improved therapeutic agents for glioblastoma multiforme. *J Control Release* 2022;350:494–513. <https://doi.org/https://doi.org/10.1016/j.jconrel.2022.08.024>.
- [4] Patil R, Portilla-Arias J, Ding H, Inoue S, Konda B, Hu J, et al. Temozolomide Delivery to Tumor Cells by a Multifunctional Nano Vehicle Based on Poly(β -L-malic acid). *Pharm Res* 2010;27:2317–29. <https://doi.org/10.1007/s11095-010-0091-0>.
- [5] Chitkara D, Mittal A, Behrman SW, Kumar N, Mahato RI. Self-Assembling, Amphiphilic Polymer–Gemcitabine Conjugate Shows Enhanced Antitumor Efficacy Against Human Pancreatic Adenocarcinoma. *Bioconjug Chem* 2013;24:1161–73. <https://doi.org/10.1021/bc400032x>.
- [6] Parveen S, Gupta P, Kumar S, Banerjee M. Lipid polymer hybrid nanoparticles as potent vehicles for drug delivery in cancer therapeutics. *Med Drug Discov* 2023:100165.
- [7] Scopel R, Falcão MA, Cappellari AR, Morrone FB, Guterres SS, Cassel E, et al. Lipid-polymer hybrid nanoparticles as a targeted drug delivery system for melanoma treatment. *Int J Polym Mater Polym Biomater* 2022;71:127–38. <https://doi.org/10.1080/00914037.2020.1809406>.
- [8] Pukale SS, Sharma S, Dalela M, Singh A kumar, Mohanty S, Mittal A, et al. Multi-component clobetasol-loaded monolithic lipid-polymer hybrid nanoparticles ameliorate imiquimod-induced psoriasis-like skin inflammation in Swiss albino mice. *Acta Biomater* 2020;115:393–409. <https://doi.org/https://doi.org/10.1016/j.actbio.2020.08.020>.
- [9] Pukale SS, Sahel DK, Mittal A, Chitkara D. Coenzyme Q10 loaded lipid-polymer hybrid nanoparticles in gel for the treatment of psoriasis like skin condition. *J Drug Deliv Sci Technol* 2022;76:103672. <https://doi.org/https://doi.org/10.1016/j.jddst.2022.103672>.
- [10] Date T, Nimbalkar V, Kamat J, Mittal A, Mahato RI, Chitkara D. Lipid-polymer hybrid nanocarriers for delivering cancer therapeutics. *J Control Release* 2018;271:60–73. <https://doi.org/https://doi.org/10.1016/j.jconrel.2017.12.016>.
- [11] Sharma S, Pukale S, Sahel DK, Singh P, Mittal A, Chitkara D. Folate targeted hybrid lipo-polymeric nanoplexes containing docetaxel and miRNA-34a for breast cancer treatment. *Mater Sci Eng C* 2021;128:112305. <https://doi.org/https://doi.org/10.1016/j.msec.2021.112305>.
- [12] Mittal A, Chitkara D, Behrman SW, Mahato RI. Efficacy of gemcitabine conjugated and miRNA-205 complexed micelles for treatment of advanced pancreatic cancer. *Biomaterials* 2014;35:7077–87. <https://doi.org/https://doi.org/10.1016/j.biomaterials.2014.04.053>.

- [13] Huang G, Zhang N, Bi X, Dou M. Solid lipid nanoparticles of temozolomide: Potential reduction of cardiac and nephric toxicity. *Int J Pharm* 2008;355:314–20. <https://doi.org/https://doi.org/10.1016/j.ijpharm.2007.12.013>.
- [14] Duwa R, Banstola A, Emami F, Jeong J-H, Lee S, Yook S. Cetuximab conjugated temozolomide-loaded poly (lactic-co-glycolic acid) nanoparticles for targeted nanomedicine in EGFR overexpressing cancer cells. *J Drug Deliv Sci Technol* 2020;60:101928. <https://doi.org/https://doi.org/10.1016/j.jddst.2020.101928>.
- [15] Liang E, Guo Z, Hu Z, Chen Z, Rehemani A, Wang J, et al. pH-Responsive expandable polycarbonate–doxorubicin conjugate nanoparticles for fast intracellular drug release. *New J Chem* 2021;45:7261–9. <https://doi.org/10.1039/D1NJ00598G>.
- [16] Tan S, Li X, Guo Y, Zhang Z. Lipid-enveloped hybrid nanoparticles for drug delivery. *Nanoscale* 2013;5:860–72. <https://doi.org/10.1039/C2NR32880A>.
- [17] Tahir N, Madni A, Correia A, Rehman M, Balasubramanian V, Khan MM, et al. Lipid-polymer hybrid nanoparticles for controlled delivery of hydrophilic and lipophilic doxorubicin for breast cancer therapy. *Int J Nanomedicine* 2019;14:4961–74. <https://doi.org/10.2147/IJN.S209325>.
- [18] Ebrahimian M, Mahvelati F, Malaekheh-Nikouei B, Hashemi E, Oroojalian F, Hashemi M. Bromelain Loaded Lipid-Polymer Hybrid Nanoparticles for Oral Delivery: Formulation and Characterization. *Appl Biochem Biotechnol* 2022;194:3733–48. <https://doi.org/10.1007/s12010-022-03812-z>.
- [19] Pang J, Xing H, Sun Y, Feng S, Wang S. Non-small cell lung cancer combination therapy: Hyaluronic acid modified, epidermal growth factor receptor targeted, pH sensitive lipid-polymer hybrid nanoparticles for the delivery of erlotinib plus bevacizumab. *Biomed Pharmacother* 2020;125:109861. <https://doi.org/https://doi.org/10.1016/j.biopha.2020.109861>.
- [20] Jatyan R, Sahel DK, Singh P, Sakhuja R, Mittal A, Chitkara D. Temozolomide-fatty acid conjugates for glioblastoma multiforme: In vitro and in vivo evaluation. *J Control Release* 2023;23:S0168-3659. <https://doi.org/10.1016/j.jconrel.2023.05.012>.
- [21] Ansari I, Singh P, Mittal A, Mahato RI, Chitkara D. 2,2-Bis(hydroxymethyl) propionic acid based cyclic carbonate monomers and their (co)polymers as advanced materials for biomedical applications. *Biomaterials* 2021;275:120953. <https://doi.org/https://doi.org/10.1016/j.biomaterials.2021.120953>.
- [22] Rana S, Singh J, Wadhawan A, Khanna A, Singh G, Chatterjee M. Evaluation of In Vivo toxicity of Novel Biosurfactant from *Candida parapsilosis* loaded in PLA-PEG Polymeric Nanoparticles. *J Pharm Sci* 2021;110:1727–38. <https://doi.org/https://doi.org/10.1016/j.xphs.2021.01.004>.
- [23] He M, Wang R, Wan P, Wang H, Cheng Y, Miao P, et al. Biodegradable Ru-Containing Polycarbonate Micelles for Photoinduced Anticancer Multitherapeutic Agent Delivery and Phototherapy Enhancement. *Biomacromolecules* 2022;23:1733–44. <https://doi.org/10.1021/acs.biomac.1c01651>.

Chapter 5

Development and evaluation of cRGD peptide-functionalized hybrid nanoconjugates of temozolomide coloaded with rapamycin in C6 cells-induced syngeneic orthotopic glioma model in rats



5.1. Introduction

Glioblastoma multiforme (GBM) is a primary brain cancer in patients, which is considered to be highly lethal with median survival rate of up to ~15 months; post-completion of the treatment, only ~25% of patients survive for more 24 months after diagnosis. The standard-of-care treatment mainly involves debulking surgery followed by radiotherapy with adjuvant chemotherapy with temozolomide. GBM, being diffusive and aggressive in nature, the treatment fails to cure tumor burden completely, resulting in the recurrence, making it an untreatable and terminal form of tumor [1,2]. Although several molecules have been tested to determine their efficacy, the outcome of the treatment is still debatable. For instance, phase 2 trials of bevacizumab, irinotecan, and temozolomide were evaluated for glioblastoma, wherein the median overall survival was found to be 12 months, similar to the control group [3]. In another study, the combination of bevacizumab and temozolomide showed a median overall survival of 37 weeks (8.51 months) and a 12-month overall survival of 31.3% [4,5]. Treatment with radiotherapy, temozolomide, and hydroxychloroquine showed an overall survival of 15.6 months. On the contrary, Nimotuzumab and rapamycin combined treatment enhanced the sensitivity to the drugs against the TMZ-resistant glioma cells, exerting higher cytotoxicity compared to TMZ alone [6]. The combined TMZ and metformin treatment demonstrated enhanced synergistic inhibition and apoptosis rate, reducing gliosphere formation and expansion in glioma stem cells [7].

The combination of therapeutics has shown significant improvement in the anti-glioma activity. However, the simultaneous delivery of multiple payloads is still challenging due to different physiochemical properties, including solubility, log p, bioavailability, BBB permeability, etc. [1]. Likewise, TMZ and rapamycin (RAP) have demonstrated significant advancements in the preclinical trials, where the TMZ and RAP given alone and in combination have shown anti-glioma activity [8–10]. Temozolomide (TMZ), a highly potent molecule, undergoes rapid hydrolysis to MTIC and converted into AIC and methyl diazonium carbocation under physiological conditions. The cytotoxicity of TMZ is exerted *viz.* methylation at susceptible nucleophilic DNA sites of N⁷ and O⁶ sites on guanine and the O³ site on adenine residues, causing DNA double-strand breaks causing cell cycle arrest at G2/M phase and eventually cell death [1]. On the other hand, rapamycin (RAP) is a potent macrocyclic lactone produced by bacteria *sp. Streptomyces hygroscopicus*, discovered in the early 1970s, was initially used as an immunosuppressant for organ transplants. Several clinical trials in phase I-III are being conducted to examine its application as an anticancer agent. RAP demonstrates

its anticancer action by inhibiting the serine/threonine site of the mammalian target of rapamycin (mTOR), impeding cell proliferation and translation process, and causing cell cycle arrest at G1 phase [11,12]. Likewise, TMZ and RAP have demonstrated significant advancements in the preclinical trials, where the TMZ and RAP given alone have shown anti-glioma activity [10,13].

Still, the co-delivery of TMZ and RAP possess limitations, primarily due to their disparate physiochemical properties, as TMZ exhibits a water solubility of 5 mg/ml, while RAP has a poor water solubility of 0.00173 mg/ml [1,12]. Several approaches have been made to deliver the molecules to the target site using organic and inorganic nanomaterials, including liposomes, polymers, lipid-polymer hybrid, porous silica nanoparticles, etc. Likewise, Xu et al. fabricated TMZ and PTX dual drug-loaded mPEG-PLGA nanoparticles, exhibiting particles of ~206 nm, with a drug loading capacity equivalent to 0.87 and 3.15% w/w of PTX and TMZ, respectively. The combined delivery system has shown better inhibition in tumor cell growth in *in vitro* and *in vivo* studies [14]. Li et al. prepared stimuli-sensitive PEGylated-poly(α -lipoic acid) copolymer to deliver PTX and DOX simultaneously for cancer therapy. The dual delivery nanosystem has shown a drug loading of 4.3% and 8.2% w/w for DOX and PTX, respectively, exhibiting effective biodistribution and tumor growth inhibition in the murine bone cancer model [15]. Naderinezhad et al. prepared DOX and CUR-loaded LipoNiosome, exhibiting specific cellular internalization and synergistic toxicity against the cancer cells [16]. Although the combinational delivery of molecules has shown promising outcomes against tumor growth, delivering certain therapeutics in combination possesses limitations, including low drug loading capacity, encapsulation efficiency, drug/carrier stability, etc. However, the hybrid carrier system approach has improved the associated limitations. For instance, Jain et al. prepared lipid-polymeric hybrid nanoparticles coloaded with MTX and beta-carotene, exhibited drug loading capacity of 8.5% and 2.85% w/w, respectively, resulting in better cellular internalization, *in vivo* antitumor efficacy, biocompatibility, and reduced the toxicity [17]. Khan et al. prepared cisplatin and curcumin-loaded lipid-polymer hybrid nanoparticles composed of lipoid S75 and chitosan exhibiting particles of 225 nm with an encapsulation of >80%, resulting in improved uptake efficiency and chemosensitization of 3D ovarian cancer spheroid model [18]. In Chapter 4, we have designed and evaluated hybrid nanoconjugates (Hybrid TMZ NCs) for delivering TMZ for the treatment of GBM, exhibiting particle size of ~100 nm with a higher drug loading capacity of 21.6% w/w. The Hybrid TMZ NCs improved *in vitro* and *in vivo* efficacy in the C6 cells-induced orthotropic rat glioma model.

The utilization of nanotechnology for co-delivering multiple payloads to the tumor cells in a single platform has shown promising outcomes in numerous *in vitro* and *in vivo* experiments. Unlike passive accumulation, receptor-based endocytosis has been shown to enhance the selectivity and active targeting of the nanocarrier system using various ligands, such as antibodies, aptamers, and cell-penetrating peptides, making it a promising approach for cancer therapeutics. Amongst, the $\alpha_v\beta_3$ and $\alpha_v\beta_5$ integrin receptors are found to be expressive in components of BBB/BBTB in many tumors and other components of tumor microenvironment, including glioblastoma, breast, prostate, melanoma, and ovarian cancer. The arginine–glycine–aspartic acid (RGD) motif (*e.g.*, cRGDyK, cRGDfC, RGD4C, and RGD10, *etc.*) are highly specific to the integrin receptors that aid in developing an active targeted delivery system that can penetrate the BBB/BBTB and effectively deliver the payload(s) to the target site of action.

In the current study, we prepared an actively targeted hybrid nanoconjugates functionalized with the cyclo(Arg-Gly-Asp-D-Phe-Cys) (cRGD) for co-delivering TMZ and RAP. The developed cRGD functionalized hybrid nanoconjugates carrying dual payloads were thoroughly evaluated for their synergistic potential in *in vitro* cell culture models and *in vivo* efficacy in the C6-induced orthotropic rat glioma model, wherein the effect on tumor burden, survival, and organ toxicity were assessed.

5.2. Experimental section

5.2.1. Materials

Temozolomide (TMZ, >98%) and coumarin-6 dye were obtained from TCI chemicals (Tokyo, Japan). Rapamycin (RAP, >99%) was procured from Alfa Aesar (ThermoFisher Scientific (Massachusetts, United States)), cRGD peptide was obtained from GL Biochem (Shanghai, China), Mal-PEG-OH (*Mn.* 5000 Da) was purchased from Xi'an ruixi Biological Technology Co., Ltd. (Shaanxi Province, China). Dulbecco's Modified Eagle Medium (DMEM), Minimum Essential Media (MEM), SnakeSkin™ Dialysis Tubing (MWCO. 10 KDa), Fetal Bovine Serum (FBS), LysoTracker™ Red DND-99, and Annexin V Ready Flow Conjugates kit were procured from ThermoFisher Scientific (Massachusetts, United States). Methoxy poly(ethylene glycol) (mPEG. 5000 Da), Tin(II) 2-ethylhexanoate, DL-lactide, and Propidium Iodide (PI) were obtained from Sigma-Aldrich (St. Louis, Missouri, United States). MTT (3-(4,5-Dimethylthiazol-2-yl)-2,5-Diphenyltetrazolium Bromide) and DMSO was

obtained from Sisco Research Laboratories (Mumbai, India). Remaining reagents and chemicals used were of analytical grade and bought from local vendors.

5.2.2. Synthesis of mPEG-poly(lactic acid) polyester copolymer (*mPEG-PLA*)

mPEG-PLA was synthesized using microwave-assisted ring-opening polymerization (ROP) of DL-lactide monomer in the presence of mPEG as a macroinitiator using tin(II) 2-ethylhexanoate as a catalyst, as described in chapter 4. Briefly, DL-Lactide (0.535 g) was polymerized with mPEG (0.465 g) at 130 °C for 1 h in the presence of a catalyst to yield the crude copolymer. The crude was purified using precipitation method by dissolving it in chloroform and precipitating it with 2-propanol followed by using diethyl ether twice. The purified copolymer was dried under vacuum and analyzed using ¹H NMR spectroscopy.

5.2.3. Synthesis of cRGD peptide-functionalized Mal-PEG-poly(lactic acid) copolymer (*cRGD-PEG-PLA*)

cRGD-PEG-PLA was synthesized in a two-step reaction, as shown in Figure 5.1B, wherein Mal-PEG-OH was initially copolymerized with DL-lactide monomer using microwave-assisted ROP, as mentioned in the previous section 5.2.2. Briefly, the Mal-PEG-OH (Mn. 5000 Da) (0.232 g) was reacted with DL-Lactide (0.267 g) in the presence of tin(II) 2-ethylhexanoate as a catalyst at 130 °C for 1 h to give Mal-PEG-poly(lactic acid) (Mal-PEG-PLA). The crude copolymer was purified using the precipitation method to yield pure copolymer. The purified Mal-PEG-PLA was then dissolved in DMSO conjugated with cRGD peptide (1:2 mass ratio) using maleimide-thiol coupling chemistry. The reaction was carried out at ambient temperature (25 °C) under nitrogen conditions for 16 h. On the following day, the crude was then dialyzed against purified water using a dialysis membrane (MWCO 3.5 KDa) for 8 h. The resulting dialysate was freeze-dried to yield the cRGD-PEG-PLA copolymer. The cRGD-PEG-PLA was analyzed using ¹H NMR spectroscopy to confirm the coupling between maleimide (Mal-PEG-PLA) and the thiol group of cysteine residue of cRGD peptide.

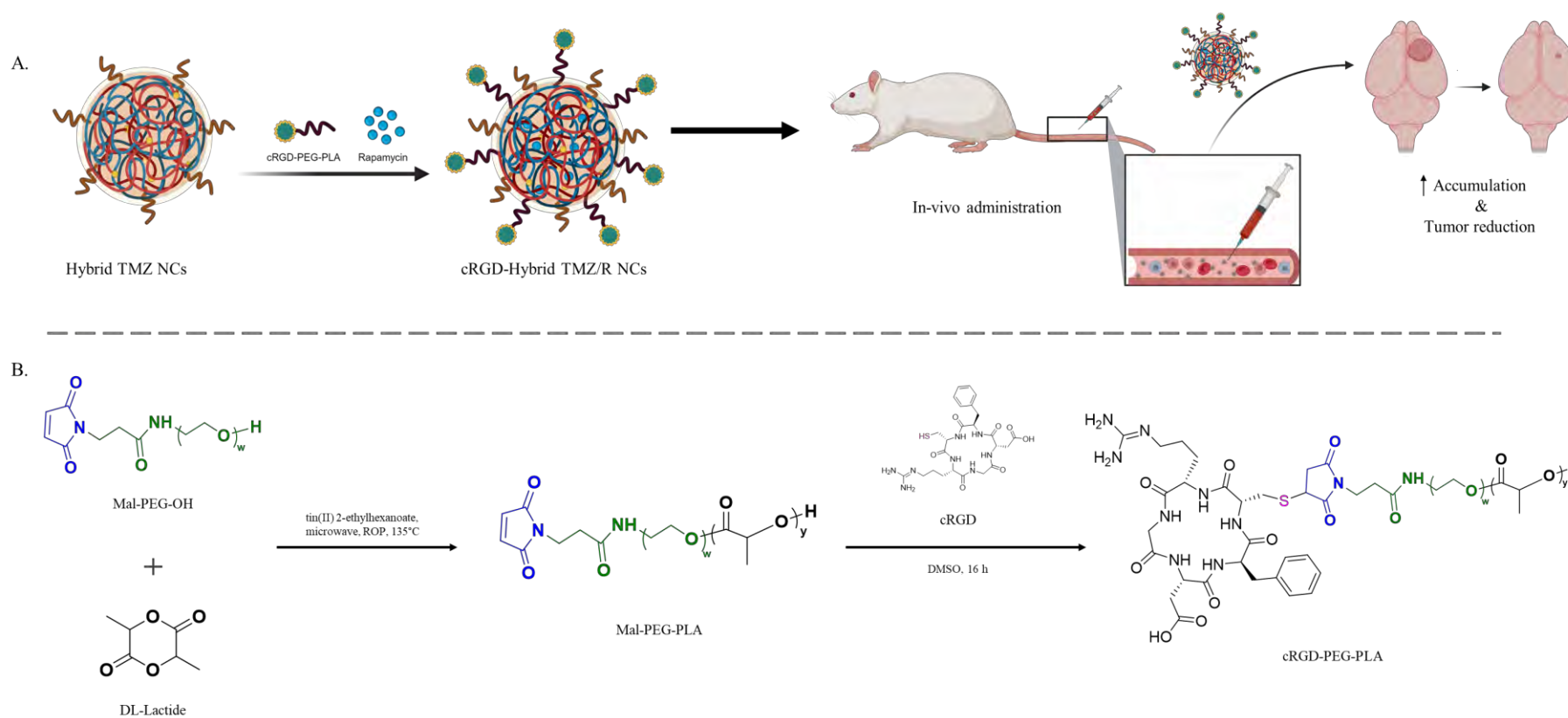


Figure 5.1. Scheme for the A) preparation and fate of nanoconjugates after *in vivo* administration and B) synthesis of cRGD-targeted poly lactide polymer (cRGD-PEG-PLA)

5.2.4. Preparation of cRGD-targeted hybrid temozolomide nanoconjugates coloaded rapamycin (*cRGD-Hybrid TMZ/R NCs*)

Initially, temozolomide nanoconjugates (TMZ NCs) were synthesized containing 40 units of TMZ, i.e., covalently attached to the polymer backbone as a pendent group, as mentioned in chapter 3. The synthesis process involves the covalent attachment of TMZ-hydrazide as a pendant to the free COOH functional groups of PEG-based polycarbonate block copolymer backbone using EDC/HoBT coupling to give TMZ NCs. Thereafter, the rapamycin-loaded cRGD-targeted hybrid temozolomide nanoconjugates (*cRGD-Hybrid TMZ/R NCs*) were prepared using the thin-film hydration method as described in chapter 4 (section 4.2.4). Briefly, TMZ NCs (75 mg), mPEG-PLA (12.5 mg), cRGD-PEG-PLA (12.5 mg), and rapamycin (2.2 mg) were dissolved in a mixture of dichloromethane and ethanol (3:1 v/v ratio) and transferred to a round bottom flask. Thereafter the organic solvent was removed using vacuum-rotary evaporator, resulting in the formation of thin film. The thin film was purged with dried nitrogen gas for 60 min, followed by thin-film dispersion under ambient conditions using phosphate-buffered saline (10 mM; pH 7.4) to give a dispersion mixture. The dispersion was then probe sonicated for 20 s at 20% amplitude under cold conditions and centrifuged at 10000 rpm for 10 min. The supernatant was obtained and evaluated for particle size, polydispersity index (PDI), and surface zeta potential (ζ). Simultaneously, the encapsulation and drug loading capacity were calculated from the weight ratio method using the below formulae:

$$\% \text{Encapsulation efficiency} = \frac{\text{Amount of drug in hybrid NCs}}{\text{Amount of drug added}} \times 100 \quad \text{eq. 5.1}$$

$$\% \text{Loading capacity} = \frac{\text{Amount of drug in hybrid NCs}}{\text{Total weight of Hybrid NCs}} \times 100 \quad \text{eq. 5.2}$$

For determining TMZ loading, briefly, 5 mg of *cRGD-Hybrid TMZ/R NCs* were taken and dissolved in DMSO: milli-Q (50:50) mixture. Afterward, the sample was diluted and evaluated using simple UV-Vis spectroscopy (at λ_{max} 328 nm) to check the concentration of TMZ present. The %loading capacity was determined as per the above-mentioned formula.

For the preparation of non-targeted hybrid nanoconjugates, the mPEG-PLA copolymer was used instead of cRGD-PEG-PLA in the hybrid formulation.

5.2.5. Cell culture studies

The glioma cell lines, C6 and U87MG, were obtained from the National Centre for Cell Sciences (NCCS, Pune, India) and were maintained in Dulbecco's Modified Eagle Medium (DMEM) and Minimum Essential Medium (MEM), respectively. Both glioma cells were complemented with 10% fetal bovine serum (FBS) and 1% penicillin/streptomycin mixture for their growth and expansion. The cells were maintained under suitable conditions at 37 °C; 5% CO₂ in an incubator and allowed to proliferate until 70% confluency for further experimentation or subculture.

5.2.5.1. Cell viability assay

The viability of C6 and U87MG glioma cells was evaluated using 3-(4,5-dimethylthiazol-2-yl)-2,5-diphenyl tetrazolium bromide (MTT) assay [19]. Briefly, the cells were seeded at a density of 5000 cells/well into a 96-well cell culture plate, kept at 37 °C/ 5% CO₂, and allowed to incubate for 24 h. Thereafter, the treatment with free TMZ, free RAP, TMZ+RAP physical mixture, Hybrid TMZ/R NCs, and cRGD-Hybrid TMZ/R NCs was given in the concentration range equivalent to 100-1500 μM and 0.5-50 μM for TMZ and RAP, respectively (for C6 cells), and 25-1000 μM and 0.5-50 μM for TMZ and RAP, respectively (for U87MG cells). After 72 h of treatment, the media was replaced with 200 μl of fresh media containing MTT (5 mg/ml) and kept for incubation at 37 °C; 5% CO₂ for 4 h. Following the formation of formazan crystals, the media was removed carefully, and 200 μl of DMSO was added to dissolve the crystals. The extent of cell viability was evaluated by measuring the absorbance at 570 and 630 nm using an Epoch microplate reader (Biotek Instruments, USA). The %cell viability was determined using the equation.

$$\% \text{Cell Viability} = \frac{\text{Sample (absorbance (570 nm)) - absorbance (630 nm)}}{\text{Control (absorbance (570 nm)) - absorbance (630 nm)}} \times 100 \quad \text{eq. 5.3}$$

5.2.5.2. Combination index analysis

The TMZ and RAP combination index was determined using Compusyn software (version 1.0). From the data observed using cytotoxicity assay of TMZ and RAP individually on C6 and U87MG cells, we have used a constant and non-constant ratio of TMZ and RAP for analysis. The Chou-Talalay method was used to analyze the combination index of the proposed drug combination. The combination index values obtained were analyzed for synergism (<1) and antagonism (>1), and the combinational ratio was determined [20].

5.2.5.3. Cell uptake assay

The cellular uptake assay of Hybrid TMZ NCs and cRGD-Hybrid TMZ NCs was performed using coumarin-6 dye as a fluorescent probe. Briefly, C6 and U87MG cells were seeded at a density of 1×10^5 cells/well into a 6-well plate and allowed to adhere for 24 h. Thereafter, the cells were treated with blank coumarin-6 dye, coumarin-6 loaded Hybrid TMZ NCs, and coumarin-6 loaded cRGD-Hybrid TMZ NCs and kept in an incubator for 4 h. Further, the old media was removed, and cells were washed with PBS (twice) and fixed with 4% paraformaldehyde for 10 min. The cells were counterstained with DAPI for 10 min to counterstain the nucleus. After that, the fixed cells were observed under fluorescent microscope (ZEISS, Germany), and respective microscopic images (DIC, DAPI, Coumarin-6, and Overlay) were acquired for the respective groups. The obtained data were interpreted using Zen Blue software V3.4 [21].

5.2.5.4. Apoptosis assay

Apoptosis analysis was performed using the Annexin-V/PI-based flow cytometry assay. Briefly, C6 and U87MG glioma cells were seeded at a density of 1×10^5 cells/well in a 6-well cell culture plate. The cells were allowed to incubate overnight at 37 °C; 5% CO₂, followed by the treatment with free TMZ, free RAP, TMZ+RAP physical mixture, Hybrid TMZ/R NCs, and cRGD-Hybrid TMZ/R NCs for 24 h. Thereafter, the cells were washed with PBS twice, followed by trypsinization, centrifuged at 1700 rpm for 5 min, and resuspended in 1X annexin binding buffer. The cells were stained with annexin-V/ propidium iodide under dark conditions for 15 min as per the manufacturer protocol. The samples were analyzed using flow cytometry (Beckman Coulter, USA) to quantify the apoptosis rate, and data was obtained and evaluated using CytExpert V3.0 software [13].

5.2.6. Development of Syngeneic orthotropic glioblastoma model in SD rats

C6-cells induced orthotropic syngeneic glioma model was developed as mentioned previously [13]. Briefly, 6-8 weeks old, male *Sprague Dawley* rats were used after the approval from the Institutional Animal Ethics Committee (IAEC) of BITS Pilani, protocol no: IAEC/RES/23/08/Rev-3/32/26. For orthotropic glioma cell implantation, the rats were initially anesthetized using intraperitoneal injection of ketamine (90 mg/kg) and xylazine (9 mg/kg), followed by placing the animals on a stereotactic apparatus. Thereafter, the head was shaved, a small incision of 3 cm was made to expose the skull, and 1 mm burr hole was created using a drill. The C6 cells (2×10^6) were injected using Hamilton's syringe at 2 mm, 3 mm, and 4 mm (x, y, and z, respectively) at a flow rate of 3 μ l/min. The burr hole was sealed with the

biodegradable wax, and an incision was sutured. Animals were then placed back in their cages for continuous observation for changes in parameters, including body weight, neurological activity, eye pigmentation, and right eye bulging, as an indicator of tumor growth. The method was validated through histopathological evaluation of brain to confirm the growth of tumor.

5.2.7. *In vivo* efficacy studies

C6 glioma tumor-bearing rats were taken randomly and allowed to recover from surgery for 9 days. From day 10th of tumor implantation, treatment was initiated comprising positive control, free TMZ, free RAP, Hybrid TMZ/R NCs, and cRGD-Hybrid TMZ/R NCs (n=5). Treatment was given intravenously (i.v.) at a dose equivalent to TMZ (10 mg/kg) and RAP (1 mg/kg) three times a week for 30 days. During the treatment phase, animals were monitored for changes in body weight, survival, and locomotion. At the termination of the treatment phase (day 40th), animals were sacrificed. The blood and major organs such as, heart, lungs, liver, kidney, and spleen, were excised for histopathological evaluation. The brain of rats were removed carefully and evaluated for their appearance, brain weight, and right-to-left hemispherical (RH/LH) width ratio.

5.2.8. Pharmacokinetics and bio-distribution study of cRGD-Hybrid nanoconjugates in C6-glioma-bearing rats

Briefly, C6-glioma-bearing rats were randomly divided into different groups and were given free TMZ, free RAP, Hybrid TMZ/R NCs, and cRGD-Hybrid TMZ/R NCs intravenously. At a dose equivalent to 10 mg/kg of TMZ and 1 mg/kg of free RAP. Free TMZ was given in normal saline and free RAP was given in solution form i.e., in 5% w/v tween 80 and 10% v/v ethanol in normal saline. 0.5 ml of blood was collected in EDTA-containing tubes at pre-determined time intervals ranging from 0.25 to 240 h. After that, 100 μ l of blood samples were taken, spiked with 5 μ l of internal standard (IS, tacrolimus), 10 μ l of 0.1 M ascorbic acid, and vortexed for 15 min for uniform mixing. After that, a hybrid method (salting out with liquid-liquid extraction) of drug extraction was adopted, wherein, initially, 50 μ l of 0.5 M ammonium sulfate as lysis salt was added and vortexed for 2 min, followed by extraction of analytes using 1200 μ l of ethyl acetate (EA) and vortexed for 30 min as mentioned in chapter 2. The samples were centrifuged at 5000 rpm for 5 min at 4 °C. The supernatant was carefully collected and transferred to vials, and the same process was repeated for the second time to extract the drug and IS. The collected organic layer was evaporated to dryness and reconstituted with 100 μ l of

mobile phase, followed by 10 μ l of sample volume injected and analyzed using developed and validated simultaneous UPLC-MS/MS method.

Liquid chromatographic separation was performed on Waters ACQUITY UPLC BEH C18 Column (2.1 \times 100 mm, 1.7 μ m). The mobile phase consisted of A) Ammonium acetate buffer with 0.1% formic acid and B) Methanol. The column temperature was maintained at 35 $^{\circ}$ C, sample temperature at 15 $^{\circ}$ C, with gradient elution at a flow rate of 0.30 ml/min with flow parameters as follows: 0-0.6 min A- hold at 60%, 0.6-0.7 min A-60% to 0%, 0.7-2.9 min A- hold at 0%, 2.9-2.95 min A-0% to 60%, 2.95-5.6 min A-60%. The concentration-time graph was plotted for the respective groups, and various pharmacokinetic parameters (C_{max} , AUC, MRT, $t_{1/2}$, Cl, V_d , and many more) were evaluated using Phoenix WinNonlin[®] (V 2.1) software using the non-compartmental model analysis.

The *in vivo* imaging system (IVIS, Lumina XRMS Series-III, Perkin Elmer, USA) was used for bio-distribution analysis. Briefly, C6-glioma cell-bearing rats (n=03/ group) were injected intravenously with DiR-loaded Hybrid TMZ NCs and DiR-loaded cRGD-Hybrid TMZ NCs. The injected rats were kept under observation for 2 and 6 h, sacrificed, followed by excision of major organs (brain, heart, lungs, liver, kidney, and spleen). After that, the organs were kept under the IVIS to determine the fluorescence intensity and organ biodistribution [19].

5.3. Statistical analysis

The obtained data are expressed as mean \pm SD and mean \pm SEM. The statistical difference was determined by analysis of variance followed by Tukey test for comparison between different groups. * p <0.05, ** p <0.01, *** p <0.001, @@ p <0.01, and #### p <0.001 was considered statistically significant.

5.4. Results

5.4.1. Characterization of cRGD peptide-functionalized Mal-PEG-poly(lactic acid) copolymer (cRGD-PEG-PLA)

Initially, mPEG-PLA was prepared using ROP of DL-lactide in the presence of mPEG as a macroinitiator using tin(II) 2-ethylhexanoate as a catalyst to yield mPEG-PLA copolymer as described in Chapter 4. Simultaneously, Mal-PEG-PLA was prepared using microwave-assisted ring-opening polymerization between DL-lactide and Mal-PEG-OH as a macroinitiator in the presence of tin(II) 2-ethylhexanoate as a catalyst. Figure 5.2A shows ¹H NMR (400 MHz, CDC13) δ 6.67 (-CH-Maleimide), 5.14 (-CO-CH-CH₃), 3.63 (-CH₂-PEG),

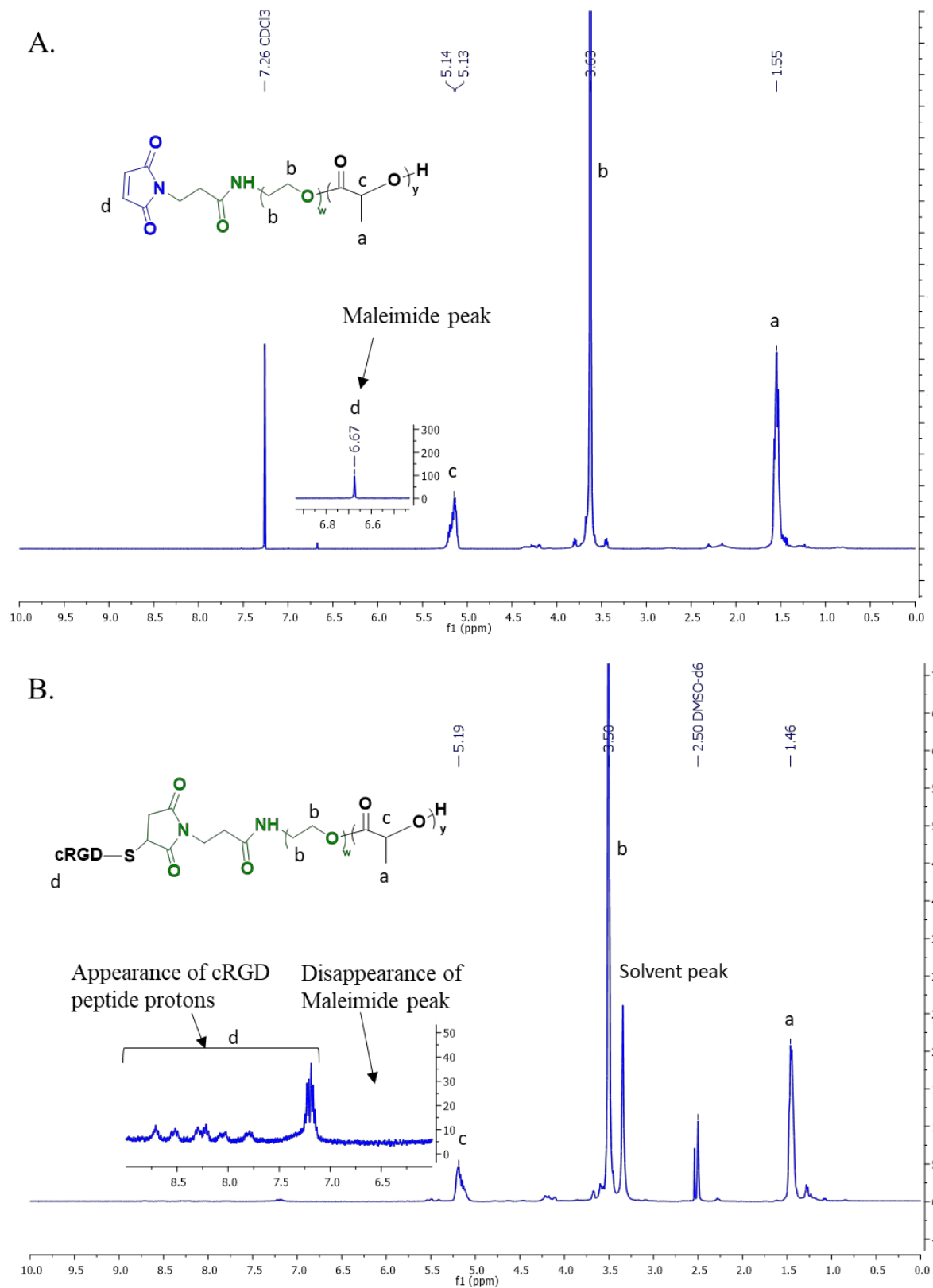


Figure 5.2. Characterisation of polymer. ¹H NMR A) Mal-PEG-PLA and B) cRGD-PEG-PLA polymer

1.55 ($\text{CH}_3\text{-CH-}$). Thereafter, the Mal-PEG-PLA was reacted with cRGD peptide using maleimide-thiol coupling chemistry to yield cRGD-PEG-PLA. Figure 5.2B depicts ^1H NMR (400 MHz, DMSO-*d*6) δ 5.19 ($-\text{CO-CH-CH}_3$), 3.50 ($-\text{CH}_2\text{-PEG}$), 1.46 ($\text{CH}_3\text{-CH-}$), presence of protons at δ 9.0-7.0 (protons of cRGD peptide) and disappearance of maleimide protons at δ 6.67 indicates the successful synthesis of cRGD-PEG-PLA.

5.4.2. Characterization of cRGD-targeted hybrid temozolomide nanoconjugates coloaded rapamycin (*cRGD-Hybrid TMZ/R NCs*)

The cRGD-Hybrid TMZ/R NCs were prepared using the thin-film hydration method. The Hybrid TMZ/R NCs depicted a particle size, PDI, and surface zeta potential of 126.62 ± 1.24 nm, 0.211 ± 0.008 , and -0.333 ± 0.095 mV, respectively, while the cRGD-Hybrid TMZ/R NCs showed a particle size, PDI, and surface zeta potential of 141.83 ± 10.05 nm, 0.233 ± 0.031 , -0.168 ± 0.03 mV, respectively (Figure 5.3). While in case of coumarin-6 loaded Hybrid TMZ NCs showed a particle size of 124.4 ± 1.91 nm (PDI. 0.144 ± 0.022) and coumarin-6 loaded cRGD-Hybrid TMZ NCs exhibited particles of 152.9 ± 1.66 nm (PDI. 0.228 ± 0.060) (Figure 5.4).

5.4.3. Combination index assay

The TMZ and RAP combination index was evaluated in C6 and U87MG glioma cells. The glioma cells were treated with free TMZ, free RAP, and TMZ+RAP physical mixture with constant and non-constant ratios to determine the combination index. In C6 glioma cells, free TMZ and free RAP depicted an IC_{50} of ~ 1133 μM and ~ 8.5 μM , respectively. On considering the cytotoxicity profiles of free drugs, the TMZ+RAP drug combination ($\text{TMZ}_{\text{var.}} + \text{RAP}_{\text{const.}}$ and $\text{TMZ}_{\text{const.}} + \text{RAP}_{\text{var.}}$) indicated a synergism with a CI value less than 1, are mentioned in Figure 5.5 B&C. Based on the obtained data, the 110:1 dose ratio of TMZ: RAP, i.e., 1100 μM :10 μM , respectively, significantly reduced cell viability. Wherein the synergistic reduction in IC_{50} of $\text{TMZ}_{\text{var.}} + \text{RAP}_{\text{const.}}$ and $\text{TMZ}_{\text{const.}} + \text{RAP}_{\text{var.}}$ was observed, equivalent to 596.4 μM and 4.08 μM , respectively (CI value <1) (Figure 5.5 A-C).

In U87MG cells, free TMZ and free RAP showed an IC_{50} of ~ 842 μM and 1.93 μM , respectively. Similarly, the constant and variable ratio of TMZ and RAP was utilized to determine the combination index (Figure 5.6 B&C). Wherein $\text{TMZ}_{\text{var.}} + \text{RAP}_{\text{const.}}$ and $\text{TMZ}_{\text{const.}} + \text{RAP}_{\text{var.}}$ depicted an IC_{50} of 233.8 μM and 0.92 μM , respectively, showing a synergism (CI value <1) at a dose ratio of 800 μM : 2 μM of TMZ and RAP, respectively, showed a reduction

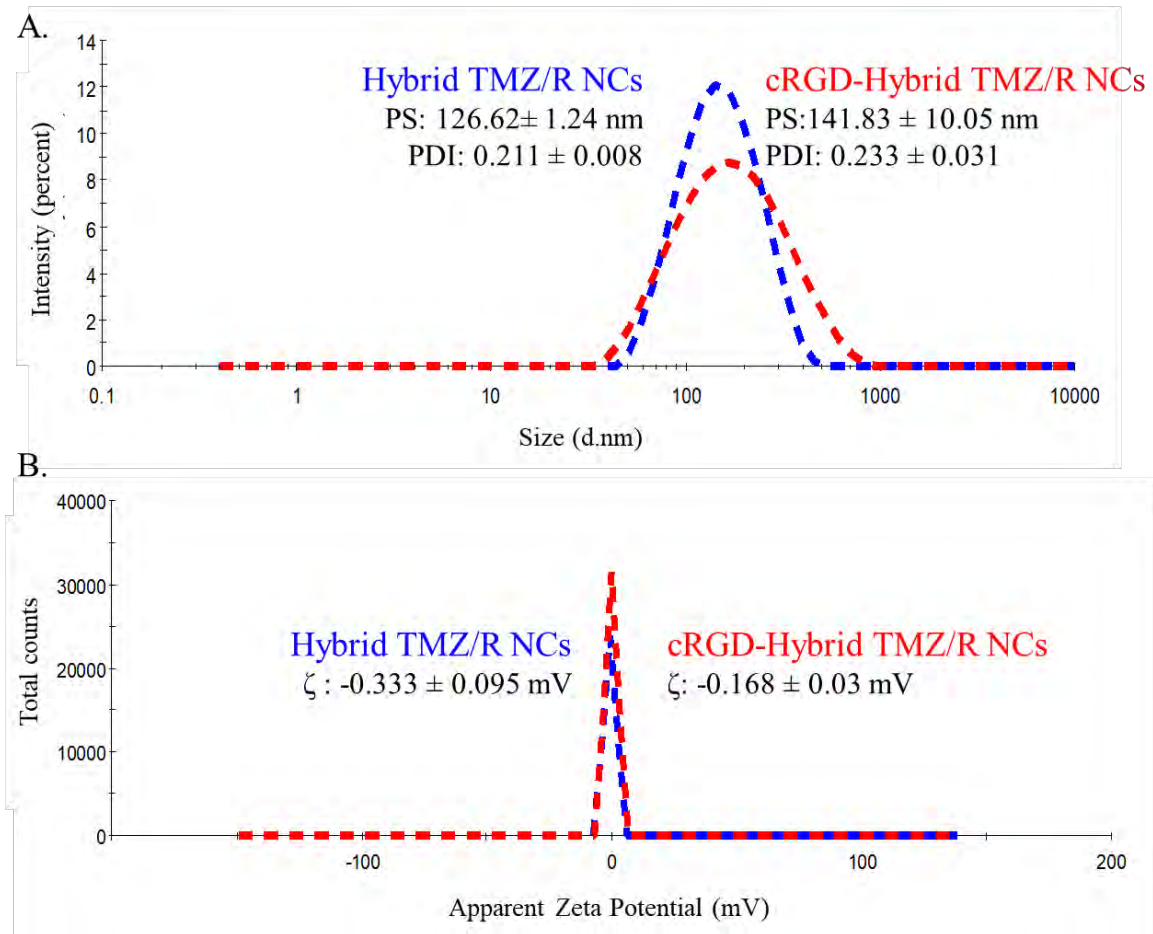


Figure 5.3. A) Particle size and B) surface zeta potential analysis of cRGD-Hybrid TMZ/R NCs

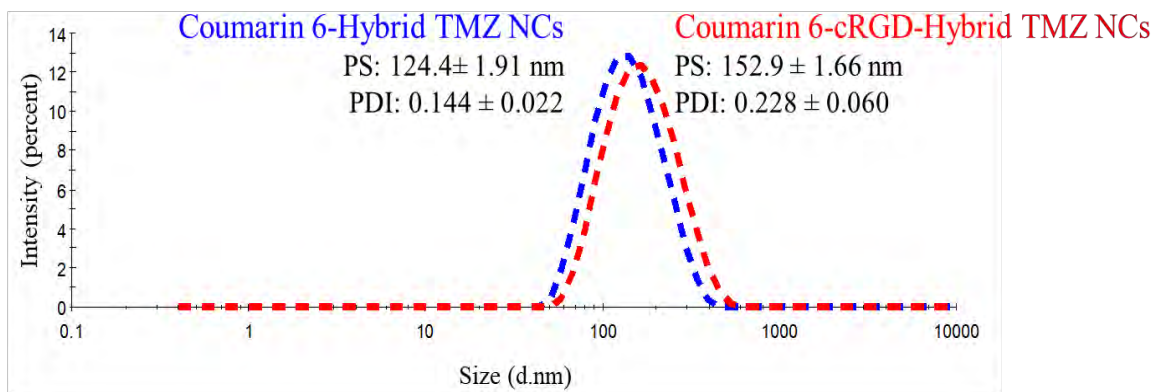


Figure 5.4. Particle size distribution of coumarin-6 dye loaded cRGD-Hybrid TMZ/R NCs

in cell viability. Thereafter, the experimentations were performed based on the observed combination index ratio of TMZ: RAP (Figure 5.6 A-C). Thus, signifying the increased potency of the combination, favourable for anti-glioma efficacy.

5.4.4. *In vitro* cytotoxicity and uptake of cRGD-Hybrid TMZ/R NCs

The cell toxicity of cRGD-Hybrid TMZ/R NCs was determined in C6 and U87MG glioma cells, as shown in Figure 5.5 & 5.6. In C6 glioma cells, treatment with Hybrid TMZ/R NCs showed an IC_{50} of $\sim 375.07 \mu\text{M}$. Surprisingly, cRGD-Hybrid TMZ/R NCs demonstrated additional improvement in IC_{50} equivalent to $\sim 282.8 \mu\text{M}$ compared to free TMZ and TMZ + RAP physical mixture with an IC_{50} of $\sim 1133 \mu\text{M}$ and $\sim 596.4 \mu\text{M}$, respectively (Figure 5.5A).

While, in U87MG cells, the Hybrid TMZ/R NCs and cRGD-Hybrid TMZ/R NCs showed an IC_{50} of 410.4 and 238.14 μM compared to free TMZ and TMZ + RAP combination with an IC_{50} of $\sim 842 \mu\text{M}$ and $\sim 233.8 \mu\text{M}$, respectively (Figure 5.6A).

The cellular uptake efficiency of cRGD-Hybrid TMZ/R NCs was determined using coumarin-6 dye as a fluorescent probe in C6 and U87MG glioma cells. The microscopic images of coumarin-6 loaded Hybrid TMZ NCs (particle size of 124.4 nm) and coumarin-6 loaded cRGD-Hybrid TMZ NCs (particle size of 152.9 nm) showed improved uptake in both glioma (C6 and U87MG) cells, compared to free coumarin 6 (Figure 5.5E & 5.6E).

5.4.5. Apoptosis assay

The extent of apoptosis rate was determined in C6 and U87MG glioma cells using the Annexin-V/PI staining method. The cells were treated with different treatment groups, including free TMZ, free RAP, TMZ+RAP physical mixture, Hybrid TMZ/R NCs, and cRGD-Hybrid TMZ/R NCs. Figure 5.5D shows the apoptosis rate in C6 cells, wherein the cRGD-Hybrid TMZ/R NCs-treated cells exhibited significant improvement in apoptosis rate of 48.25% (early apoptosis: 45.67% and late apoptosis: 2.58%). While, Hybrid TMZ/R NCs showed an apoptosis rate of 41.81% (early apoptosis: 39.46% and late apoptosis: 2.35%) compared to free TMZ with an apoptosis rate of 18.08% (early apoptosis: 18.46% and late apoptosis: 2.87%), free RAP with apoptosis rate of 21.33% (early apoptosis: 14.77% and late apoptosis: 3.31%), and TMZ+RAP physical mixture with an apoptosis rate of 22.51% (early apoptosis: 20.65% and late apoptosis: 1.86%).

In U87MG cells, cRGD-Hybrid TMZ/R NCs showed an improved apoptosis rate of 57.2% (early apoptosis: 9.34% and late apoptosis: 47.86%), while the Hybrid TMZ/R NCs

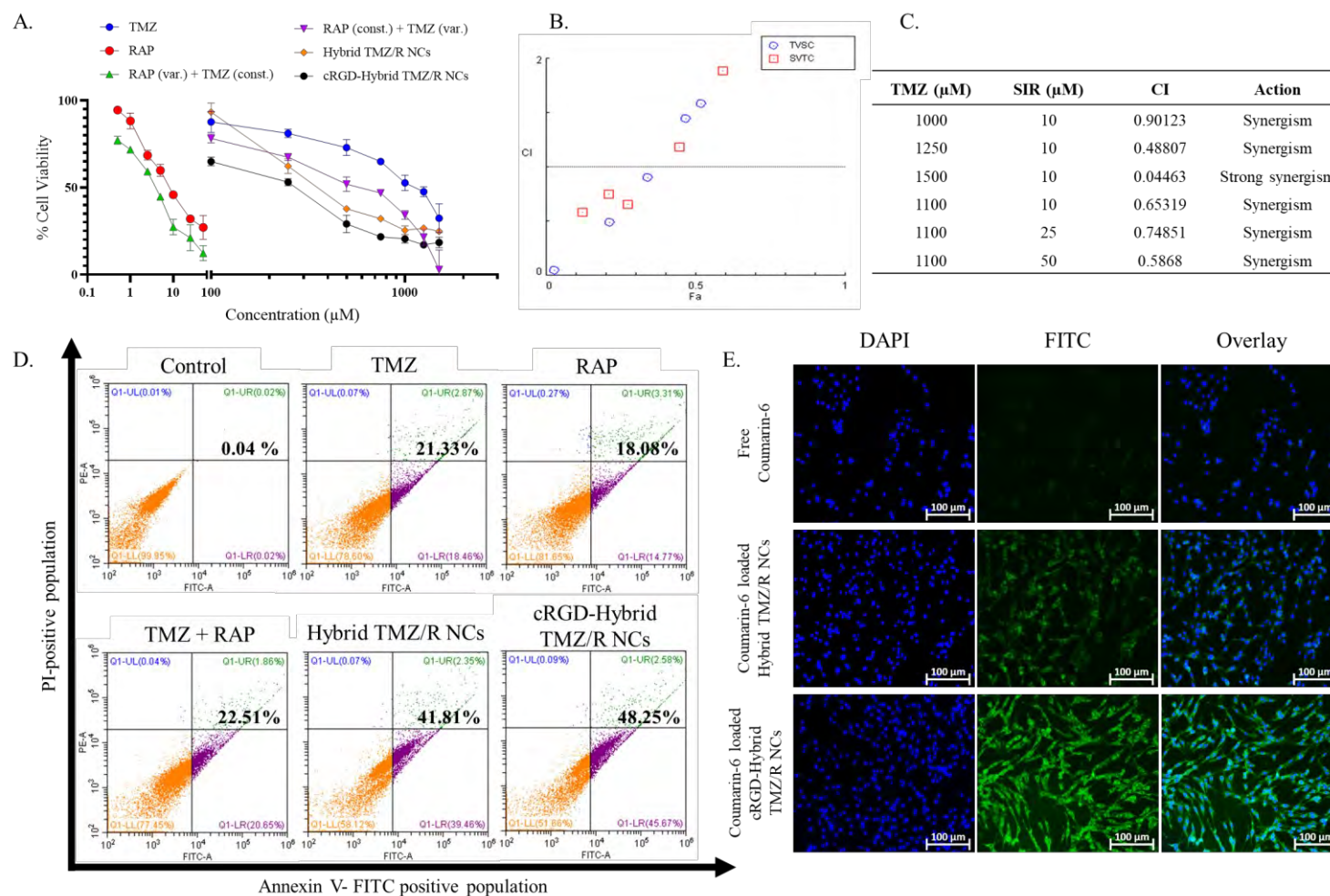


Figure 5.5. *In vitro* evaluation of cRGD-Hybrid TMZ NCs in C6 glioma cells. A) Cell cytotoxicity assay B) & C) Combination index analysis for TMZ, RAP, and its combination using Chou-Talalay method. D) Annexin-V-FITC/PI-based apoptosis assay E) & F) Cellular uptake determination using coumarin-6 dye as a fluorescent probe

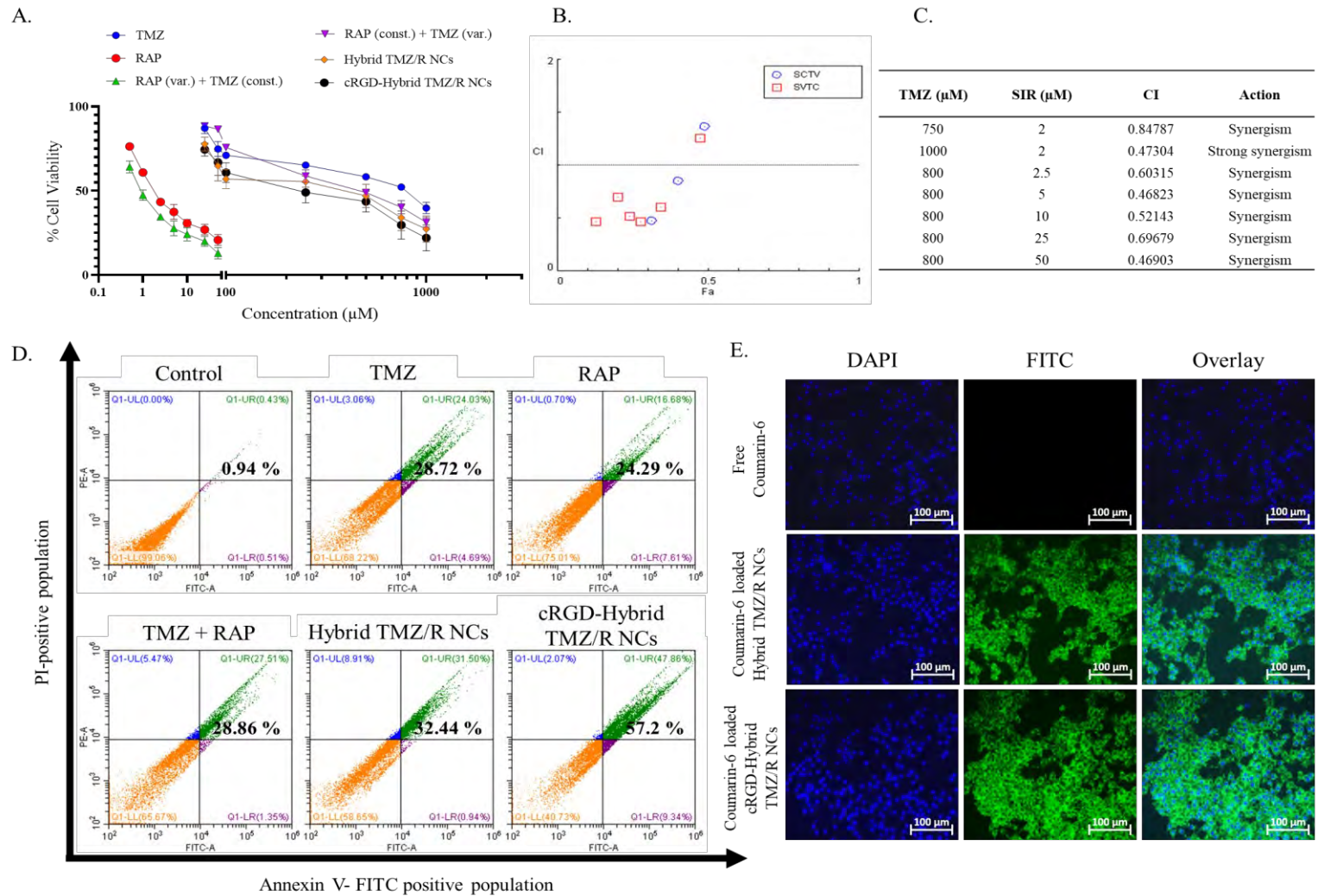


Figure 5.6. *In vitro* evaluation of cRGD-Hybrid TMZ NCs in U87MG glioma cells. A) Cell cytotoxicity assay B) & C) Combination index analysis for TMZ, RAP, and its combination using Chou-Talalay method. D) Annexin-V-FITC/PI-based apoptosis assay E) Cellular uptake determination using coumarin-6 dye as a fluorescent probe

exhibited an apoptosis rate of 32.44% (early apoptosis: 0.94% and late apoptosis: 31.50%), compared to free TMZ with an apoptosis rate of 28.72% (early apoptosis: 4.69% and late apoptosis: 24.03%), free RAP with apoptosis rate of 24.29% (early apoptosis: 7.61% and late apoptosis: 16.68%), and TMZ+RAP combination with an apoptosis rate of 28.86% (early apoptosis: 1.35% and late apoptosis: 27.51%) (Figure 5.6D).

5.4.6. *In vivo* efficacy of cRGD- Hybrid TMZ/R NCs in C6 cells induced orthotropic rat glioma model

In vivo antitumor efficacy of cRGD-Hybrid TMZ/R NCs was determined in the C6 cells induced orthotropic syngeneic glioma model in male *Sprague Dawley* rats (Figure 5.7). After the C6 cell implantation, tumor was allowed to develop for 9 days. On the 10th day, animals were treated i.v. with free TMZ, free RAP, Hybrid TMZ/R NCs, and cRGD-Hybrid TMZ/R NCs at a dose equivalent to 10 mg/kg and 1 mg/kg for TMZ and RAP thrice a week for the next 30 days. The positive control group animals were treated with normal saline exhibited 100% mortality within 15 days after initiation of treatment, while treatment with free TMZ, free RAP, and Hybrid TMZ/R NCs showed mortality up to 40, 60, and 20%, respectively, after 30 days of treatment. On the contrary, no mortality was observed in cRGD-Hybrid TMZ/R NCs-treated animals till the completion of the treatment (Figure 5.7D).

Interestingly, after the glioma model implantation, a marked body weight reduction was observed in all the animals; thereafter, the animals started to recover their body weight after the initiation of the treatment phase. Furthermore, the physiological parameters were also observed in animals, including change in brain weight, hemispherical width ratio (RH/LH), and physical appearance to confirm the tumor growth. It was evident that the positive control animals treated with normal saline exhibited increased brain weight and RH/LH hemispherical width ratio than the normal control group. While free TMZ and free RAP-treated animals showed a nominal reduction in brain weight and RH/LH hemispherical width ratio. At the same time, treatment with Hybrid TMZ/R NCs and cRGD-Hybrid TMZ/R NCs demonstrated a statistically significant reduction in the brain weight and the RH/LH hemispherical width ratio, indicating the effectiveness of the developed combinational delivery system *in vivo* compared to the free drugs (Figure 5.7). Simultaneously, the histopathological analysis of the brain of the positive control group animals exhibited the presence of mononuclear/ tumoral cell infiltration in the right hemisphere of the brain at the site of injection. While, no such observation has been made in the left hemisphere of the brain (uninjected site) (*data not shown*), depicting normal

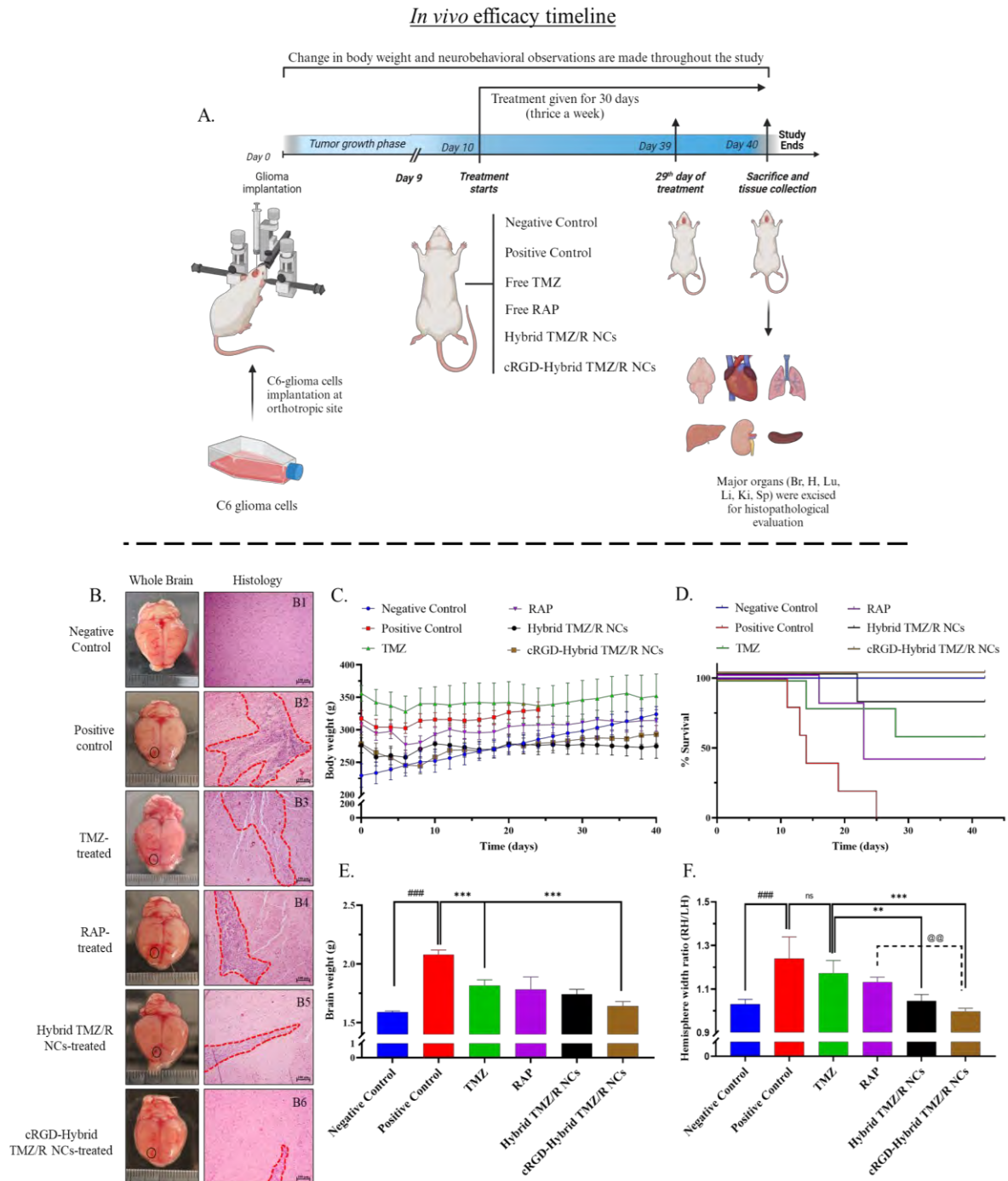


Figure 5.7. *In vivo* efficacy of cRGD-Hybrid TMZ NCs in C6 cells induced orthotopic syngeneic glioma model in rats. A) Scheme for the *in vivo* study design. B) Representative brain images of treatment groups and B1-B7) brain histopathology (H&E) evaluation of the right hemisphere of brain (injection site). C) and E) mean body and brain weight of treated animals, D) and F) hemispherical width ratio (RH/LH) and Kaplan-Meier survival plot of treated animals, respectively (scale bar: 100 μ m) (*, **, ***, @@, ### signifies p value <0.05, <0.01, <0.001, <0.01, and <0.001 respectively)

morphology of the brain tissue. Treatment with free TMZ and free RAP expressed a minimal reduction in mononuclear cell infiltration. In contrast, a marked decrease in tumor cell infiltration was observed in Hybrid TMZ/R NCs and cRGD-Hybrid TMZ/R NCs-treated animals. Similarly, the Kaplan Meier survival plot also indicated no mortality in cRGD-Hybrid TMZ/R NCs-treated animals compared to 100% mortality in the positive control group, analogous to negative control animals, exhibiting the efficiency of the cRGD-Hybrid TMZ/R NCs carrying dual payload against glioma therapy (Figure 5.7).

5.4.7. Histopathological evaluation of cRGD-Hybrid TMZ/R NCs in glioma-bearing rats

The H&E staining was performed to understand the toxicity of cRGD-Hybrid TMZ/R NCs in vital organs, including the heart, lungs, liver, kidney, and spleen (Figure 5.8). The negative control (sham group) exhibited normal histopathological parameters of the heart tissues, including the syncytial arrangement of fibers with intercalated disks. All treatment groups, including a positive control group, showed normal pathophysiology of the heart, comparable to healthy animals. Furthermore, the positive control group exhibited mononuclear / tumor cell infiltration in the lungs, indicating tumor development and metastasis toward the lungs. The treatment with free TMZ and free RAP exhibited minimal histology improvement with the presence of a significant number of mitotic cell infiltration in the lungs. The Hybrid TMZ/R NCs and cRGD-Hybrid TMZ/R NCs treated lungs demonstrated a marked reduction in mitotic cell infiltration, indicating the effectiveness of the combination therapeutics using the hybrid nanoconjugate delivery system. The histopathology of the negative control group reveals the normal architecture of hepatocytes, bile duct, central vein, and other hepatic components. Nevertheless, the positive control group, as well as the free TMZ and free RAP treated group, exhibited degeneration of hepatic components, especially the hepatocytes, indicating adverse effects on the liver. On the contrary, Hybrid TMZ/R NCs and cRGD-Hybrid TMZ/R NCs exhibited improvement in the hepatocytic components with healthy liver architecture, i.e., normal hepatocytes, central vein, kupffer cells, bile duct cells, etc. At the same time, the positive control and free TMZ-treated animals exhibited altered kidney histopathology, including increased peritubular space, atrophic renal tubules, glomerulus tufts, renal tubules, etc. The free RAP-treated animals showed thickening of renal tubules and glomerulus tufts with a reduction in the peritubular spaces; yet, the treatment with Hybrid TMZ/R NCs and cRGD-Hybrid TMZ/R NCs improved the histopathology of kidney components towards the normal comparable to the healthy animals. The spleen is considered to be a vital component for removing affected red and white blood cells. Administering the

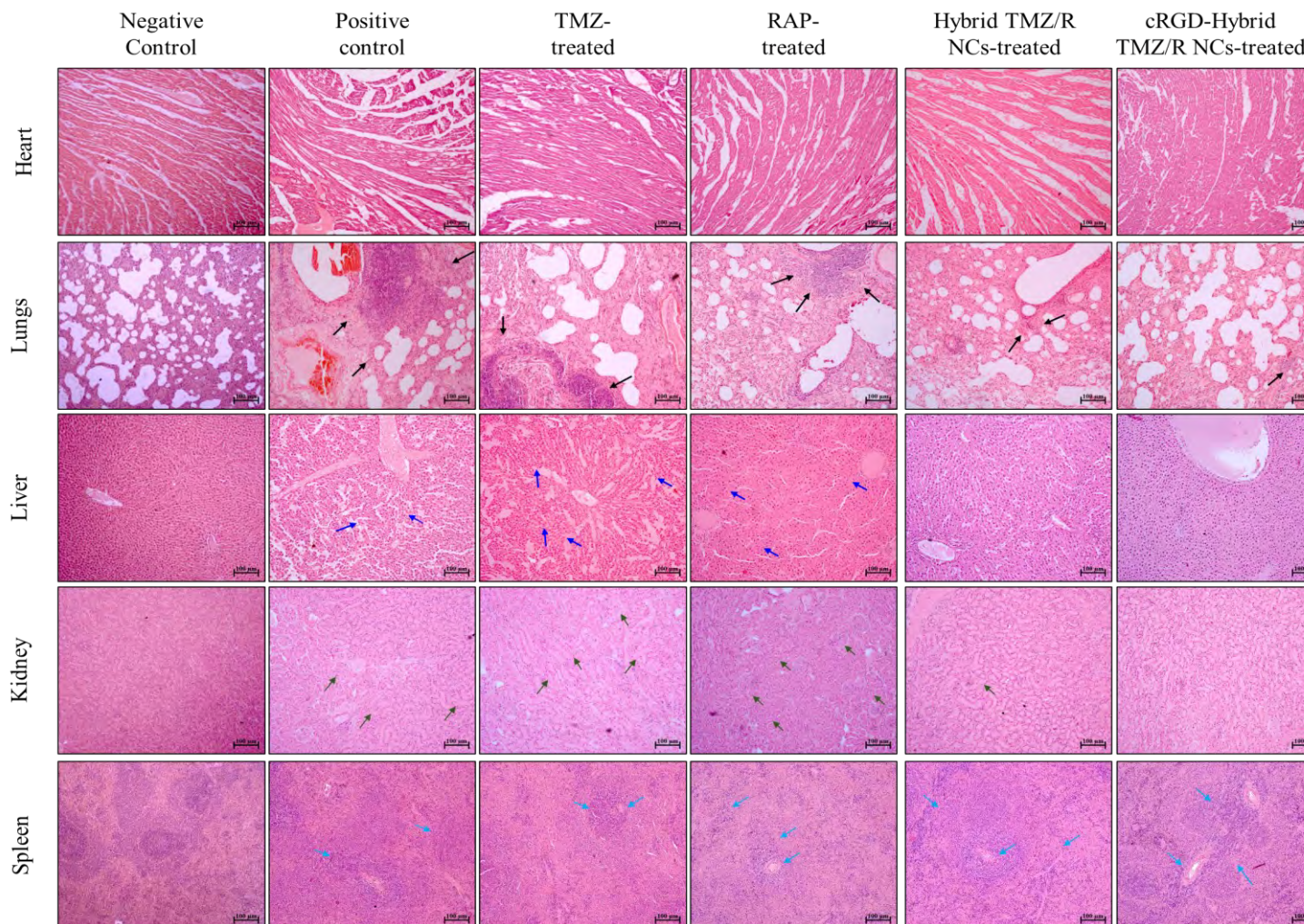


Figure 5.8. Histopathological toxicity (H&E) evaluation of cRGD-Hybrid TMZ/R NCs in major organs (heart, lungs, liver, kidney, and spleen) in C6-glioma tumour bearing animals (scale bar: 100 μ m) (Black arrow: mononuclear cell infiltration in lungs, blue arrow: degeneration of hepatocytes in liver, green arrow: atrophic renal tubules with abnormal peritubular space, light blue arrow: moderate white and red pulp depletion)

molecules/nanomaterials to blood directly interacts with RBC and WBC; therefore, understanding the effect is paramount. Wherein treatment with free TMZ and RAP exhibited moderate white and red pulp depletion. However, Hybrid TMZ/R NCs and cRGD-Hybrid TMZ/R NCs showed improvement in the splenic components with minimal toxicity (Figure 5.8).

5.4.8. Pharmacokinetics and bio-distribution study of cRGD-Hybrid nanoconjugates in C6-glioma-bearing rats

Pharmacokinetics study was performed in C6-glioma-bearing rats, wherein, the tumor-bearing rats were divided into free TMZ, free RAP, Hybrid TMZ/R NCs, and cRGD-Hybrid TMZ/R NCs. The whole blood concentration-time profile for various analytes (RAP, TMZ, TMZ-A, TMZ-H, and AIC) in treated animals are shown in figure 5.9 and various pharmacokinetic parameters (C_{max} , AUC, MRT, $t_{1/2}$, Cl, V_d , etc) were recorded using non-compartment analysis (Table 5.1). For RAP, improvement in pharmacokinetic parameters were observed such as free RAP treated group exhibited a half-life of 86.19 ± 1.23 h compared to half-life of 63.24 ± 2.25 and 57.27 ± 4.86 h for Hybrid TMZ/R NCs and cRGD-Hybrid TMZ/R NCs, respectively. Interestingly, a marked reduction in the volume of distribution from 10667.27 ± 1115.96 to 4261.94 ± 901.29 and 5032.88 ± 632.95 ml/kg for Hybrid TMZ/R NCs and cRGD-Hybrid TMZ/R NCs was observed, respectively. The pharmacokinetic parameters for all the analytes including RAP, TMZ, TMZ-A, TMZ-H, and AIC are mentioned in table 5.1. On contrary, the TMZ conjugated to polymeric backbone did not exhibited breakdown into TMZ, TMZ-A, TMZ-H, or AIC.

The biodistribution study was performed in C6-glioma-bearing rats, wherein the DiR-loaded Hybrid TMZ NCs and DiR-loaded cRGD-Hybrid TMZ NCs were administered intravenously. At 2 and 6 h, the rats were euthanized, and organs were isolated and observed under *in vivo* imaging system for the fluorescence intensity. Interestingly, an intense fluorescent signal was observed in the brain after administering DiR-loaded cRGD-Hybrid TMZ/R NCs at 6 h of administration compared to the DiR-loaded Hybrid TMZ/R NCs; wherein a less to minimal fluorescent signal was observed in tumor-bearing brain, indicating the beneficial outcome of cRGD peptide functionalization in improved BBB permeability (Figure 5.10).

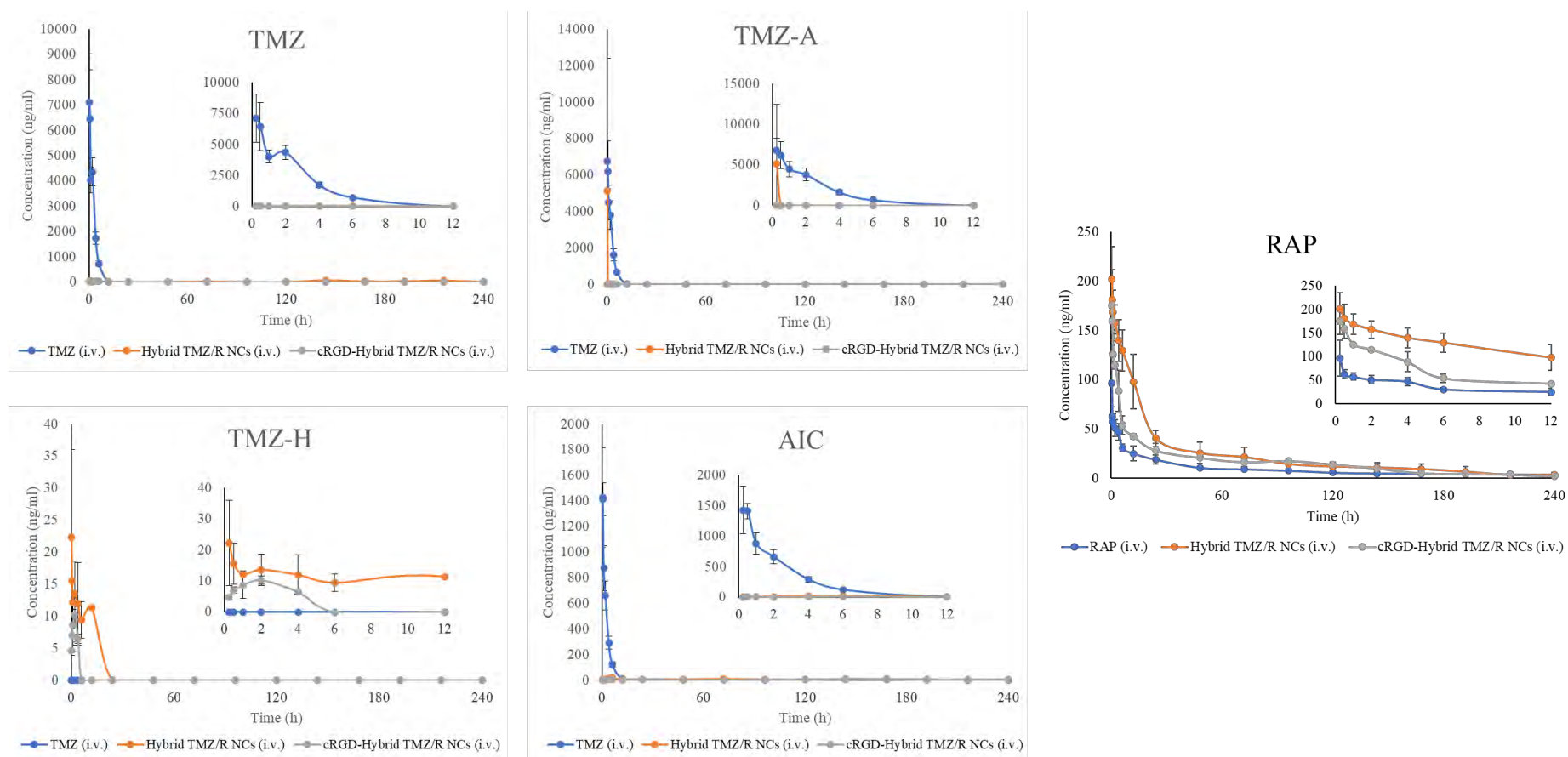


Figure 5.9. Pharmacokinetic concentration-time profile of TMZ, TMZ-A, TMZ-H, AIC and RAP in whole blood after intravenous (i.v.) administration of free TMZ, free RAP, Hybrid TMZ/R NCs, and cRGD-Hybrid TMZ/R NCs in C6-glioma bearing rats. Data represented as mean \pm SD

Table 5.1. Pharmacokinetic parameters of TMZ, TMZ-A, TMZ-H, AIC and RAP after intravenous (i.v.) administration of free TMZ, free RAP, Hybrid TMZ/R NCs, and cRGD-Hybrid TMZ/R NCs in C6-glioma bearing rats. Data represented as mean \pm SEM

Pk Parameters	Treatment														
	Free TMZ				Hybrid TMZ/R NCs				cRGD-Hybrid TMZ/R NCs				Free RAP	Hybrid TMZ/R NCs	cRGD-Hybrid TMZ/R NCs
Analyte	AIC	TMZ	TMZ-A	TMZ-H	AIC	TMZ	TMZ-A	TMZ-H	AIC	TMZ	TMZ-A	TMZ-H	RAP	RAP	RAP
C _{max} (ng/mL)	1198.16 \pm 332.34	4684.93 \pm 744.98	4823.48 \pm 617.66	n.d.	n.d.	n.d.	n.d.	n.d.	n.d.	n.d.	n.d.	n.d.	68.14 \pm 8.31	249.59 \pm 6.05	193 \pm 41.24
T _{1/2} (h)	1.70 \pm 0.14	1.52 \pm 0.13	1.38 \pm 0.12	n.d.	n.d.	n.d.	n.d.	n.d.	n.d.	n.d.	n.d.	n.d.	86.19 \pm 1.23	63.24 \pm 2.25	57.27 \pm 4.86
AUC _(0-last) (ng.h/mL)	5566.55 \pm 381.51	17211.91 \pm 2022.16	17845.18 \pm 2542.03	n.d.	n.d.	n.d.	n.d.	n.d.	n.d.	n.d.	n.d.	n.d.	2437.17 \pm 199.62	4670.41 \pm 330.54	3944.35 \pm 278.88
AUC _(0-∞) (ng.h/mL)	5580.88 \pm 377.65	17914.22 \pm 1645.48	17015.66 \pm 1541.43	n.d.	n.d.	n.d.	n.d.	n.d.	n.d.	n.d.	n.d.	n.d.	2925.19 \pm 310.14	4899.75 \pm 445.32	4121.62 \pm 282.08
AUMC _(0-last) (ng.h/mL)	216604.27 \pm 49687.16	48336.24 \pm 5393.90	54850.48 \pm 5124.18	n.d.	n.d.	n.d.	n.d.	n.d.	n.d.	n.d.	n.d.	n.d.	182209.67 \pm 43765.60	236493.62 \pm 18942.31	258049.04 \pm 14208.75
AUMC _(0-∞) (ng.h/mL)	220079.34 \pm 48930.08	48938.01 \pm 5733.87	55959.22 \pm 5164.43	n.d.	n.d.	n.d.	n.d.	n.d.	n.d.	n.d.	n.d.	n.d.	359905.73 \pm 93318.21	310217.14 \pm 59925.88	315643.20 \pm 27532.86
MRT (h)	38.63 \pm 6.36	2.67 \pm 0.42	2.06 \pm 0.31	n.d.	n.d.	n.d.	n.d.	n.d.	n.d.	n.d.	n.d.	n.d.	123.54 \pm 18.11	62.99 \pm 7.78	76.64 \pm 5.39
V _z (mL/kg)	642.60 \pm 190.48	2.94.04 \pm 47.69	304.56 \pm 40.22	n.d.	n.d.	n.d.	n.d.	n.d.	n.d.	n.d.	n.d.	n.d.	10667.27 \pm 1115.96	4261.94 \pm 901.29	5032.88 \pm 632.95
Cl (mL/h/kg)	325.70 \pm 127	146.59 \pm 18.21	148.60 \pm 15	n.d.	n.d.	n.d.	n.d.	n.d.	n.d.	n.d.	n.d.	n.d.	86.12 \pm 9.26	51.32 \pm 4.92	60.85 \pm 4.27

n.d.: not detected

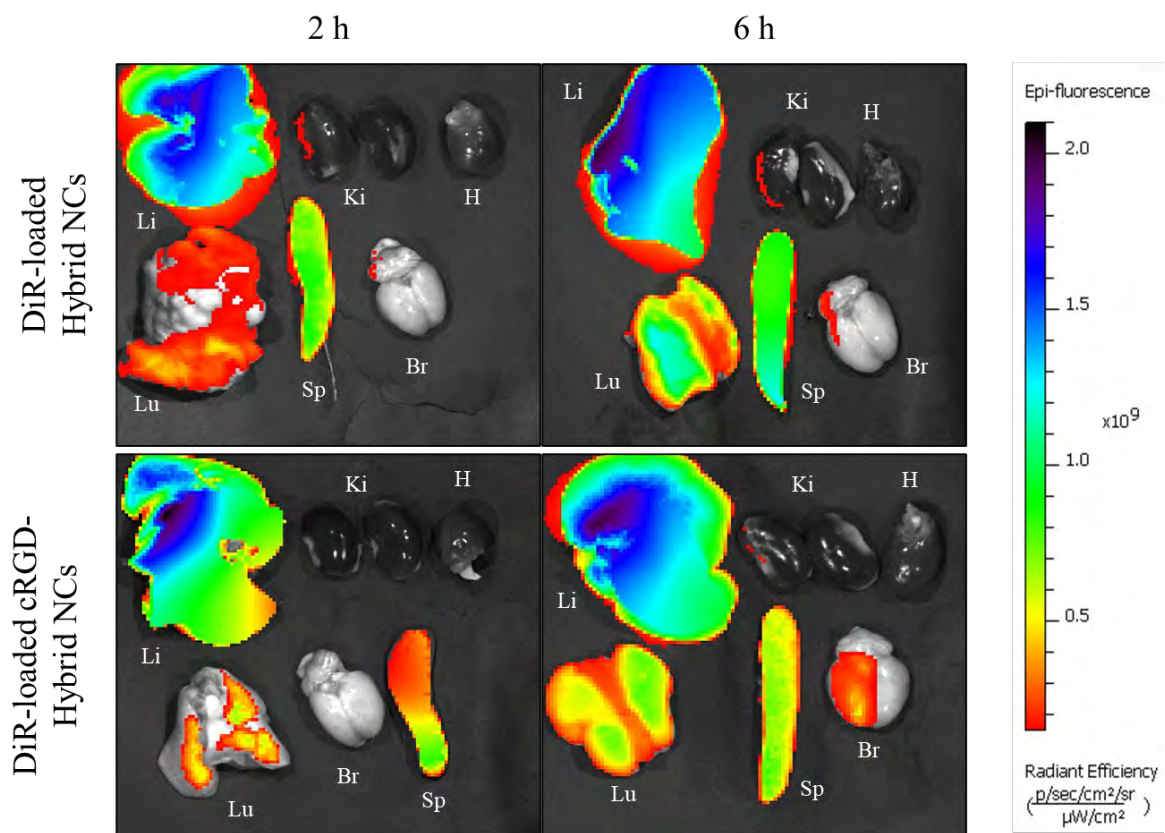


Figure 5.10. Biodistribution of cRGD-Hybrid nanoconjugates in glioma bearing rats (Br: Brain, H: Heart, Lu: Lungs, Li: Liver, Ki: Kidney, and Sp: spleen)

5.5. Discussion

Glioblastoma multiforme (GBM) is considered as the most common type of malignant and aggressive brain tumor, primarily accounting for ~16% of brain and CNS-related tumors. GBM is a type IV glioma characterized by its dedifferentiated, angiogenic, multiforme structure, making it more lethal. Temozolomide (TMZ) is considered as the standard of care chemotherapy with surgical resection and radiotherapy. Regardless of treatment, the probability of the tumor relapses is significantly higher, making it more lethal. TMZ, being a potent molecule, possesses several physiochemical limitations such as short life, quick clearance, and low brain bioavailability, which leads to sub-therapeutic outcomes and the development of resistance and finally results in tumor relapse [1]. Several other molecules are administered simultaneously to support the treatment outcome against the GBM, including mTOR inhibitors, such as rapamycin (sirolimus), temsirolimus, and ridaforolimus. These rapalogues are known to inhibit mTORC1 activity, which remains upregulated in tumor growth and progression. One well-known rapalogue commonly known as rapamycin (RAP), isolated from soil bacterium *Streptomyces hydropiscus*, is known to show its antitumor outcome, viz. inhibition of mTOR downstream pathway. Although RAP is known to bind strongly to the mTORC1 domain and demonstrate its antitumor outcome, the molecule still lacks clinical translation for glioma treatment. This could be mainly ascribed due to the low solubility, bioavailability (~15%), poor pharmacokinetic behavior, and side effects, including leukopenia, thrombocytopenia, renal, cardiac impairment, hyperlipidaemia, etc., making it more challenging for its deployment in the treatment of GBM [22].

Although both the molecules, TMZ and RAP, demonstrate the antitumor action against the GBM differently i.e., TMZ exhibits its action viz. DNA alkylation while RAP shows its action, viz. inhibition of multiple downstream proliferative pathways (PI3K/Akt/mTOR) involved in tumor survival and growth. When administered together, both compounds work synergistically to strengthen the effectiveness of the treatment outcome, specifically by overcoming the development of resistance. Likewise, Li et al. observed the molecular effect of mTOR inhibitor and TMZ against glioma, wherein the combination treatment with TMZ and RAP markedly improved the cellular cytotoxicity and rate of apoptosis compared to the individual counterpart [23]. In phase 2 open-label interventional clinical trials, the combination of albumin-bound rapamycin (nab-rapamycin) was evaluated with various drugs in combination including nab-sirolimus and temozolomide, nab-sirolimus and bevacizumab, nab-sirolimus and lomustine, nab-sirolimus and marizomib (MRZ), nab-sirolimus and

temozolomide + radio treatment for the treatment of high-grade, recurrent glioma and newly diagnosed glioblastoma. Meanwhile, treatment with nab-rapamycin and temozolomide showed better median progression-free survival and overall survival of 11.7 and 13.8 months compared to the other treatment combinations [24].

Nevertheless, the TMZ and RAP combination carry ample advantages over the conventional treatment; still, the outcome of therapy is nominal. It is mainly observed due to different physiochemical properties of the drug, including TMZ being a hydrophilic molecule with a solubility of 5 mg/ml and high permeability. At the same time, rapamycin is considered to be highly hydrophobic with $\log p$ of >4 , solubility of 0.00173 mg/ml, making it highly challenging to deliver simultaneously across the BBB and to the target site of action [1,25]. Several other attempts have been made to overcome the hindrance in improving the prognosis of the GBM, either *via* encapsulation, surface adsorption, complexation, conjugation, or a hybrid carrier approach. For instance, Mujokoro et al. evaluated the effect of co-delivery of methotrexate and curcumin using PLGA-based copolymer. The dual delivery system exhibited the encapsulation efficiency of 77.2% and 86.1% at drug loading efficiency of 6.5% and 15.5% w/w for CUR and MTX, respectively, exhibiting improved cytotoxicity compared to individual treatment [26]. Xu et al. prepared mPEG-PLA copolymer-based drug delivery system for the combined delivery of TMZ and PTX to evaluate chemotherapeutic efficacy against GBM. The dual drug delivery system was prepared using double emulsion method, which yielded particles of ~206 nm with an encapsulation of 90% and 65%, at drug loading of 0.871% and 3.15% w/w for PTX and TMZ, respectively. The PTX/TMZ-NPs exhibited a synergistic outcome by inhibiting tumor growth compared to the physical mixture alone in the subcutaneous xenograft U87 mice model [14]. Furthermore, functionalization with cell targeting ligands is also known to enhance the selective targeting towards the targeted site compared to the non-targeted counterpart. Xin et al. prepared low-density lipoprotein receptor-related protein (LRP) targeted PEG-PCL nanoparticles functionalized with Angiopep peptide for glioma. The ANG-NP exhibited improved endocytosis, transport across the BBB model *in vitro*, and enhanced accumulation in tumoral region U87MG glioma tumor-bearing mice compared to non-targeted nanoparticles [27]. Similarly, Chen et al. fabricated Peptide-22 and c(RGDfK) functionalized liposomes for transport across the BBB and BBTB. *In vitro* and *in vivo* experiments confirmed that active targeting with peptides effectively improved uptake efficiency with higher cellular uptake and higher brain tumor distribution compared to plan liposomal preparation [28].

The current chapter focuses on the fabrication of cell-penetrating peptide cRGD functionalized hybrid TMZ nanoconjugates that can co-deliver TMZ and RAP with different physiochemical properties across the BBB/BBTB for the treatment of glioblastoma multiforme. The cRGD peptide-functionalized copolymer was prepared to give cRGD-PEG-PLA copolymer. Similarly, Mazumdar et al. prepared the cRGD coupled with the maleimide group to give a peptide-functionalized polycarbonate cholesterol-based lipopolymeric nanocarrier for targeting cancer [29]. After that, the polycarbonate block polymer conjugated with TMZ (*mPEG-b-P(CB- $\{g-COOH; g-TMZ_{40}\}$)* (TMZ NCs), as reported in chapter 4, was mixed with mPEG-PLA/ cRGD-PEG-PLA, followed by preparation of nano-dispersion using thin-film hydration method to yield the Hybrid TMZ/R NCs and cRGD-Hybrid TMZ/R NCs. The Hybrid TMZ/R NCs gave the particle size and PDI of 126.62 ± 1.24 nm and 0.211 ± 0.008 and surface zeta potential of -0.333 ± 0.095 mV (Figure 5.3). The Hybrid TMZ NCs exhibited a particle size of 105.7 nm and PDI of 0.106 (Chapter 4); this could be attributed due to the encapsulation of RAP into the Hybrid TMZ NCs resulted in a slight increase in particle size from 105.7 nm to 126.2 nm. Likewise, Mittal et al. observed a similar outcome in the preparation of different molecular weights of PLGA-based nanoparticles wherein all grades of polymer (ranging MW 14-213 KDa) exhibited the drug-loaded nanoparticles with slightly higher particle size compared to the blank nanoparticles [30]. Interestingly, on cRGD functionalization, the particle size was increased to 141.83 ± 10.05 nm, PDI of 0.233 ± 0.031 with uniform morphology, and surface zeta potential of -0.168 ± 0.03 mV. Likewise, Thamake et al. prepared PLGA nanoparticles coated with alendronate and exhibited a higher particle size of 235 nm compared to 191 nm of non-targeted nanoparticles [31].

Quader et al. prepared $\alpha v \beta 3$ and $\alpha v \beta 5$ integrins targeting cRGD peptide-functionalized polymeric micelles exhibiting faster and higher penetration in U87MG-based 2D and 3D-spheroids compared to those without cRGD [32]. Similarly, cRGD-Hybrid TMZ NCs exhibited better uptake efficiency than non-targeted counterparts, as shown in Figure 5.5E & 5.6E. In the previous chapter, we have reported the cytotoxicity of TMZ with IC_{50} equivalent to ~ 1125 μM and ~ 866 μM with an apoptosis rate of 15.5% and 21.33% in C6 and U87MG glioma cells, respectively. In the current study, we have found the IC_{50} of TMZ and RAP of ~ 1133 μM and 8.5 μM . Thereafter, the combination index (CI) was determined using the Chou-Talalay method, providing the theoretical basis of the isobologram and median effect equation, allowing the quantitative estimation of drug combination interactions, wherein CI value < 1 , $= 1$, and > 1 , shows the synergism, additive, and antagonism pharmacodynamic outcome of the

drug combination. In C6 glioma cells, the TMZ: RAP molar ratio equivalent to 100:1, 110:1, 125:1, 150:1, 110:2.5, and 110:5 exhibited synergism with $CI < 1$. Based on the above data, we have selected the TMZ: RAP molar ratio equivalent to 110:1 for further experimentation in C6 glioma cells (Figure 5.5 A-C). In U87MG cells, the TMZ: RAP molar ratio equivalent to 750:2, 1000:2, 800:2.5, 800:5, 800:10, 800:25, and 800:50 showed synergism with $CI < 1$. Similarly, we have selected TMZ: RAP molar ratio equivalent to 800:2, as per the IC_{50} of individual drugs for further experimentation (Figure 5.6 A-C). After the determination of the combination index of the drug combination, the similar TMZ: RAP ratio was loaded into the nanocarrier system, i.e., Hybrid TMZ/R NCs and cRGD-Hybrid TMZ/R NCs, and evaluated for further *in vitro* assays. Interestingly, the Hybrid TMZ/R NCs and cRGD-Hybrid TMZ/R NCs exhibited IC_{50} of 375.07 and 282.8 μM in C6 and 410.4, and 238.14 μM in U87MG glioma cells, respectively (Figure 5.5A and 5.6A). The apoptosis rate of the free drug and nanoconjugates were evaluated in C6 and U87MG glioma cells, wherein free TMZ, free RAP, and TMZ+RAP physical mixture exhibited a total apoptosis rate of 18.08%, 21.33%, and 22.51%, respectively. On encapsulation into the nanocarrier system, the Hybrid TMZ/R NCs and cRGD-Hybrid TMZ/R NCs showed a total apoptosis rate of 41.81% and 48.25%, respectively, in C6 glioma cells (Figure 5.5D). In U87MG glioma cells, the free TMZ, free RAP, and TMZ+RAP combination exhibited a total apoptosis rate of 28.72%, 24.29%, and 28.86%, respectively. The Hybrid TMZ/R NCs and cRGD-Hybrid TMZ/R NCs exhibited a total apoptosis rate of 32.44% and 57.2%, respectively (Figure 5.6D). A similar outcome was shown in multiple reports that encapsulation of drugs into nanoparticles will aid in the improvement of the apoptosis rate in cancer cells [33,34]. Furthermore, Yu et al. observed that the functionalization with the cRGD cell-penetrating peptide results in an additional improvement in the apoptosis rate compared to the non-targeted counterpart [35].

After confirming the *in vitro* activity of the TMZ and RAP combination with cRGD surface functionalization to carrier system, the developed system was evaluated for its *in vivo* efficacy activity in the C6 cells induced syngeneic orthotropic rat glioma model. The animals were continuously observed for changes in physiological parameters to confirm tumor growth. The glioma-bearing rats were randomly divided into different treatment groups, namely, negative control, positive control, free TMZ, free RAP, Hybrid TMZ/R NCs, and cRGD-Hybrid TMZ/R NCs. After the completion of treatment, the major organs were excised for histopathological toxicity evaluation. The excised rat brain was evaluated for change in brain weight and RH/LH hemispherical width ratio, wherein it was observed that the positive control

brain showed RH/LH hemispherical width ratio of >1 , indicating the successful development of the rat glioma model. While treatment with Hybrid TMZ/R NCs and cRGD-Hybrid TMZ/R NCs exhibited a statistically significant reduction in the RH/LH ratio ($p < 0.01$, 0.001) compared to the TMZ-treated group, respectively (Figure 5.7F). As reported previously in Chapter 4, the RH/LH ratio was found to be elevated (>1) in the case of C6 cells glioma-bearing rats. Moreover, the animals treated with cRGD-Hybrid TMZ/R NCs showed no sign of mortality during the study period. In contrast, the positive control animals died within 15 days after the initiation of treatment (Figure 5.7). The histopathological toxicity analysis was performed using H&E staining, indicating no significant sign of toxicity with the cRGD-Hybrid TMZ/R NCs in all majorly excised organs (Figure 5.8). While in the positive control, a significant number of mononuclear/tumor cells were observed in the brain and lungs; upon treatment with Hybrid TMZ/R NCs and cRGD-Hybrid TMZ/R NCs, a significant reduction in cell infiltration was observed. Furthermore, a similar trend was observed in the liver, kidney, and spleen, wherein mild to moderate organ toxicity was observed in the case of positive control, TMZ, and RAP-treated animals, especially liver with hepatocyte degeneration; kidney with atrophic renal tubules, increased peritubular space; and spleen with mild to moderate depletion in the red and white pulp. In previous studies, it is well reported that the utilization of biocompatible and biodegradable polycarbonate and polyester copolymers showed no signs of toxicity in animals and further aided the delivery of payload to the site of action. Likewise, no such toxicity was observed in Hybrid TMZ/R NCs and cRGD-Hybrid TMZ/R NCs treated animals, indicating the effectiveness and biocompatibility of the combinational delivery against the glioma. Thereafter, pharmacokinetics study was performed in C6-glioma-bearing rats, wherein, the hybrid nanoconjugate exhibited reduction in the half-life, volume of distribution, and improvement in the C_{max} and AUC compared to the free RAP treated animals (Figure 5.8, table 5.1). The reduction in the half-life of RAP was observed due to the encapsulation of RAP into the Hybrid TMZ/R NCs and cRGD-Hybrid TMZ/R NCs and reduction in the non-specific distribution of the RAP in the organs compared to the free RAP, eventually resulted in lowered organ toxicity in glioma bearing animals. Interestingly, the conjugated TMZ to the polymeric system did not exhibited breakdown into free TMZ, TMZ-A, TMZ-H, and AIC. Similarly, it is well reported that the amide bond between the temozolomide and the polymeric backbone is comparatively much stronger and requires higher energy to break compared to the imidazotetrazine ring. However, the ring is highly susceptible to undergo hydrolysis into its metabolites even under physiological conditions, where, the amide bond remains intact [36,37].

Thus, we hypothesize that the conjugated TMZ hydrolyzed to give the methyl diazonium ion, which is known to show the alkylation of the DNA susceptible sites. After that, a biodistribution study of cRGD-Hybrid TMZ nanoconjugates was performed in C6 cells glioma-bearing SD rats to understand the fate of nanocarrier after injection. At a specific time (2 and 6 h), major organs were evaluated for their fluorescent signal using the IVIS system. Wherein an intense signal was observed at 6 h post-injection in cRGD-Hybrid TMZ NCs compared to a minimal signal was seen in non-targeted counterpart, indicating the role of cRGD peptide in transversing the BBB. Similarly, several reports suggested the role of cell-penetrating peptides aiding in the transverse of the nanocarrier system across the BBB for their effective therapeutic outcome [32,38,39].

5.6. Conclusion

Glioblastoma is considered the deadliest form of brain tumor, which poses a substantial challenge to the conventional form of treatment. Multiple drug combinations have been given with TMZ to overcome the limitations associated with the treatment. Still, the outcome remains elusive, which is mainly attributed due to the disparate physiochemical properties of the treatment combination involved, making it much harder to reach the optimal concentration at the target site of action. However, in response to the drug-related challenges, a hybrid-based approach has been developed, integrating conjugation with encapsulation strategy for hydrophilic and hydrophobic molecules, which have shown promising outcomes in various facets of drug delivery. Such hybrid approach aids in improved encapsulation efficiency, loading capacity, uptake by tumor cells, cytotoxicity towards cancer cells, and penetration through the blood-brain and blood-tumor barriers.

Furthermore, the surface functionalization with cRGD peptide on the hybrid nanoconjugates improved cellular uptake and apoptosis rate and reduced the IC_{50} in C6 and U87MG glioma cells. After that, *in vivo* administration of TMZ and RAP using cRGD-Hybrid TMZ/R NCs has improved the *in vivo* efficacy profile of the drug combination, with marked improvement in the brain parameters and survival of rats. The comprehensive histopathological assessment demonstrated a substantial reduction in the tumor cells within the brain with minimal signs of toxicity observed to heart, lungs, liver, kidney, and spleen. Also, the biodistribution of the cRGD-Hybrid TMZ NCs elucidated the improved accumulation in the brain, indicating the role of functionalization of cRGD cell-penetrating peptide.

Overall, the hybrid nanoconjugate approach with an amalgamation of polymer(s) and surface functionalization could be an effective and better strategy for delivering multiple therapeutic payloads. Such therapeutic strategies offer a promising avenue in addressing a wide range of diseases, potentially transforming the landscape of brain tumor therapeutics.

5.7. References

- [1] Jatyan R, Singh P, Sahel DK, Karthik YG, Mittal A, Chitkara D. Polymeric and small molecule-conjugates of temozolomide as improved therapeutic agents for glioblastoma multiforme. *J Control Release* 2022;350:494–513. <https://doi.org/https://doi.org/10.1016/j.jconrel.2022.08.024>.
- [2] Mohammed S, Dinesan M, Ajayakumar T. Survival and quality of life analysis in glioblastoma multiforme with adjuvant chemoradiotherapy: A retrospective study. *Reports Pract Oncol Radiother* 2022;27:1026–36.
- [3] NCT00979017. Avastin/Temozolomide/Irinotecan for Unresectable/Multifocal Glioblastoma Multiforme 2009. <https://clinicaltrials.gov/study/NCT00979017?cond=NCT00979017&rank=1&tab=history> (accessed March 30, 2024).
- [4] NCT00501891. Bevacizumab in Combination With Metronomic Temozolomide for Recurrent Malignant Glioma 2007. <https://clinicaltrials.gov/study/NCT00501891?cond=NCT00501891&rank=1&tab=history> (accessed March 30, 2024).
- [5] Desjardins A, Reardon DA, Coan A, Marcello J, Herndon JE, Bailey L, et al. Bevacizumab and daily temozolomide for recurrent glioblastoma. *Cancer* 2012;118:1302–12.
- [6] NCT00486603. Hydroxychloroquine, Radiation, and Temozolomide Treating Patients With Newly Diagnosed Glioblastoma Multiforme 2007. <https://clinicaltrials.gov/study/NCT00486603?cond=NCT00486603&rank=1&tab=history> (accessed March 30, 2024).
- [7] Yu Z, Zhao G, Xie G, Zhao L, Chen Y, Yu H, et al. Metformin and temozolomide act synergistically to inhibit growth of glioma cells and glioma stem cells in vitro and in vivo. *Oncotarget* 2015;6:32930.
- [8] Luchman HA, Stechishin ODM, Nguyen SA, Lun XQ, Cairncross JG, Weiss S. Dual mTORC1/2 blockade inhibits glioblastoma brain tumor initiating cells in vitro and in vivo and synergizes with temozolomide to increase orthotopic xenograft survival. *Clin Cancer Res* 2014;20:5756–67.
- [9] Cloughesy TF, Yoshimoto K, Nghiemphu P, Brown K, Dang J, Zhu S, et al. Antitumor

- activity of rapamycin in a Phase I trial for patients with recurrent PTEN-deficient glioblastoma. *PLoS Med* 2008;5:e8.
- [10] Arcella A, Biagioni F, Oliva MA, Bucci D, Frati A, Esposito V, et al. Rapamycin inhibits the growth of glioblastoma. *Brain Res* 2013;1495:37–51.
- [11] Koehl GE, Schlitt HJ, Geissler EK. Rapamycin and tumor growth: mechanisms behind its anticancer activity. *Transplant Rev* 2005;19:20–31.
- [12] Kahan BD. Sirolimus: a comprehensive review. *Expert Opin Pharmacother* 2001;2:1903–17.
- [13] Jatyan R, Sahel DK, Singh P, Sakhuja R, Mittal A, Chitkara D. Temozolomide-fatty acid conjugates for glioblastoma multiforme: In vitro and in vivo evaluation. *J Control Release* 2023;23:S0168-3659. <https://doi.org/10.1016/j.jconrel.2023.05.012>.
- [14] Xu Y, Shen M, Li Y, Sun Y, Teng Y, Wang Y, et al. The synergic antitumor effects of paclitaxel and temozolomide co-loaded in mPEG-PLGA nanoparticles on glioblastoma cells. *Oncotarget* 2016;7:20890.
- [15] Li Y, Hou H, Zhang P, Zhang Z. Co-delivery of doxorubicin and paclitaxel by reduction/pH dual responsive nanocarriers for osteosarcoma therapy. *Drug Deliv* 2020;27:1044–53.
- [16] Naderinezhad S, Amoabediny G, Haghirsadat F. Co-delivery of hydrophilic and hydrophobic anticancer drugs using biocompatible pH-sensitive lipid-based nano-carriers for multidrug-resistant cancers. *RSC Adv* 2017;7:30008–19.
- [17] Jain A, Sharma G, Kushwah V, Garg NK, Kesharwani P, Ghoshal G, et al. Methotrexate and beta-carotene loaded-lipid polymer hybrid nanoparticles: A preclinical study for breast cancer. *Nanomedicine* 2017;12:1851–72.
- [18] Khan MM, Madni A, Tahir N, Parveen F, Khan S, Jan N, et al. Co-delivery of curcumin and cisplatin to enhance cytotoxicity of cisplatin using lipid-chitosan hybrid nanoparticles. *Int J Nanomedicine* 2020:2207–17.
- [19] Sharma S, Pukale S, Sahel DK, Singh P, Mittal A, Chitkara D. Folate targeted hybrid lipopolymeric nanoplexes containing docetaxel and miRNA-34a for breast cancer treatment. *Mater Sci Eng C* 2021;128:112305.

<https://doi.org/https://doi.org/10.1016/j.msec.2021.112305>.

- [20] Zhang N, Fu J-N, Chou T-C. Synergistic combination of microtubule targeting anticancer fludellone with cytoprotective panaxytriol derived from panax ginseng against MX-1 cells in vitro: experimental design and data analysis using the combination index method. *Am J Cancer Res* 2016;6:97.
- [21] Pukale SS, Sharma S, Dalela M, Singh A kumar, Mohanty S, Mittal A, et al. Multi-component clobetasol-loaded monolithic lipid-polymer hybrid nanoparticles ameliorate imiquimod-induced psoriasis-like skin inflammation in Swiss albino mice. *Acta Biomater* 2020;115:393–409. <https://doi.org/https://doi.org/10.1016/j.actbio.2020.08.020>.
- [22] Zaytseva YY, Valentino JD, Gulhati P, Evers BM. mTOR inhibitors in cancer therapy. *Cancer Lett* 2012;319:1–7.
- [23] Li B, Zhou C, Yi L, Xu L, Xu M. Effect and molecular mechanism of mTOR inhibitor rapamycin on temozolomide-induced autophagic death of U251 glioma cells. *Oncol Lett* 2018;15:2477–84.
- [24] NCT03463265. Nab-sirolimus in Recurrent High Grade Glioma and Newly Diagnosed Glioblastoma 2018. <https://clinicaltrials.gov/study/NCT03463265?cond=NCT03463265&rank=1> (accessed March 29, 2024).
- [25] DrugBank. Sirolimus n.d. <https://go.drugbank.com/drugs/DB00877> (accessed March 29, 2024).
- [26] Mujokoro B, Madani F, Esnaashari SS, Khosravani M, Adabi M. Combination and co-delivery of methotrexate and curcumin: preparation and in vitro cytotoxic investigation on glioma cells. *J Pharm Innov* 2020;15:617–26.
- [27] Xin H, Sha X, Jiang X, Zhang W, Chen L, Fang X. Anti-glioblastoma efficacy and safety of paclitaxel-loading Angiopep-conjugated dual targeting PEG-PCL nanoparticles. *Biomaterials* 2012;33:8167–76. <https://doi.org/https://doi.org/10.1016/j.biomaterials.2012.07.046>.
- [28] Chen C, Duan Z, Yuan Y, Li R, Pang L, Liang J, et al. Peptide-22 and cyclic RGD functionalized liposomes for glioma targeting drug delivery overcoming BBB and BBTB. *ACS Appl Mater Interfaces* 2017;9:5864–73.

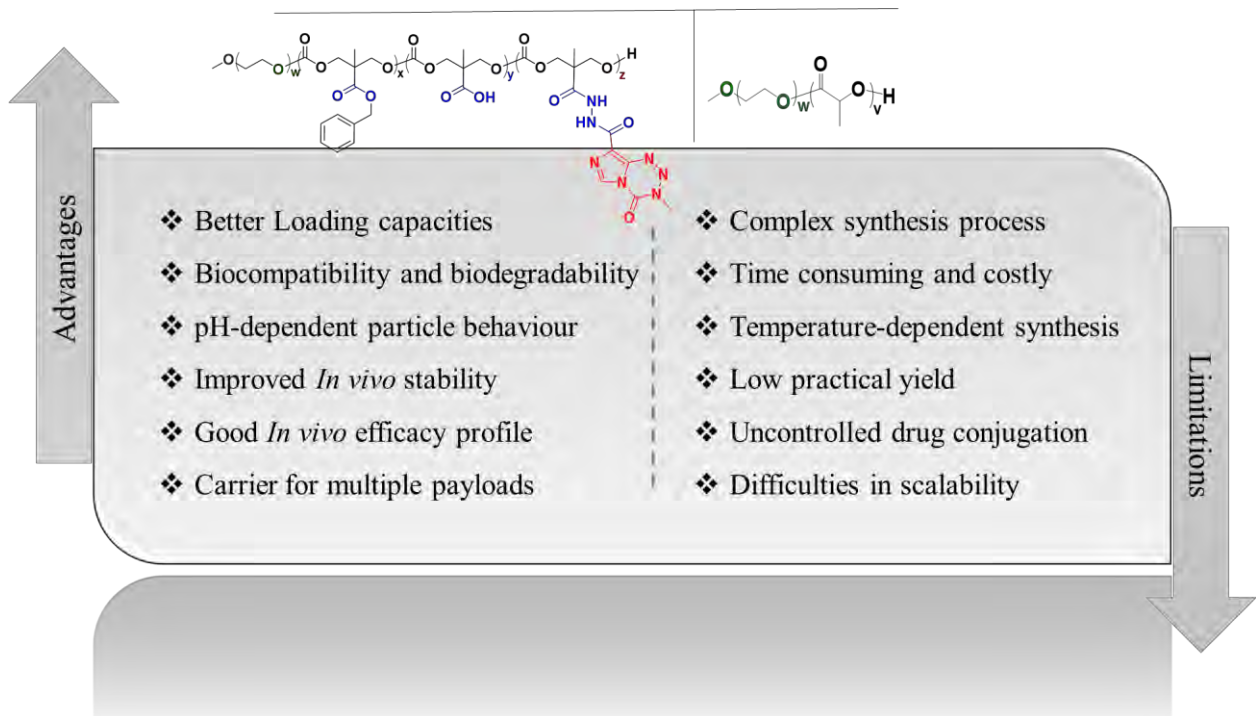
- [29] Mazumdar S, Narisepalli S, Singh AK, Chitkara D, Mittal A. Enhanced anti-tumor efficacy and tumor accumulation of Tamoxifen through cRGD functionalized cholesterol based lipopolymeric nanoparticles for targeted breast cancer therapy. *J Drug Deliv Sci Technol* 2023;90:105173.
- [30] Mittal G, Sahana DK, Bhardwaj V, Kumar MNVR. Estradiol loaded PLGA nanoparticles for oral administration: effect of polymer molecular weight and copolymer composition on release behavior in vitro and in vivo. *J Control Release* 2007;119:77–85.
- [31] Thamake SI, Raut SL, Gryczynski Z, Ranjan AP, Vishwanatha JK. Alendronate coated poly-lactic-co-glycolic acid (PLGA) nanoparticles for active targeting of metastatic breast cancer. *Biomaterials* 2012;33:7164–73.
- [32] Quader S, Liu X, Chen Y, Mi P, Chida T, Ishii T, et al. cRGD peptide-installed epirubicin-loaded polymeric micelles for effective targeted therapy against brain tumors. *J Control Release* 2017;258:56–66.
- [33] Yuan Q, Han J, Cong W, Ge Y, Ma D, Dai Z, et al. Docetaxel-loaded solid lipid nanoparticles suppress breast cancer cells growth with reduced myelosuppression toxicity. *Int J Nanomedicine* 2014:4829–46.
- [34] Abdel-Hakeem MA, Abdel-Haseb OM, Abdel-Ghany SE, Cevik E, Sabit H. Doxorubicin loaded on chitosan-protamine nanoparticles triggers apoptosis via downregulating Bcl-2 in breast cancer cells. *J Drug Deliv Sci Technol* 2020;55:101423.
- [35] Yu X, Song Y, Di Y, He H, Fu D, Jin C. Enhanced tumor targeting of cRGD peptide-conjugated albumin nanoparticles in the BxPC-3 cell line. *Sci Rep* 2016;6:31539.
- [36] Mirzaei S, Khalilian MH, Taherpour AA. Mechanistic study of the hydrolytic degradation and protonation of temozolomide. *RSC Adv* 2015;5:41112–9. <https://doi.org/10.1039/C5RA04680G>.
- [37] Sun H, Yan L, Chang MYZ, Carter KA, Zhang R, Slyker L, et al. A multifunctional biodegradable brush polymer-drug conjugate for paclitaxel/gemcitabine co-delivery and tumor imaging. *Nanoscale Adv* 2019;1:2761–71. <https://doi.org/10.1039/C9NA00282K>.
- [38] Tapia-Arellano A, Gallardo-Toledo E, Ortiz C, Henríquez J, Feijóo CG, Araya E, et al. Functionalization with PEG/Angiopep-2 peptide to improve the delivery of gold nanoprisms to central nervous system: In vitro and in vivo studies. *Mater Sci Eng C*

2021;121:111785.

- [39] Bode GH, Coué G, Freese C, Pickl KE, Sanchez-Purrà M, Albaiges B, et al. An in vitro and in vivo study of peptide-functionalized nanoparticles for brain targeting: The importance of selective blood–brain barrier uptake. *Nanomedicine Nanotechnology, Biol Med* 2017;13:1289–300.

Chapter 6

Conclusions and future prospective



6.1. Conclusions

Glioblastoma multiforme (GBM) is a heterogeneous type of malignancy that arises from neoplastic glial cells, representing one of the most lethal forms of brain cancer. The conventional treatment involves temozolomide (TMZ), a second-generation DNA alkylating agent capable of crossing the blood-brain barrier (BBB) and used as a standard-of-care chemotherapeutic agent with debulking surgery and radiotherapy. Despite its potency, TMZ faces limited (<1%) brain bioavailability, thereby rendering the drug with sub-therapeutic outcomes. Therefore, higher doses of TMZ are given, resulting in dose-dependent toxicities. Such a treatment approach only improves the survival of the patient with a limited scope. However, to overcome the limitations of TMZ monotherapy, the treatment in combination with second-line chemotherapeutics is highly preferred. The mTOR inhibitors, such as rapalogues, offer anti-tumor potential by modulating the downstream pathway of the PI3K/Akt/mTOR in cancer. Such therapeutic combinations could serve as a potential approach to glioma treatment. Nevertheless, the simultaneous delivery of multiple payloads remains challenging due to differing physiochemical behaviors, including solubility, log p, bioavailability, BBB/BBTB permeability, etc. Overall, the primary goal of the current work is to design, synthesize, and characterize the polymeric nanocarrier platform that can simultaneously deliver both hard-to-deliver hydrophilic and hydrophobic molecules across the BBB/BBTB and enhances the therapeutic efficacy using targeted and simultaneous delivery of multiple payloads in combating glioma. Chapter 1 details an extensive overview of glioblastoma multiforme (GBM), encompassing its incidences, pathogenesis, and factors responsible for cancer progression and survival. Certain treatment approaches are available in the market to treat various cancers. However, the presence of the BBB/BBTB makes the therapeutics ineffective, creating a hindrance in achieving the actual potential of the therapeutics. Thereby limiting the scope of viable treatment options. However, the chapter describes the viable therapeutic strategies, particularly combining TMZ with mTOR inhibitors for glioma therapy. Furthermore, the delivery of the combination therapeutics across the BBB/BBTB using the nanocarrier, polymer-drug conjugation, and actively targeted polymer-hybrid approach were thoroughly discussed.

Chapter 2 covers the development of the analytical method and its validation using simple ultraviolet-visible (UV-Vis) spectroscopy for TMZ-H for the quantitation of the drug molecule in the polymeric conjugate of temozolomide. Thereafter, an HPLC-UV-based analytical

method for rapamycin, temozolomide (TMZ), and its derivatives (TMZ-A, TMZ-BOC, TMZ-H, AIC) have been developed, followed by its thorough validation as per the ICH guidelines. The developed method was utilized to determine the purity of the synthesized analytes. After that, a highly sensitive, UPLC-MS/MS-based simultaneous method was developed for RAP, TMZ, and its derivatives and validated as per the ICH guidelines. The developed method exhibited a linearity over the range of 0.976 to 1000 ng/ml in whole blood as a biological matrix. The developed and validated method could be utilized for *in vivo* pharmacokinetics of analytes in animals.

Chapter 3 covers the design, synthesis, and characterization of the amphiphilic polymeric conjugate of TMZ (mPEG-b-P(CB-{g-COOH; g-TMZ_n})). The polycarbonate-based polymeric drug conjugate was synthesized to address the drug-related limitations, such as loading, encapsulation, and stability of the molecule. The process was initiated by synthesizing mPEG-polycarbonate-based copolymer possessing free COOH as free pendent groups, followed by covalent conjugation of temozolomide hydrazide using EDC/HoBt coupling. The resulting conjugates of TMZ, (mPEG-b-P(CB-{g-COOH; g-TMZ₂₀}), mPEG-b-P(CB-{g-COOH; g-TMZ₄₀}), mPEG-b-P(CB-{g-COOH; g-TMZ₆₀})), depicted the loading efficiency of 16.8%, 28.82%, and 37.99% w/w for 20, 40, and 60 units of TMZ units, respectively. After that, the nanodispersion of nanoconjugates was prepared and evaluated based on the particle size and surface morphology using DLS and SEM, respectively, at pH 5.0, 6.0, and 7.4, demonstrated varying particle sizes based on the units of TMZ units attached. mPEG-b-P(CB-{g-COOH; g-TMZ₂₀} demonstrated size ranging from 237.1 to 323.7, mPEG-b-P(CB-{g-COOH; g-TMZ₄₀} showed an average particle size ranging from 90.9 to 207.2, while, mPEG-b-P(CB-{g-COOH; g-TMZ₆₀} exhibited an average particle size from 497.8 to 552 nm. The stability of nanoconjugates in the biological environment is an important aspect that can impact the therapeutic outcome. As reported in the literature, the tumor vasculature junctions usually get compromised with intercellular gaps ranging from 60-300 nm with loose endothelial junctions. Accordingly, colloidal and TMZ stability of mPEG-b-P(CB-{g-COOH; g-TMZ₂₀} and mPEG-b-P(CB-{g-COOH; g-TMZ₄₀} NPs under physiological conditions was investigated. The colloidal stability assay indicated no significant change in particle size at 4 °C up to 7 days, whereas, at 37 °C, a substantial change in particle size was observed from day 1 and day 2 in mPEG-b-P(CB-{g-COOH; g-TMZ₂₀} and mPEG-b-P(CB-{g-COOH; g-TMZ₄₀}, respectively. The same samples were analyzed for the %TMZ remaining, wherein mPEG-b-P(CB-{g-

COOH; g-TMZ₂₀) and (mPEG-b-P(CB-{g-COOH; g-TMZ₄₀}) showed a half-life of 4.03 and 5.88 h, respectively compared to 1.8 h for free TMZ.

Chapter 4 mainly addresses the stability perspective of the TMZ molecule and the *in vitro* and *in vivo* fate were explored. Although the TMZ loading capacity was significantly improved after conjugation, the stability perspective is still a concern. To overcome this, in the current chapter, we prepared a hybrid system comprised of polymer-TMZ conjugate ((mPEG-b-P(CB-{g-COOH; g-TMZ₄₀})) and mPEG-PLA using a thin film hydration method. The resulting hybrid TMZ nanoconjugates (Hybrid TMZ NCs) showed particles of 105.7 ± 0.99 nm with a narrow polydispersity index of 0.106 ± 0.033 and a surface zeta potential of ζ : -6.79 ± 1.61 mV. The UV-stability studies were performed for the %TMZ remaining, indicating the improved stability of >120 h with a half-life of ~194 h under physiological conditions. Afterward, hybrid TMZ nanoconjugates were characterized for their *in vitro* cell-based assay, showing improved cellular toxicity, uptake, and apoptosis rate in C6 and U87MG glioma cells. Furthermore, a C6-induced syngeneic orthotropic glioma model in *Sprague Dawley* rats was developed, followed by an evaluation of efficacy and toxicity of Hybrid TMZ NCs, indicating marginal improvement in the brain physiology, survival rate, change in body weight, and reduced organ toxicity compared to the free TMZ. Thus, such a strategy could be explored to deliver various drugs to target the glioma.

In Chapter 5, we proposed to actively functionalize the hybrid nanoconjugates with the cyclo(Arg-Gly-Asp-D-Phe-Cys) (cRGDfC, or cRGD), composed of a mixture of polycarbonate and polyester block copolymer that can co-deliver hydrophilic TMZ and hydrophobic rapamycin molecule for the treatment of GBM. The cRGD-targeted RAP-loaded Hybrid TMZ NCs (cRGD-Hybrid TMZ/R NCs) were prepared by using thin film hydration of (mPEG-b-P(CB-{g-COOH; g-TMZ₄₀}), mPEG-PLA, cRGD-PLA, and RAP. The resulting colloidal dispersion indicated particle size, PDI, and surface zeta potential of 141.83 ± 10.05 nm, 0.233 ± 0.031 , and -0.168 ± 0.03 mV, respectively. The cRGD-Hybrid TMZ/R NCs exhibited plentiful advantages, including improved uptake efficiency, cellular toxicity, and apoptosis rate in C6 and U87MG glioma cells. Thereafter, *in vivo*, the efficacy of actively targeted nanoconjugates has improved brain parameters, including brain weight, right-to-left brain hemispherical width (RH/LH) ratio, and survival and reduced the tumor burden and organ toxicity compared to free drug counterpart. The comprehensive histopathological assessment demonstrated a substantial reduction in the tumor cells within the brain with minimal signs of

toxicity observed in the heart, lungs, liver, kidney, and spleen in the C6-cells induced syngeneic orthotropic glioma model in rats. Simultaneously, the pharmacokinetic study was performed in C6-glioma-bearing animals, indicating reduced circulation half-life and volume of distribution and improved the C_{max} , AUC, and clearance of RAP, post-treatment with cRGD-Hybrid TMZ/R NCs. Further, *in vivo* tissue bio-distribution was performed in C6-glioma-bearing rats, where the cRGD-Hybrid TMZ/R NCs exhibited an intense signal in tumor-bearing brain and liver at 6 h of administration, indicating the beneficial outcome of cRGD peptide functionalization with improved BBB permeability.

Overall, the hybrid nanoconjugate approach with an amalgamation of polymer(s) and surface functionalization could be an effective and better strategy for delivering multiple therapeutic payloads. Such therapeutic strategies offer a promising avenue in addressing a wide range of diseases, potentially transforming the landscape of brain tumor therapeutics.

6.2. Future prospective

The current work primarily targets to design, synthesize, and characterize the actively targeted amphiphilic hybrid carrier system that can co-deliver both hydrophilic (TMZ) and hydrophobic (Rapamycin) molecules simultaneously, *viz.* overcoming the barriers involved from the site of injection to its intended site of action, i.e., to the brain to exploit its synergistic therapeutic potential against hard-to-treat brain cancer. However, the efforts made in advancements in the therapeutic outcome in mitigating glioma. Nevertheless, there is and will be scope for improvement. Several aspects of our experiments could be studied in detail for future nanomedicine translation from bench to bedside.

The following could be the possible future direction of current research:

1. The amphiphilic polymer was synthesized as per the unit calculation method. Still, a minor change in the number of units could lead to variability in the therapeutic to toxic outcome. However, stringent control over the number of units of TMZ as a pendant group is required.
2. Different targeting ligands (small and large molecules) could be explored for *in vivo* therapeutic outcomes.
3. Different types of biocompatible polymers or the mixture of monomers for polymerization could be explored to deliver various kinds of payload, either using conjugation, complexation, or encapsulation.

4. The developed polymeric hybrid nanocarrier could be explored for other routes of administration, such as oral and nose-to-brain delivery.
5. Different pendant groups could be attached, such as cationic groups/lipids for nucleic acid delivery, amino acids for improved biocompatibility, or labeling dye as a diagnostic/tracking agent.
6. The degradation pattern/profile of the polymer-drug conjugate could be explored to better understand the fate after *in vivo* administration.
7. Determining the cross-talk between the molecules delivered using developed polymer hybrid nanoconjugates after *in vivo* administration could be explored, including resistance pathway, apoptosis, ROS, autophagy, mitophagy, etc.
8. Apart from TMZ and RAP, other combinations of hydrophilic and hydrophobic molecules could be explored using the polymer hybrid nanoconjugate approach.

ANNEXURES



ANNEXURE-I**List of Patents**

S. No.	Details of Patent
1	Deepak Chitkara, Prabhjeet Singh , Deepak Kumar Sahel, Reena Jatyan, Anupama Mittal, Polymeric Nano-Formulation For Delivery Of Temozolomide And Method Of Preparing The Same, Indian Patent Application no. 202311047526, Filed on 14 th July 2023

ANNEXURE-II**List of Publications****Publication from Thesis**

S. No.	Details of Publications
1	Prabhjeet Singh , Deepak Kumar Sahel, Reena Jatyan, Kiran Bajaj, Anupama Mittal, Deepak Chitkara. "Enhancing Temozolomide <i>In Vivo</i> Stability and Efficacy Through Hybrid Nanoconjugate Approach for Improved Glioblastoma Multiforme Treatment." Asian Journal of Pharmaceutical Sciences (2023): Accepted for Publication (Impact factor: 10.7)
2	Reena Jatyan, Prabhjeet Singh , Deepak Kumar Sahel, Y. G. Karthik, Anupama Mittal, and Deepak Chitkara. "Polymeric and small molecule-conjugates of temozolomide as improved therapeutic agents for glioblastoma multiforme." Journal of Controlled Release 350 (2022): 494-513. (Impact factor: 10.5)
3	Prabhjeet Singh , Anupama Mittal, Deepak Chitkara. "cRGD-Functionalized Nanohybrid Conjugates Delivering Temozolomide and Rapamycin for Treating Glioblastoma Multiforme: <i>In vitro</i> and <i>In vivo</i> Evaluation." Advanced Science (2024): Submitted (Impact factor: 14.3)
4	Prabhjeet Singh , Anupama Mittal, Deepak Chitkara. "Simultaneous Estimation of Rapamycin, Temozolomide and its Metabolites Using UPLC-ESI-MS/MS and its Application to Pharmacokinetics in C6-glioma Bearing Animals." Analytica Chimica Acta (2024): Submitted (Impact factor: 5.7)
5	Prabhjeet Singh , Aditi Singh, Shruti Shah, Jalpa Vataliya, Anupama Mittal, and Deepak Chitkara. "RNA interference nanotherapeutics for treatment of glioblastoma multiforme." Molecular Pharmaceutics 17, no. 11 (2020): 4040-4066. (Impact factor: 4.5)

Publication from Allied work

S. No.	Details of Publications
1	Reena Jatyan, Deepak Kumar Sahel, Prabhjeet Singh , Rajeev Sakhuja, Anupama Mittal, and Deepak Chitkara. "Temozolomide-fatty acid conjugates for glioblastoma multiforme: In vitro and in vivo evaluation." Journal of Controlled Release 359 (2023): 161-174. (Impact factor: 10.5)
2	Paramita Saha, Prabhjeet Singh , Himanshu Kathuria, Deepak Chitkara, and Murali Monohar Pandey. "Self-assembled lecithin-chitosan nanoparticles improved rotigotine nose-to-brain delivery and brain targeting efficiency." Pharmaceutics 15, no. 3 (2023): 851 (Impact factor: 4.9)
3	Imran Ansari, Prabhjeet Singh , Anupama Mittal, Ram I. Mahato, and Deepak Chitkara. "2, 2-Bis (hydroxymethyl) propionic acid based cyclic carbonate monomers and their (co) polymers as advanced materials for biomedical applications." Biomaterials 275 (2021): 120953 (Impact factor: 12.8)
4	Saurabh Sharma, Sudeep Pukale, Deepak Kumar Sahel, Prabhjeet Singh , Anupama Mittal, and Deepak Chitkara. "Folate targeted hybrid lipo-polymeric nanoplexes containing docetaxel and miRNA-34a for breast cancer treatment." Materials Science and Engineering: C 128 (2021): 112305. (Impact factor: 8.45)

ANNEXURE-III**List of Awards and Conferences**

S. No.	Award
1	Awarded with Innovation in Science Pursuit for Inspired Research (INSPIRE)-JRF-2019 and SRF-2022 from Department of Science and Technology (DST), GOI (DST-INSPIRE-JRF/SRF)
2	Awarded with Oral Presentation at “National Science Festival 2023”, on the occasion of National Science Day organised by Society of Young Biomedical Scientists, India and SMS medical college, Jaipur, held on February 27 th -28 th , 2023
3	Aditi Vaidya, Prabhjeet Singh , Anupama Mittal, Deepak Chitkara, Polymeric and Small Molecule Conjugation Strategy Delivering Temozolomide for the Treatment of Glioblastoma Multiforme, presented at National Science Festival at SMS Medical College, Jaipur, Under the aegis of Society of Young Biomedical Scientists (SYBS), India, held on February 27 - 28, 2023 (Poster Presentation)
4	Jalpa Vataliya, Shruti Shah, Prabhjeet Singh , Deepak Chitkara, Tumor Microenvironment and Targeted Nano-Delivery in Glioblastoma Multiforme, presented at BITS International Conference on Life Science Research & its Interface with Engineering and Allied Sciences (LSRIEAS 2018), organised by BITS-Pilani, Pilani campus, Rajasthan 333031, held on November 1-3, 2018 (Poster presentation)
5	Shruti Shah, Jalpa Vataliya, Prabhjeet Singh , Deepak Chitkara, Deregulated Pathways of Glioblastoma Multiforme, presented at BITS International Conference on Life Science Research & its Interface with Engineering and Allied Sciences (LSRIEAS 2018), organised by BITS-Pilani, Pilani campus, Rajasthan 333031, held on November 1-3, 2018 (Poster presentation)
6	Aditi Singh, Jalpa Vataliya, Prabhjeet Singh , Deepak Chitkara, Mi-RNA Therapeutics for Treatment of Glioblastoma Multiforme, presented at BITS International Conference on Life Science Research & its Interface with Engineering and Allied Sciences (LSRIEAS 2018), organised by BITS-Pilani, Pilani campus, Rajasthan 333031, held on November 1-3, 2018 (Poster presentation)

ANNEXURE-IV

Biography of supervisor

Dr. Deepak Chitkara completed his B. Pharmacy degree in 2004 from the University Institute of Pharmaceutical Sciences (UIPS), Panjab University, Chandigarh, Punjab. Thereafter, he obtained his M.S. (Pharm.) in Pharmaceutics from the Department of Pharmaceutics, National Institute of Pharmaceutical Education and Research (NIPER), SAS Nagar, Punjab, followed by completion of his Ph.D. in Pharmaceutical Sciences, National Institute of Pharmaceutical Education and Research (NIPER), S.A.S. Nagar (Mohali), Punjab. During his Ph.D. tenure, he was a visiting research scholar at the University of Tennessee Health Science Center (UTHSC), Memphis, TN, USA, for one year. He continued his research practice with Prof. Ram I. Mahato at the University of Nebraska Medical Center (UNMC), Omaha, NE, USA, as a post-doctoral research associate in the field of miRNA therapeutics for treating pancreatic cancer. Then, he joined the Birla Institute of Technology and Science (BITS)-Pilani, Vidya Vihar Campus, Pilani, Rajasthan. Currently, he is working as an Associate Professor at the Department and focuses on various tasks, including research, teaching, administration, entrepreneurship, and many more. His research primarily focuses on designing and synthesizing different biocompatible, non-viral nano-based delivery systems for small molecules, oligonucleotides (miRNA, mRNA), plasmids, and CRISPR/Cas genome editing tools. His lab is well equipped with the equipment required to synthesize polymers, develop formulations, and evaluate *in vitro* and *in vivo*. He has written and been granted several funded grants from various government (DST, DBT, ICMR) and pharmaceutical industries. His in-depth research work has been published with >80 publications in peer-reviewed journals, and he is the editor of one book and two special issues from the Journal of Controlled Release on Brain Targeting and Protein and Peptide Therapeutics for the Journal of Pharmacology and Experimental Therapeutics. He has filed 11 Indian patents and one international PCT patent application, of which 5 Indian patent applications have been granted.



He is the coordinator (University-wide) of the Intellectual Property Enablement and Commercialization (IPEC) vertical under the Research and Innovation Division of BITS Pilani. Dr. Chitkara's role is central to ensuring that the university's intellectual assets are protected,

managed, and leveraged effectively to benefit society and the economy. He is involved in several key responsibilities and activities aimed at managing and facilitating the intellectual property (IP) and technology transfer processes. His efforts help bridge the gap between academic research and real-world applications, enabling the translation of BITS Pilani technologies into commercial products and services.

He is also the coordinator of the DST-supported BITS-Technology Enabling Centre established with the support from the Technology, Translation and Innovation Division of DST, Government of India, with an objective of creating a regional ecosystem to promote a culture of innovation and indigenous technology development in the state of Rajasthan. Dr. Chitkara is be involved in fostering collaborations with other universities, research institutions, government bodies, and the private sector to enhance the commercialization opportunities in the state.

Dr. Chitkara is also the founding director of a faculty-led nanotechnology-based start-up (Nanobrid Innovations Private Limited) incubated at Pilani Innovations and Entrepreneurship Development Society at BITS-Pilani to further take up the commercialization activities. The Company has commercialized a skin care range (Nanobrid Inskin) wherein four products has been launched through their own e-commerce platform (www.inskin.in) as well as other e-commerce platforms including amazon and flipkart.

Biography of Co-supervisor

Prof. Gaikwad Anil Bhanudas is a Professor at Department of Pharmacy, Birla Institute of Technology and Science Pilani (BITS Pilani), Pilani Campus. He did his Master's and Ph.D. from the Department of Pharmacology and Toxicology, NIPER, SAS Nagar. He was awarded a Doctoral Sandwich Fellowship from DAAD (German Academic Exchange Services) during his doctoral studies. He visited reputed overseas institutes as a visiting scientist in the Department of Medicine/Nephrology, Albert Einstein College of Medicine, NY, USA, and Nephrological Center, Medizinische Poliklinik, Ludwig-Maximilians-University, Munich, Germany, in 2010 and 2008, respectively. His research grants are from SERB, UGC, DBT, ICMR, and CSIR. Till date, he has provided essential and novel evidences on histone post-translational modifications and the protective axis renin-angiotensin system in the development of diabetic kidney diseases. He has contributed to several book chapters published by Elsevier and has 84 peer-reviewed research and review publications published in reputed international journals such as *Drug Discovery Today*, *Cardiovascular Research*, *Pharmacological Research*, *British Journal of Pharmacology*, *BBA- Molecular Basis of Disease*, *Food and Function*. He has supervised one PDF and seven Ph.D. students and, at present, is guiding one RA and six Ph.D. students. He is also serving as an Associate Editor for *Frontiers in Endocrinology Journal* (Cardiovascular Endocrinology section), Renal Pharmacology section of the *Frontiers in Pharmacology Journal*, and *BMC Pharmacology and Toxicology Journal*. Also, he is an international reviewer for grant applications from the South African Medical Research Council and the Netherlands under the Innovational Research Incentive Scheme.



ANNEXURE-V

Biography of Research Scholar

Mr. Prabhjeet Singh is currently working as a Ph.D. Scholar with Dr. Deepak Chikara, Associate Professor, and Prof. Gaikwad Anil Bhanudas, Professor, since August 2018 at Department of Pharmacy, Department of Pharmacy, Birla Institute of Technology & Science, Pilani, Rajasthan. He completed his Bachelor's in Pharmacy (B.Pharm) in 2016 from Pt. B.D. Sharma, University of Health Sciences, Rohtak, Haryana. He got his Master's in Pharmacy (M.Pharm) degree in Pharmacology in 2018 from Jamia Hamdard, Hamdard University, New Delhi. He was awarded a Gold medal and first-rank certificate for his excellent academic performance during his M.pharm. tenure. Thereafter, he joined the Ph.D. at the Department of Pharmacy, Birla Institute of Technology & Science, Pilani, Rajasthan, as a Junior Research Fellow (JRF). Afterward, he was granted with "Innovation in Science Pursuit for Inspired Research (INSPIRE) (DST-INSPIRE) fellowship from DST, Government of India, and later awarded with Senior Research Fellow (SRF) in 2022. During his Ph.D. tenure, he has published ~10 publications in peer-reviewed Journals such as *Asian Journal of Pharmaceutical Sciences*, *Molecular Pharmaceutics*, *Journal of Controlled Release*, *Biomaterials*, *Materials Science and Engineering: C*. His research mainly focuses on designing, synthesis, and evaluating biocompatible nanocarrier platform through chemical modifications for delivering hard-to-deliver hydrophilic and hydrophilic molecules to treat glioblastoma multiforme. His research resulted in the filing of 01 Indian Patent with complete specification. He was awarded the best oral presentation (national conference) and selected for oral presentation (International conference) for presenting his research against brain tumors.

